University of Florence
Department of Pharmaceutical Sciences

Scuola di Dottorato in Scienze
PhD in Chimica e Tecnologia del Farmaco – XXII ciclo
Curriculum: Pharmaceutical technology (CHIM/09)

Micro- and nano-carriers to improve technological and biopharmaceutical properties of drugs from plants

Benedetta Isacchi

Supervisor
Prof. F.F. Vincieri

Coordinatore della Scuola di Dottorato
Prof. E. Teodori

Aim

The aim of this PhD work was to develop micro- and nano-carriers for some drugs derived from plants. Vegetal world is a big box, containing numerous potential therapeutic molecules but many of them suffer of poor biopharmaceutical properties which affect their effectiveness. Micro- and nano-carriers represent formulation technologies which can hugely modify drug release profile, absorption, distribution and elimination for the benefit of improving product efficacy and safety, as well as patient convenience and compliance.
The molecules investigated in the present project were artemisinin, isolated from *Artemisia annua* L., verbascoside, purified from *Lippia citriodora* H.B.K. and resveratrol, derived from *Vitis vinifera* L.

Artemisinin is a sesquiterpene lactone having an unusual endoperoxyl moiety which is essential for the activity. The molecule has a poor bioavailability due to its little solubility both in oil and water and it is not stable decomposing by the opening of the lactone ring or lacking the endoperoxide moiety (Klayman DL, 1985).
Verbascoside is a phenylpropanoid molecule represented by two sugar moieties (glucose and rhamnose), a phenylpropanoid structure (caffeic acid) and a phenylethanol moiety. It is very water soluble (up to 30 mg/mL) but in aqueous media it is unstable and it undergoes to degradation which is correlated to the pH (Sinico C, 2008). The main reaction involved in this process is the hydrolysis of the caffeic acid moiety which led to the formation of an inactive molecule.
Resveratrol is a stilbenoid molecule having a low solubility in aqueous media, with a poor bioavailability and high propensity to oxidize (Walle T, 2004; Trela BC, 1996; Wenzel E, 2005). Resveratrol exists as two possible geometric isomes: *cis*- (*Z*) and *trans*- (*E*). The *trans*- form can undergo isomerisation to the *cis*- form when exposed to ultraviolet irradiation but this isomer is inactive. (Prokop J, 2006). This isomerization is very fast and represent a very huge problem for the use of trans-resveratrol in pharmaceutical and cosmetic applications (Wang Y, 2002).

These three molecules having very different structures and as a consequence distinctive problematics related to their scarce solubility and/or poor stability were chosen to solve some practical aspects related to their therapeutically use but also as model structures to substantiate how pharmaceutical technology may deeply affect bioavailability profile of drugs.
Carriers with different characteristics were developed and tested for evaluating their efficacy and versatility as Troy's horses. It is clear that making new formulations without trying their real application or therapeutic capability seems only a style exercise.
Many efforts were done in order to test *in vivo* the innovative formulations. So, many links and collaborations with other researchers' groups were created, believing deeply in an international sharing of knowledge.

I. Artemisinin

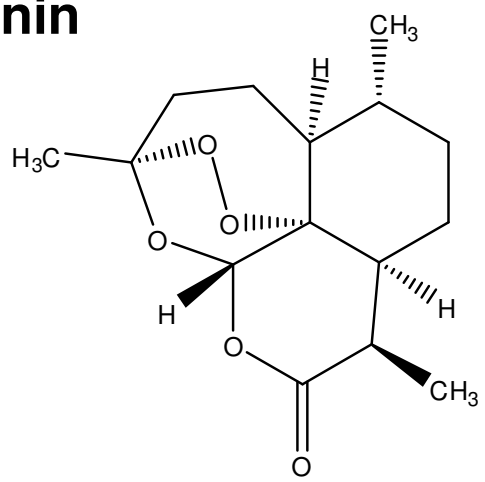

I.1. Introduction

I.1.1. Artemisinin: Hystory

Artemisinin (*qinghaosu*), an endoperoxide sesquiterpene lactone isolated from *Artemisia annua* L. a plant derived from Traditional Chinese Medicine, which was used for at least 2000 years to treat fever and malaria (Klayman DL, 1985; Duffy PE, 2004; Meshnick SR, 1998). Its earliest recorded use dates as far back as 340 BC when Ge Hong of the East Jin dynasty described this herbal medicine in *The Handbook of prescription for emergencies*. In 1596, The Chinese herbalist Li Shizhen recommended that patients with fever take a handful of *qinghaosu* , soak it in a sheng (about 1 liter) of water, squeeze out the jouice and drink it all (Efferth T, 2009).
Nowadays, artemisinin is considered one of the most important secondary metabolite and bioactive constituent (Klaiman DC, 1985; van Agtmael MA, 1999; Heppner DG, 1998). Now is available commercially in China, Vietnam and other countries as an antimalarial drug.

I.1.2. Artemisinin: Source

Malaria continues to be a major global killer disease despite continuous efforts to reduce its toll. Each year at least a million people die with more than 80% of these in Africa south of the Sahara. Within this number, pregnant women and children under five years of age account for the majority of the victims (WHO, UNICEF, 2005).
The widespread development of resistance in malaria parasites against the cheapest antimalarials such as chloroquine and to a lesser extent quinine has prompted a search for alternative treatments. In remote regions patients often first consult traditional herbalists and healers before visiting the nearest clinic or hospital (usually only when symptoms worsen). Because of its efficacy against both uncomplicated and severe malaria, there is a global demand for artemisinin and its derivatives, which are the active compounds against falciparum malaria. The increased demand has led to fears of a future shortage if increased cultivation of *Artemisia annua* L., the source of artemisinin is not pursued. The non-governmental organisations Anamed (Action for Natural Medicine) and Medicos Descalzos (Barefoot doctors) have set up programs for small scale cultivation and local utilization of herbal formulations of *A. annua* L. (Hirt HM, 2000).
Artemisia annua L. (sweet or annual wormwood, member of Asteraceae family) is an annual herbaceous plant with a strong fragrance endemic to the northern parts of Chahar and Suiyuan Provinces in China, at 1000-1500 m above sea level (Wang CW, 1961)

where it is known as *qinghao* 青蒿 (green herb) and used as a remedy for chills and fevers since more than 2000 years (Klaiman DC, 1985; Hien TT, 1993). Artemisia is now growing in many European countries and has also become naturalized in North America. *A. annua* is an interesting source of essential oils (Simon JE, 1990), however, its economical importance is mainly determined by being probably the only species of genus Artemisia able to synthesize artemisinin (Baraldi R, 2008). In 1972, the active ingredient was isolated and first named *qinghaosu* (essence of *qinghao*), and then later renamed artemisinin (Meshnick SR, 2002). In the 1979 its structure was fully elucidated.

I.1.3. Artemisinin: Chemical properties

Artemisinin presents many problems due to its poor biopharmaceutical properties. First of all, it has low bioavailability due to its low solubility. Artemisinin metabolizes quickly in vivo and has an initial burst effect and high peak plasma concentration (Chen Y, 2009). It is not very stable and easly decomposes, most probably by the opening of the lactone ring, due to its unusual peroxy group (Klayman DL, 1985). It is difficult for drug crystals to disperse homogeneously because of their hydrophobicity in solution or blood. In addition, a greater number of injections is necessary because of the short-duration effect (Chen Y, 2009).

I.1.4. Artemisinin: Antimalarian activity

Artemisinin is considered a potent antimalarial drug, even against chloroquine- and quinine-resistant *Plasmodium falciparum* and other malaria-causing parasites (Meshnick SR, 1998; Baraldi R, 2008). At the moment, artemisinin is the basis of a large family of drugs recommended by the World Health Organization to fight malaria in the countries where highly resistant strains of the protozoan have been certified (Baraldi R, 2008).
Its chemical action on the human organism has not yet completely clarified. The theory more realistic seems that in *Plasmodia* species, the cleavage of the endoperoxide moiety of artemisinin is facilitated by haeme-iron. Erythrocyte haemoglobin serves as an amino acid source for *Plasmodium* trophozoites and schizonts. The parasites take up haemoglobin and degrade it in their food vacuoles (Shenai BR, 2000). The release of haeme-iron during haemoglobin digestion facilitates the cleavage of the endoperoxide moiety of artemisinin by an iron(II) Fenton reaction. Thereby, reactive oxygen species, such as hydroxyl radicals and superoxide anions, are generated. They damage the membranes of food vacuoles and lead to auto-digestion (Krishna S, 2004).
Artemisinin offers impressive effects including characteristics of 'high efficacy, fast-action and low-toxicity', and is regarded as 'a breakthrough in the history of antimalarial drugs' (Heppner DG, 1998). It is a potent blood schizonticide with a minimum inhibitory concentration of 0.1 µM (De Vries PJ, 1996).

I.1.5. Artemisinin: Pharmacological effects

It has been found to be effective also against other infectious diseases including hepatitis B (Romero MR, 2005) and parasites that cause schistosomiasis (Bormann S, 2001; Utzinger J, 2001). More recently, artemisinin and its derivatives (expecially its water soluble derivative artesunate) have been shown to be effective also against numerous types of tumors, including breast cancer, human leukemia, colon, and small-cell lung carcinomas (Efferth T, 2001; Singh NP, 2001). Artemisinin is a therapeutic molecule to control human cancers with reduced side-effects (Firestone GL, 2009). Artemisinin is also selectively toxic to cancer cells because of their high iron content; *in vitro* in the presence of iron, induces apoptosis (Singh NP, 2004), and is lethal towards human leukaemia (Lai

H, 1995) and breast cancer cells (Singh NP, 2001). Normal cells pick up less iron and have better intracellular regulation of iron content, they are significantly less susceptible to artemisinin (Lai H, 2006). Artemisinin is able to prevent breast cancer development in rats. In addition, breast tumors in artemisinin-fed rats were significantly fewer and smaller in size when compared with controls. These data indicate that artemisinin may be a potent cancer-chemoprevention agent (Lai H, 2006).

Curcumin

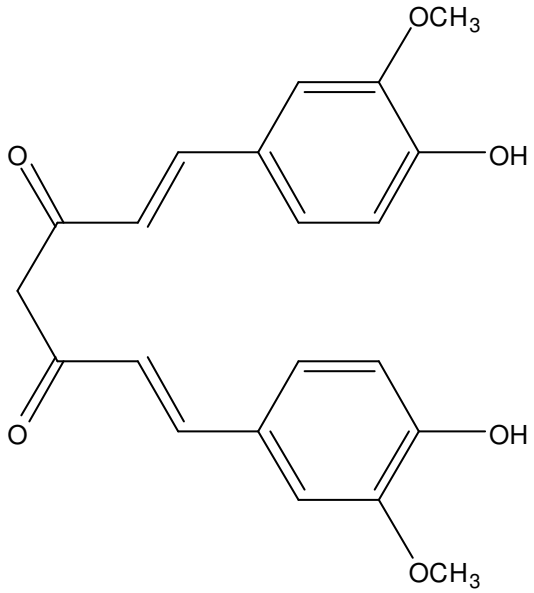

I.1.6. Curcumin: Source

Curcumin, diferuloylmethane isolated from the rhizomes of the *Curcuma longa* L. (Zingiberaceae family) plant, a perennial herb widely cultivated in tropical regions of Asia and extensively used for imparting colour and flavour to food (Shoba G, 1998).

I.1.7. Curcumin: Antimalarian activity

Studies both *in vitro* with *P. falciparum* and *in vivo* with a rodent model of malaria (*P. berghei*) have indicated that curcumin has also an antimalarial activity against sensitive and multidrug resistant parasites (Reddy RC, 2005; Nandakumar DN, 2006).
The target of curcumin is not known, although it has been suggested to be the PfATP6 protein (Reddy RC, 2005), which has already been implicated as a potential candidate of artemisinin-resistance in malaria (Eckstein-Ludwig U, 2003).

I.1.8. Curcumin: Pharmacological activity

Curcumin has been shown to regulate a number of biological responses (Araujo CC, 2001). Curcumin has been shown to have antitumoral properties (Kuttan G, 2007). Additionally, curcumin and, to a lesser extent, its metabolites have been shown to have immunomodulatory activities which may also contribute to the beneficial effects of curcumin against autoimmune diseases and cancer (Jagetia GC, 2007; Sandur SK, 2007).

In addition to its anti-tumorigenic, anti-oxidant, and antinflammatory effects, curcumin has been shown to possess anti-microbial activity (Araujo CC, 2001; Rasmussen HB, 2000). Curcumin has been shown to hinder Leishmania (Koide T, 2002) and Trypanosoma (Nose M, 1998) viability.

I.1.9. Artemisinin-based combination therapy (ACT)

Malaria continues to be one of the major public problems in Africa, Asia and Latin America. The World Health Organisation (WHO) has racommended that all the antimalarians must be combined with an artemisinin component (artemisinin-based combination therapy ACT) for use as first line treatment against malaria. This class is now first line policy in most malaria-endemic countries (Ioset JR, 2009; Eastman RT, 2009).

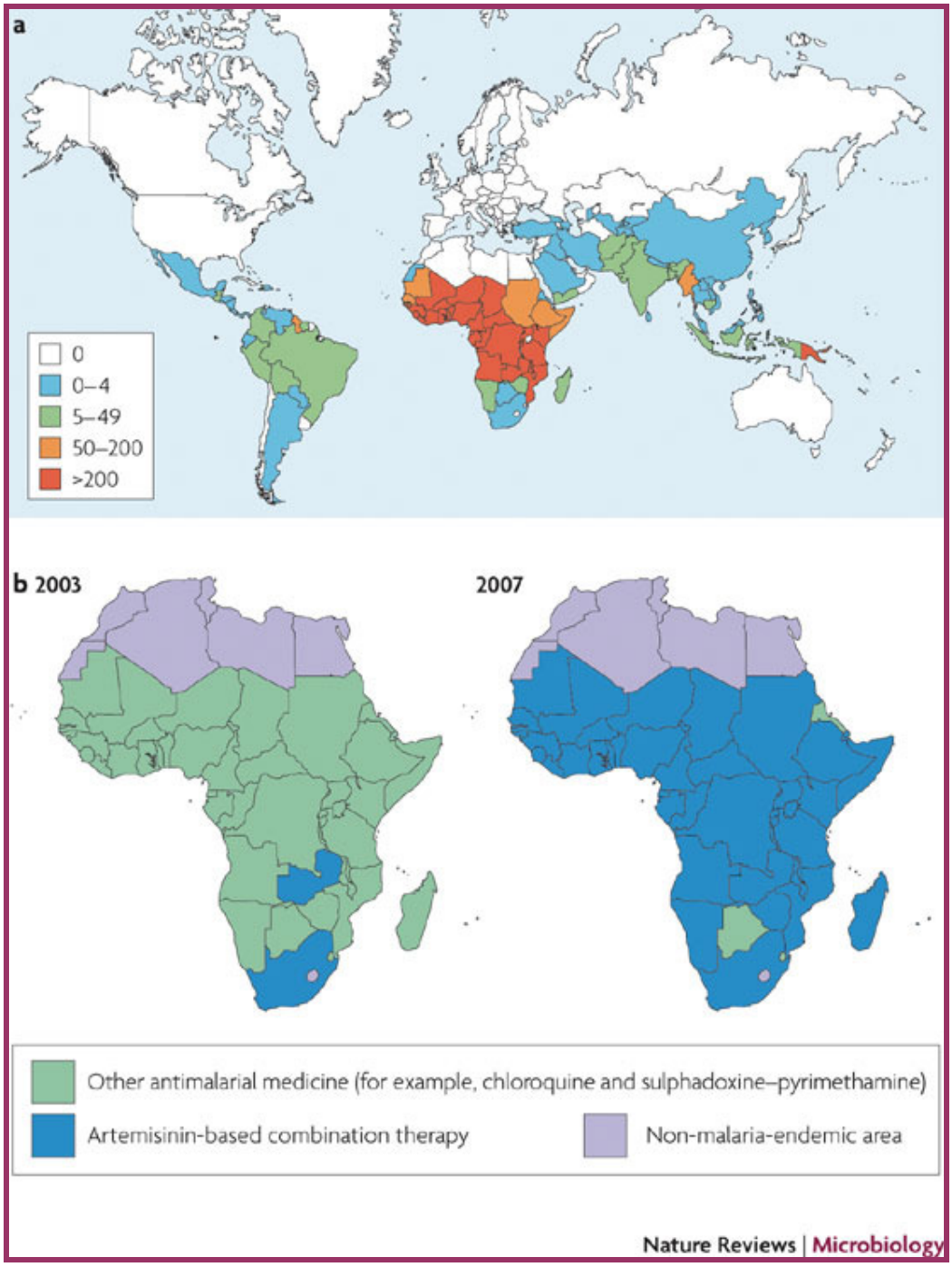

Fig 1. (a) The worldwide incidence of malaria and (b) the rapid adoption of ACT across the sub-Saharan Africa (Nature Review Microbiology, 2009).

In the figure **1 (a)**, incidence of malaria worldwide in 2006, stratified per 1000 population, was estimated. Cases in Africa constituted 86% of the global total, Southeast Asia accounted for 9% and the eastern of Mediterranean regions had 3%. *Plasmodium falciparum* was found to be responsible for over 75% of the cases in most of sub-Saharan African countries but was second to *Plasmodium vivax* in most countries outside of Africa (WHO, 2008). In the figure **1 (b)**, the official first-line antimalarian policy in Africa in 2003 and 2007, demonstrating the dramatic shift from a diversity of first line antimalarials (typically chloroquine or sulphadoxine-pyrimethamine) towards the adoption of artemisinin-based combination therapies (UNICEF, 2007).
It is now widely accepted that the emergence of artemisinin resistance in natural parasite populations of *P. falciparum* may be only a question of time. In order to delay the development of resistance and thus prolong the efficacy of artemisinin and its derivatives, artemisinins have been paired with other drugs in so-called artemisinin combination therapies (ACT) (Martinelli A, 2008). These have however been criticized due to the pharmacokinetic mismatches between the two drugs within the combination and to the fact that resistance versus the non-artemisinin component of the combination is commonly present (Hastings IM, 2006).
Curcumin has been recently proposed as an attractive partner drug for artemisinins, due to its short half-life (1–2 h), closely matching that of artemisinin, its relative abundance and cost effectiveness (Reddy RC, 2005; Nandakumar DN, 2006). Artemisinin and curcumin show an additive interaction in killing *P. falciparum* in culture with; IC50 for artemisinin and curcumin are 45-50 nM and 15-18 µM, respectively (Nandakumar DN, 2006).
In view of its abundance, non-toxic nature and demonstrated therapeutic effects in a variety of human diseases, it will be useful to further investigate the potential of curcumin in developing low-cost antimalarial therapies (Reddy RC, 2005).

I.2. Materials and methods

I.2.1. Chemicals and standards

All the solvents used for the extraction and HPLC analysis (MeOH, *n*-hexane, dichloromethane, and acetonitrile) were HPLC grade from Merck (Darmstadt, Germany); 85% formic acid was provided by Carlo Erba (Milan, Italy). Water was purified by a Milli-Q_{plus} system from Millipore (Milford, MA). Solution NaCl 0.9%, Fresenius Kabi, Italy. Artemisinin was purchased from Sigma (Sigma-Aldrich srl, Milan, Italy). Curcumin purchased from Extrasynthese (Milan, Italy). 18:0/18:0 PEG 2000 was purchased by Spectra2000 srl (Rome, Italy), italian seller for Avanti Polar (Canada). Egg phosphatidylcholine (Phospholipon90G, P90G) were kindly obtained from Natterman Phospholipids, Gmb. Cholesterol, dicetylphosphate and stearylamine were analytical grade and were purchased from Aldrich (Milan, Italy). Phosphotungstic acid and copper grids with carbon film 150 mesh were purchased from Società Italiana Chimici (Rome, Italy).
Artemisinin reference standard (ST3105, batch no. C005641) which was used for the quantification of artemisinin, was kindly provided by Sigma-tau (Pomezia, Rome, Italy).
Rutin trihydrate reference standard (batch no. K12408717, standard purity 88.17%, considering the content of residual solvents, moisture and amount of impurities) which was used for the quantification of polymethoxylated flavonoids, was kindly provided by Indena Research Laboratories (Settala, Milan, Italy).
Curcumin standard was used for the quantification of curcumin, was kindly provided by Extrasynthese (Milan, Italy).

I.2.2. Plant material and growth condition

Seeds of Artemisia *annua* L. (a gift from a private collection site near Bologna, Italy) were sown in 1x1 m nursery beds in April and germinated in greenhouse. One month old seedlings were then transplanted into pots containing peat and the obtained plantlets were then transferred outside where they were allowed to acclimate for 4 weeks before planting in the experimental field located in a flat land site 11°37' E and 44°300' N in the Po Valley, Italy, with an intra-row and inter-row spacing of 0.2 and 1 m, respectively. The plants were sampled randomly and the different parts of the flowering tops (leaves and inflorescences) were harvested at different time during the vegetative phase (pre-flowering, full bloom and post-flowering), separated manually, weighted and stored frozen at -20°C until analysis to check the artemisinin and flavonoid concentrations. Plant dried material used for the analyses at pre-flowering, full bloom and post-flowering were 24.17, 3.7 and 20.30 g, respectively, for the inflorescence and 14.20, 3.4 and 8.20 g for leaves.

I.2.3. Preparation of the extracts

Leaves and inflorescences at different developmental stages were lyophilized and cut into small pieces with an Osterizer. The samples were exhaustively extracted at room temperature by maceration with 100 mL of hexane for 72 h. The eluates were subsequently taken to dryness under reduced pressure to obtain the crude extracts.

I.2.4. Preparation of the samples for HPLC/DAD/ESI MS analysis

Three samples of 10 mg of dried *n*-hexane extract (accurately weighed) were suspended in 2 mL acetonitrile in a volumetric flask and sonicated for 30 min. The suspensions were filtered and each of the sample solutions was injected three times. Quantification of artemisinin was performed by the MS detection while flavonoids were quantified by UV detection at 280 nm. Calibration curves were obtained from a methanolic solution of the reference standards containing artemisinin or rutin with the concentrations ranging between 0.01 and 2.0 mg/mL. All calibration levels (n=5) were measured six times. Results were calculated using the peak areas.

I.2.5. Analytical HPLC/DAD characterization

The HPLC analyses were performed using a HP 1100 Liquid Chromatograph (Agilent Technologies, Palo Alto, CA, USA) equipped with a HP 1040 Diode Array Detector (DAD), an automatic injector, an auto sampler and a column oven and managed by a HP 9000 workstation (Agilent Technologies, Palo Alto, CA, USA). Separations were performed on a reversed phase column Purospher® Star RP-18, namely Hibar® Prepacked column RT (250 x 4.6 mm) with particle size 5 mm (Merck, Darmstadt, Germany).
The eluents were H_2O at pH 3.2 by formic acid and acetonitrile. The following multi-step linear gradient was applied:

Time (min.)	CH3CN (%)	H2O/HCOOH pH=3.2 (%)
0.1	50	50
15	50	50
20	100	0
23	100	0
28	50	50

The system was operated with a flow of 1 mL/min and with the oven temperature at 26°C; the injection volume was 20 µL. Before HPLC analysis, each sample was filtered through a cartridge-type sample filtration unit with a polytetrafluoroethylene (PTFE) membrane (d=13 mm, porosity 0.45 µm, Lida manufacturing Corp.) and immediately injected.
Chromatograms were recorded at 240, 280, 350 nm to detect flavonoids and any other constituents and at the wavelength of 420 nm in order to detect the amount of curcumin in combined liposomes.

I.2.6. Analytical HPLC/ESI MS characterization

The HPLC system described above was interfaced with a HP 1100 MSD API-electrospray (Agilent Techologies, Palo Alto, CA, USA). The interface geometry, with an orthogonal position of the nebulizer with respect to the capillary inlet, allowed use of analytical conditions similar to those used for HPLC/DAD analysis in order to achieve the maximum sensitivity of ESI values. The same column, time period and flow rate were used during the HPLC/ESI MS analyses. Mass spectrometry operating conditions were optimised in order to achieve maximum sensitivity values: negative and positive ionisation mode, scan spectra from *m*/Z 100 to 800, was used with a gas temperature of 350°C, nitrogen flow rate of 10 L min^{-1}, nebulizer pressure 30 psi, quadrupole temperature 30°C, Capillary voltage 3500V. The applied fragmentors were in the range 80–180 V. Full scan spectra from m/z 100 to 800 in the positive ion mode were obtained (scan time 1 s).
Identification of constituents was carried out by HPLC/DAD and HPLC/ESI MS analysis, and/or by comparison and combination of their retention times, UV-Vis and mass spectra of the peaks with those of authentic standards when possible, or isolated compounds or characterised extracts as well as based on literature data.

I.2.7. Statistical analysis

Data of physiological variables were analyzed by ANOVA using PC SAS version 8.2 (SAS Institute Inc., Cary, NC, USA). Means and standard errors are presented. The concentrations were compared using the General Linear Model Procedure with the LSD test. Differences referred to as significant had a *P* value less than 0.05.

I.2.8. Formulations

I.2.8.1. Production of liposomes

Multilamellar vesicles were prepared according to the film hydratation method (Bangham AD, 1965). P90G, cholesterol and artemisinin were dissolved in chloroform. The organic solvent were vacuum evaporated and the dry lipid film was hydratated by addition of bidistilled water or physiological solution (Buffer at pH=7.4 or NaCl 0.9% v/v). The dispersion was stirred with a mechanical stirrer for 30 minutes with a waterbath at the constant temperature of 38°C. In order to reduce the dimensions of the vesicles from MLV to LUV, an high pressure homogenizer Emulsiflex C3® was used at the applied pressure of 150000 kPa for 60 seconds. Then the liposomes were characterized by different techniques.

I.2.8.2. Production of liposomes with superficial charge

Multilamellar vesicles were prepared according to the film hydratation method (Bangham AD, 1965), as described above. Negatively and positively charged vesicles were prepared

by using either dicetylphosphate (dihexadecylphosphate) or stearylamine, respectively, as a charge inducer. Dicetylphospahate or stearylamine was weighted together with P90G, cholesterol and artemisinin. In order to reduce the dimensions of the vesicles, an high pressure homogenizer Emulsiflex C3® was used, as described above.

I.2.8.3. Production of PEGylated liposomes

Multilamellar vesicles were prepared according to the film hydratation method (Bangham AD, 1965), as described above. 18:0/18:0 PEG 2000 was weighted together with P90G, cholesterol and artemisinin in order to obtain stealth liposomes. In order to reduce the dimensions of the vesicles, an high pressure homogenizer Emulsiflex C3® was used, as described above.

I.2.8.4. Production of artemisinin-curcumin loaded liposomes

Multilamellar vesicles were prepared according to the film hydratation method (Bangham AD, 1965), as described above. Artemisinin, curcumin, P90G, and cholesterol were weighted together with the perspective of combined therapy. In order to reduce the dimensions of the vesicles, an high pressure homogenizer Emulsiflex C3® was used, as described above.

I.2.9. Characterization of liposomes

I.2.9.1. Dynamic Light Scattering (DLS)

Dynamic Light Scattering is an ALV CGS-3 system (Malvern Instruments, Malvern, UK) equipped with a JDS Uniphase 22 mW He–Ne laser operating at 632.8 nm, an optical fiber-based detector, a digital LV/LSE-5003 correlator and a temperature controller (Julabowater bath) set at 25 °C. Time correlation functions were analyzed to obtain the hydrodynamic diameter of the particles (Z_h) and the particle size distribution (polydispersity index, PDI) using the ALV-60X0 software V.3.X provided by Malvern. Autocorrelation functions were analyzed by the cumulants method (fitting a single exponential to the correlation function to obtain the mean size (Z_{ave}) and polydispersity index (PDI)) and CONTIN (to fit a multiple exponential to the correlation function to obtain particle size distributions). The diffusion coefficients calculated from the measured autocorrelation functions were related to the hydrodynamic radius of the particles via the Stokes–Einstein equation

$$Z_h = (k_B T q^2)/(3\pi\eta\Gamma)$$

where Z_h is the hydrodynamic radius of the particles,
k_B is the Boltzmann constant,
T is the absolute temperature,
η is the solvent viscosity,
Γ is the decay rate,
q is the scattering vector

$$q = [4\pi n \sin(\Phi/2)]/\lambda$$

in which n is the refractive index of the solution,
Φ is the scattering angle,
λ is the wavelength of the incident laser light.
Scattering was measured in an optical quality 4 mL borosilicate cell at a 90° angle.

I.2.9.2. Electrophoretic mobility

Zeta potentials (ζ-potentials) of the liposome systems were measured using a Malvern Instruments Zetamaster 5002. For all samples, an average of three measurements at stationary level was taken. The cell used was a 5 × 2 mm rectangular quartz capillary. The temperature was kept constant at 25°C by a Haake temperature controller. The zeta potential was calculated from the electrophoretic mobility, μ_E, using the Henry correction to Smoluchowski's equation.

I.2.9.3. Trasmission electron microscopy (TEM): 'negative contrast'

A drop (10 µL) of vesicle dispersion diluted 10-times was applied to a carbon film-covered copper grid. Most of the dispersion was blotted from the grid with filter paper to form a thin film speciment, which was stained with a phosphotungstic acid solution 1% w/v in sterile water. The samples were dried for 3 minutes and than they were examined under a JEOL 1010 electron microscope and photographed at an accelerating voltage of 64 kV.

I.2.9.4. Trasmission electron microscopy (TEM): 'encapsulation method'

Liposomal dispersions were fixed with Karnovski's solution overnight, washed with cacodylate solution buffer and then fixed with osmium tetroxide in sodium cacodylate buffer (1:1) for 1 h. Following post fixation, the samples were dehydrated in 30%, 50%, 70%, 80%, 95% and 100% acetone solutions and embedded in epon-araldite resin.
Ultra-thin sections of liposomal dispersions were obtained with a LKB NOVA ultramicrotome using a diamond knife and stained with an alcoholic solution of uranyl acetate, followed by a solution of concentrated bismuth subnitrate. These sections were examined under a JEOL 1010 electron microscope and photographed.

I.2.9.5. Encapsulation efficacy (EE%)

Free artemisinin was removed by means of dialysis. Liposomal formulation was transferred in a dialysis bag. This dialysis bag was stirred in 800 mL of aqueous medium (used for rehydrating the lipid film) at room temperature for 2 hours. The aqueous medium was refreshed once. The content of the liposomes with the cleaned surface were quantified by HPLC/DAD/ESI MS analysis using artemisinin, rutin triidrate and curcumin as external standards for artemisinin, flavonoid and curcumin respectively.
The artemisinin encapsulation yield is expressed as the so-called entrapment efficiency. The EE is defined as the percentual amount of artemisinin entrapped in the vesicles in relation to the total amount of artemisinin present during the vesicle formation and entrapment procedure.
EE(%) = {(amount of artemisinin entrapped in the vesicles)/(total amount of artemisinin used)}×100.

I.2.10. *In vivo* experiment: pharmacokinetic study

I.2.10.1. Mice

Male CD1 mice (25-30 g) were used for the study of pharamacokinetic profile.
The animal were placed in the experimental room 4 days before the test for acclimatization. The animals were fed a standard laboratory diet and tap water *ad libitum* and kept at 23±1°C with a 12-h light/dark cycle, light at 7 AM. All experiments were carried

out in accordance with the European Communities Council Directive of 24 November 1986 (86/609/EEC) for experimental animal care. All efforts were made to minimize the number of animals used and their suffering.

I.2.10.2. Pharmacokinetic study

Sixty mice were randomly separated into three groups. One group of mice received artemisinin dissolved in DMSO 10% v/v at the dosage of 10 mg/kg i.p. and the other two groups were given artemisinin-loaded conventional and PEGylated liposomes dissolved in NaCl 0.9% v/v at the same dosage of artemisinin. From jugular vein, blood samples were collected into heparinized tubes (to prevent blood coagulation) at 0, 10, 30 min, 1, 2, 3, 4, 6 and 24 hours after i.p. injection. Blood samples were centrifuged at 2000 rpm for 20 min at 17°C to separate plasma from other blood elements. The obtained plasma was stored at -20°C prior to analysis.

I.2.10.3. Calibration curves

The calibration curve was determined by constant volume of blank plasma with increasing concentration of artemisinin (0-100 µM, final concentration of artemisinin) dissolved in methanol 0.3% v/v. My dilution scheme was:

solution	µM	dilution
a	100	-
b	50	solution **a**/2
c	10	solution **b**/5
d	6	solution **a**/1.67
e	5	solution **c**/2
f	2	solution **c**/5
g	1	solution **f**/2
h	0.5	solution **g**/2
i	0.2	solution **g**/5
l	0.1	solution **i**/2
m	0.05	solution **l**/2
n	0	only plasma

I.2.10.4. Sample pre-treatment

Because of the complex nature of plasma, a pre-treatment procedure is often needed to remove protein and potential interferences prior to HPLC/MS/MS analysis. Protein precipitation is commonly used for fast sample clean-up and disrupting protein–drug binding. Each sample, including each point of the calibration curve, were diluted 7 times with acetonitrile in order to precipitate plasma proteins. Each sample was vortexed for 15 seconds and centrifuged at 10000 rpm for 2.5 minutes. 200 µL of each sample were transferred in 96-well format plates, which resulted in shorter sample preparation time.

I.2.10.5. Analytical HPLC/MS/MS characterization

An Applied Biosystems-Sciex (Toronto, Canada) API 4000 bench-top Triple-Quad Mass Spectrometer equipped with the TurboIonSpray source was used. The TurboIonSpray source operated under positive ion mode at a voltage of 5000V and with a “turbo” gas flow of 10 L/min of air heated at 150°C. Collision activated dissociation (CAD) MS/MS was performed through the LINAC Q2 collision cell, operating with 10mT or pressure of nitrogen as collision gas.

Declustering Potential (DP), Collision Exit Potential (CXP) and Collision Energy (CE) were automatically optimized for Artemisinine by the "Quantitation Optimization" option. The resulting DP was +30 Volts. Optimal CE and CXP were found at 15 V and 12 V respectively. MS and MS/MS spectra were collected in continuous flowmode by connecting the Infusion pump directly to the TurboIonSpray source. The quantitation experiments were undertaken by using a Series 1100 Agilent Technologies (Waldbronn, Germany) CapPump coupled to an Agilent Micro ALS autosampler, both being fully controlled from the API 4000 data system. Liquid chromatography was performed using an Agilent Zorbax Eclipse XDB-C18 3.5µm, 3 × 150 mm HPLC column (Waldbronn, Germany). Column flow was 0.4 mL/min using an aqueous solution of 85% Acetonitrile containing 0.1% formic acid. The eluent from the column was directed to the TurboIonSpray probe without split ratio. The data were processed using the Analyst 1.4.1 proprietary software. The molecular ion (283 m/Z) was selected in the first quadrupole and two fragments 151 m/Z (MRM 1 as quantifier transition) and 209 m/Z (MRM 2 as qualifier transition) were monitored in the third quadrupole.

	m/Z
MRM 1	283→151
MRM 2	283→209

I.2.10.6. Data analysis

Analysis of artemisinin concentrations in plasma was performed with a computerised program (Syphar, version 4.0; SIMED) using a two-compartment model on the basis of the extended least squares regression method with the Powell minimisation algorithm, and elimination from the central compartment. The AUC was determined by trapezoidal rule and was extrapolated to 24 h. AUC values were determined for the period 0–24 h. C_{max} was the observed peak value. The elimination half-life ($t_{\beta 1/2}$) was determined as 0.693/β (where β is the elimination rate constant, obtained by the equation $dC/dt = -\beta C$, where C is the concentration and t is time); CL was calculated by dividing the dose by the AUC_{0-24h} (Gibaldi M, 1982).

I.2.10.7. Statistics

Statistical analysis was carried out using GraphPad Version 4. PK parameters were analysed with the two-way analysis of variance (ANOVA) test and Duncan's post-hoc test. Data are reported as mean±S.D. unless otherwise stated. A P-value <0.05 was considered significant.

I.2.11. *In vivo* experiment: antiplasmodian activity

I.2.11.1. Mice

Female BALB/c mice (20-25 g) were used for the study of antimalarian activity.
The animals were fed a standard laboratory diet and tap water *ad libitum* and kept at 22±1°C with a 12 h light/dark cycle, and 60% humidity regulated environment. All experiments were carried out in accordance with the European Communities Council Directive of 24 November 1986 (86/609/EEC) for experimental animal care. All efforts were made to minimize the number of animals used and their suffering.

I.2.11.2. Inoculation of parasites

A cryopreserved isolate of the virulent rodent malaria parasite strain *Plasmodium berghei* (NK 65), originally from the Istituto Superiore di Sanità (Rome, Italy) is a specific mouse malaria and does not infect man. Immediately after thawing, the isolate was injected i.p. in a mouse that later served as a donor. Then, parasite strain was maintained by weekly serial passage of blood from donor mouse to other mice. The parasitaemia was checked daily. A thin smear of peripheral blood from the tail vein was taken, Giemsa stained and observed under an immersion optical microscope (David AF, 2004). When the count of the infected red blood cells is 20-30%, blood was taken from venous ocular sinus and was diluted with isotonic saline solution. Each mouse was inoculated i.p. with 200 µL *inoculum*, which is constituted by $1x10^7$ infected erythrocytes.

I.2.11.3. In vivo antiplasmodial activity

Antiplasmodial activity was evaluated using the 4-day suppressive test described by Peters and coworkers (Peters W, 1975; David AF, 2004; Fidock DA, 2004) employing *P. berghei* NK 65.
Each Balb/c mouse was inoculated i.p. with 200 µL of *inoculum*, which is constituted by $1x10^7$ infected erythrocytes. Mice were divided in 4 groups, each group is constituted by 2 animals:

- negative control, mice were injected i.p. with 200 µL of bidistilled water
- positive control, mice were injected i.p. with artesunate 50 mg/kg
- conventional liposomes, mice were injected with artemisinin delivered at 10 mg/kg.

Artesunate and the formulation were injected daily for one week, starting 24 hors after infection of mice with *inoculum* ($1x10^7$ red blood cells/mL infected with *P. berghei*).
The parasitaemia was checked 3, 5 and 7 days after infection. A thin smear of peripheral blood from the tail vein was taken, coloured with Giemsa 10% and observed at the immersion optical microscope 100x. The level of parasitaemia was determined counting the number of infected red blood cells. The reduction of parasitaemia was calculated by the following formula

$$100\ (A–B/A)$$

where A is the percentage of parasitaemia in the negative control group and B is the percentage of parasitaemia in the tested groups (Tona L, 1998).
During the whole experiment, the survival of the animals was assessed.

I.3. Results and discussion

I.3.1. Content of artemisinin and flavonoids at various developmental stages of the plant

Artemisinin and bioactive flavonoids were identified from aerial parts (inflorescences and leaves) of *Artemisia annua* plants and were quantified by HPLC/DAD/ESI MS analyses during different developmental stages: pre-flowering, full bloom and post-flowering.
Artemisinin (*qinghaosu*), an endoperoxide sesquiterpene lactone, is considered the most important secondary metabolite and bioactive constituent (Klaiman DC, 1985; van Agtmael MA, 1999; Heppner DG, 1998). Its relativel low yields can vary considerably, depending on the plant material, growing conditions and seasonal and geographic variations: in the plant it is generally present in the shoots and seeds (Abdin MZ, 2003) with highest levels in field grown leaves and flowers (0.01-1.4% dry weight; van Agtmael MA, 1999) where artemisinin is sequestered in glandular trichomes (Duke MV, 1994).
Although its total synthesis has been achieved (the total organic synthesis gives low yields and is uneconomical due to its complex structure), its extraction from the plant still

represents the only reliable resource (Klaiman DC, 1985; De Vries PJ, 1996; Van Geldre E, 1997) even if the required annual targets of 20-22 t/yr of artemisinin are not being achieved (RBM, 2005; WHO, 2005). At present, commercial artemisinin is mainly extracted from selected heedings (artemisinin high yelds, up to 2%), but they are still affected by pedoclimatic variations.
Artemisinin concentration vary with genotype (Charles DJ, 1990; Jain DC, 1996), plant tissue and time of harvesting (Laughlin JC, 1993, 1995; Morales M, 1993; Ferreira JFS, 1996), and is influenced by soil and climatological conditions (Van Geldre E, 1997; Vaz APA, 2006).
In view of the scarcity of artemisinin and of its actual high demand in the world, it is important, therefore, to establish the conditions that favour the increase of these metabolites together with the content of artemisinin at various stages of the vegetative life of the plant.
Artemisinin determination in Italian ecotypes of *A. annua* would provide information about its utilization for commercial production of this compound.
Previous studies have pointed out that other secondary metabolites of plants, such as the polymethoxyflavonoids casticin and artemetin present in the phytocomplex can enhance the bioavailability or the activity of artemisinin against *P. falciparum* (Elford BC, 1987). In particular, casticin was found to be active in inhibiting some cytophysiological activities of the parasite (Yang SL, 1995).

I.3.1.1. Analytical HPLC/DAD/ESI MS characterization

In the chromatogram at 280 nm of the *n*-hexan extract of *Artemisia annua* L., four flavonoids were detected, namely eupatin, an unseparable mixture of chrysoplenetin and casticin, and artemetin, previously isolated and identified in the aerial parts of a selected breeding of *Artemisia annua* L. (Bilia AR, 2002).

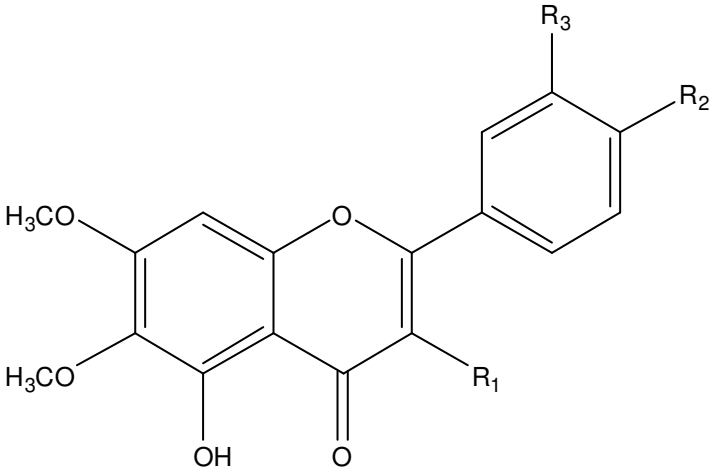

flavonoid	**R_1**	**R_2**	**R_3**
eupatin	-OH	$-OCH_3$	-OH
casticin	$-OCH_3$	$-OCH_3$	-OH
chrysoplenetin	$-OCH_3$	-OH	$-OCH_3$
artemetin	$-OCH_3$	$-OCH_3$	$-OCH_3$

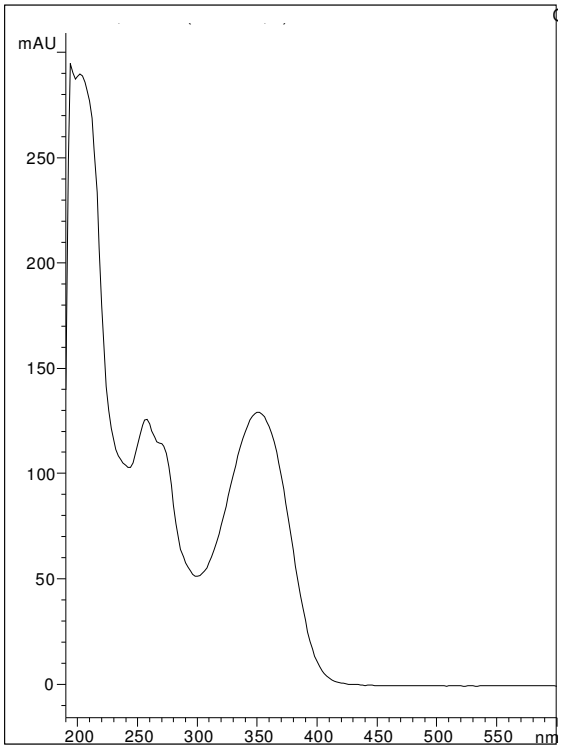

Identification of flavonoids was carried out by HPLC/DAD and HPLC/ESI MS analysis, UV-Vis and mass spectra of the peaks with those of authentic standards when possible, or isolated compounds and, and/or by comparison and combination of their retention times, or characterised extracts as well as based on literature data. The UV spectrum of polymethoxylated flavonoids is rapresented in figure **2**. Polymethoxylated flavonoid were quantified at 280 nm using rutin trihydrate reference standard as external standard.

flavonoid		**m/Z**
eupatin	$[M+H]^+$	361
casticin	$[M+H]^+$	375
chrysoplenetin	$[M+H]^+$	375
artemetin	$[M+H]^+$	389

Fig 2. UV spectrum of flavonoids.

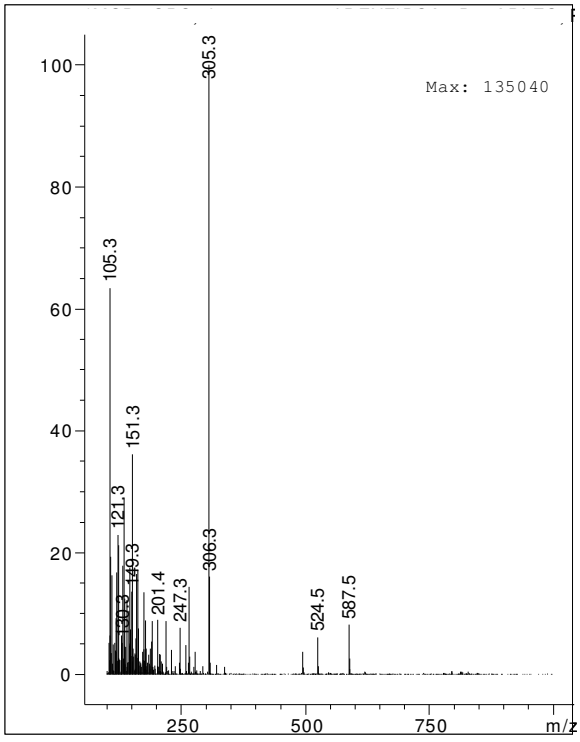

Identification of artemisinin was carried out by HPLC/ESI MS analysis and mass spectra of the peaks with that of authentic standard. Artemisinin reference standard was also used for the calibration of artemisinin. Mass spectrum (fig **3**) were optimized in scan modality, positive polarity and fragmentor of 120 V.

		m/Z
artemisinin	$[M+Na]^+$	305

Fig 3. Mass spectrum of artemisinin.

I.3.1.2. Content of polymethoxylated flavonoids

All the constituents were found in both leaves and inflorescences at all the developmental stages. Nevertheless, their distribution pattern vary with both plant component and developmental stage. Among flavonoids, the highest yields were obtained for an

inseparable mixture of the two isomers casticin/chrysoplenetin followed by artemetin and eupatin.
Eupatin (fig **4**) was found in very low concentrations in all plant parts and during all the developmental stages. In leaves, eupatin level increased from 0.035 mg 100 g^{-1} dried herbal drug (DHD) at pre-flowering to 0.69 mg 100 g^{-1} DHD at post-flowering. The highest contents were measured in full bloom and post-flowering inflorescences (1.08 and 1.11 mg 100 g^{-1} DHD, respectively).

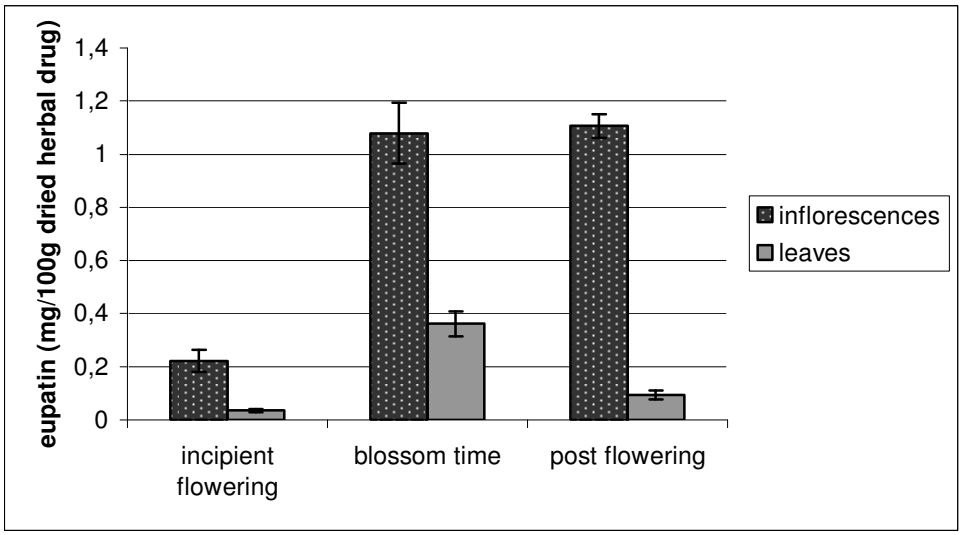

Fig 4. Eupatin contents in the different developmental stages of *A. annua*.

Casticin and chrysoplenetin (fig **5**) reached similar highest contents during full bloom in both inflorescences and leaves (39.2 and 36.2 mg 100 g^{-1} DHD, respectively). Significantly lower levels were measured during pre- and post-flowering in both plant organs.

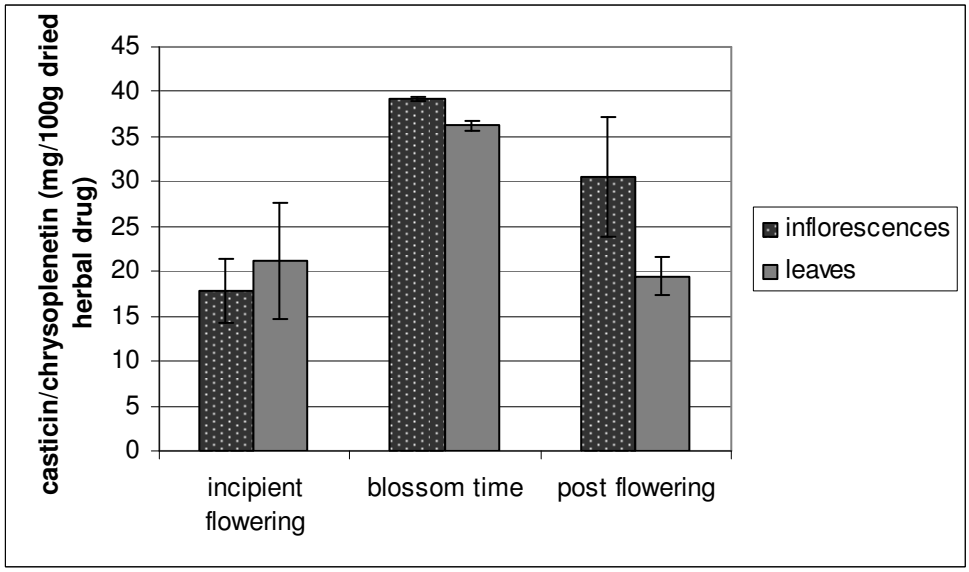

Fig 5. Casticin/Chrisoplenetin contents in the different developmental stages of *A. annua*.

The fourth flavonoid, artemetin (fig **6**), had a different distribution pattern. The highest concentration was again found at blossom time and it was higher in leaves (14.2 mg 100 g^{-1} DHD) than in the inflorescences (11.1 mg 100 g^{-1} DHD). The latter content was not statistically different to those observed in the inflorescences during pre- and post-flowering. On the contrary, during these stages, artemetin concentrations in the leaves significantly decreased compared to the level recorded at full bloom.

The total levels of flavonoids were thus higher at full bloom with similar values in both plant organs (about 50 mg 100 g^{-1} DHD).

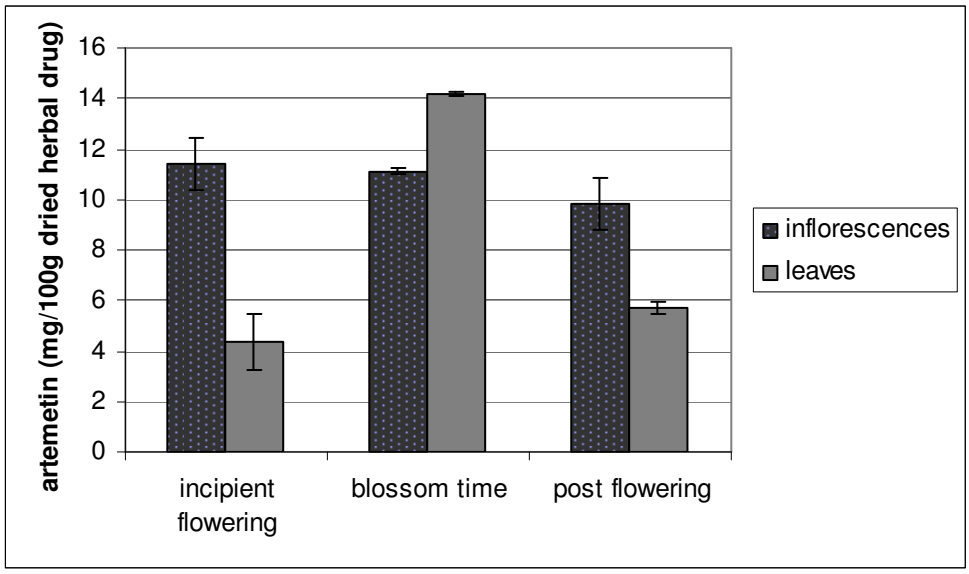

Fig 6. Artemetin contents in the different developmental stages of *A. annua*.

I.3.1.3. Content of artemisinin

Concerning the distribution pattern of artemisinin (fig **7**), the highest levels were reached in both leaves and inflorescences at full bloom (54.1 and 44.0 mg 100 g^{-1} DHD, respectively) with the former value significantly higher than the latter. In pre- and post-flowering, artemisinin levels reached lower concentration in analyzed plant organs. Significant differences were observed during pre-flowering with the highest level (25.2 mg 100 g^{-1} DHD) in the inflorescences, almost two times more than the value obtained in the leaves. At post-flowering these plant organs contained only one-tenth of the content recorded during blossom time. No significant differences were observed in the leaves at pre- and post-flowering.

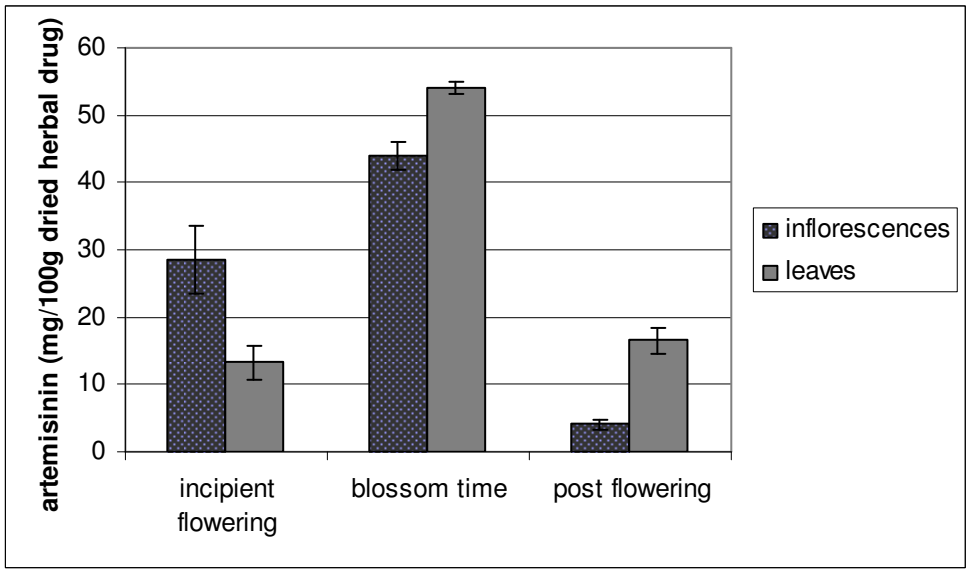

Fig 7. Artemisinin contents in the different developmental stages of *A. annua*.

It is interesting to observe that both total flavonoids (eupatin, casticin, chrysoplenetin and eupatin) and artemisinin showed higher values in aerial parts at full bloom (fig **8**), when the

total amount of the polyphenols was about twice the values observed during incipient and post-flowering stages. On the other hand, artemisinin content was only 40 and 20% at pre- and post-flowering, respectively, in comparison with the values measured at blooming.

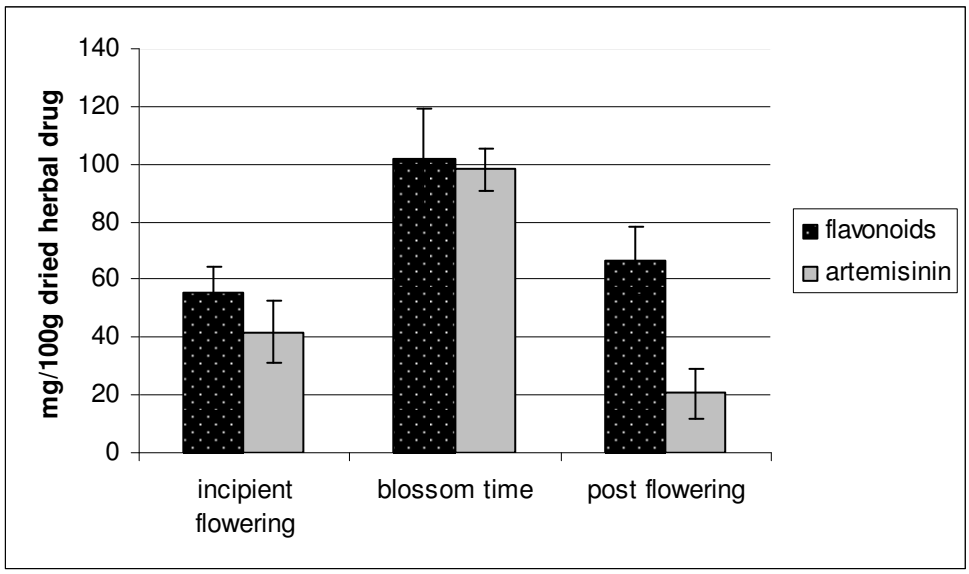

Fig 8. Content of total flavonoids and artemisinin during the investigated developmental stages of *A. annua*.

Several reports have shown that artemisinin concentration changes, not only during the vegetative growth, but it varies considerably also in the different plant components between strain origin (Laughlin JC, 2002). Furthermore, reports differ regarding the stage at which the highest content of artemisinin occurs during plant development: just before flowering (Acton N, 1985; ElSohly HN, 1990; Liersh R, 1986; Woerdenbag HJ, 1991; 1993), or at the point of full blooming (Ferreira JFS, 1995; Morales M, 1993; Pras N, 1991; Singh A, 1988). Since these differences may be attributable to climatic conditions, ecotype, cultural practices or a combination of these factors, it is worthwhile to determine experimentally the time of peak artemisinin concentration for any area of production and for any ecotype rather than to rely only on published data. We demonstrated that the tested ecotype, yielded the maximum artemisinin content at full bloom in both leaves and inflorescences where, as proposed for other glanded biotypes (Duke MV, 1994; Ferreira JFS, 1995), this sesquiterpenoid compound accumulates almost exclusively in the subcuticular space of capitate glandular trichomes that are abundantly present on the surfaces of leaves and flower organs of these plants (Rotondi, personal communication). At this stage of development, the artemisinin concentration varied from 0.04 to 0.05% of plant dried weight, in the range of the relatively low average of artemisinin concentration in plants of European origin (0.03-0.22; Charles DJ, 1991; Trigg PI, 1990).
Besides, in the fully bloomed plants flavonoids also accumulate more in both plant organs (0.05% dried weight), with foliage and inflorescences yielding about equal amounts. To our knowledge these are is the first results on flavonoid content in *A. annua* L., regarding plant phenological stages and, therefore for obtaining the highest yields of both artemisinin and polyphenol compounds.

I.3.2. Formulations of artemisinin

I.3.2.1. Conventional liposomes

In all the experiments reported, mixtures of soy phosphatidylcholines (P90G) were used as the main vesicle forming amphiphile. The phosphatidylcholines are amphiphiles, all of which have the same zwitterionic head group (phosphocholine) linked to glycerol through the oxygen atom at *sn*-3 of glycerol. Each of the two hydroxyl groups at *sn*-1 and *sn*-2 is esterified with a fatty acid with the following percentage composition:

fatty acid	**%**
linoleic acid	66.5
palmitic acid	12.9
oleic acid	10.5
linolenic acid	5.7
stearic acid	4.4

P90G was used in combination with cholesterol, which alters the organization and mechanical properties of the lipid bilayers (McMullen TPW, 1995).
In the table all the constituents of the bilayer of conventional liposomes were indicated with their molar ratio:

molecule	**MW**	**molar ratio**	**mg/mL**
P90G	760	5	33
cholesterol	386.66	0.6	2
artemisinin	282	2	5

It is well-known that dry lipid films form spontaneously large multilamellar vesicles upon addition of an aqueous phase. This is, however, erroneous. When dry lipid films are hydratated the lamellae swell and grow into thin lipid tubules. Additional energy has to be dissipated into the system in order to produce smaller and less lamellar liposomes (Lasch J, 2003). Liposomes were homogenized by high pressure emulsificator in order to make their sizes smaller and size distribution narrower. In addition, homogenization is useful in order to improve liposomal physical stability in terms of sedimentation or floating. Even if the vesicles are stearically stabilized, smaller size (70-200 nm) and good size homogeneity is of advantage for prolonged circulation (Liu D, 1992). So, different pressure for changeable time were applied to liposomal empty samples in order to find the best balance between size and polidispersity index. Results derived from DLS analysis:

pressure (kPa)	**time (s)**	**mean diameter (nm)**	**PDI**
50 000	60	103.57	0.619
75 000	20	127.48	0.921
75 000	60	124.14	0.530
75 000	100	165.58	0.821
100 000	20	90.56	0.637
100 000	60	128.30	0.456
100 000	100	117.29	0.508
125 000	20	119.02	0.008
125 000	60	190.01	0.620
125 000	100	65.58	0.911
150 000	60	112.64	0.213

The best results is obtained applying to the sample the pressure of 150 000 kPa for 60 seconds. So, artemisinin-loaded liposomes were emulsified following these optimized parameters. Results derived from DLS:

aqueous medium	artemisinin (mg/ml)	Mean diameter (nm)	PDI	Zeta potential (mV)
bidistilled water	–	183.0±39.60	0.27±0.05	–17.5±1.20
bidistilled water	5	180.1±1.74	0.31±0.06	–32.3±0.78
NaCl 0.9%	5	136.2±42.27	0.54±0.07	–17.7±1.74

The sample rehydrated with physiological solution (NaCl 0.9% v/v) was polydispersed (PDI>0.4), but analyses were always repeatable.
Different cholesterol/P90G ratio were tried in order to improve the encapsulation efficacy (EE%) of our formulations. As we expected, all the obtained EE, summarized in the following table, are low; this is attribuible to the hydrophobicity of the drug that the formulations delivered. Results derived from HPLC/DAD/ESI MS analysis:

chol/P90G	EE (%)
0.20	8.98
0.33	2.93
0.47	6.91
0.60	12.54
0.73	13.38
0.87	13.82
1.00	10.02

When the ratio cholesterol/P90G is 0.20, the vesicles appeared sphere-shaped at the electron microscopy. When the ratio was increased, the encapsulation efficacy is better, but, this higher amount of cholesterol can be related with unusual tridimensional structure (detailed explanation will follow below, in the section related to transmission electron microscopy).

I.3.2.2. Liposomes with superficial charge

Negatively and positively charged vesicles were prepared by using either dicetylphosphate (dihexadecylphosphate, DP, 4.84 mg/ml final concentration) or stearylamine (SA, 2.38 mg/ml final concentration), respectively, as a charge inducer. P90G was used in combination with dicetylphosphate or stearylamine, with the aim of preventing vesicle fusion (Sada E, 1988).
In the table all the constituents of the bilayer of liposomes were indicated with their molar ratio:

molecule	MW	molar ratio	mg/mL
P90G	760	5	33
cholesterol	386.66	0.6	2
SA	269.51	1	2.38
DP	546.85	1	4.84
artemisinin	282	2	5

Results derived from DLS analysis:

artemisinin (mg/ml)	P90G (mg/ml)	Chol. (mg/ml)	SA (mg/ml)	DP (mg/ml)	Mean diameter (nm)	PDI	Zeta potential (mV)
–	33	2	–	–	183.0±39.6	0.27±0.05	–17.5±1.2
5	33	2	–	–	180.1±1.74	0.31±0.06	–32.3±0.78
5	33	2	2.38	–	191.8±37.5	0.42±0.03	–61.8±4.2
5	33	2	–	4.84	135.6±28.1	0.45±0.04	–46.4±1.7

These samples were polydispersed (PDI>0.4), but analyses were always repeatable. Moreover, the mean size of positively charged liposomes was large if compared with those containing dicetylphosphate; this is due to the presence in the bilayer, of the highly hydrophilic amphiphile stearylamine that increase the vesicle surface energy which causes vesicle enlargement (Fang JY, 2001).
Results derived from HPLC/DAD/ESI MS analysis:

SA	DP	EE (%)
+	–	14.56±1.57
–	+	23.14±0.51

As shown in the table, the formulations presented a high encapsulation efficiency (EE%). It is interesting to note that SA liposomes showed an encapsulation efficiency that was lower than that of the DP vesicles. This could be due to the higher energy required for artemisinin-incorporating vesicle formation when SA was present in the lipid phase. In fact, in the preparation of SA-containing liposomes, emulsification was less efficient in comparison with the preparation of negatively charged.

I.3.2.3. Trasmission Electron Microscopy

The homogeneity and morphology of liposomes can also be visualized by electron microscopy (Meyer HV, 1998; 1999; 2000; 2001; Ulrich AS, 1999). The spheroidal shape of lipid vesicles with their bimolecular arrangement of the amphiphiles is known since the pioneering work of Bangham *et al.* (Bangham AD, 1964; 1965), who originally called these aggregates *spherulites* (Bangham AD, 1964). These aggregates are also called phospholipids vesicles (Papahadjopoulos D, 1974) which has been simplified in the past to lipid vesicles (Szoka F Jr, 1980), artificial vesicles (Ingolia TD, 1978) or just vesicles (Fendler JH, 1982; Rosoff M, 1996). Vesicles is used as a general term and includes all types (often spherical) of single or multicompartment closed bilayer structures, regardless of their chemical composition (Fendler JH, 1982; Fuhrhop JH, 1984).
Two different techniques were used in order to visualize vesicles: the 'negative contrast' and the 'encapsulation method'. The first is very quick and easy to perform, while the second one, typically used for observing skin samples, needs many days to prepare the slice of the sample.

I.3.2.3.a. Trasmission Electron Microscopy: "negative contrast"

The samples were diluted 10 times in order to photograph isolated vesicles and to measure their sizes. There is a perfect correlation between the dimension measured by Dynamic Light Scattering DLS (around 200 nm) and those visualized at the electron microscopy. Dimensions measured by DLS, data were presented as a mean of particle sizes, assuming that observed structure were sphere-shaped. Electron microscopy can confirm this.

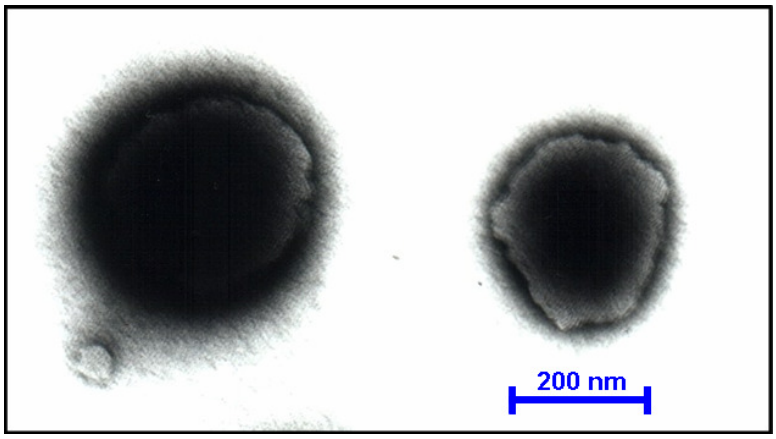

Fig 9. LUV: large unilamellar vesicles.
Mean diameter 100-500 nm.

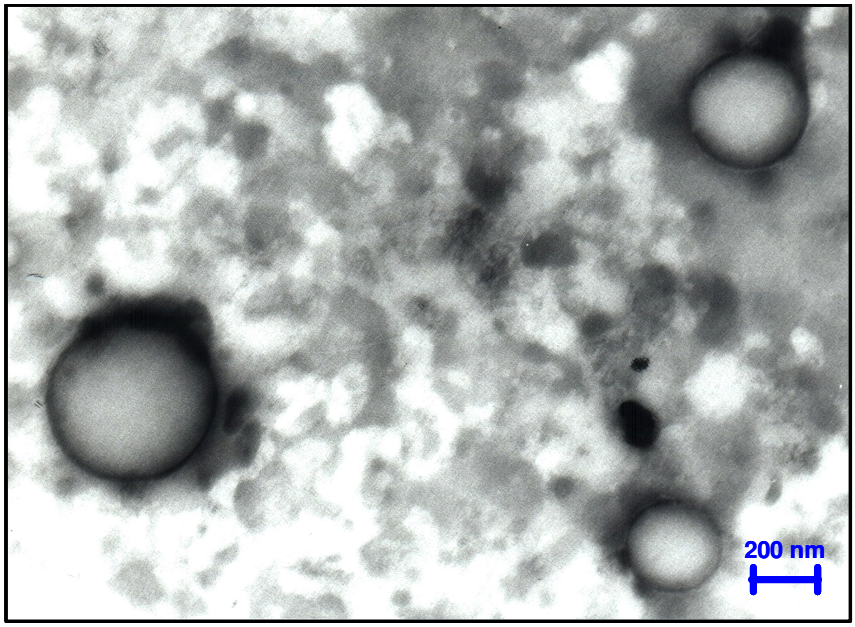

Fig 10. LUV: large unilamellar vesicles.
Mean diameter 100-500 nm.

I.3.2.3.b. Trasmission Electron Microscopy: "encapsulation method"

Ultra-thin sections of liposomal dispersions were obtained with a ultramicrotome, examined under electron microscope and photographed. The slice of liposomal dispersion can show the lamellarity together with the dimensional analysis. Obviously, multilamellar (10 bilayers) and oligolamellar (2-5 bilayers) vesicles were bigger than UVs and sometimes they appeared coalesced. In order to overcome this problem of potential fusion of the vesicles, liposomes with superficial charge were prepared.

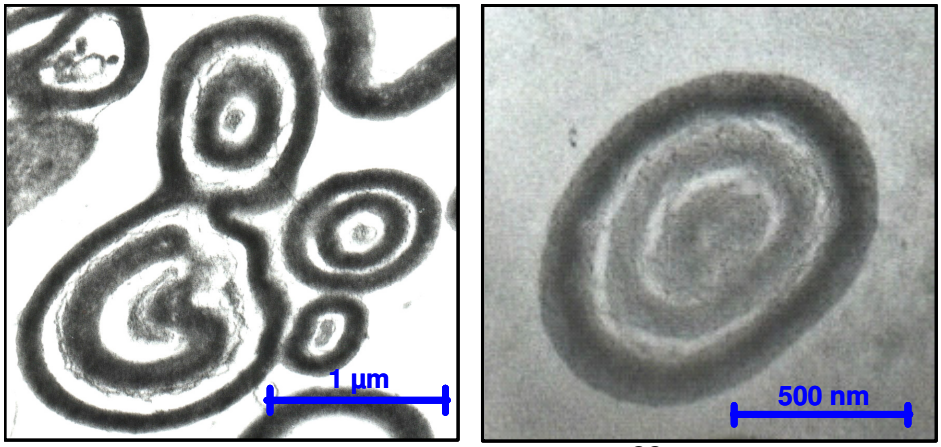

Fig 11. OLV: oligolamellar vesicles.
Mean diameter 0.1-10 µm, typically 1 µm.

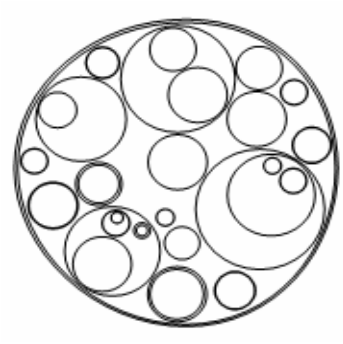

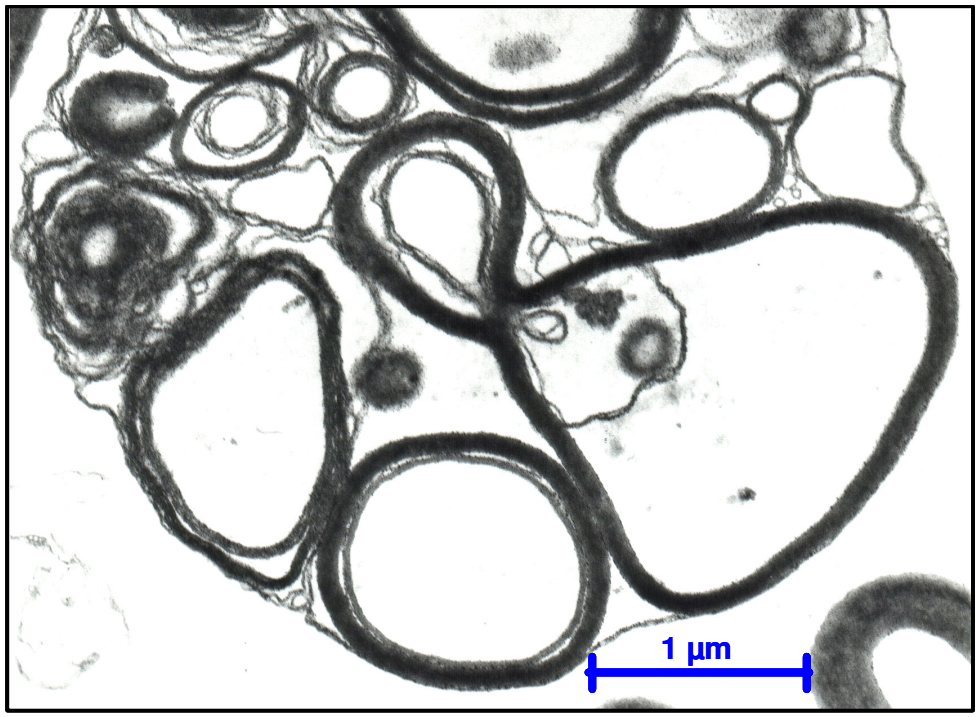

Fig 12. MVV: multivesicular vesicles. Schematic representation and real electron micrograph.

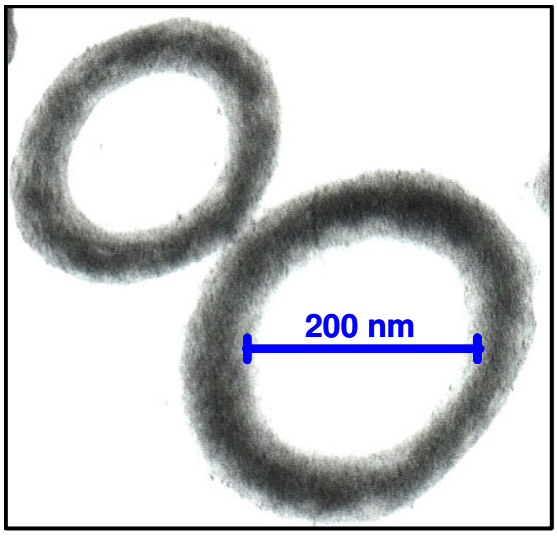

Fig 13. LUV: large unilamellar vesicles. Mean diameter 100-500 nm.

Physical instabilities of lipid vesicle systems involve vesicle aggregation and fusion (possibly leading to vesicle precipitation and formation of flat bilayers) (Crommelin DJA, 1994; Leung D, 1996). Lipid vesicles are generally not a thermodynamically stable state of amphiphiles and do not form 'spontaneously' (without input of external energy); they are only kinetically stable, kinetically trapped systems (Laughlin RG, 1997; Lasic DD, 1990; 1999; Horbaschek K, 2000; Luisi PL, 2001).
The mean size, the lamellarity and the physical stability of the vesicles not only depend on the chemical structure of the amphiphiles used, but also on the method of vesicle preparation. It must be generally noted that any hydrophobic drug is likely to affect the phase diagram of its liposomal carrier, hence great care has to be taken to characterize the corresponding behaviour of the loaded system (Peleg-Shulman T, 2001; Fatouros DG, 2001; Stoye I, 1998; Fahr A, 2001; Ardhammar M, 1999). Summarizing the type of lipid used, the preparation method and the molecule loaded influenced the shape of the system. But there is something else. In addition, unexpected structures, different from vesicles, were appeared at the transmission electron microscopy, if the cholesterol is added to the P90G with a ratio of about 0.60 (fig **14**).

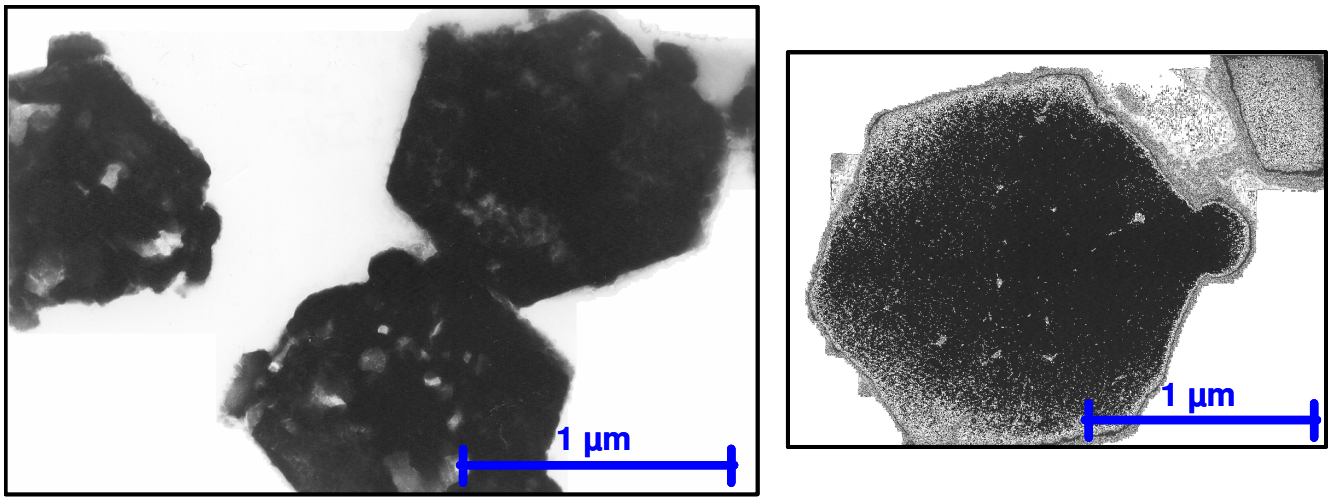

Fig 14. Tridimensional unexpected structures obtained if the chol/P90G ratio is 0.6.

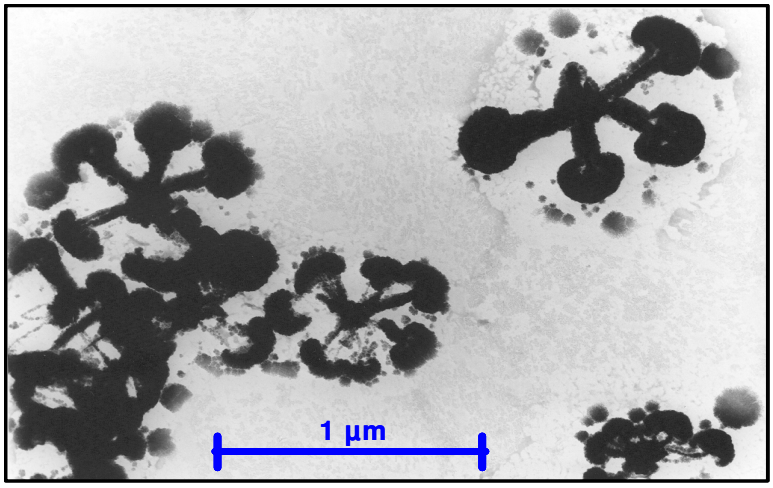

Fig 15. Skeleton of the previous hexagonal structure.

It can be related to the fact that also the amount of cholesterol affects the morphology of the tridimensional aggregates. An explanation may be derived from literature.

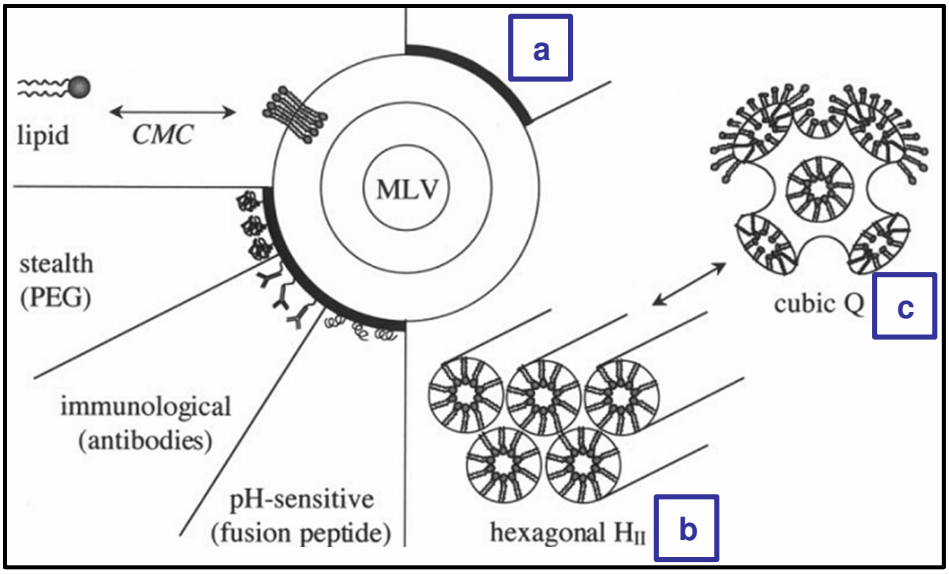

Fig 16. Overview of lipid phase transitions and polymorphism.

Lipid polymorphism is described as an essential aspect to consider in the rational design of liposomes for drug delivery, and has been well reviewed (Gerasimov OV, 1999; Maurer N, 1999; Hafez IM, 2001). Concerning the lamellar phase, the most common is that assumed by the vesicles (fig **16a**), but other morphologies, such as the inverted hexagonal phase H_{II} or various cubic phases *Q* can be observed, as summarized in figure **16** (Ulrich AS, 2002). The hexagonal phase (fig **16b**) consists of an array of cylindrical rods, wherein the lipids are oriented with their headgroups towards the aqueous core. Cubic phases (fig **16c**) are made up of bicontinuous surfaces, such that every point of the internal surface of this macroscopic assembly has access to the external aqueous space via aqueous channels, and any lipid molecule may exchange places with another in the same monolayer simply by diffusion (Shah JC, 2001).
Surprising also in the case of samples obtained using mixtures of cholesterol/P90G it is possible to observe such aggregates. Thus, if the cholesterol is added to the P90G with a ratio of about 0.60, vesicles were present as aggregates related to inverted hexagonal phase as reported in figure **14**.
These unusual structures are now under further physical-chemical investigations in order to clarify their formation and stability.

I.3.2.4. PEGylated liposomes

When liposomes were proposed as vehicles for drug delivery, their major disadvantage was discover: typical liposome composition rapidly exited the bloodstream and accumulated in the Kupffer cells in the liver, as well as in spleen macrophages (Senior JH, 1987). An excess of empty liposomes were administered in order to overcome this problem (Patel KR, 1983). However, blocking RES is not the most appropriate approach for human therapy. The real breakthrough was achieved with the discovery of polymer-modified long-circulating liposomes (Lasic DD, 1995). Coating uncharged colloidal particles with non-ionic hydrophilic polymers, such as PEG, renders them stable against non specific interactions and self-aggregation, because the hydration repulsion and the steric barrier prevent close approach (Ulrich AS, 2002; Allen C, 2002). Explanation of the phenomenon of PEGylated liposomes involve the formation of a 'conformational cloud' by flexible liposomes-grafted polymers over the liposomal surface (Torchilin VP, 1994) and the decreased rate of plasma protein adsorption on the hydrophilic surface of PEGylated liposomes (Lasic DD, 1991). The incorporation of PEG into so-called 'stealth' liposomes establishes a steric barrier that delays their recognition by the mononuclear phagocyte system. As consequence, circulation times of conventional liposomes (typically several minutes) have been increased this way up to many hours (Ulrich AS, 2002).
In the table all the constituents of the bilayer of PEGylated liposomes were indicated with their molar ratio:

molecule	MW	molar ratio	mg/mL
P90G	760	5	33
cholesterol	386.66	0.6	2
18:0/18:0 PEG 2000	2805.497	0.25	6.2
artemisinin	282	2	5

Results derived from DLS analysis:

NaCl 0.9%	artemisinin (mg/ml)	P90G (mg/ml)	Chol. (mg/ml)	18:0/18:0 PEG 2000 (mg/ml)	Mean diameter (nm)	PDI	Zeta potential (mV)
+	–	33	2	–	136.2±42.27	0.22±0.07	–17.7±1.74

+	5	33	2	6.2	132.6±8.78	0.39±0.01	−17.5±1.85

The mean size of PEGylated liposomes was similar to conventional liposomes but the polidyspersity index was higher, because of the presence of PEG in the bilayers.

I.3.3. *In vivo* experiment: pharmacokinetic study

I.3.3.1. Calibration curves

The calibration curve (R^2=0.999) was determined by constant volume of blank plasma with increasing concentration of artemisinin (0-100 µM, final concentration of artemisinin) dissolved in methanol 0.3% v/v.

theoretical µM	real µM	accuracy
50	42.4	84.9
10	9.89	98.9
6	6.05	101.0
5	5.17	103.0
2	1.96	97.9
1	0.984	98.4
0.5	0.476	95.1
0.2	0.205	103.0
0.1	0.086	86.0
0.05	0.0452	90.3

I.3.3.2. Pharmacokinetic study

There are no clues in literature about the parenteral dosages of artemisinin and only a study on β-artemether-loaded liposomes is reported (Chimanuka B, 2002). This study showed the successful treatment of *Plasmodium berghei* infected mice at the dosage of β-artemether of 4.8 mg/kg (Chimanuka B, 2002). In our preliminary studies a dosage of artemisinin of 10 mg/kg was tested to evaluate the pharmacokinetic performance of liposomes versus artemisinin solubilized in DMSO 10% v/v.
In order to select the best way of parenteral administration, the properties of the carrier were considered. Regardless of the circulation time of an intravenously injected liposomal dose, however, the majority will eventually be taken up by the mononuclear phagocyte system (Ulrich AS, 2002). Subcutaneous injection has been the route of administration most extensively investigated for targeting to the lymphatic system (Oussoren C, 1998). When intramuscular injected, liposomes with the particle size above 100 nm remain at the injection site and act as sustained drug release system for manteining prolonged drug concentration in the blood compartment (Storm G, 2000). Intraperitoneally administration of liposomal drugs has been shown to reduce systemic toxicity (Alberts DS, 1996) and prolong the blood circulation of liposomes caused by slow absorption of the liposomes from the abdominal cavity (Sadzuka Y, 1997). The AUC of spleen and liver were lower after i.p. injection than after i.v. injection (Lin YY, 2009). I.p. administration was selected as the most suitable for our needs.

Both artemisinin-loaded conventional and PEGylated liposomes increased the pharmacokinetic parameters of artemisinin such as C_{max}, $AUC_{0\text{-}24h}$ and $t_{1/2\beta}$. In addition, delivered artemisinin reduced CL compared to free artemisinin (control) as described in the following table and in fugures **17** and **18**.

	artemisinin	conventional liposomes	PEGylated liposomes
C_{max} (µM±SD)	0.25±0.08	1.11±56.00	1.04±0.01
AUC $_{0\text{-}24h}$ (µM/h)	0.132	0.836	0.899
$t_{1/2\beta}$ (h)	0.38	0.67	2.02
CL (mL/h)	63.11	9.97	9.20

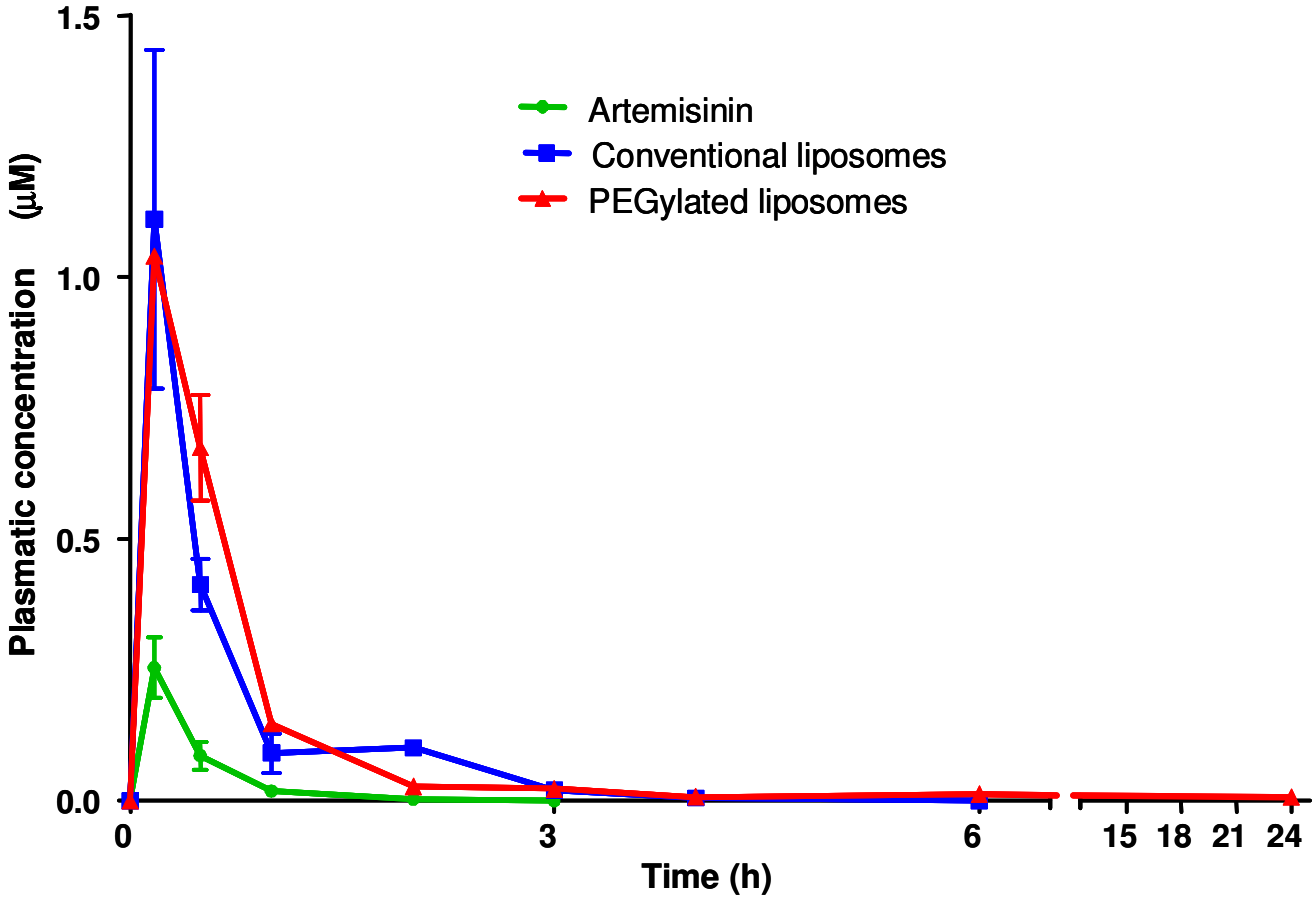

Fig 17. Pharmacokinetic profile of free artemisinin versus artemisinin-loaded liposomes.

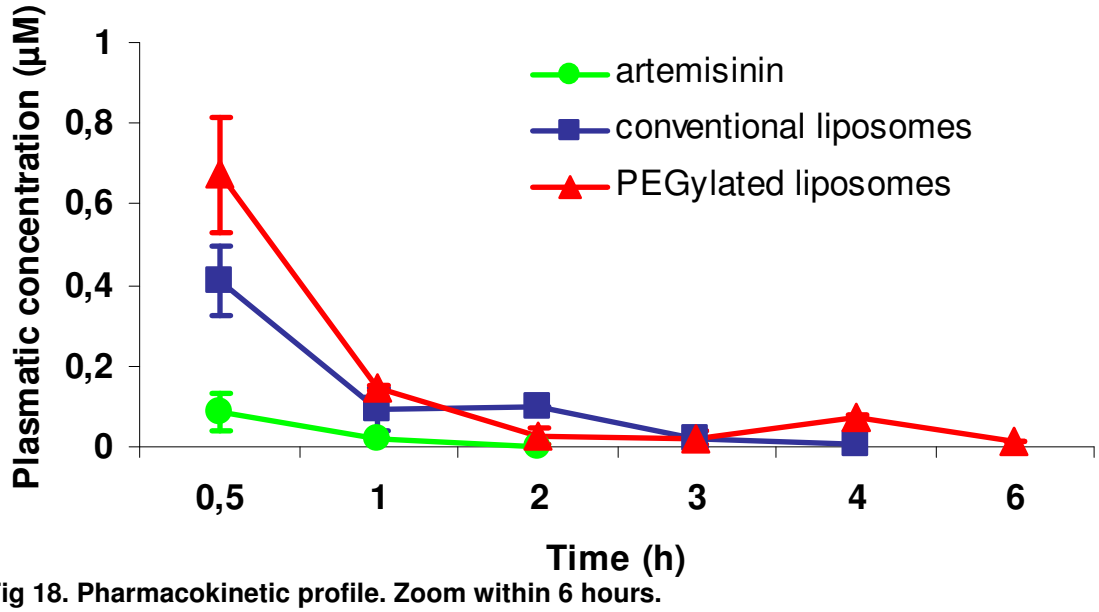

Fig 18. Pharmacokinetic profile. Zoom within 6 hours.

The plasma maximum concentration of free artemisinin was increased 4.4 and 4.2 folds more in conventional and stealth liposomes, respectively.
AUC values, determined for the period 0–24 h, was increased about 6 times more in both of the liposomal formulations in comparison with free artemisinin.
$t_{1/2\beta}$ was 0.38 h for artemisinin. However, incorporation of artemisinin into liposomes prolonged $t_{1/2\beta}$ to 0.67 h and 2.02 h for conventional and stealth liposomes, respectively. Compared with the $t_{1/2\beta}$ of free artemisinin, the ones of artemisinin in conventional and stealth liposomes were much lengthened by 1.7 and 5.3 folds, respectively. The effect of formulation was much better in PEGylated liposomes because of steric stabilizing effect of PEG on liposome surface. An additional hydration layer on the surface of liposomes resulted that liposomes cannot be recognized by macrophages and RES as foreign particles, and are spared phagocytic clearance (Lian T, 2001).
Free artemisinin was so rapidly cleared from plasma that the remained artemisinin was hardly detected in the plasma at 1 h after dosing. The clearance of artemisinin from blood plasma could be decreased by importing liposomes as drug carriers. Both liposomal formulations showed much longer blood circulation time than free artemisinin. It took about 3 h to be cleared from plasma for conventional liposomes. In the case of PEGylated liposomes, artemisinin was still detectable after 24 hours.
Concluding, the artemisinin-loaded liposomes have proper physical characteristics as drug carrier for parenteral administration in terms of particle size, polydispersity index and zeta potential. From *in vivo* studies, it could be concluded that encapsulation into liposomes is a reasonable method to prolong the circulating time of artemisinin in blood plasma. In addition, the effect of formulation on the half-life of artemisinin was enhanced by inclusion of PEG into liposomes.

I.3.4. *In vivo* experiment: antiplasmodial activity

Artemisinin at the dosage of 10 mg/Kg was administred i.p. delivered in conventional liposomes to *Plasmodium berghei* infected mice. Artesunate (Sigma Aldrich) at the dosage of 50 mg/Kg was administred i.p. as well, as positive control.

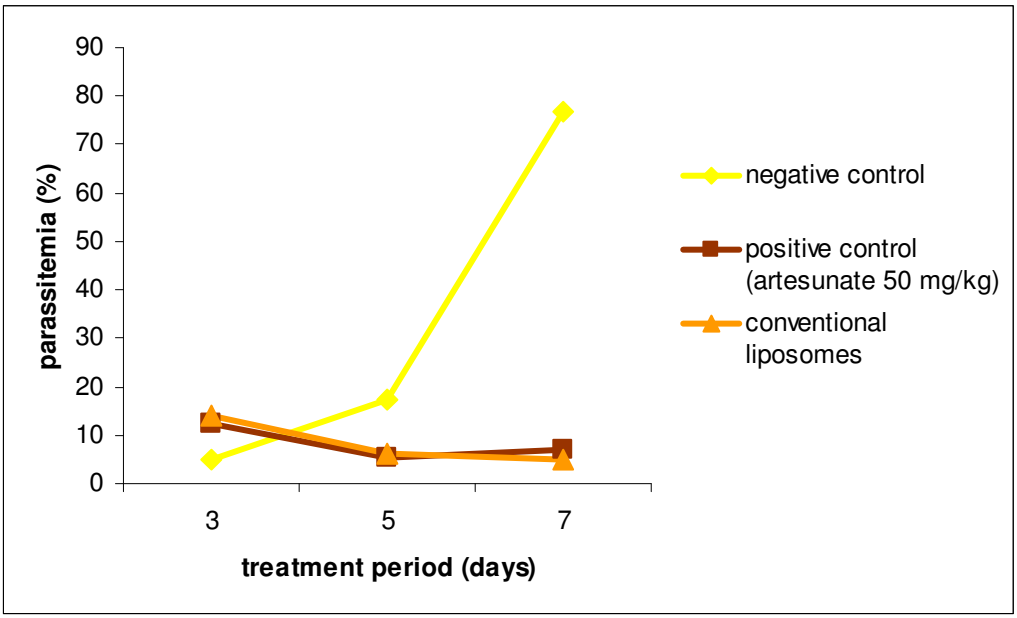

Fig 19. Parasitaemia of *Plasmodium berghei* infected mice treated with conventional artemisinin-loaded liposomes. Each group conteined two mice.

The parasitaemia in the mice was followed for 7 days. The results are presented in figure **19** and take into account the pattern of the parasitaemia in each group. Each value of percentage of parasitaemia is a daily mean value of two mice per group. The reduction of the percentage of parasitaemia is monitored for verifying the antiplasmodial *in vivo* activity. At the beginning of the treatment there were no differences in parasitaemia in any of the groups.
In the negative control group, the percentage of parasitaemia increase progressively so all the mice were infected in the right way; in the positive control group, antiplasmodial activity of artesunate was effective during the whole experiment so, the results will be reliable.
On the fifth day of treatment, the parasitaemia reached around 17.4% in the negative control group, 5.3% in the positive control group and 6.0% in the conventional liposomes group, respectively. On the seventh day of treatment, the parasitaemia reached around 76.7% in the negative control group, 7.0% in the positive control group and 5.0% in the conventional liposomes group, respectively. In the mice treated with artemisinin-loaded conventional liposomes, the percentage of parasitaemia had the same trend of the positive control group.

I.3.5. Artemisinin-curcumin loaded liposomes

Artemisinin-based combination therapy is now the first line policy in most malaria-endemic countries (Ioset JR, 2009; Eastman RT, 2009) in order to delay the development of resistance. Curcumin has been recently proposed as an attractive partner drug for artemisinins (Reddy RC, 2005; Nandakumar DN, 2006).
So, liposomes delivering both of these antimalarian drugs were producted. Before preparing artemisinin-curcumin loaded liposomes , a screening of curcumin-loaded liposomes was done. The lipidic film was rehydrated with buffer solution at different pH values, ranging from 5 to 7.4. The best results, in terms of size (<200 nm) and polidispersity index (about 0.20), were obtained using the highest tested value of pH. Then, liposomes delivering both of the two antimalarian drugs were prepared. Results derived from DLS analysis:

artemisinin (mg/mL)	curcumin (mg/mL)	ratio chol/P90G	mean diameter (nm)	PDI	Zeta potential (mV)
-	-	0.2	183.0±39.6	0.27±0.05	–17.5±1.20
5	-	0.2	180.1±1.74	0.31±0.06	–32.3±0.78
5	2	0.2	71.0±4.14	0.36±0.05	–21.2±2.95
5	5	0.2	310.6±37.19	0.47±0.09	–18.8±0.25
1	5	0.2	316.0±10.01	0.22±0.06	–21.6±0.78

When curcumin had an initial concentration of 2 mg/mL, the size is very low and the system was quite homogeneous. When the concentration of curcumin is 5 mg/mL, artemisinin and curcumin loaded liposomes had size bigger than artemisinin or curcumin loaded liposomes. The emulsification of these formulations was more difficult, but the mean diameter is acceptable considering the intraperitoneally administration as perspective. Results derived from HPLC/DAD/ESI MS analysis:

artemisinin		curcumin	
mg/mL	EE%	mg/mL	EE%
5	22.87±0.28	2	54.78±0.13
5	15.71±0.12	5	25.37±0.18
1	12.55±0.99	5	25.62±0.18

The encapsulation efficacies were satisfactory for every combination of concentration of the two drugs. There was no competition between two hydrophilic molecules to enter into the vesicles. These formulations will be suitable for *in vivo* administering.

I.4. Future perspectives

Physical-chemical investigations will be developed for understanding the potential use of the tridimensional structures that we had observed at the electron microscopy in order to finger out the role of the cholesterol in the lamellar phase and in the morphology.
Improved pharmacokinetic parameters of PEGylated liposomes are encouraging and these carriers will be tested in *Plasmodium berghei* infected mice for testing their antiplasmodial activity and their enhancement in comparison with conventional liposomes.
Artemisinin-curcumin loaded liposomes will be developed with the aim of producing an appropriate formulation to be suggested as an artemisinin-based combination therapy.

I.5. References

- Abdin MZ, Israr M, Rehman RU, Jain SK. **2003**. Artemisinin, a novel antimalarial drug: biochemical and molecular approach for enhanced production. *Planta Med.* 69, 289-299.
- Acton N, Klayman DL. **1985**. Artemisitene, a new sesquiterpene lactone endoperoxide from *Artemisia annua*. *Planta Med.* 5, 441-442.
- Alberts DS, Liu PY, Hanningan EV, *et al.* **1996**. Intraperitoneal cisplatin plus intravenous cyclophosphamide versus intravenous cisplatin plus intravenous cyclophosphamide for stage III ovarian cancer. *NEJM* 335: 1950.
- Allen C, *et al.* **2002**. Controlling the Physical Behavior and Biological Performance of Liposomes Formulation through Use of Surface Grafted Poly(ethylene glycol). *Biosci. Reps.* 22:225–250.
- Araujo CC, LeonLL. **2001**. Biological activities of *Curcuma longa* L., Mem Inst. Oswaldo Cruz 96, 723–728.
- Ardhammar M, *et al.* **1999**. In vitro membrane penetration of modified peptide nucleic acid (PNA). *J. Biomol. Struct. Dyn.* 17, 33–40.
- Bangham AD, Horne RW. **1964**. *J Mol Biol* 8, 660–8.
- Bangham AD, Standish MM, Watkins JC. **1965**. Diffusion of univalent ions across the lamellae of swollen phospholipids. *J Mol Biol*. 13, 238-252.
- Baraldi R, Isacchi B, Predieri S, Marconi G, Vinecieri FF, Bilia AR. Distribution of artemisinin and bioactive flavonoids from *Artemisia annua* L. during plant growth. *Biochemical Systematics and Ecology* 36 (2008) 340-348.
- Bilia AR, Melillo de Malgalhaes P, Bergonzi MC, Vincieri FF. 2006. Simultaneous analysis of artemisinin and flavonoids of several extracts of *Artemisia annua* L. obtained from a commercial sample and a selected cultivar. *Phytomedicine* 13, 487-493.
- Bilia, A.R., Lazari, D., Messori, L., Taglioli, V., Temperini, C., Vincieri, F.F. **2002**. Simple and rapid physico-chemical methods to examine action of antimalarial drugs: its application to *Artemisia annua* L. constituents. *Life Sci.* 70, 769-778.
- Bormann S, Szlezak N, Faucher JF, Matsiegui PB, Neubauer R, Biner RK, Lell B, Kremsner PG, **2001**. Artesunate and praziquantel for the treatment of *Schistosoma haematobium* infections: a double-blind randomized. Placebo-controlled study. *J. Infect. Dis.* 184, 1363-1366.
- Charles DJ, Cebert E, Simon JE, **1991**. Characterization of the essential oil of *Artemisia annua* L. *J. Essent. Oil Res.* 3, 33-39.
- Charles DJ, Simon JE, Wood KV, Heinstein P. **1990**. Germplasm variation in artemisinin content of *Artemisia annua* using an alternative method of artemisinin analysis from crude plant-extracts. *J. Nat. Prod.* 53, 157-160.
- Chen Y, Xianfu L, Hyunjin P, Greever R. **2009**. Study of artemisinin nanocapsules as anticancer drug delivery systems. *Nanomedicine*. 5, 316-322.
- Chimanuka B, Gabriels M, Detaevernier MR, Plaizier-Vercammen JA. **2002**. Preparation of β-artemether liposomes, their HPLC-UV evaluation and relevance for clearing recrudescent parasitaemia in *Plasmodium chabaudi* malaria-infected mice. *Journal of Pharmaceutical and Biomedical Analysis*. 28, 13-22.
- Crommelin DJA, Schreier H. **1994**. In: Kreuter J, editor. Colloidal drug delivery systems. New York: Marcel Dekker. 73–190.
- David AF, Philip JR, Simon RC, Reto B, Solomon N. **2004**. Antimalarial drug discovery: efficacy models for compound screening. *Nat. Rev.* 3, 509–520.
- De Vries PJ, Dien TK, **1996**. Clinical pharmacology and therapeutic potential of artemisinin and its derivatives in the treatment of malaria. *Drugs* 52 (6), 818-836.
- Donrop AM, Day NPJ. **2007**. The treatment of severe malaria. *Trans. R. Soc. Trop. Med. Hyg.* 101, 633-634.
- Duffy PE, Mutabingwa TK. **2004**. Drug combinations for malaria: time to ACT?. *Lancet* 363, 3-4.

- Duke MV, Paul RN, El Sohly HN, Sturtz G, Duke SO. **1994**. Localization of artemisinin and artemisitene in foliar tissues of glanded and glandless biotype of *Artemisia annua* L. *Int. J. Plant Sci.* 155, 365-372.
- Eastman RT, Fidock DA. **2009.** Artemisinin-besed combination therapies: a vital tool in efforts to eliminate malaria. Nature Review Microbiology, AOP.
- Eckstein-Ludwig U, Webb RJ, van Goethem ID, East JM, Lee AG, Kimura M, O'Neill PM, Bray PG, Ward SA, Krishna S. **2003**. Artemisinins target the SERCA of *Plasmodium falciparum. Nature* 424, 957–961.
- Efferth T, Dunstan H, Sauerbrey A, Miyachi H, Chitambar CR. **2001**. The anti-malarial artesunate is also active against cancer. *Int. J. Oncol*. 18 (767), 773.
- Efferth T. **2009**. Artemisinin: a versatile weapon from TCM. In herbal drug: Ethnomedicine to Modern Medicine 173-194. Springer-Verlag Berlin Heidelberg.
- El Sohly HN, Croom Jr EM, El Feraly FS, El Sherei MM. **1990**. A large-scale extraction technique of artemisinin from *Artemisia annua*.*J.Nat. Prod*. 53, 1560-1564.
- Elford BC, Roberts MF, Phillipson JD, Wilson RJ. **1987**. Potentiation of the antimalarial activity of qinghaosu by methoxylated flavones. *Trans. R. Soc. Trop. Med. Hyg.* 81, 434-436.
- Fahr A, Seelig J. **2001**. Liposomal formulations of Cyclosporin A: a biophysical approach to pharmacokinetics and pharmadocynamics. *Crit. Rev. Ther. Drug. Carrier Syst*. 18, 141–172.
- Fang JY, Hong CT, Chiu WT, Wang YY. **2001**. Effect of liposomes and niosomes on skin permeation of enoxacin. *Int. J. Pharm*. 219, 61–72.
- Fatouros DG, Antimisiaris SG. **2001**. Physicochemical properties of liposomes incorporating hydrachlorothiazide and chlorothiazide. *J. Drug Target* 9, 61–74.
- Fendler JH. **1982**. Membrane mimetic chemistry. New York: Wiley.
- Ferreira JFS, Janick J. **1996**. Distribution of artemisinin *Artemisia annua*. In: Janick J (Ed.), Progress in New Crops. ASHS Press, Arlington, VA, 579-584.
- Ferreira JFS, Simon JE, Janik J. **1995**. Developmental studies of *Artemisia annua* L.: flowering and artemisinin production under greenhouse and field conditions. *Planta Med.* 61, 167 and 170.
- Fidock DA, Rosenthal PJ, Croft SL, Brun R, Nwaka S. **2004**. Antimalarial drug discovery: efficacy models for compound screening. *Nature Reviews Drug Discovery* 3, 509–520.
- Firestone GL, Sundar S. **2009**. Anticancer activities of artemisinin and its bioactive derivatives. *Expert reviews in molecular medicine* 11, e32.
- Fuhrhop JH, Mathieu J. **1984**. *Angew Chem* 96, 124–37.
- Gerasimov OV, *et al.* **1999**. Cytosolic drug delivery using pH- and light-sensitive liposomes. *Adv. Drug. Deliv. Rev*. 38, 317–338.
- Gibaldi M, Perrier D. **1982**. *Pharmacokinetics*. New York: Marcel Dekker Inc.
- Hafez IM, Cullis PR. **2001**. Roles of lipid polymorphism in intracellular delivery. *Adv. Drug Deliv. Rev.* 47, 139–148.
- Hastings IM, Watkins WM. **2006**. Tolerance is the key to understanding antimalarial drug resistance. *Trends in Parasitology* 22, 71–77.
- Heppner DG, Ballou VR. **1998**. Malaria in 1998: advances in diagnosis, drugs and vaccine development. *Curr. Opin. Infect. Dis.* 11 (5), 519-530.
- Hien TT, White NJ. **1993**. Qinghaosu. *Lancet* 341, 603-608.
- Hirt HM. **2000**. Clinical Results of the Use of *Artemisia annua* Tea. Anamed Coordination, Winnenden, Germany.
- Horbaschek K, Hoffmann H, Hao J. **2000**. *J Phys Chem B* 2781–4.
- Ingolia TD, Koshland DE Jr. **1978**. *J Biol Chem* 253, 3821–9.
- Ioset JR, Kaur H. Simple field assays to check quality of current artemisinin-based antimalarian combination formulation. PLoS ONE 4(9), e7270.
- Jagetia GC, Aggarwal BB. **2007**. ‘‘Spicing up” of the immune system by curcumin. *Journal of Clinical Immunology* 27, 19–35.

- Jain DC, Mathur AK, Gupta MN, Singh AK, Verma RK, Gupta AP, Kumar S. **1996**. Isolation of high artemisinin-yielding clones of *Artemisia annua. Phytochemistry* 43, 993-1001.
- Klaiman DC. **1985**. Quinghaosu (artemisinin): an antimalarial drug from China. *Science* 228, 1049-1055.
- Koide T, Nose M, Ogihara Y, Yabu Y, Ohta N. **2002**. Leishmanicidal effect of curcumin in vitro. *Biol. Pharm. Bull*. 25, 131–133.
- Krishna S, *et al.* **2004**. Artemisinins: mechanisms of action and potential for resistance. *Drug Resist. Updat*. 7, 233–244.
- Kuttan G, Kumar KB, Guruvayoorappan C, Kuttan R. **2007**. Antitumor, antiinvasion, and antimetastatic effects of curcumin. *Advances in Experimental Medicine and Biology* 595, 173–184.
- Lai H, Singh NP. **1995**. Selective cancer cell cytotoxicity from exposure to dihydroartemisinin and holotransferrin. *Cancer Lett.* 91, 41–46.
- Lasic DD, Martin F. **1995**. Stealth liposomes. CRC Press, Boca Raton.
- Lasic DD, Martin FG, Gabizon A, Huang SK, Papahadjopoulos D. **1991**. *Biochim Biophys. Acta.* 1070, 187.
- Lasic DD. **1990**. *J Colloid Interface Sci* 140, 302–4.
- Lasic DD. **1999**. *J Liposome Res*. 9, 43–52.
- Laughlin JC, Heazlewood GN, Beattie BM. **2002**. Cultivation of *Artemisia annua* L. In: Wright, C.W. (Ed.), Artemisia. Taylor & Francis, London, N.Y., pp. 160-195.
- Laughlin JC. **1993**. Effect of agronomic practices on plant yield and antimalarial constituents of *Artemisia annua* L. *Acta Hortic.* 331, 54-61.
- Laughlin JC. **1995**. The influence of distribution of antimalarial constituents in *Artemisia annua* L. on time and method of harvest. *Acta Hortic*. 390, 67-73.
- Laughlin RG. **1997**. *Colloids Surf A* 128, 27–38.
- Leung D, Lasic DD. **1996**. In: Barenholz Y, Lasic DD, editors. Handbook of nonmedical applications of liposomes, vol. III. Boca Raton: CRC Press, 31–41.
- Lian T, Ho RJY. **2001**. Trends and developments in liposome drug delivery systems. *J Pharm Sci* 90, 667–80.
- Liersh R, Soicke H, Stehr C, Tullner HU. **1986**. Formation of artemisinin in *Artemisia annua* during one vegetation period. *Planta Med*. 52, 387-390.
- Lin YY, Li JJ, Chang CH, Lu YC, Hwang JJ, Tseng YL, Lin WJ, Ting G, Wang HL. **2009**. Evaluation of Pharamacokinetics of ^{111}In_labeled VNB-Pegylated liposomes after i.p. and i.v. administration in a tumor/ascites mouse model. Cancer Biotherapy and Radiopharmaceuticals 24(4), 453-460.
- Liu D, Huang L. **1992**. *Liposomes research* 2, 57.
- Luisi PL. **2001**. *J Chem Educ* 78, 380–4.
- Lusch J, Weisseg V, Brandl M. **2003**. Preparation of liposomes. In Liposomes 2nd edition, edited by Torchilin V and Weisseg V. Oxford University Press, pag.4.
- Martinelli A, Rodrigues LA, Cravo P. **2008**. *Plasmodium chabaudi*: Efficacy of artemisinin + curcumin combination treatment on a clone selected for artemisinin resistance in mice. *Experimental Parasitology* 119, 304–307.
- Maurer N, *et al.* **1999**. Lipid-based systems for the intracellular delivery of genetic drugs. *Mol. Membr. Biol.* 16, 129–140.
- McMullen TPW, McElhaney RN. **1995**. *Biochim Biophys Acta* 1234, 90–8.
- Meshnick SR. **1998**. Artemisinin antimalarials mechanism of action and resistance. *Medecine Tropicale* 58, 13-17.
- Meshnick SR. **2002.** Artemisinin: mechanisms of action, resistance and toxicity. *International Journal for Parasitology* 32, 1655–1660.
- Meyer HW, Richter W. **2001**. Freeze-fracture studies on lipids and membranes. Micron 32, 615–44.
- Meyer HW, *et al.* **1998**. Minimal radius of curvature of lipid bilayers in the gel phase state correspond to the dimension of biomembrane structures ‘‘caveolae’’. *J. Struct. Biol.* 124, 77–87.

- Meyer HW, *et al.* **2000**. Hydration of DMPC and DPPC at 4 degrees C produces a novel subgel phase with convex-concave bilayer curvatures. *Chem. Phys. Lipids* 105, 149–166.
- Meyer HW, Bunjes H, Ulrich AS. **1999**. Morphological transitions of brain sphingomyelin are determined by the hydration protocol: ripples re-arrange in plane, and sponge-like networks distintegrate into small vesicles. *Chem. Phys. Lipids* 99, 111–123.
- Morales M, Charles DJ, Simon JE. **1993**. Seasonal accumulation of artemisinin in *Artemisia annua* L. *Acta Hortic.* 344, 416-420.
- Nandakumar DN, Nagaraj VA, Vathsala PG, Rangarajan P, Padmanaban G. **2006**. Curcumin-artemisinin combination therapy for malaria. *Antimicrobial Agents and Chemotherapy* 50, 1859–1860.
- Nose M, Koide T, Ogihara Y, Yabu Y, Ohta N. **1998**. Trypanocidal effects of curcumin in vitro. *Biol. Pharm. Bull*. 21, 643–645.
- Oussoren C, Velinova M, Scherphof G, van der Want JJ, van Rooijen N, Storm G. **1998**. Lymphatic uptake and biodistribution of liposomes after subcutaneous injection IV. Fate of liposomes in regional lymph nodes. *Biochimica et Biophysica Acta* 1370, 259-272.
- Papahadjopoulos D, Kimelberg HK. **1974**. *Prog Surf Sci* 4, 141–232.
- Patel KR, Li MP, Baldeschwieler JD. **1983**. *Proc. Natl. Acad. Sci.* USA 80, 6518.
- Peleg-Shulman T, *et al.* **2001**. Characterization of steric alloys stabilized cisplatin liposomes by nuclear magnetic resonance. *Biochim. Biophys. Acta.* 1510, 278–291.
- Peters W, Portus JH, Robinson BL. **1975**. The four day suppressive in vivo antimalarial test. *Ann. Trop. Med. Parasitol.* 69, 155–171.
- Pras N, Visser JF, Batterman S, Woerdenbag HJ, Malingre TM, Lugt CB. **1991**. Laboratory selection of *Artemisia annua* L. for high artemisinin yielding types. *Phytochem. Anal*. 2, 80-83.
- Radko SP, Chrambach A. **1999**. Capillary electrophoresis of subcellular-sized particles. *J. Chromatogr. B. Biomed. Sci. Appl.* 722, 1–10.
- Rasmussen HB, Christensen SB, Kvist LP, Karazmi A. **2000**. A simple and efficient separation of the curcumins, the antiprotozoal constituents of *Curcuma longa. Planta Med*. 66, 396–398.
- RBM **2005**. Roll Back Malaria, Meeting on the Production of Artemisinin and ACTS. 2nd Draft Report. Available from http://rbm.who.int/mmss/library.html.
- Reddy RC, Vatsala PG, Keshamouni VG, Padmanaban G, Rangarajan PN. **2005**. Curcumin for malaria therapy. *Biochemical and Biophysical Research Communications* 326, 472–474.
- Romero MR, Efferth T, Serrano MA, Castano B, Macias RI, Briz O, Marin JJ. **2005**. Effect of artemisinin/artesunate as inhibitors of hepatitis B virus production in an *in vitro* system. *Antivir Res.* 68, 75-83.
- Rosoff M. **1996.** editor. Vesicles. *Surf. Sci. Ser*. 62.
- Sada E, Katoh S, Terashima M, Tsukiyama K-I. **1988**. *Biotechnol Bioeng* 32, 826–30.
- Sadzuka Y, Nakai S, Miyagishima A, *et al.* **1997**. Effects of administered route on tissue distribution and antitumor activity of PEG-coated liposomes containing adriamycin. *Cancer Lett* 111, 77.
- Sandur SK, Pandey MK, Sung B, Ahn KS, Murakami A, Sethi G, Limtrakul P, Badmaev V, Aggarwal BB. **2007**. Curcumin, demethoxycurcumin, bisdemethoxycurcumin, tetrahydrocurcumin and turmerones differentially regulate anti-inflammatory and anti-proliferative responses through a ROS-independent mechanism. *Carcinogenesis* 28, 1765–1773.
- Senior JH. **1987**. CRC Crit. Rev. Ther. Drug Carrier Syst. 3, 123.
- Shah JC, Sadhale Y, Chilukuri DM. **2001**. Cubic phase gels as drug delivery systems. *Adv. Drug. Deliv. Rev*. 47, 229–250.
- Shenai BR, *et al.* **2000**. Characterization of native and recombinant falcipain-2, a principal trophozoite cysteine protease and essential hemoglobinase of Plasmodium falciparum. *J. Biol. Chem*. 275, 29000–29010

- Shoba G, Joy D, Joseph T, Majeed M, Rajendran R, Srinivas PS. **1998**. Influence of piperine on the pharmacokinetics of curcumin in animals and human volunteers. *Planta Medica* 64, 353–356.
- Singh A, Vishwarkarma RA, Husain A. **1988**. Evaluation of *Artemisia annua* strains for higher artemisinin production. *Planta Med.* 54, 475-476.
- Singh NP, Lai H. **2004**. Artemisinin induces apoptosis in human cancer cells, *Anticancer Res.* 24, 2277–2280.
- Singh NP, Lai H. **2001**. Selective toxicity of dihydroartemisinin and holotransferrin toward human breast cancer cells. *Life Sci.* 70, 49-56.
- Storm G, Crommelin D, Senior J. **2000**. Liposomes for local sustained drug release. Sustained-release injection products. Interpharm press, Denver, Colorado; 137-180.
- Stoye I, Schroder K, Muller-Goymann CC. **1998**. Transformation of a liposomal dispersion containing ibuprofen lysinate and phospholipids into mixed micelles—physico-chemical characterization and influence on drug permeation through excized human stratum corneum. *Eur. J. Pharm. Biopharm.* 46, 191–200.
- Szoka F Jr, Papahadjopoulos D. **1980**. *Annu Rev Biophys Bio eng* 9, 467–508.
- Tona L, Kambu K, Ngimbi N, Cimanga K, Vlietinck AJ. **1998**. Antiamoebic and phytochemical screening of some Congolese medicinal plants. *J. Ethnopharmacol*. 61, 57–65.
- Torchilin VP, Omelyanenko VG, Papisov MA, Bogdanov Jr. AA, Trubetskoy VS, Herron JN. **1994**. *Biochim Biophys. Acta*. 1195, 11.
- Trigg PI. **1990**. Qinghaosu (artemisinin) as an antimalarial drug. *Econ. Med. Plant Res.* 3, 20-55.
- Ulrich AS. **2002**. Biophysical Aspects of Using Liposomes as Delivery Vehicles. *Bioscience Reports* 22, No. 2.
- Ulrich AS, *et al.* **1999**. Ultrastructural characterization of peptide-induce membrane fusion and peptide self-assembly in the lipid bilayer. *Biophys. J.* 77, 829–841.
- UNICEF. Malaria and children: progress in intervention coverage (UNICEF, New York, **2007**).
- Utzinger J, Xiao S, N'Goran EK, Berquist R, Tanner M. **2001**. The potential of artemether for the control of schistosomiasis. *Int.J. Parasitol*. 31, 1549-1562.
- van Agtmael MA, Eggelte TA, van Boxtel CJ. **1999**. Artemisinin drugs in the treatment of malaria: from medicinal herb to registered medication. *Trends Pharmacol. Sci.* 20 (5), 199-205.
- van Geldre E, Vergauwe A, van den Eeckhout E. **1997**. State of the production of the antimalarial compound artemisinin in plants. *Plant Mol. Biol*. 33, 199-209.
- Vaz APA, Scaranari C, Batista LAR, Figueira GM, Sartoratto A, Magalhaes PM. **2006**. Biomassa e composicao quımica de genotipos melhorados de especies medicinais cultivadas em quatro municıpios paulistas. *Pesqui. Agropecu. Bras*. 41, 869-872.
- Wang CW. **1961**. The Forests of China, with a Survey of Grassland and Desert Vegetation, vol. 5. Harvard University, Maria Moors Cabot Foundation, Cambridge, MA, pp. 171-187.
- WHO 2005. World Malaria Report. Available from http://rbm.who.int/wmr2005/pdf/WMReport.
- WHO, UNICEF, **2005**. World Malaria report 2005, section II: malaria burden. Available from http://www.rbm.who.int/wmr2005/html/1-2.htm.
- WHO. World malaria report **2008** (WHO, Geneva 2008).
- Woerdenbag HJ, Luers JFJ, van Uden W, Pras N, Malingre TM, Alfermann AW. **1993**. Production of the new antimalarial drug in shoot cultures of *Artemisia annua* L. *Plant Cell Tissue Organ Cult.* 32, 247-257.
- Woerdenbag HJ, Pras N, Bos R, Visser JF, Hendriks H, Malingre TM. **1991**. Analysis of artemisinin and related sesquiterpenoids from *Artemisia annua* L. by combined gas chromatography/mass spectrometry. *Phytochem. Anal*. 2, 215-219.
- Yang SL, Roberts MF, O'Neill MJ, Bucat F, Phillipson JD. **1995**. Flavonoids and chromenes from *Artemisia annua. Phytochemistry* 38, 255-257.

II. Verbascoside, acteoside

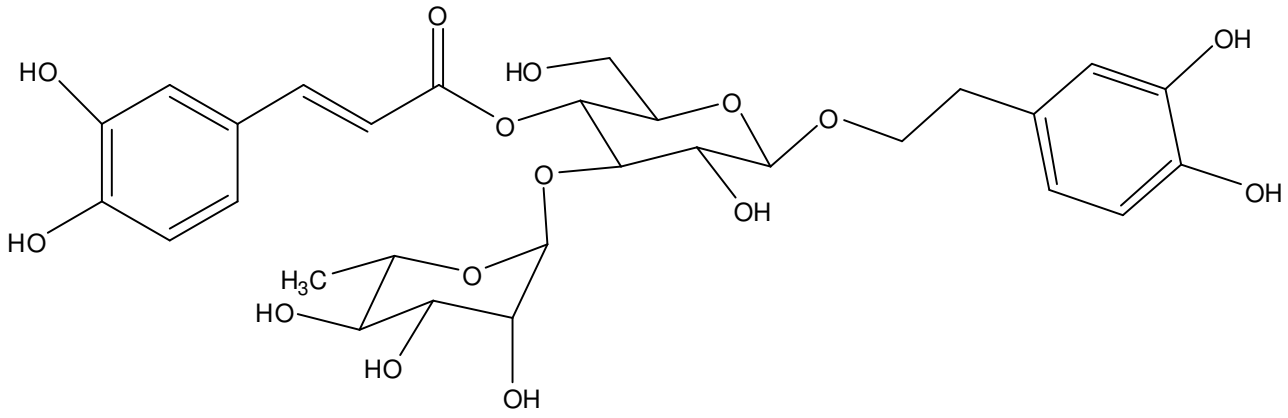

II.1. Introduction

II.1.1. Hystory

Verbascoside is a phenylpropanoid glycoside widely spread in nature (Scogin R, 1992). Because of their broad presence in the vegetal world, there was much confusion in the literature regarding the name and structures of phenylethanoid glycosides. In the 1963, verbascoside was isolated for the first time from *Verbascum sinatum* (Scrophulariaceae), but its structure was not determined at that time (Scarpati ML, 1963). Verbascoside was isolated again in 1966 from *Syringa vulgaris* (Oleaceae) and its structure determined to be β-(3,4-dihydroxyphenyl)ethyl-*O*-α-L-rhamnopyranosyl (1”→3”)-β-D-(4-*O*-caffeoyl)glucopyranoside, but it was named as acteoside (Birkofer R, 1968). In 1982 Andary *et al.* found that the structure of verbascoside and acteoside were identical (Andary C, 1982). A year later, kusaginin was isolated from *Clerodendron tricholomum* (Verbenaceae) and subsequently shown to be identical to verbascoside = acteoside (Sakurai A, 1983).

II.1.2. Source

Verbascoside has been reported from 14 angiosperm families (44 genera, 71 species). This distribution of verbascoside contains many families traditionally clustered in a Scrophulariaceae-Lamiales complex (Scogin R, 1992). It is isolated from several medicinal plants of different families such as Verbenaceae, Oleaceae, Buddlejaceae, Lamiaceae, Scrophulariaceae (Küpeli E, 2007; Scogin R, 1992), including plants of the Traditional Chinese Medicine (Jiangshu Botanic Institute, 1991).
Lemon verbena, *Lippia citriodora* H.B.K. is an aromatic shrub belonging to the Verbenaceae family, which is widely used all over South America and was introduced into Europe in the 17th century. It is cultivated mainly due the lemon-like aroma emitted from its leaves that are utilized for the preparation of herbal tea, which is reputed to have antispasmodic, antipyretic, sedative and digestive properties (Carnat P, 1999; Pascual CJ, 2001; Santo-Gomes R, 2005; Valentao J, 1999). Lemon verbena has a long history of folk uses in treating asthma, spasms, cold, fever, flatulence, colic, diarrhoea, indigestion, insomnia and anxiety (Carnat P, 1999).

II.1.3. Chemical properties

Verbascoside is a diglycoside ester of the caffeic acid which, upon hydrolysis, yields caffeic acid, glucose, rhamnose and 3,4-dihydroxyphenylethanol (Scogin R, 1992). This molecule is very water soluble (up to 30 mg/mL) but it is unstable and it undergoes to degradation that depends upon its concentration (Sinico C, 2008). Degradation products were analyzed by mass spectrometry which pointed out that the main reaction involved in this process is the leakage of the caffeic acid moiety and the opening of the two emiacetal groups.

II.1.4. Analgesic activity

Methanol or ethanol sequential extracts of *Buddleja globosa* leaves produce a dose-dependent antinociceptive activity, as observed through different algesiometric tests. The major metabolites involved in sequential extracts antinociception mechanism are verbascoside and 7-O-luteolin glycoside (Backhouse N, 2008). Verbascoside showed topical and oral analgesic effects (Backhouse N, 2008).
Verbascoside exhibit analgesia (writhing and tail pressure methods) and a weak sedation (prolongation of pentobarbital-induced anaesthesia and methamphetamine-enhanced locomotor activity) by the oral administration (Nakamura T, 1997). However, in a study about the anxiolytic and sedative properties of infusions of *Aloysia triphylla* in normal volunteers, no difference was observed between plant or placebo (Wannmacher L, 1990).
A topical preparation of *Verbena officinalis* L. showed anti-inflammatory and analgesic activities (Calvo MI, 2006).
Verbascoside has been reported for its antinociceptive and anti-inflammatory activity (Küpeli E, 2007), together with its ability for inhibiting the formation of PGE2, the tumor necrosis factor-α, nitric oxide, suppressing the inducible nitric oxide synthase, the enzymatic activity of cyclooxygenase and for exerting a protective action against oxygen free radical-induced peroxidative damage to biomembranes (Lee JL, 2005; Liu MJ, 2003).

II.1.5. Pharmacological effects

The literature regarding the biological activities of this compound is significant: indeed concerning anti-inflammatory, anti-ulcerogenic and antispasmodic activity (Küpeli E, 2007; Korkina LG, 2007; Hausmann M, 2007; Fleer H, 2007; Penido C, 2006; Lau CW, 2004; Diaz AM, 2004), antiproliferative properties and inhibition of telomerase (Efferth T, 2007; Lee KW, 2007), immunomodulatory (Akbay P, 2002), antioxidant (Bilia AR, 2008; Lee JY, 2005) and antibacterial activity (Didry N, 2002).
Mostly of the plants containing verbascoside as a major constituent are traditionally used in the treatment of inflammatory diseases. This activity may be attributed, at least in part, to the selective 5-lipoxygenase inhibition and potent *in vitro* free radical scavenging action of verbascoside and some other phenylpropanoid derivatives (Deepak M, 1999). The high redox potential as electron donor of verbascoside, protects cells against glucose oxidase-mediated cytotoxicity and apoptosis (Chiou WF, 2004), and a preventive potential may be attributed to the treatment of oxidative stress-mediated diseases (Kim SS, 2005).
Verbascoside showed a stronger COX-2 inhibition activity (23.1±2.0% at a concentration of 10^{-4} M and IC_{50} = 0.69 mM) than towards COX-1. A structure–activity relationship suggests that the presence of more than one sugar unit increases the steric hindrance which prevents the molecule getting easily to the active site of the enzyme (Sahpaz S, 2002).
Verbascoside showed inhibitory effect on histamine and bradykinin-induced contractions and oral antiinflammatory activity (Schapova E, 1998).

Verbascoside impairs endothelial NO-mediated aortic relaxation partially through of agonist-induced endothelial Ca^{2+} mobilization and Ca^{2+}-dependent NO production and subsequent suppression of cyclic GMP formation. This action, if occurring in small vessels *in vivo*, may contribute to the reported anti-inflammatory effect of verbascoside against NO-mediated vascular permeability-related acute oedema (Lau CW, 2004).
Verbascoside showed a photoprotective effect against UV-B induced cellular death, evaluated by challenge experiments using *E. coli* (Avila Acevedo JG, 2005).
An aqueous extract of *Verbena officinalis* had a neuroprotective effect against β-amyloid peptide, important cytotoxic factor in the Alzheimer's disease; a pre-treatment with this extract attenuated the toxicity of Aβ in primary cultures of cortical neurons (Lai SW, 2006).

II.2. Materials and methods

II.2.1. Plant material

Verbascoside was extracted with an hydroalcoholic solution (EtOH 80%) of dried leaves of cultivated *Lippia citriodora* H.B.K. (Verbenaceae) harvested in 2004, a gift from Aboca (Pistrino di Citerna, PG, Italy), lot n. 4L0466.

II.2.2. Chemicals and standards

Ethanol was analytical reagent grade from Riedel-de Haen (Seelze, Germany). All the solvents used for the extraction and HPLC analysis (MeOH, *n*-hexane, dichloromethane, and acetonitrile) were HPLC grade from Merck (Darmstadt, Germany); 85% formic acid was provided by Carlo Erba (Milan, Italy). Water was purified by a Milli-Q_{plus} system from Millipore (Milford, MA). Solution NaCl 0.9%, Fresenius Kabi, Italy. Verbascoside was purchased from IRB Istituto di Ricerche Biotecnologiche of Altavilla Vicentina. Egg phosphatidylcholine (Phospholipon90G, P90G) were kindly obtained from Natterman Phospholipids, Gmb. Cholesterol was analytical grade and were purchased from Aldrich (Milan, Italy). Carboxymethylcellulose Sodium Salt (CMC), Fluka Chemie GmbH, Steinheim, Germany. Naloxone hydrochloride (> 99%), tramadol (> 99%), ketorolac (≥ 99%), (Sigma, St. Louis, USA). Morphine hydrochloride (> 99%) was from S.A.L.A.R. Pregabalin (> 99%) was purchased from Chem Pacific, Baltimore. Size esclusion column chromatography was carried out on Sephadex LH-20 (Amersham Biosciences AB, Uppsala, Sweden). TLC (plates of silica gel 60 F254, Merck, Damrastatt Germany). β-CD (kleptose) was purchased from Rochette and D_2O was purchased from Sigma Aldrich.
Verbascoside reference standard (purity 98% by HPLC/DAD/ESI MS, GC, NMR) from IRB Istituto di Ricerche Biotecnologiche of Altavilla Vicentina.

II.2.3. Isolation of verbascoside

500 g of herbal drug were exhaustively extracted with an hydroalcoholic solution (EtOH 80%). This extract was concentrated to dryness in a rotavapor under reduce pressure and controlled temperature (30°C) and lyophilised. 34.75 g of dried extract was obtained (6.96 % with respect to the HD). 5 g of the extract (about 12% of verbascoside by HPLC/DAD/ESI MS, fig **20**) were dissolved in 5 mL EtOH 50% and purified with a Sephadex LH-20 column chromatography (length 50 cm, diameter 4 cm) using EtOH 50%. Fractions were analysed by TLC plates of silica gel 60 F254; solvent $CHCl_3$/MeOH 7:3) using vanilline 5% in MeOH and H_2SO_4 1%. Purity of isolated verbascoside (700 mg, 81.2%) was assessed by HPLC/DAD/ESI MS analysis using verbascoside reference standard (purity 98% by HPLC/DAD/ESI MS, GC, NMR). Verbascoside was re-

crystallised from MeOH to obtain pure compound (510 mg, purity > 98%). Purification of verbascoside from the extract was repeated 6 times.

II.2.4. Analytical HPLC/DAD characterization

The HPLC system consisted of a HP 1100 L instrument with a Diode Array Detector and managed by a HP 9000 workstation (Agilent Technologies, Palo Alto, CA, USA). The column was a Varian Polaris TM C18-E (250 mm x 4.6 mm i.d., 5 (m) maintained at 26°C with a pre-column of the same phase. The eluents were H_2O at pH 3.2 by formic acid and acetonitrile. The following multi-step linear gradient was applied:

Time (min.)	CH3CN (%)	H2O/HCOOH pH=3.2 (%)
0.1	13	87
10	15	85
20	25	75
23	25	75
25	95	5
28	95	5

Total time of analysis was 28 min, equilibration time was 10 min, flow rate was 0.8 mL/min, injection volume was 10 µL and oven temperature 26°C. The UV-vis spectra were recorded between 220–500 nm and the chromatographic profiles were registered at 240, 330 and 350 nm.

II.2.5. Analytical HPLC/ESI MS characterization

The HPLC system described above was interfaced with a HP 1100 MSD API-electrospray (Agilent Technologies, Palo Alto, CA, USA). The interface geometry, with an orthogonal position of the nebulizer with respect to the capillary inlet, allowed use of analytical conditions similar to those used for HPLC/DAD analysis in order to achieve the maximum sensitivity of ESI values. The same column, time period and flow rate were used during the HPLC/ESI MS analyses. Mass spectrometry operating conditions were optimised in order to achieve maximum sensitivity values: negative and positive ionisation mode, scan spectra from *m*/Z 100 to 800, was used with a gas temperature of 350°C, nitrogen flow rate of 10 L min^{-1}, nebulizer pressure 30 psi, Quadrupole temperature 30°C, Capillary voltage 3500V. The applied fragmentors were in the range 80–180 V. Identification of constituents was carried out by HPLC/DAD and HPLC/ESI MS analysis, and/or by comparison and combination of their retention times, UV-Vis and mass spectra of the peaks with those of authentic standards when possible, or isolated compounds or characterised extracts as well as based on literature data.

II.2.6. Formulations

II.2.6.1. Production of liposomes

Multilamellar vesicles were prepared according to the film hydratation method (Bangham AD, 1965). P90G and cholesterol were dissolved in chloroform. The organic solvent were vacuum evaporated and the dry lipid film was hydratated by addition of a verbascoside aqueous solution or a verbascoside physiological solution (NaCl 0.9%). The dispersion was stirred with a mechanical stirrer for 30 minutes with a waterbath at the constant

temperature of 38°C. Glass beads were used to increase the contact surface between the lipidic film and the verbascoside solution. In order to reduce the dimensions of the vesicles from MLV to LUV, an high pressure homogenizer Emulsiflex C3® was used at the applied pressure of 150000 kPa for 30 seconds. Then the liposomes were characterized by different techniques.

II.2.6.2. Production of ethosomes

Multilamellar vesicles were prepared according to the film hydratation method (Bangham AD, 1965) as describe above for liposomes. In the case of ethosomes, the dry lipid film was hydrated by addition of a verbascoside hydroalcolic solution (EtOH 30%), stirring for 1 hour. The size of ethosomes was reduced form MLV to LUV by sonicator.

II.2.6.3. Inclusion complex preparation

Co-freeze dried technique was used to prepare the inclusion complex of verbascoside and β-cyclodextrin. A mixture of verbascoside and β-cyclodextrin at different molar ratio was solubilized in water and this solution was stirred for 3 h in the dark. After equilibration the solution was frozen and freeze dried.

II.2.7. Characterization of formulations

II.2.7.1. Characterization of liposomes and ethosomes

II.2.7.1.a. Dynamic Light Scattering (DLS)

Dynamic Light Scattering is an ALV CGS-3 system (Malvern Instruments, Malvern, UK) equipped with a JDS Uniphase 22 mW He–Ne laser operating at 632.8 nm, an optical fiber-based detector, a digital LV/LSE-5003 correlator and a temperature controller (Julabowater bath) set at 25 °C. Time correlation functions were analyzed to obtain the hydrodynamic diameter of the particles (Z_h) and the particle size distribution (polydispersity index, PDI) using the ALV-60X0 software V.3.X provided by Malvern. Autocorrelation functions were analyzed by the cumulants method (fitting a single exponential to the correlation function to obtain the mean size (Z_{ave}) and polydispersity index (PDI)) and CONTIN (to fit a multiple exponential to the correlation function to obtain particle size distributions). The diffusion coefficients calculated from the measured autocorrelation functions were related to the hydrodynamic radius of the particles via the Stokes–Einstein equation

$$Z_h = (k_B T q^2)/(3\pi\eta\Gamma)$$

where Z_h is the hydrodynamic radius of the particles,
k_B is the Boltzmann constant,
T is the absolute temperature,
η is the solvent viscosity,
Γ is the decay rate,
q is the scattering vector

$$q = [4\pi n \sin(\Phi/2)]/\lambda$$

in which n is the refractive index of the solution,
Φ is the scattering angle,
λ is the wavelength of the incident laser light.

Scattering was measured in an optical quality 4 mL borosilicate cell at a 90° angle.

II.2.7.1..b. Trasmission electron microscopy (TEM)

A drop (10 µL) of vesicle dispersion diluted 10-times was applied to a carbon film-covered copper grid. Most of the dispersion was blotted from the grid with filter paper to form a thin film specimen, which was stained with a phosphotungstenic acid solution 1% w/v in sterile water. The samples were dried for 3 minutes and than examined and photographed with a Zeiss EM 109 transmission electron microscope at an accelerating voltage of 80 kV.

II.2.7.1.c. Encapsulation efficacy (EE%)

Verbascoside-incorporated vesicles were separated from the not encapsulated material by gel chromatography on Sephadex G-50. This method is satisfactory for solutes less than 7 kDa (Zuidam NJ, 2003). 200 µL of liposomal dispersion were added on the top of a minicolumn containing a dry matrix (G-50 gel bed). The not entrapped material was removed by centrifugation at 1000 g for 3 minutes. Liposomes with the cleaned surface were collected as eluates and free-verbascoside remained inside the minicolumn. Verbascoside was quantified by HPLC/DAD analysis using pure verbascoside (purity 98% by HPLC/DAD/ESI MS, GC, NMR) as external standard.

II.2.7.2. Inclusion complex characterization

II.2.7.2.a. NMR analyses

Proton spectra and 2D-NMR NOESY and ROESY experiments were carried out in a Bruker DRX 600 MHz and Bruker DRX 400 MHz.
NOESY mixing time was 900ms and ROESY spin-lock time of 350ms.

II.2.7.2.b. Job's plot

A solutions of verbascoside 10 mM was mixed in different ratios (ranging from 0.1 to 0.9) with solution of β-CD in D_2O (10 mM) to obtain final solutions of 10 mM and ratios of guest/[β-CD +guest] ranging from 0.1 to 0.9. All samples were filtered before NMR analysis and were allowed to equilibrate at 298 K for at least 15 minutes prior to acquisition. Each spectrum was calibrated and the chemical shift displacements were recordered. The construction of the continuous variation plot required 2D COSY and ROESY experiments for most of the data points; they were useful to determine the chemical shift displacements where overlapping resonances (Zouvelekis D, 2002) and line broadering fenomena occurred.

II.2.7.2.c. Diffusion Ordered SpectroscopY

DOSY experiments were carried out in a Bruker DRX 600 MHz. DOSY was carried out using a spectrometer equipped with a 5 mm triple indirect detection probe capable of providing pulsed field gradients of up to 60 G/cm. Between 8 and 25 measurements, each of 4–64 transients, of diffusion-attenuated stimulated echo spectra were made for each sample, using z field gradient strengths between 3 and 60 G/cm spaced at equal intervals of gradient squared. The data were then processed using least-squares fitting of peak heights to derive estimated diffusion coefficients and standard errors from the attenuation of signal as a function of the square of field

gradient pulse area. The gradient strength was logarithmically incremented in 32 steps from 2% up to 95% of the maximum gradient strength. Diffusion times and gradient pulse durations were optimised for each experiment in order to achieve a 95% decrease in resonance intensity at the largest gradient amplitude; typically, diffusion times (D) between 60 and 100 ms, gradient strength (δ * 0.5) between 2.5 and 3.6 ms and spoil gradient strength of 6 ms. Gradient strength, g in the z direction was calibrated by D_{H_2O} = 2.3 x 10^{-9} m^2/s)1 at 298 K using a 90% H2O/ 10% D2O mixture. After Fourier transformation and baseline correction, the diffusion dimension of the 2D DOSY spectra was processed by means of the Bruker Topspin software package.

II.2.8. Stability

II.2.8.1. Stability test of verbascoside-loaded liposomes

Liposomal formulation was kept at 4°C±1°C and its stability was studied over 6 months. At fixed time intervals (once a week for the first month and than once a month) liposomes were assayed for their drug content after disruption of purified vesicles with methanol. Verbascoside chemical stability was checked by HPLC/DAD analysis. Physical stability of vesicular dispersion was investigated by DLS measurements and by TEM visualization.

II.2.8.2. Stability test of the inclusion complex

The inclusion complex was kept at room temperature covered by sunlight and its stability was studied within 1 month. A water solution of β-cyclodextrin 15 mM (closed to saturation) was prepared and verbascoside was added at different concentration: 0.1, 2 and 5 mg/mL. At fixed time intervals (every 5 days) an aliquote of these three solutions was collected in order to quantified the content of verbascoside still present in β-cyclodextrin solution. Verbascoside chemical stability was checked by HPLC/DAD analysis.

II.2.9. *In vitro* experiment: skin permeation studies

In vitro experiments were performed in triplicate (at least five times in order to achieve statistical significance) using skin fragments excised from new born pigs (Sinico C, 2006). The subcutaneous fat was carefully removed and the skin was cut into squares of 3 × 3 cm^2 and randomized. The skin, previously frozen at –18°C, was placed at +4°C 1 day before the experiments and, one hour before the start of the experiments, was pre-equilibrated in 0.9% NaCl solution at +25°C. Circular pieces of this skin were fixed on vertical Franz diffusion cells (Franz TJ, 1975). The receiver compartment (volume 7 cm^3; effective diffusion area 0.636 cm^2) was filled with 0.9% NaCl solution, which was constantly stirred with a small magnetic bar and thermostated at 37°C throughout the experiments. A hydroxyethylcellulose gel containing verbascoside or verbascoside-loaded liposomes (200 µL) were applied to each of the skin pieces and the donor compartment was closed by means of a cork and sealed with parafilm in order to achieve occlusive conditions. At hourly intervals up to 24 h, the receiver solution was removed, the chamber was refilled with fresh pre-thermostated 0.9% NaCl solution, and the samples were analyzed by HPLC/DAD to determine the amount of permeated verbascoside. At the end of the experiment the skin surface was washed 3 times with 0.9% NaCl solution and then removed and dried with filter paper. The amount of drug accumulated into the skin was evaluated after dermis-epidermis separation. The stratum corneum was removed by stripping with tapes of Tesa® film. A piece of skin was separated into epidermis and

dermis by pressing the skin surface against a hot plate (60°C) and peeling off the epidermis. The layers were soaked separately and then exposed to four sonication cycles of 30 min each in an ultrasound bath. Finally, the obtained solutions were concentrated and the verbascoside content quantified by HPLC/DAD.

II.2.10. *In vivo* experiment: antihyperalgesic activity

II.2.10.1. Rats

Male Sprague-Daloley albino rats (180-200 g) from Harlan (S. Piero al Natisone, Italy) were used. Four rats were housed per cage. The cages were placed in the experimental room 24 h before the test for acclimatization. The animals were fed a standard laboratory diet and tap water *ad libitum* and kept at 23±1°C with a 12-h light/dark cycle, light at 7 AM. All experiments were carried out in accordance with the European Communities Council Directive of 24 November 1986 (86/609/EEC) for experimental animal care. All efforts were made to minimize the number of animals used and their suffering.

II.2.10.2. Administration of tested substances

Drugs were dissolved in isotonic (NaCl 0.9%) saline solution or dispersed in carboxymethylcellulose sodium 1% solution immediately before use; it depends on the route of administration. Drug concentrations were prepared so that the necessary dose could be administered in a volume of 10 mL kg^{-1} by i.p. and p.o. injection.

II.2.10..3. Animal models of neuropathic pain

II.2.10.3.a. Chronic constriction injury (CCI)

A peripheral mono neuropathy was produced in adult rats by placing loosely constrictive ligatures around the common sciatic nerve according to the method described by Bennett (Bennett GJ, 1988). Rats were anaesthetised with chloral hydrate. The common sciatic nerve was exposed at the level of the middle of the thigh by blunt dissection through biceps femoris. Proximal to sciatica's trifurcation, about 1 cm of the nerve was freed of adhering tissue and four ligatures (3/0 silk tread) were tied loosely around it with about 1 mm spacing. The length of the nerve thus affected was 4-5 mm long. Great care was taken to tie the ligatures such that the diameter of the nerve was seen to be just barely constricted when viewed with 40x magnification. In every animal, an identical dissection was performed on the opposite side except that the sciatic nerve was not submitted to constrictive ligature ligated. The left paw was untouched.

II.2.10.3.b. Monoiodioacetate injection (MIA)

Joint damage was induced by a single intra-articular injection of 2 mg of sodium monoiodioacetate into the left knee joint of anaesthetised rats in a total volume of 25 µL. The dose of monoiodoacetate was chosen based on previous literature (Guingamp C, 1997) and in-house dose-response data using 0.5, 1 and 2 mg.

II.2.10.4. In vivo tests

II.2.10.4.a. Paw-pressure test

The pharmacological assay is carried out using the paw-pressure test (Leighton CE, 1988), in the two animal models of neuropathic pain described above. The instrument exerts a force which is applied at a constant rate (32 g per second) with a cone-shaped pusher on the upper surface of the rat hind paw. The force is continuously monitored by a pointer moving along a linear scale. The pain threshold is given by the force which induces the first struggling from the rat. An arbitrary cut off value of 250 g was adopted. Those mice scoring less than 40 g or over 75 g in the pretest were rejected (25%). The pain threshold was measured before (pretest) and 15, 30 and 45 min after the beginning of the test.

II.2.10.4.b. Rota-rod test

The apparatus consisted of a base platform and a rotating rod with a diameter of 3 cm and a non slippery surface, The rod was placed at a height of 15 cm from the base. The rod, 30 cm in length, was divided into five equal sections by six disks. Thus, up to five rats were tested simultaneously on the apparatus, with a rod-rotating speed of 16 rpm. The integrity of motor coordination was assessed on the basis of the number of falls from the rod in 30 s. Those mice scoring less than three and more than six falls in the pretest were rejected (20%). The performance time was measured before (pretest) and 15, 30 and 45 min after the beginning of the test. A total of 4-5 rats per group were tested.

II.2.10.4.c. Statistics

All experimental results are given as the mean ± SEM. An analysis of variance ANOVA, followed by Fisher's Protected Least Significant Difference procedure for post-hoc comparison, were used to verify significance between two means. Data were analyzed with the StatView software for the Macintosh. *P* values of less than 0.05 were considered significant.

II.3. Results and discussion

II.3.1. Isolation of verbascoside

Commercial dried plant material (*Lippia citriodora* H.B.K.) was exhaustively extracted with hydroalcoholic solution (EtOH 80%) as described in the experimental part. The macerates were filtered and evaporated under reduced pressure and lyophilized to obtain a dried extract which was analysed by HPLC/DAD/ESI MS. The presence of verbascoside in the extract was assessed by comparison of its t_R with the authentic sample verbascoside international standard and it was confirmed by UV and NMR data. Verbascoside resulted about 12% of the dried extract calculated using international standard (fig **20**).

II.3.1.1. Analytical HPLC/DAD/ESI MS characterization

Chromatograms were acquired at different wavelengths for monitoring the diverse classes of compounds that can be present in the extract of leaves of *Lippia citriodora* H.B.K. (fig **20**). The different registered wavelengths were: 240 nm for monitoring iridoids, 330 nm for monitoring phenylpropanoids and 350 nm for monitoring flavonoids.

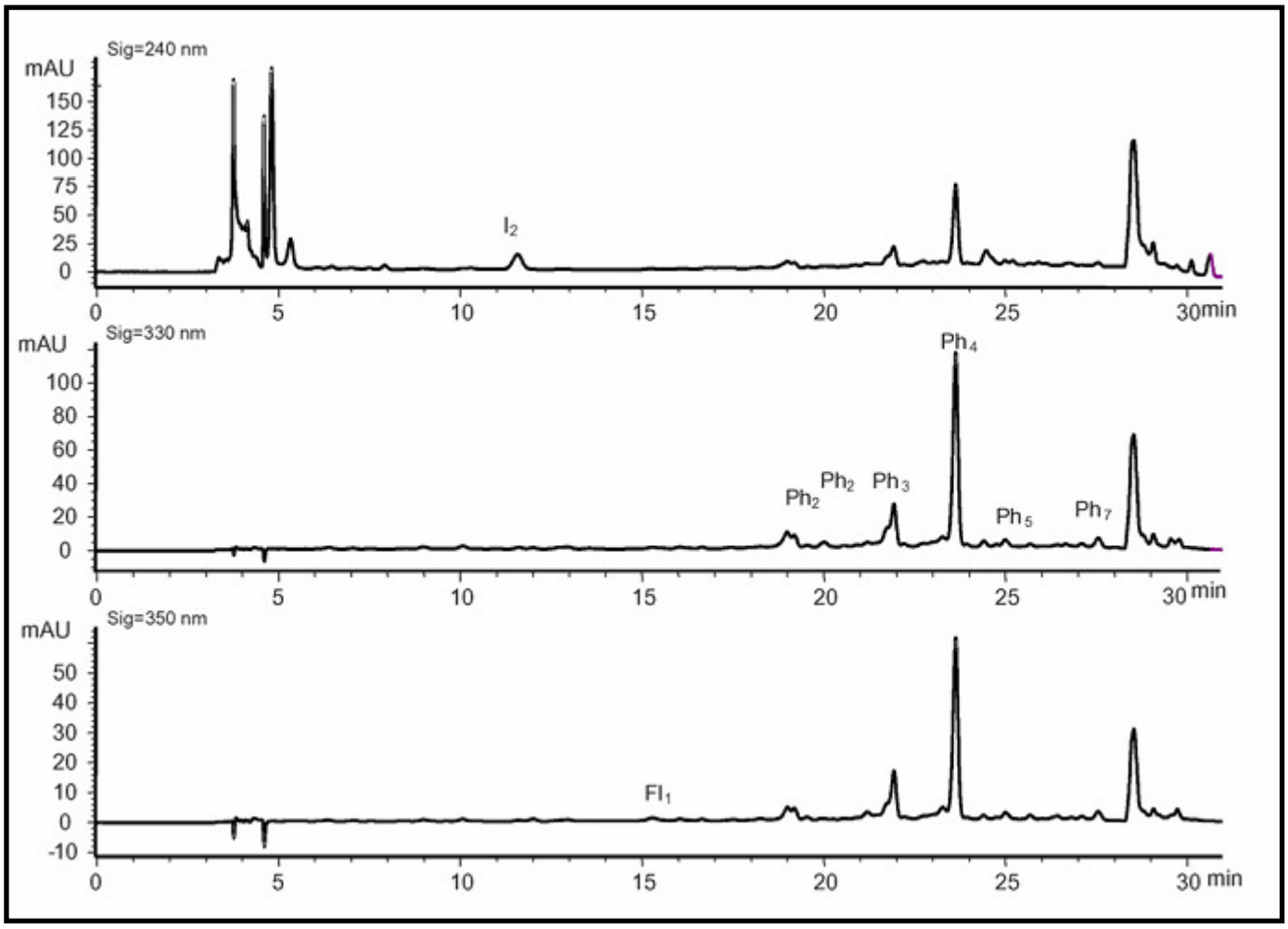

Fig 20. Chromatographic profiles at 240, 330 and 350 nm of a representative sample of *Lippia citriodora* H.B.K. leaf extracts. I=iridoids; Ph=phenylpropanoids derrivatives; Fl=flavonoids derivatives.

At the wavelenght of 240 nm, only one iridoid was identified as verbenalin (figure **21**, I_2 in fig **20**).

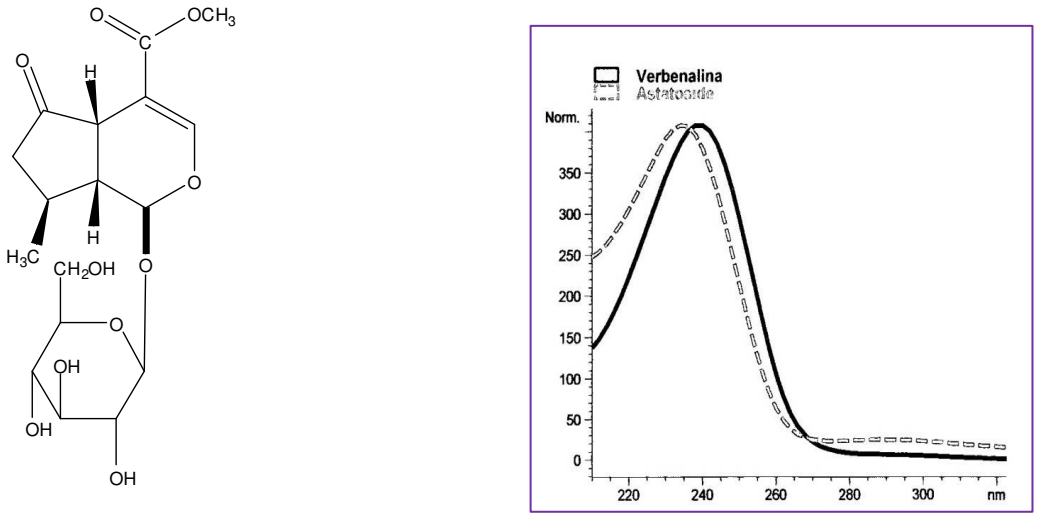

Fig 21. Chemical structure and UV spectrum of verbenalin.

At the wavelenght of 330 nm, many phenylpropanoids derivates were evidenced: β-OH-isoverbascoside, verbascoside, isoverbascoside, eukovoside and its isomer (figure **22**, $Ph_{2,3,4,5,7}$ respectively in fig **20**).

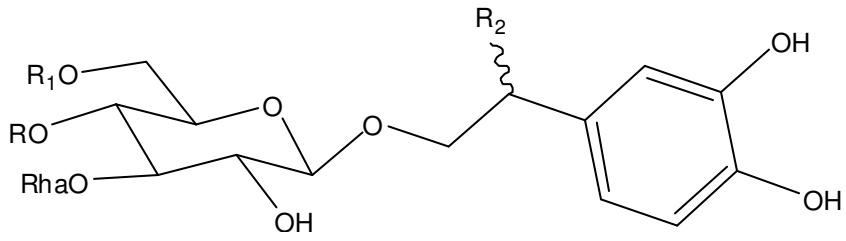

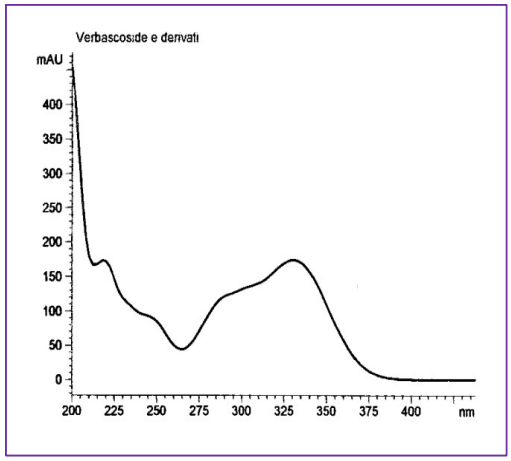

β-OH-isoverbascoside	**R**=H; **R_1**= caffeic acid; **R_2**=OH
verbascoside	**R**= caffeic acid; **R_1**=H; **R_2**=H
isoverbascoside	**R**=H; **R_1**= caffeic acid; **R_2**=H

Fig 22. Chemical structure and UV spectrum of phenylpropanoids derivates.

At the wavelenght of 350 nm, only one flavonoid derivates was identified as luteolin-7-*O*-diglucuronide (figure **23**, Fl_1 in fig **20**).

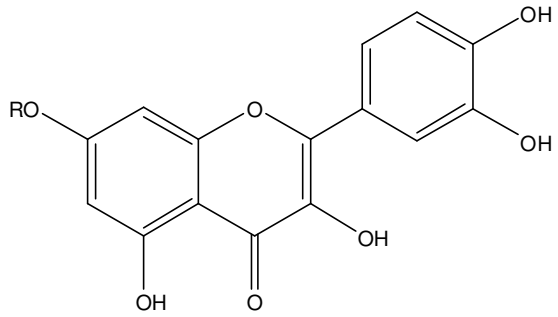

R=diglucuronyl

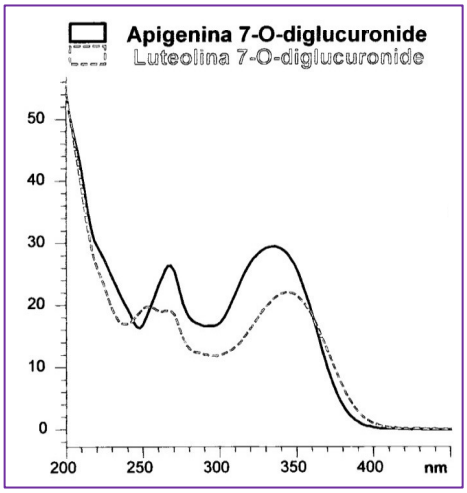

Fig 23. Chemical structure and UV spectrum of as luteolin-7-*O*-diglucuronide.

Than, pure verbascoside was obtained by size exclusion chromatography (Sephadex LH-20) eluting with ethanol (50%) and by recrystallization with methanol. Its good separation with Sephadex LH-20 in one purification step could represent a method easily applied at the industrial scale. This method is proposed as a fast and efficient tool for the isolation and purification of verbascoside recovering more than 85% of the constituent present in the crude dried extract (purity > 98%, determined by HPLC/DAD/ESI MS and confirmed by NMR).
The advantages of this method include high recovery of the target product, short and well defined separation times, narrow bands which lead to good sensitivity, freedom from sample loss because solutes do not interact with stationary phase and the possibility to use “ecologically friendly” solvents.

II.3.2. Formulations

II.3.2.1. Production and characterization of liposomes and ethosomes

In the table all the constituents of the bilayer of conventional liposomes were indicated with their molar ratio:

molecule	MW	molar ratio	mg/mL
P90G	760	2.5	23
cholesterol	386.66	0.5	2.2
verbascoside	624	2	15

These ratios were optimized starting from values reported in a precedent paper of our group (Sinico C, 2008). In the case of verbascoside, it is a molecule very hydrophilic, so the lipidic films were rehydrated with a solution of this drug dissolved in water, in a physiological solution (NaCl 0.9% v/v) or, in the case of ethosomes, in EtOH 30% v/v.
All the obtained dimensional analysis were summarized in the following tables.
Results derived from DLS analysis for liposomes:

NaCl 0.9%	Verbascoside (mg/ml)	P90G (mg/ml)	Chol. (mg/ml)	Mean diameter (nm)	PDI
–	–	23	2.2	177.8	0.15
–	15	23	2.2	155.0	0.15
+	–	23	2.2	98.2±4.1	0.13
+	15	23	2.2	120.1±14.8	0.16

Results derived from DLS analysis for ethosomes:

EtOH 30%	Verbascoside (mg/ml)	P90G (mg/ml)	Chol. (mg/ml)	Mean diameter (nm)	PDI	Zeta potential (mV)
+	15	23	2.2	239.9±1.5	0.6±0.1	-39.6±0.3

In the case of liposomes, all the prepared formulations had a size very low, suitable not only for a topical delivery system but also for a parenteral administration. The polidispersity indexes (PDI) were less than 0.2, that means that the system is quite monodisperse.
Conversely, the size of ethosomes were still acceptable but their PDI were not. The addition of ethanol in this percentage (30% v/v) to the bilayer act as enhancer of skin penetration (Touitou E, 1997), but verbascoside is not stable in this hydroalcoholic solution: the formulation started to become brownish. The *in vitro* test (Franz's cell), described below, will be deluding. Ethosomes will be not developed more.
After minicolumn centrifugation on sephadex G-50, useful for cleaning the liposomal surfaces from unentrapped drug, the encapsulation efficacy was evaluated. Results derived from HPLC/DAD/ESI MS analysis for liposomes:

NaCl 0.9%	Emulsiflex 150.000 KPa 30 s	Sephadex G-50	Mean diameter (nm)	PDI	EE (%)
+	+	+	120.15±14.85	0.16	91.44±1.28

As we expected, the encapsulation efficacy of an water-soluble drug was very high.
Liposomal formulation seemed to be a potential delivery for carrying *in vivo* verbascoside.

II.3.2.2. Production and characterization of the inclusion complex

Cyclodextrins are cyclic oligosaccharides consisting of six to eight D-glucose units (α, β and γ-CD, respectively) linked at C1 and C4 carbons (Bakkour Y, 2006). Due to their particular structure characterised by a hydrophobic internal cavity and a hydrophilic

external surface, they are able to entrap a variety of organic compounds. Cyclodextrins are widely applied in pharmaceutical and food industry, as they enhance the aqueous solubility of poorly water-soluble substances and they modify the physico-chemical properties of drugs and protect labile substances from oxidations or thermal and chemical degradations (Szejtli J, 1988; Bakkour Y, 2006). This type of inclusion complexes are able to reduce the volatility of fragrances and perfumes (Bakkour Y, 2006), to give a greater stabilization, to control the release and other wanted properties of the included compounds (Szejtli J, 1988). In food industry they are used as additives to improve the taste (Szejtli J, 2005) and to control the enzymatic browning of different foods (Astray G, 2009).

II.3.2.2.a. NMR analyses

Nuclear magnetic resonance is one of the most powerful and versatile methods for the elucidation of molecular structure and dynamics. It is also very well suited to study molecular complexes and their properties (Fielding L, 2000). Therefore it has been widely used for studying inclusion complexes formed by cyclodextrins (Dodjiuk H, 2004). The success of NMR spectroscopy in this field is due to its ability to study complex chemical systems and to determine stoichiometry, association constants, and conformations of molecular complexes, as well as to provide information on the symmetry and dynamics. NMR provides a detailed picture of the inclusion complexes, at least through four different and independent pieces of information (Schneider HJ, 1998). In the first place, one can simply measure complexation shifts, i.e. the difference between free and bound resonance frequency (in ppm) for the same nucleus; secondly, one can take advantage of through-space proximity of nuclei on the host and the guest molecule, by means of ROESY; third one can build a Job's plot and finally one can measure a decreasing of the diffusion coefficient, due to the fact that when the verbascoside is included, it assumes the same (slower) dynamic behaviour of cyclodextrin (Brand T, 2005). First of all, the difference between the chemical shifts of free and complexed verbascoside for the same nucleus were measured in order to understand which proton were mainly involved in the complexation. In figures **24** and **25**, the ^{1}H NMR spectra of verbascoside in D_2O and verbascoside in a satured solution of β-CDs.

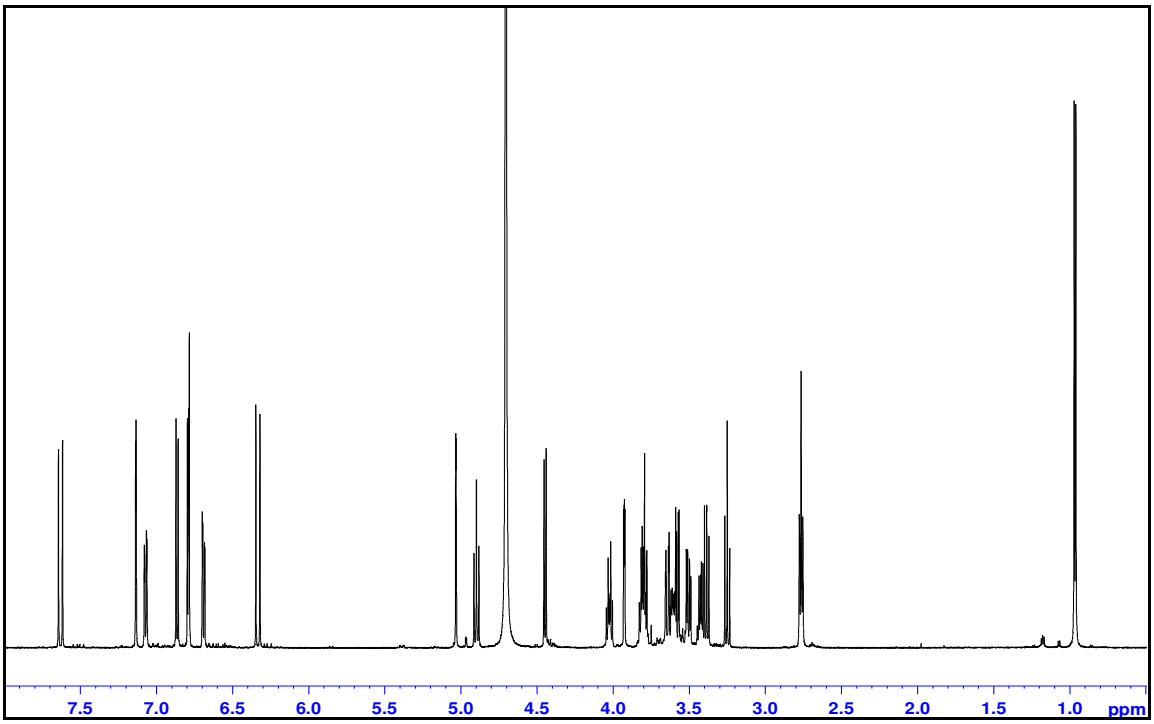

Fig 24. ^{1}H NMR spectrum of verbascoside in D_2O

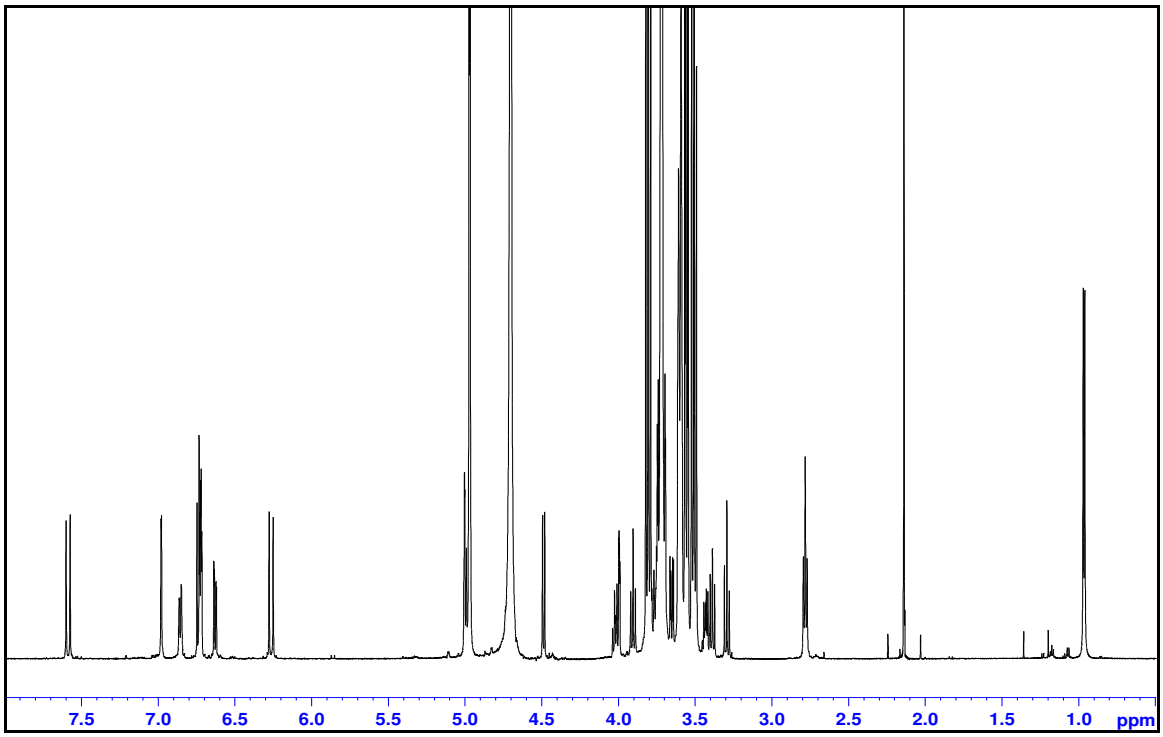

Fig 25. ^{1}H NMR spectrum of verbascoside-βCDs complex in D_2O.

Following table reports the complexation shifts Δδ for verbascoside alone and in presence of β-cyclodextrin. This compound features a certain scatter in the complexation shifts. The assignment of the peaks was unambiguously made by 2D spectra like COSY.

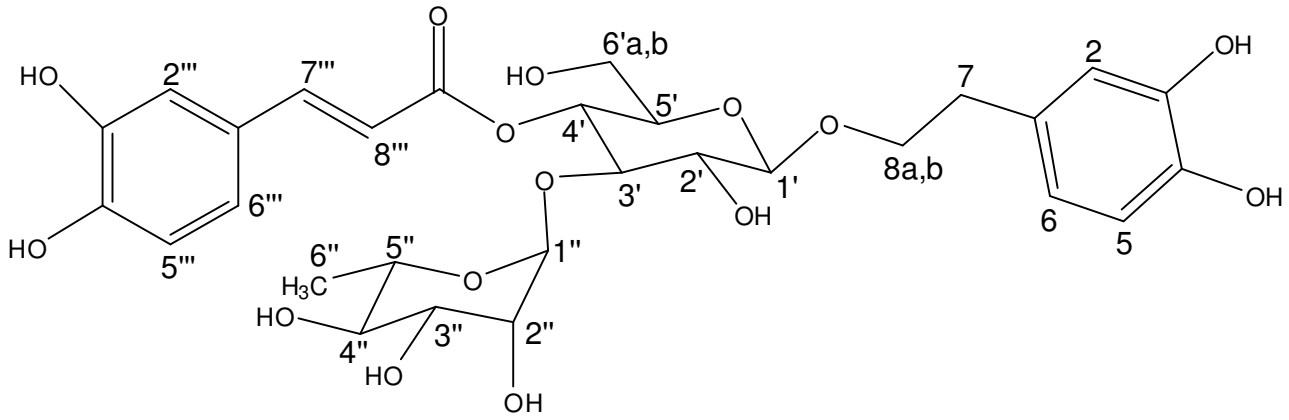

δ (ppm) verbascoside	δ (ppm) verbascoside-βCDs complex	Δδ (ppm)	No. H		
					aglycon
6.7919	*		1	d	**H-2**
6.7869	*		1	d	**H-5**
6.6902	6.6295	0.0607	1	dd	**H-6**
2.7647	2.7831	0.0184	2	dd	**H-7a,b**
4.0241	4.0180	0.0061	1	m	**H-8a**
3.7933	3.9056	0.1123	1	m	**H-8b**
					glucose
4.4466	4.4889	0.0423	1	d	**H-1'**
3.3849	3.3885	0.0036	1	dd	**H-2'**
3.8040	*		1	dd	**H-3'**
4.8975	4.9707	−0.0732	1	dd	**H-4'**
3.6438	*		1	m	**H-5'**
3.4226	*		1	dt	**H-6'a**
3.5038	*		1	dd	**H-6'b**
					rhamnose
5.0322	5.0033	0.0289	1	d	**H-1''**
3.9266	3.9967	−0.0701	1	dd	**H-2''**
3.5773	3.6542	−0.0769	1	dd	**H-3''**
3.2499	3.2944	−0.0445	1	t	**H-4''**
3.6100	*		1	m	**H-5''**
0.9653	0.9661	−0.0008	3	d	**H-6''**
					caffeoyl
7.1349	6.9808	**0.1541**	1	d	**H-2'''**
6.8641	6.7981	0.0660	1	d	**H-5'''**
7.0709	6.8569	**0.2140**	1	dd	**H-6'''**
7.6299	7.5877	0.0422	1	d	**H-7'''**
6.3335	6.2645	0.0690	1	d	**H-8'''**

* Peaks were completely or partially submerged, so it was not possible to figer out the chemical shift, neither with the help of bidimensional spectra.

The complexation shifts Δδ for verbascoside alone and in presence of β-cyclodextrin involved all the nuclei, so this is the a clue that an interaction between host and guest happened. The signals assigned to the protons H2''' and H6''' of the caffeoyl moiety were the most affected with or without the presence of β-CDs; in addition, the signals of these protons were isolated, not overlapped with peaks of the β-cyclodextrin, so can be monitored in order to understand the stoichiometry ratio of the complex by Job's plot analysis. In the figure **26** an enlargement of the 1H spectrum shows the Δδ in ppm in the aromatic region related to H2''' and H6'''.

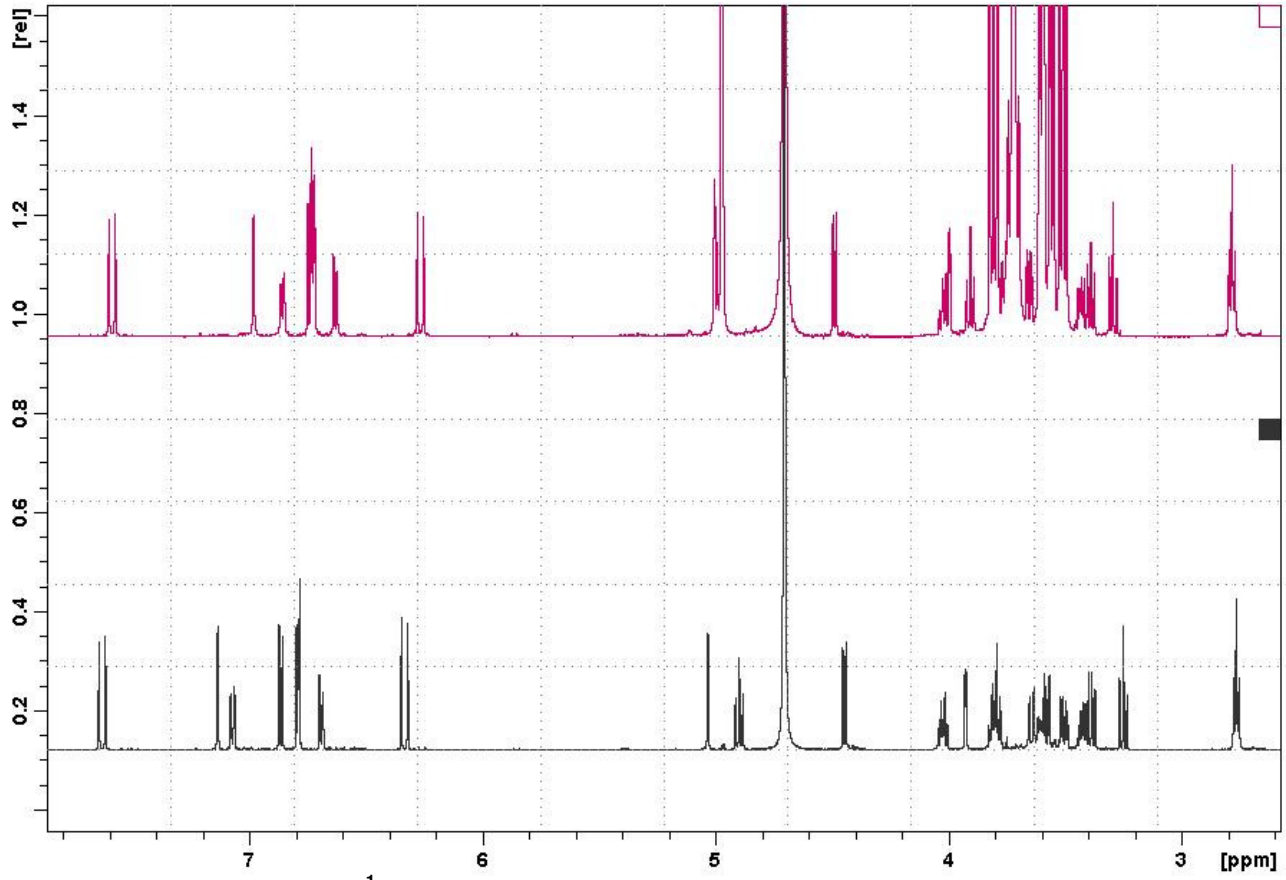

Fig 26. Zoom of overlapped ^{1}H NMR of verbascoside with (up) or without (down) the presence of β-CDs.

Starting from monodimensional NMR spectroscopy, protons H2''' and H6''' of the caffeic acid moiety of verbascoside were involved in the formation of the complex between verbascoside and β-CDs.
Secondly, one can take advantage of through-space proximity of nuclei on the host and the guest molecule, by means of ROESY; the network of intermolecular contacts for verbascoside included in β-CDs is depicted in figures **27** and **28**. The most relevant interactions are between the sugar proton H3' and the protons H2''', H5''' and H6''' of the caffeic acid moiety of verbascoside: these data confirm a deep inclusion of drug with the aromatic tail in the hydrophobic pocket of β-CDs, oriented toward the primary hydroxyl rim.

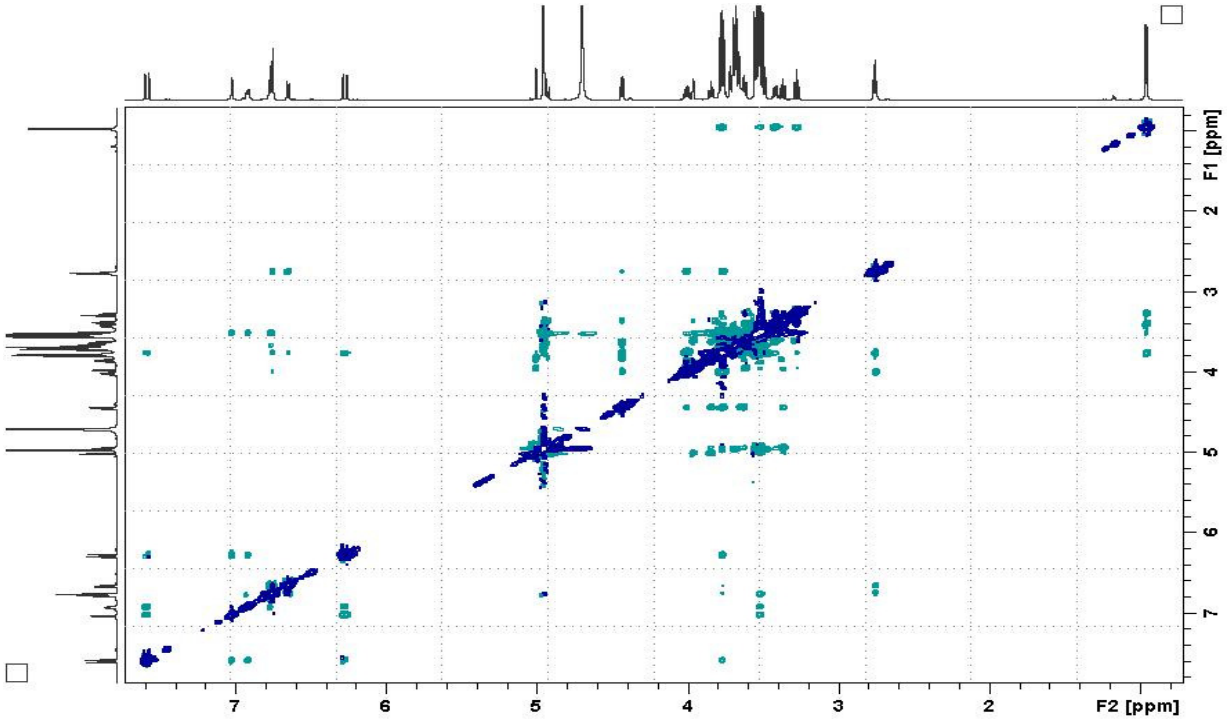

Fig 27. 2D ROESY spectrum of verbascoside-βCDs complex in D_2O.

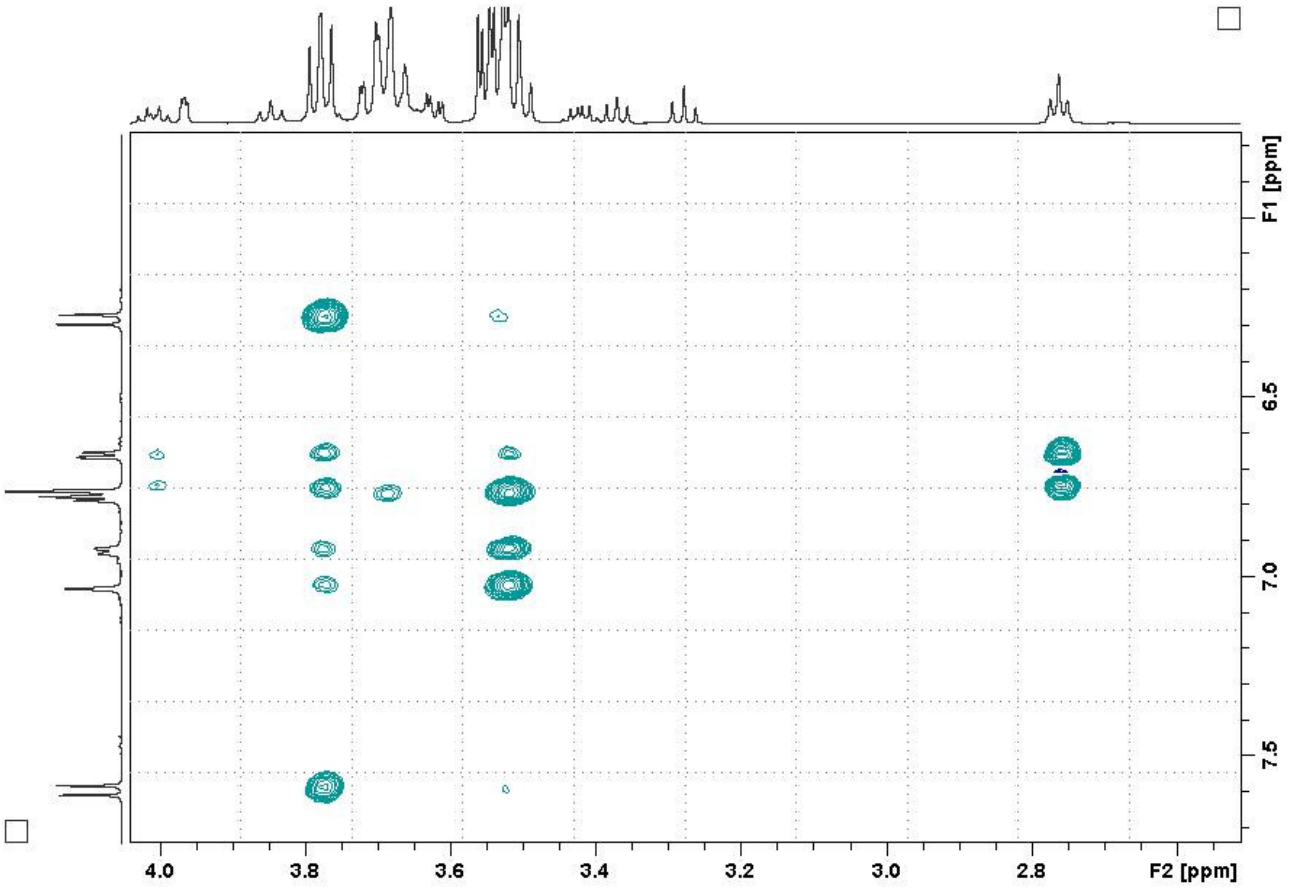

Fig 28. Partial 2D ROESY spectrum where cross peaks between H3' of β-CDs and H2''' and H6''' were found out.

The absence of other intermolecular contacts is a first strong indication of the existence of one well-defined 1:1 complex only. Different adduct stoichiometries (for example, β-CDs/guest 2:1) would necessarily lead to other contacts, e.g. involving the dihydroxyphenylethanol and β-CyD or two different β-CDs molecules. This conclusion is also confirmed by the Job's plot analysis discussed below. Figure **29** shows a representation of the interaction of verbascoside with β-cyclodextrin.

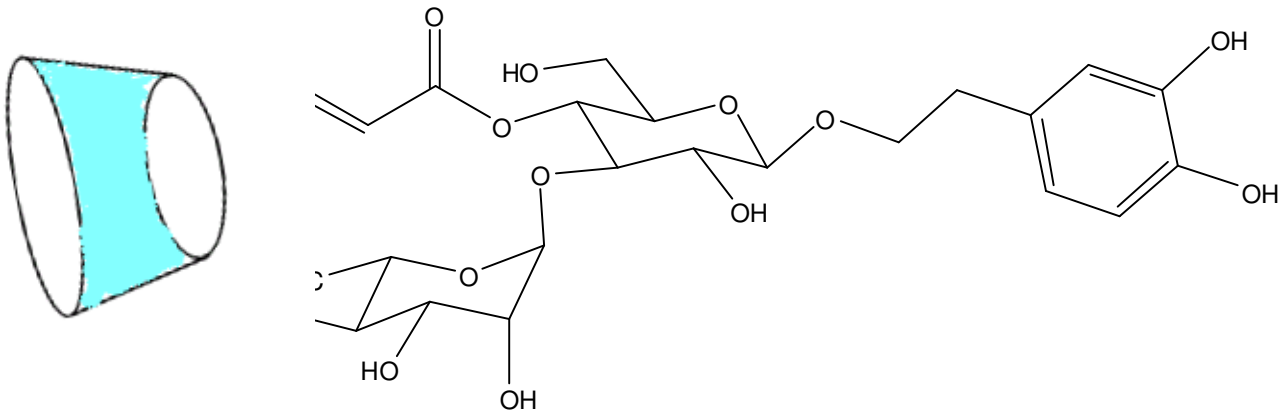

Fig 29. Schematic representation of verbascoside and its interaction with β-CDs.

In the case of verbascoside induced proton shifts and intermolecular ROE signals demonstrated that the caffeoyl moiety is deeply inserted in the cyclodextrin cavity.
H2''' and H6''' were selected for monitoring $\Delta\delta_{obs}$ during the continuous variation method because their shifts were more considerable and their peaks do not overlap with others.

II.3.2.2.b. Job's plot

A molecule and β-CDs may be in fast, intermediate or slow exchange with the complex molecule-β-CDs on the ^{1}H NMR time-scale (Connors KA, 1987). When a molecule and β-CDs are in a slow exchange with their complex, two signals for one specific proton can be seen in the spectrum, corresponding to complexed and uncomplexed molecule. When they are in a fast exchange, only one signal for a specific proton is observed. In the case of verbascoside and β-CDs, they are in a fast exchange and the doubt about the stoichiometry can be ascertained by a Job's plot.
An important step of a molecular complex is to determine its stoichiometry. This is frequently obtained by applying the method of continuous variations (Job's plot) (Connors KA, 1987; Job P, 1928; Bratu I, 2004; Zouvelekis D, 2002; Fielding L, 2000; Dodziuk H, 2004). This method is often applied with various analytical techniques, such as ^{1}H NMR, UV–vis spectroscopies or circular dichroism. In each case, the Job plot is based on the spectral change observed either for the host or the guest (Landy D, 2007).
Values of the experimentally observed spectral parameter (usually chemical shifts that are sensitive to complex formation) are determined for varying host (H) to guest (G) mole ratios where the sum of their concentrations is kept constant (Ejchart A, 2006; Job, 1928). The data are plotted as the product of guest mole fraction and its complexation induced shift versus host mole fraction (fig **30**). The ratio of mole fractions $X_G : X_H$ at the position of the maximum indicates the complex stoichiometry (Ejchart A, 2006).

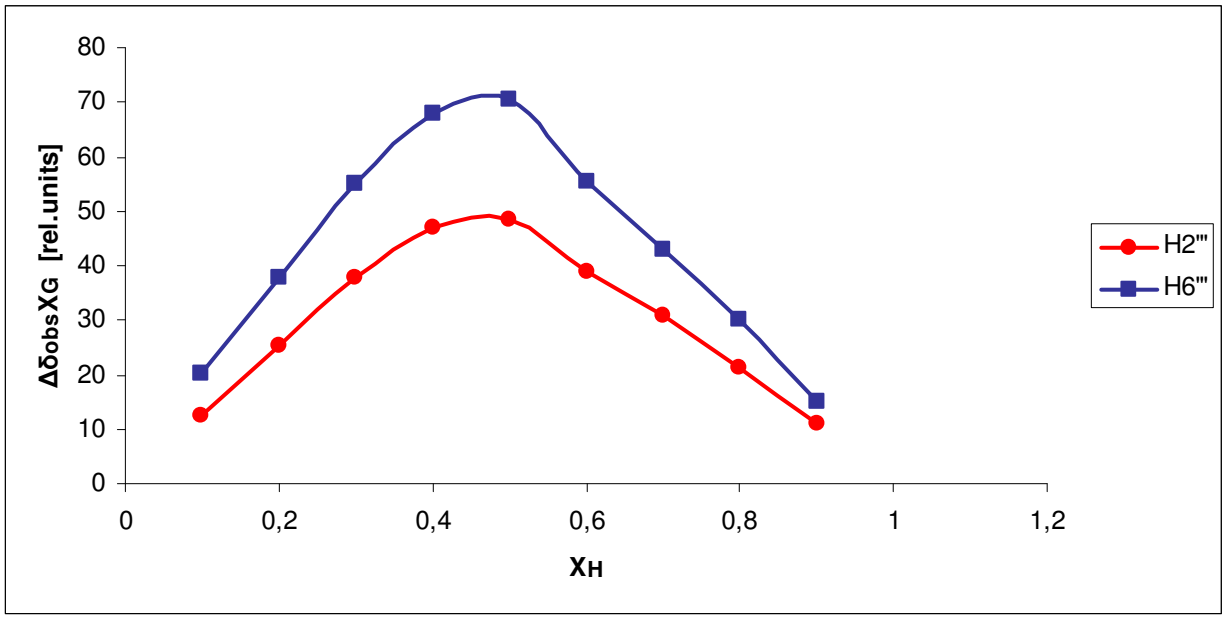

Fig 30. Job's plot

The Job's plots confirmed the 1:1 inclusion complex. The complexation happened when the ratio of mole fractions $X_G : X_H$ is 0.5 : 0.5.

II.3.2.2.c. Diffusion Ordered SpectroscopY

DOSY experiments were carried out in order to establish the inclusion of verbascoside in the β-CDs cavity. DOSY is based on diffusion coefficients which are different for free and complexed molecules and whose measurements make it possible to determine the binding constant between β-CDs and verbascoside.
While the above data provide a complete picture of the complex structure, they do not lend themselves to speculations on the magnitude of the association constant. This is due to the fact that the system is in fast exchange (on the NMR timescale) and consequently one observes resonances falling at the weighted average between the positions of the free and bound form. Nowadays is very easily performed on NMR instruments equipped with *z*-gradient coils (Johnson CS jr, 1999) in order to determinate the apparent binding constant by diffusion experiment. It is necessary to measure the diffusion coefficient of the guest alone D_F, of the host alone D_H, and of the mixture D_{mix}, in solution (Fielding L, 2000). Then, provided the host is large enough, one can approximate the diffusion coefficient of the bound complex to that of the host alone ($D_B \approx D_H$), which amounts to saying that complexation is only a minor perturbation to the host. In such a case, the following equation holds:

$$x_B = \frac{D_F - D_{mix}}{D_F - D_B} \approx \frac{D_F - D_{mix}}{D_F - D_H}$$

where x_B is the mole fraction of the bound drug.
The DOSY spectra in figure **31** clearly demonstrate that in the presence of β-CDs the translational diffusion of verbascoside is sizably slowed down with respect to the free drug, although it is not completely reduced to that of the macrocycle.

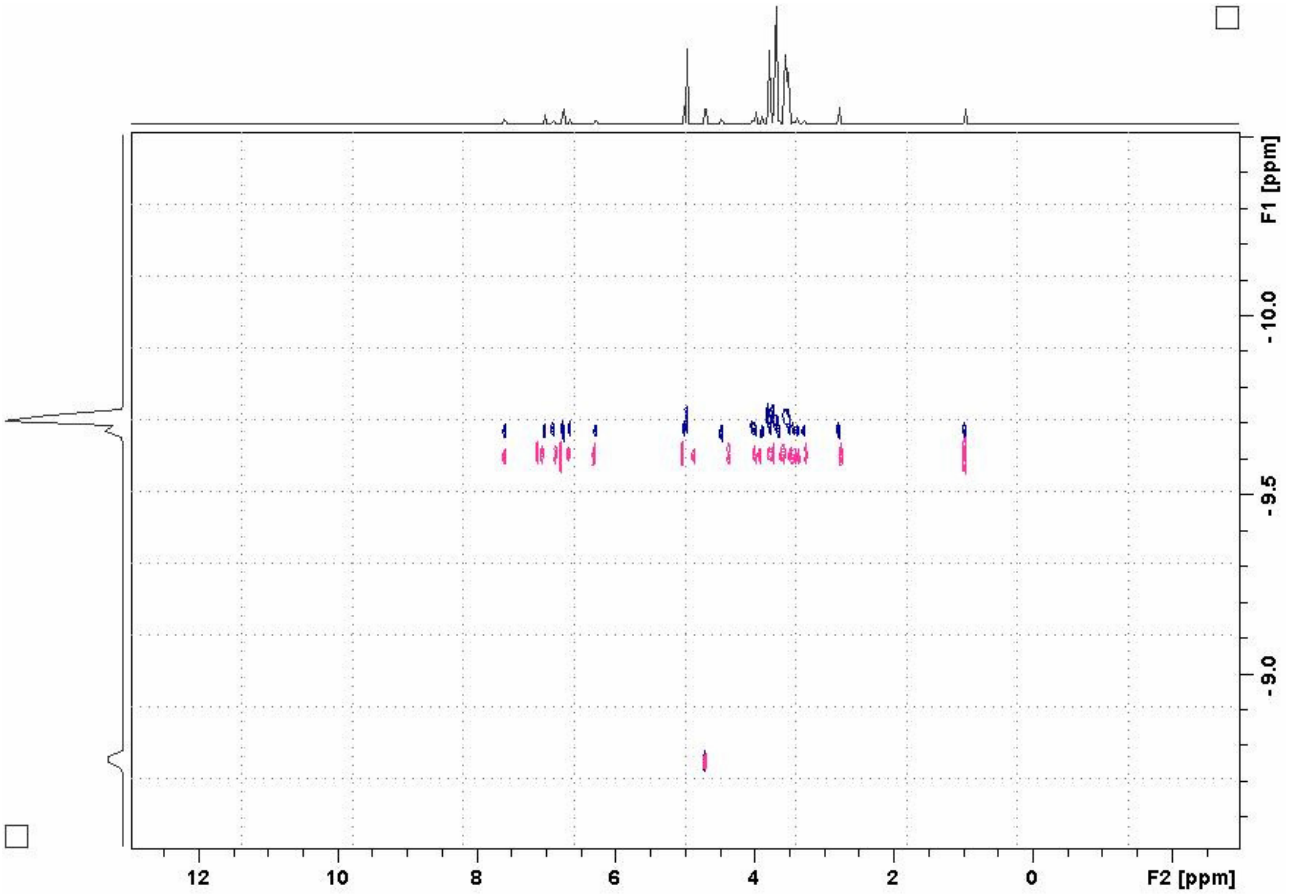

Fig 31. Overlapped DOSY of verbascoside with (up) or without (down) the presence of β-CDs.

sample in D_2O		diffusion	diffusion rate (m/s^2)
verbascoside	D_F	–9.611	2.45×10^{-10}
β-CDs	$D_B \approx D_H$	–9.714	1.93×10^{-10}
verbascoside + β-CDs	D_{mix}	–9.685	2.06×10^{-10}

This confirms that we are indeed in the presence of a free/bound equilibrium, and by means of the previous equation:

$$\frac{(2.45 - 2.06) \times 10^{-10}}{(2.45 - 1.93) \times 10^{-10}} = \frac{0.39}{0.52} = 0.75$$

We can estimate the extent of inclusion to about $x_B \approx 75\%$ for verbascoside in D_2O; owing to the approximations introduced above, no more accurate figures can be provided.
Diffusion ordered spectroscopy (DOSY), a high-resolution NMR technique which was used extensively to study supramolecular aggregates and solubilisation processes.
Compared to other techniques NMR spectroscopy provides a superior method to study complexation phenomena , because guest and host molecules are simultaneously observed at the atomic level.

II.3.3. Stability

II.3.3.1. Stability test of verbascoside-loaded liposomes

The physical stability of a liposome formulation is determined by its colloidal behaviour and its ability to retain the cargo for long periods during storage. The liposomes should ideally remain intact upon dilution or changes in the ionic strength, as typically encountered during administration. From a thermodynamical point of view it is notable that plain liposomes are not at equilibrium but represent kinetically trapped systems. Hence, their structures are relatively stable upon dilution, whereas thermodynamically reversible systems such as micelles and microemulsions would immediately aggregate or disintegrate (Chung H, 2001). If the liposomal dispersion is physically stable, phenomena of aggregation, disaggregation or fusion of the vesicles will not occur.
Chemical stability of the lipids during storage is another point of concern, especially against hydrolysis, and in the case of unsaturated lipid chains also against oxidation (Ulrich AS, 2002). If the liposomal dispersion is chemically stable, phenomena of leakage and chemical degradation of the delivered drug will not happen.
Verbascoside-loaded liposomes were kept at 4℃±1℃ for 3 months and their physical and chemical stability were assessed.

day after preparation	mean diameter (nm)	retained verbascoside (%)
1	120.15±14.85	100±0.2
7	120.95±22.27	97±1.4
30	125.97±19.09	97±1.2
90	163.26±19.85	91±3.4
180	-	83±2.7

Stability studies (DLS measurements and TEM visualization) pointed out that vesicles were physically stable for 90 days and neither verbascoside leakage nor vesicle size alteration occurred during this period. Moreover, no verbascoside degradation occurs over the whole period. This results suggest that verbascoside concentration in the aqueous phase of the vesicles is always closed to saturation.

II.3.3.2. Stability test of the inclusion complex

The inclusion complex was kept at room temperature covered by sunlight and verbascoside chemical stability was checked within 1 month.

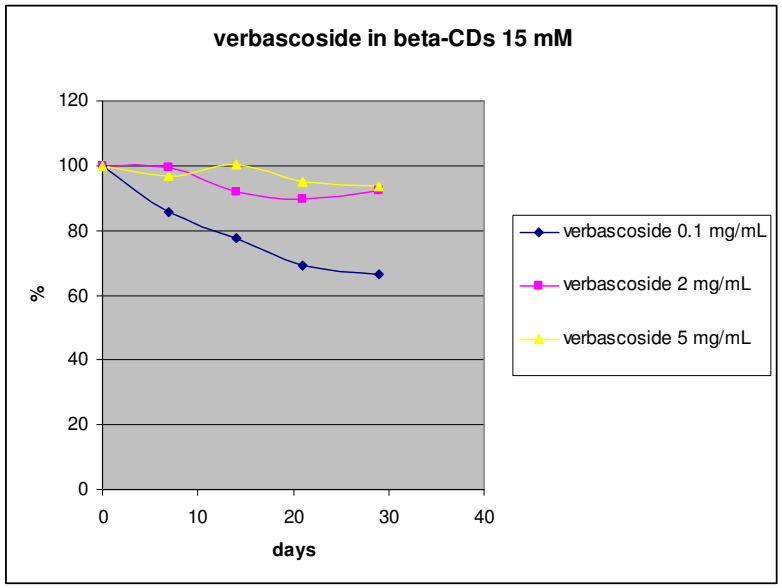

Fig 32. Stability in time of verbascoside-β-CDs inclusion complex.

The inclusion complexes containing verbascoside at concentrations of 2 and 5 mg/mL were stable for the whole tested period; verbascoside, cheched by HPLC/DAD analysis, is not degradated for more than 95%.

II.3.4. *In vitro* experiment: skin permeation studies

A Franz diffusion cell methodology has been performed with the aim to understand if carriers like liposomes or ethosomes will be able to delivery verbascoside, once topically applied, to deeper subcutaneous regions.
Results of *in vitro* permeation study of different formulations through pig skin were summarized in the following table (SC strato corneum; E epidermis; D derma).

formulation	Permeated drug (µg x cm^2)	Accumulated drug (µg x cm^2)		
		SC	E	D
verbascoside	–	–	–	–
verbascoside-loaded liposomes	–	430±75	75±18	–
verbascoside-loaded ethosomes	–	17.72±1.5	0.90±0.01	–

Results reported in table show that verbascoside-loaded liposomes promoted drug accumulation into the stratum corneum, but they did not give rise to any significant transdermal verbascoside delivery. Verbascoside crossed the skin layers to the epidermis only with a low amount. Ethosomes were really deluding and it make no sense to develop this kind of formulation with additional studies or *in vivo* experiments.

II.3.5. *In vivo* experiment: antihyperalgesic activity

The antihyperalgesic activity of pure verbascoside was investigated in two animal models of neuropathic pain: CCI and MIA. In the MIA model, the intra-articular injection of sodium monoiodioacetate produce an inflammation; so drugs able to revert this hyperalgesia will be active against chronic inflammation. On the other hand, in the case of CCI model, a peripheral mono neuropathy was produced in rats thank to the constriction of sciatic nerve; so drugs able to revert this hyperalgesia will be active against neuropathic pain. To the best of our knowledge no study has been reported on the activity of verbascoside on neuropathic pain, a widespread disorder induced by autoimmune diseases, drug or toxin exposure, infections, metabolic insults or trauma. As a consequence, nerve damage may cause muscle weakness, altered functionalities and sensitivity, and a chronic pain syndrome characterized by allodynia (pain elicited by a nonnoxious stimulus) and hyperalgesia (increased pain response to a noxious stimulus) which can persist long after the initial injury is resolved (Woolf CJ, 1999). The underlying molecular mechanisms are still not completely understood, and as a consequence, treatment is unsatisfactory in many cases (Syndrup SH, 1999). Therefore, there is an urgent need to develop novel therapeutics for an effective treatment of neuropathic pain.
In the Paw pressure test, paw withdrawal threshold was measured exerting a force that increases at constant rate (32 g/s). Stimulus at which rats withdrew the paw was recorded before treatment and after drug administration at different times (15, 30, 45 and 60 min). The results represent means ± SEM of the mechanical threshold expressed as grams.
Figure **33** shows the positive controls used as reference compounds in both of the two models of neuropathic pain in the rat paw-pressure test.

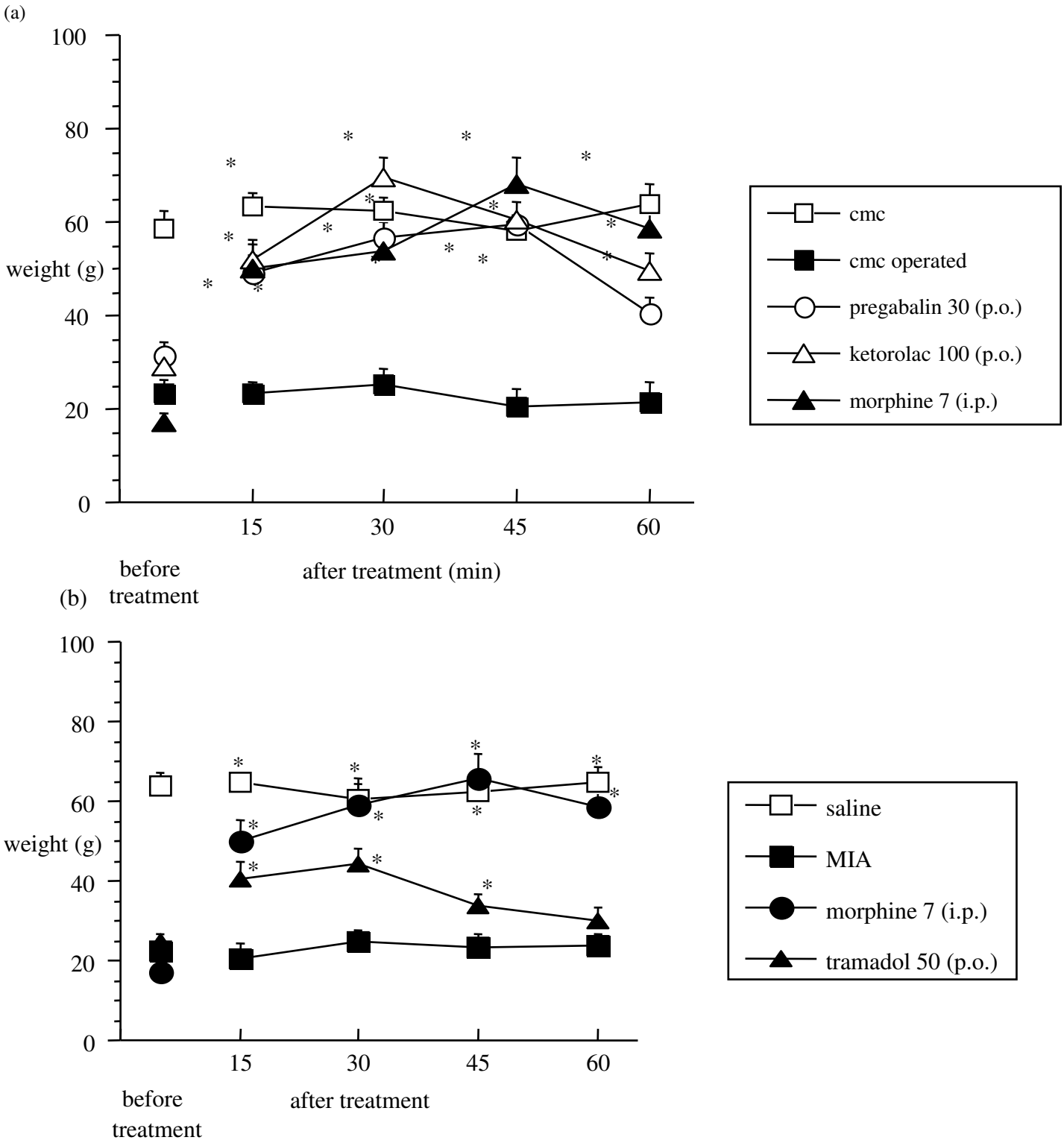

Fig 33. Positive controls used as reference compounds in a chronic constriction injury of the sciatic nerve (a) and in an intra-articular injection of sodium monoiodoacetate (b) in the rat paw-pressure test.

II.3.5.1. In vivo antihyperalgesic activity: comparison of the behaviour of verbascoside and verbascoside-loaded liposomes administered intraperitoneally

Verbascoside was unable to increase the pain threshold in naïve animals, showing the lack of any analgesic activity at the dosages of 50 and 100 mg/kg i.p. (fig **34**). We can, therefore, exclude that the antihyperalgesic activity of verbascoside was a consequence of its analgesic properties.

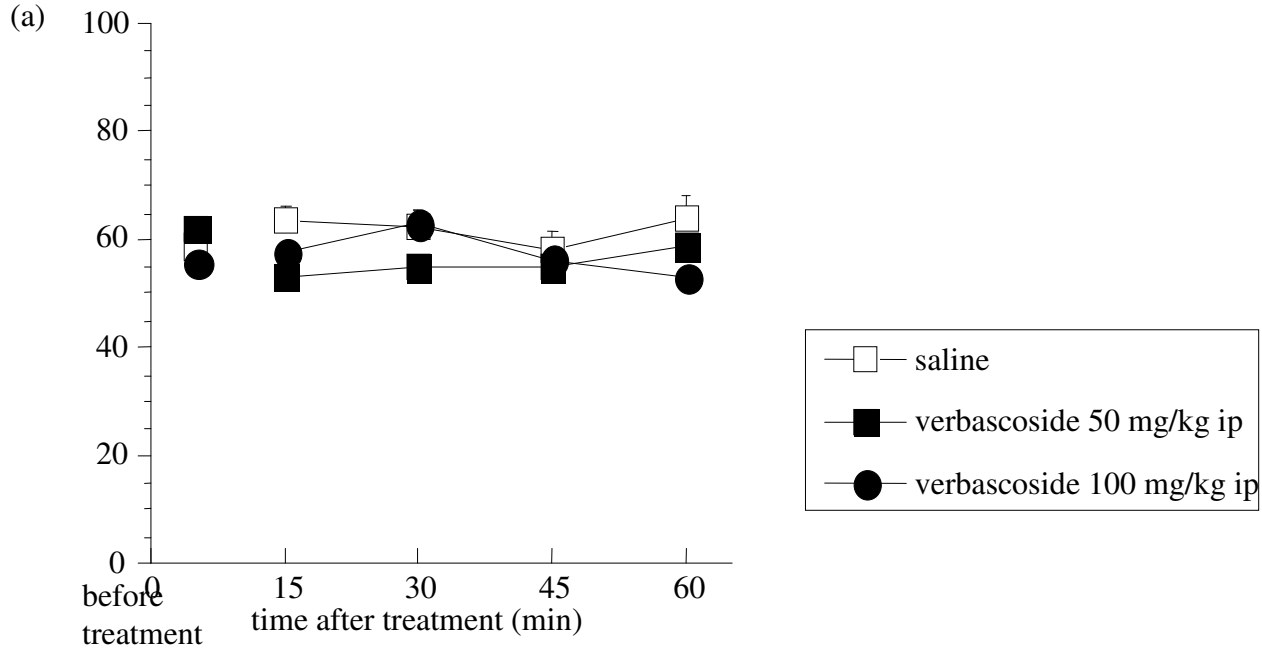

Fig 34. At the dosages of 50 and 100 mg/kg i.p. verbascoside shows the lack of any analgesic activity, in the rat paw-pressure test.

The antihyperalgesic effect of verbascoside was not prevented by pre-treatment with the opioid antagonist naloxone, suggesting that verbascoside does not require the activation of the opioid system to reverse hyperalgesia (data not shown).
First of all, there were no suggestions about the active dosage (if existing) of verbascoside i.p. in these animal models. So, several dosage of pure verbascoside, dissolved in physiological solution, were administered in order to find the active and the lowest dosage.
Verbascoside, when administered intraperitoneally at the dose of 100 mg/kg reverted the mechanical hyperalgesia, evaluated in the paw pressure test in CCI treated rats (fig **35A**). The antihyperalgesic effect started 15 min after administration and persisted up to 30-45 min. By contrast in the controlateral paw the pain perception remained unchanged.
In the case of MIA treated rats (fig **35B**) verbascoside was active 15 min after administration and persisted up to 30-45 min, when administered intraperitoneally (i.p.) at the same dosage of 100 mg/kg.

A liposome formulation containing verbascoside 100 mg/kg administered i.p. showed a longer lasting antihyperalgesic effect in comparison with a 100 mg/kg verbascoside saline solution. The effect appeared 15 min after administration and persisted up to 60 min in both models investigated (fig **35A,B**). The intensity of the effect of the liposome formulation was comparable to that showed by the verbascoside saline solution (fig **35A,B**).

Effect of verbascoside and of verbascoside-loaded liposomes in a chronic constriction injury of the sciatic nerve (CCI) evaluated in the Paw-pressure test.

treatment i.p.	Paw pressure test in rats (g)											
	before treatment		after treatment									
			15 min.		30 min.		45 min.		60 min.		75 min.	
	sn	dx	sn	dx	sn	dx	sn	dx	sn	dx	sn	dx
verbascoside 50 mg/kg	61.9±1.2	30.0±1.2	53.0±3.7	35.6±2.4	55.0±1.2	24.4±2.4	55.0±1.2	22.2±1.2				
verbascoside 100 mg/kg	55.9±1.2	29.6±1.2	57.6±1.7	38.9±1.0*	63.0±2.1	42.0±1.2*	56.3±1.5	37.6±1.1*	53.0±0.7	32.2±0.9		
verbascoside-loaded liposomes 100 mg/kg	55.9±1.2	30.0±0.8	55.2±1.4	37.2±1.1*	58.5±1.6	42.8±1.5*	60.9±2.0	45.9±1.2*	56.1±2.0	38.7±1.6*	51.1±1.4	33.1±0.9

*P<0.05 in comparison with pretest dx (antihyperalgesic effect).

Effect of verbascoside and of verbascoside-loaded liposomes in an intra-articular injection of sodium monoiodoacetate (MIA) evaluated in the Paw-pressure test.

treatment 100 mg/kg i.p.	Paw pressure test in rats (g)											
	before treatment		after treatment									
			15 min.		30 min.		45 min.		60 min.		75 min.	
	sn	dx	sn	dx	sn	dx	sn	dx	sn	dx	sn	dx
verbascoside 50 mg/kg	60.9±1.2	31.7±2.1	53.0±3.7	39.6±2.3*	52.0±1.2	31.7±1.0	53.0±1.2	30.0±1.6				
verbascoside 100 mg/kg	55.9±1.2	32.3±3.1	56.6±1.7	42.0±2.5*	64.0±2.1	44.6±1.0*	56.1±1.5	36.8±1.1*	51.0±0.7	31.3±1.3		
verbascoside-loaded liposomes 100 mg/kg	54.9±1.2	32.3±0.7	55.3±1.4	39.3±0.7*	58.7±1.6	43.0±0.8*	59.9±2.0	45.7±0.7*	56.4±2.0	38.7±1.0*	50.1±1.4	34.3±0.4

*P<0.05 in comparison with pretest dx (antihyperalgesic effect).

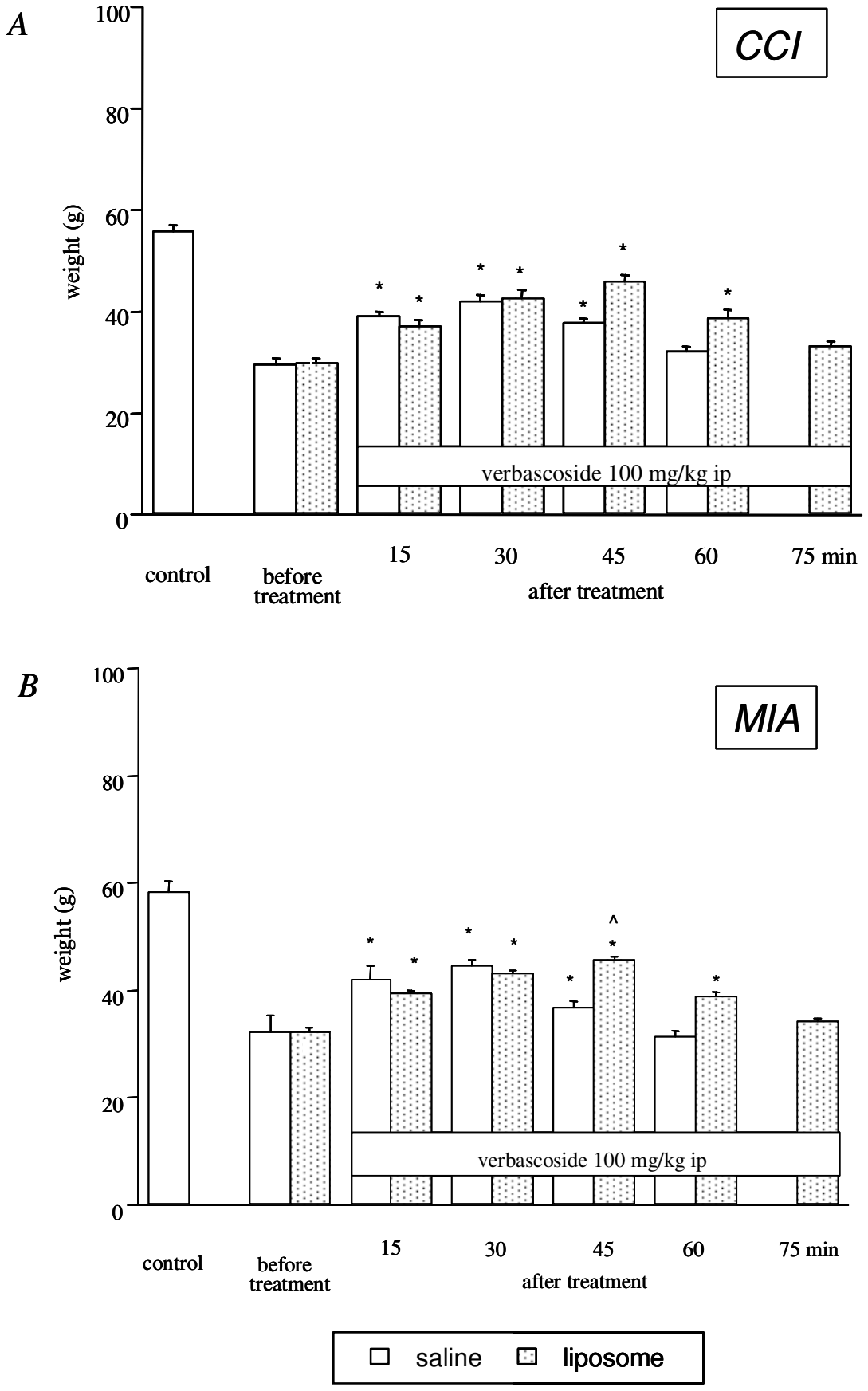

Fig 35. Effect of verbascoside and of verbascoside-loaded liposomes in a chronic constriction injury of the sciatic nerve (A) and in an intra-articular injection of sodium monoiodoacetate (B) evaluated in the Paw-pressure test.

II.3.5.2. In vivo antihyperalgesic activity: comparison of the behaviour of verbascoside and verbascoside-βCDs inclusion complex administered orally

Verbascoside was also effective against mechanical hyperalgesia when orally administered. At the doses of 300 and 600 mg/kg p.o. (fig **36**) as well as 50 and 100 mg/kg i.p. (fig **34**), verbascoside was unable to increase the pain threshold in naïve animals, showing the lack of any analgesic activity.

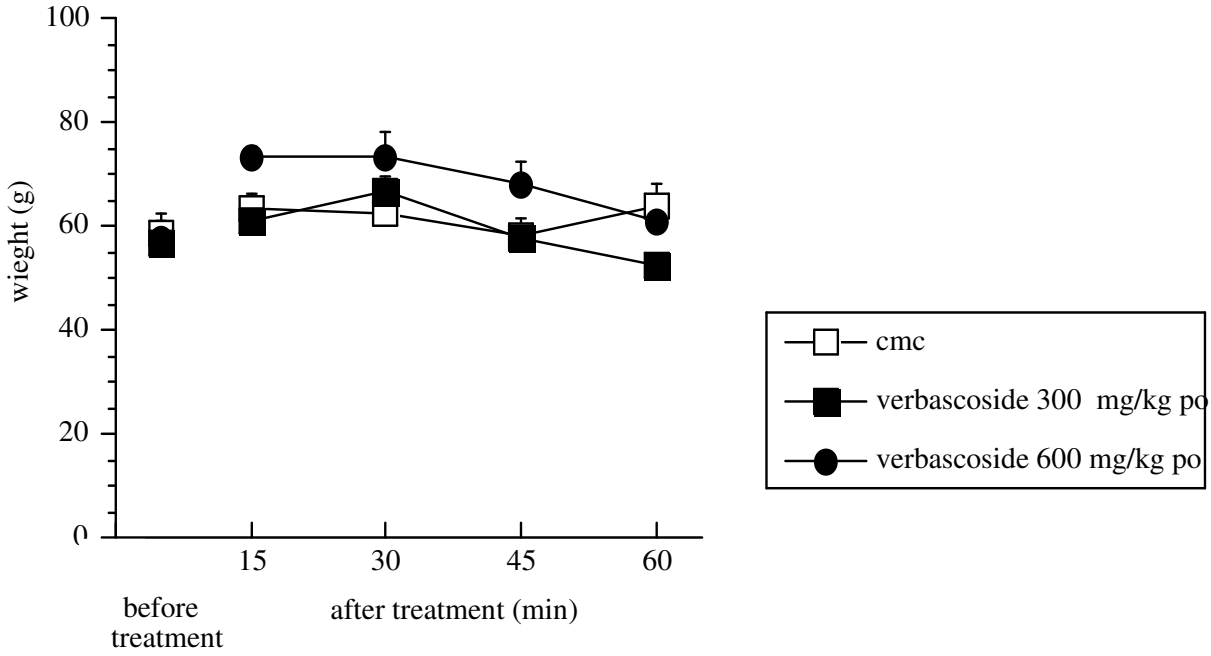

Fig 36. At the dosages of 300 and 600 mg/kg p.o., verbascoside shows the lack of any analgesic activity, in the rat paw-pressure test.

At the dosages of 300 and 600 mg/kg p.o. it reverted the hyperalgesia induced by both CCI (fig **37A**) and MIA injection with a long lasting effect (fig **37B**): the antihyperalgesic effect started 15 after administration and was still significant at 45 min.

Conversely by the liposomal formulation, a β-cyclodextrin formulation containing verbascoside 300 mg/kg showed the same antihyperalgesic profile of 300 mg/kg verbascoside saline solution when orally administered in both CCI (fig **37A**) and MIA injected (fig **37B**) rats.

Effect of verbascoside and of verbascoside-β-CDs complex in a chronic constriction injury of the sciatic nerve (CCI) evaluated in the Paw-pressure test.

treatment p.o.	Paw pressure test in rats (g)											
	before treatment		after treatment									
			15 min.		30 min.		45 min.		60 min.		75 min.	
	sn	dx	sn	dx	sn	dx	sn	dx	sn	dx	sn	dx
verbascoside 300 mg/kg	56.7±1.4	34.6±0.8	60.8±4.2	47.5±0.8*	66.6±3.0	52.4±0.8*	57.5±0.8	45.0±1.7*	52.5±0.8	38.3±1.0		
verbascoside-β-CDs complex 300 mg/kg	55.0±3.5	34.2±1.6	58.3±4.4	45.8±1.6*	64.1±2.1	51.7±2.1*	55.8±1.6	42.5±0.8*	55.8±1.6	36.7±1.4		
verbascoside 600 mg/kg	57.5±3.7	33.3±2.9	73.3±2.0 ^	50.0±4.0*	73.3±5.0^	60.8±5.1*	68.3±4.3 ^	58.3±7.2*	60.8±4.7	45.0±4.3*	48.3±5.2	36.7±2.9

*P<0.05 in comparison with pretest dx (antihyperalgesic effect).

Effect of verbascoside and of verbascoside-β-CDs complex in an intra-articular injection of sodium monoiodoacetate (MIA) evaluated in the Paw-pressure test.

treatment 300 mg/kg p.o.	Paw pressure test in rats (g)											
	before treatment		after treatment									
			15 min.		30 min.		45 min.		60 min.		75 min.	
	sn	dx	sn	dx	sn	dx	sn	dx	sn	dx	sn	dx
verbascoside 300 mg/kg	56.8±1.4	31.7±0.6	56.7±1.4	38.5±0.6*	55.7±1.4	43.9±1.0*	54.7±1.4	38.9±0.7*	58.7±1.4	30.7±1.0		
verbascoside-β-CDs complex 300 mg/kg	54.0±3.5	31.7±0.6	55.1±3.5	37.5±0.4*	55.3±3.5	45.0±1.0*	53.0±3.5	39.2±0.4*	55.3±3.5	35.0±0.7		
verbascoside 600 mg/kg	56.5±3.7	30.0±2.4	55.5±3.7	44.2±3.4*	58.5±3.7	50.0±3.0*	57.4±3.7	41.7±1.7*	57.8±3.7	35.0±1.0		

*P<0.05 in comparison with pretest dx (antihyperalgesic effect).

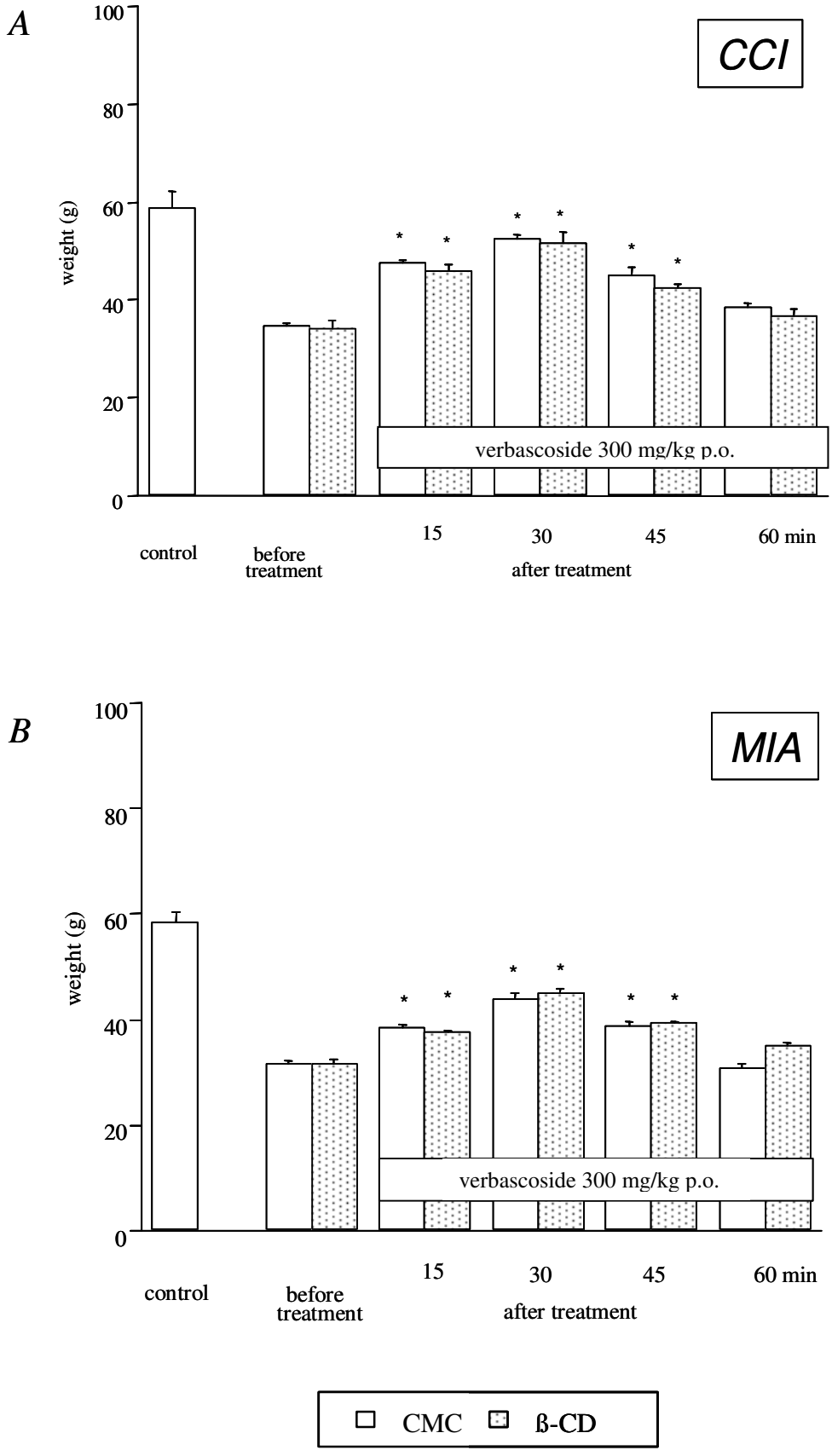

Fig 37. Effect of verbascoside and of verbascoside-βCDs complex in a chronic constriction injury of the sciatic nerve (A) and in an intra-articular injection of sodium monoiodoacetate (B) evaluated in the Paw-pressure test.

II.3.5.3. Rota rod test

The safety of verbascoside was also demonstrated. Verbascoside did not modify animals' gross behaviour at the highest effective doses. The Rota-rod test was also employed to unmask any alterations of the motor coordination induced by the compound investigated. The number of falls from the rotating rod showed the lack of any impairment in the motor coordination of animals treated with verbascoside in comparison with the control group, ruling out that the results obtained were due to animals' altered viability. During each session the number of falls of mice with unaltered locomotor activity decreases since animals learn how to balance on the rotating rod. The results were summarized in the following table.

treatment	**dose (mg/kg) p.o.**	**before treatment**	**after treatment**		
			15 min.	**30 min.**	**45 min.**
CMC		3.6 ± 0.3	2.2 ± 0.4	1.9 ± 0.3	1.2 ± 0.3
verbascoside	1000	3.9 ± 0.4	2.5 ± 0.3	2.1 ± 0.3	0.7 ± 0.2

Each value represents the mean of 5 mice.

II.4. References

- Akbay P, Calis I, Ündeger U, Basaran N, Basaran AA. **2002**. *In vitro* immunomodulatory activity of verbascoside from *Nepetya ucrainica* L. *Phytoter Res* 16(6): 593-595.
- Andary C, Wylde R, Laffite C, Privat G, Winternitz F. Phytochemistry. **1982**, 21, 1123.
- Astray G, Gonzalez-Barreiro C, Mejuto JC, Rial-Otero R, Simal-Gandara JA. **2009**. A review on the use of cyclodextrins in foods. *Food hydrocolloids*. 23, 1631-1640.
- Avila Acevedo JG, Castaneda CMC, Benitez FJC, Duran DA, Barroso VR, Martinez CG, Munoz LJL,Martinez CA, Romo de Vivar A. **2005**. *Fitoterapia*. 76, 301-309.
- Backhouse N, Delporte C, Apablaza C, Farías M, Goïty L, Arrau S, Negrete R, Castro C, Miranda H. **2008**. Antinociceptive activity of *Buddleja globosa* (matico) in several models of pain. *Journal of Ethnopharmacology* 119, 160–165.
- Bakkour Y, Vermeersch G, Morcellet M, Boschin F, Martel B, Azaroual N. **2006**. Formation of cyclodextrin inclusion complexes with doxycyclin-hyclate: NMR investigation of their characterization and stability. *Journal of Inclusion Phenomena and Macrocyclic Chemistry* 54, 109-114.
- Bangham AD, Standish MM, Watkins JC. **1965**. Diffusion of univalent ions across the lamellae of swollen phospholipids. *J Mol Biol* 13, 238-252.
- Bennett GJ, Xie YK. **1988**. A peripheral mononeuropathy in rat that produces disorders of pain sensation like those seen in man. *Pain* 33(1), 87-107.
- Bilia AR, *et al.* **2002.** *J Pharm Sci* 91, 2265–2270.
- Bilia AR, Giomi M, Innocenti M, Gallori S, Vincieri FF. **2008**. HPLC/DAD/ESI-MS analysis of the constituents of aqueous preparations of verbena and lemon verbena and evaluation of the antioxidant activity. *J Pharm Biomed Anal* 46, 463-470.
- Birkofer R, Kaiser C, Thomas UZ. **1968**. *Naturforsch, Bchem. Sci*. 23, 1051.
- Brand T, Cabrita EJ, Berger S. **2005**. Intermolecular interaction as investigated by NOE and diffusion studies. *Prog. Nucl. Magn. Reson. Spectrosc*. 46, 159-196.
- Bratu I, Gavira-Vallejo JM, Hernanz A, Bogdan M, Bora G. **2004**. *Biopolymers* 73, 451.
- Calvo MI. **2006**. Anti-inflammatory and analgesic activity of the topical preparation of *Verbena officinalis* L. *J Ethnopharmacol* 107, 380-382.
- Chiou WF, Lin LC, Chen CF. **2004**. Acteoside protects endothelial cells against free radical-induced oxidative stress. *Journal of Pharmacy and Pharmacology* 56, 743–748.
- Chung H, *et al.* **2001**. Oil components modulate physical characteristics and function of the natural oil emulsions as drug or gene delivery system. *J. Control Release* 71, 339–350.
- Connors KA. **1987.** Binding constant. Wiley Interscience, New York.
- Deepak M, Umashankar DC, Handa SS. **1999**. Verbascoside—a promising phenylpropanoid. *Indian Drugs* 36, 336–345.
- Diaz AM, Abad MJ. **2004.** *Life Sciences* 74, 2515-2526.
- Didry N, Seidel V, Dubreuil L, Tillequin F, Bailleul F. **1999**. *J.of Ethnoph.* 67, 197-202.
- Dodjiuk H, *et al.* **2004.** *Chirality* 16, 90-105.
- Efferth T, Lee PCH, Venkata S, Badireenath Konkimalla VS, Kaina B. **2007**. From traditional Chinese medicine to rational cancer therapy. *Trends in Molecular medicine* 13(8), 353-361.
- Ejchart A, Kozmiski W. **2006**. NMR of cyclodextrin and their complexes; In: Cyclodextrin and their complexes. Edited by Dodziuk H. Wiley-VCH. p.243.
- Fielding L. **2000**. Determination of Association Constants (K_a) from Solution NMR Data. *Tetrahedron* 56, 6151-6170.
- Fleer H, Verspohl EJ. **2007**. Antispasmodic activity of an extract from *Plantago lanceolata* L. and some isolated compounds. *Phytomedicine* 14(6), 409-415.
- Franz TJ. **1975**. Percutaneous absorption: on the relevance of *in vitro* data. *J. Invest. Dermatol.,* 64:190–5.

- Guingamp C, Gegout-Pottie P, Philippe L, Terlain B, Netter P, Gillet P. **1997**. Mono-iodoacetate-induced experimental osteoarthritis: a dose-response study of loss of mobility, morphology, and biochemistry. *Arthritis Rheum* 40(9), 1670-1679.
- Hausmann M, Obermeier F, Paper DH, Balan K, Dunger N, Menzel K, Flak W, Schoelmerich J, Herfarth H, Rogler G. **2007**. *In vivo* treatment with herbal phenylethanoid acteoside ameliorates intestinal inflammation in dextran sulphate sodium-induced colitis. *Clin Exp Immunol* 148(2), 373-381.
- Jiangshu Botanic Institute, Institute of Materia Medica CAMS, Kunming Botanic Institute. **1991**. *Xinhua Bencao Gangyao II*; Scientific and Technical Press: Shanghai.
- Job P. **1928**. Formation and stability of inorganic complexes in solution. *Ann. Chim*. 9, 113-203.
- Johnson CS Jr. **1999**. Diffusion ordered nuclear magnetic resonance spectroscopy: principles and applications. *Prog. Nucl. Magn. Reson. Spectrosc*. 34, 203-256.
- Kim SS, Son YO, Chun JC, Kim SE, Chung GH, Hwang KJ, Lee LC. **2005**. Antioxidant property of an active component purified from leaves of paraquat-tolerant *Rhemannia glutinosa. Redox Report* 10, 11–318.
- Koltzenburg M. **1998**. Painful neuropathies. *Curr Opin Neurol* 11, 515-521.
- Korkina LG, Mikhalchik E, Suprun MV, Pastore S, Dal Toso R. **2007**. Molecular mechanisms underlying wound healing and anti-inflammatory properties of naturally occurring biotecnologically produced phenylpropanoid glycosides. *Cell Mol Biol* 30, 84-91.
- Kupeli E, Sahin FP, Yesilada E, Calis I, Eze N. **2007**. *In vivo* anti-inflammatory and antinociceptive activity of phenolic compounds from *Sideritis stricta. Zeitschrift für Naturforschung C* 62, 519–525.
- Lai SW, Yu MS, Yuen WH, Chuen-Chung Chang R. **2006**. *Neuropharmacology* 50, 641-650.
- Landy D, Tetart F, Truant E, Blanch F, Fourmentin S, Surpateanu G. **2007**. Development of a competitive continuous variation plot for the determination of inclusion compound stoichiometry. *J Incl Phenom Macrocycl Chem* 57, 409-413.
- Lau CW, Chen ZY, Wong CM, Yao X, He Z, Xu H, Huang Y. **2004**. Attenuated endothelium-mediated relaxation by acteoside in rat aorta: Role of endothelial [Ca^{2+}] and nitric oxide/cyclic GMP pathway. *Life Sci* 75(10), 1149-1157.
- Lee JY, Woo ER, Kang KW. **2005**. Inhibition of lipopolysaccharide-inducible nitric oxide synthase expression by acteoside trough blocking of AP-1 activation. *J Ethnopharmacol* 97, 561-566.
- Lee KW, Kim HJ, Lee YS, Park HJ, Choi JW, Ha J, Lee KT. **2007**. Acteoside inhibits human promyelocytic HL-60 leukemia cell proliferation via inducing cell cycle arret at G0/G1 phase and differentiation into monocyte. *Carcinogenesis* 28(9), 1928-1936.
- Leighton GE, Hill RG, Hughes J. **1988**. Intrathecal injection of a opioid agonist produces hyperalgesia in the guinea pig. *Eu J Pharmacol* 157(1-2), 241-242.
- Liu MJ, Li JX, Guo HZ, Lee KM, Qin L, Chan KM. **2003**. The effects of verbascoside on plasma lipid peroxidation level and erythrocyte membrane fluidity during immobilization in rabbits: a time course study. *Life Sciences* 73, 883–892.
- Nakamura O, Okuyama E, Tsukada A, Yamazaki M, Satake H, Nishibe S, Deyama T, Moriya A, Maruno M, Nishimura H. **1997**. Acteoside as analgesic principle of Cedron (*Lippia triphylla*) Peruvian Medicinal Plant. *Chem Pharm Bull* 45(3), 499-504.
- Penido C, Costa KA, Futuro DO, Paiva SR, Kaplan MAC, Figueiredo MR, Henriques MGMO. **2006**. Anti-inflammatory and anti-ulcerogenic properties of *Stachytarpheta cayennensis* (L.C. Rich) Valh. *J Ethnopharmacol* 104(1-2), 225-233.
- Sahpaz S, Garbacki N, Tits M, Bailleul F. **2002**. Isolation and pharmacological activity of phenylpropanoid esters from *Marrubium vulgare. Journal of Ethnopharmacology* 79, 389–392.
- Sakurai A, Katu T. **1983**. *Bull. Chem.Soc. Jpn*. 56, 1573.
- Scarpati ML, Monache D. **1963**. *Ann. Chim*. 53, 356.

- Schapova E, Winter de Vargas M, Chaves C, Bridi R, Zuanazzi J, Henriques A. **1998**. Antinflammatory and antinociceptive activities of extracts and isolated compounds from *Stachytarpheta cayennensis. Journal of Ethnopharmacology* 60, 53–59.
- Schneider H.-J, Kacket F, Rüdiger V. **1998**. NMR Studies of Cyclodextrins and Cyclodextrin Complexes. *Chem. Rev.* 98, 1755-1785.
- Scogin R. **1992**. The distribution of acteoside among angiosperms. *Biochemical Systematics and Ecology* 20(5), 477-480.
- Sinico C, Caddeo C, Valenti D, Fadda AM, Bilia AR, Vincieri FF. **2008**. Liposomes as carriers for verbascoside: stability and skin permeation studies. *Journal of liposomes research* 18, 83-90.
- Sinico C, Valenti D, *et al.* **2006**. Cutaneous delivery of 8-methoxypsoralen from liposomal and niosomal carriers. *J. Drug Del. Sci. Tech.* 16(2), 115–20.
- Syndrup SH, Jensen TS. **1999**. Efficacy of pharmacological treatments of neuropathic pain: an update and effect related to mechanism of drug action. *Pain* 83, 389-400.
- Szejtli J, Szente L. **2005.** Elimination of bitter, disgusting tastes of drugs and foods by cyclodextrins. *European Journal of Pharmaceutics and Biopharmaceutics* 61, 115–125.
- Szejtli J. **1988**. Cyclodextrin Technology; Kluwer Accademic: Dordrecht.
- Touitou E, Dayan N, Eliaz M. **1997**. Ethosomes:novel vesicular carriers for enhanced skin delivery. *Pharm Res* 14, S305.
- Ulrich AS. **2002**. Biophysical Aspects of Using Liposomes as Delivery Vehicles. *Bioscience Reports* 22, No. 2,.
- Wannmacher L, Fuchs FD, Paoli CL, Fillman HS, Gianlupi A, Lubianca JF, Hassegawa CY, Guimaraes FS. **1990**. Plants employed in the treatment of anxiety and insomnia: II. Effect of infusions of *Aloysia triphylla*, on experimental anxiety in normal volunteers. *Fitoterapia* 61, 449–453.
- Woolf CJ, Mannion RJ. **1999**. Neuropathic pain: Aetiology, symptoms, mechanisms, and management. *Lancet* 353, 1959-1964.
- Wu D, Chen A, Johnson CS. **1995**. *J Magn Reson A* 115, 260.
- Zouvelekis D, Yannakopoulou K, Mavridis IM, Antoniadou-Vyza E. **2002**. The self-association of the drug ametacin and its interactions and stabilization with β-cyclodextrin in aqueous solution as inferred from NMR spectroscopy and HPLC studies.
- Zuidam NJ, de Vrueh R, Crommelin DJA. **2003**. Characteization of liposomes, In: Liposomes 2nd edition Oxford University Press edited by Torchilin V and Weisseg V, pag 53.

III. *trans*-Resveratrol

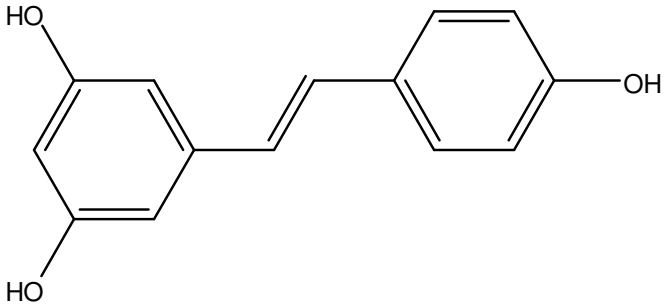

III.1. Introduction

The non-flavonoid phytoalexin trans-resveratrol (trans-3,5,4′-trihydroxystilbene) and its various derivatives are widely distributed in Gymnosperms and Dicotyledons (Gorham J, 1980; Ingham JL, 1976). *trans*-Resveratrol was discovered in 1976 in the grape vine, *Vitis vinifera* L., and was observed to occur there as a response to fungal infection or injury (Langcake P, 1976) is produced by plants in response to infection by the pathogen Botrytis cinerea (Delmas D, 2006). It is also induced in response to a variety of stress conditions, such as pedoclimatic conditions, exposure to ozone, sunlight and heavy metals (Bavaresco L, 2003).Later studies revealed trans-resveratrol in grape skins (Creasy LL, 1988; Jeandet P, 1991, 1995; Roggero JP, 1995) and more recently in wines (Goldberg DM, 1994, 1995; Vrhovsek U, 1995). *trans*-Resveratrol has been suggested as a cause for reduced CHD mortality in wine drinkers and numerous studies describe potential mechanisms by which trans-resveratrol could reduce heart disease (Trela BC, 1996). The roots of *P. cuspidatum* are traditionally used as a remedy or prevention for allergic inflammatory diseases, hyperlipidemia and cancer (Kimura Y, 2001). Resveratrol is known to have potent anti-inflammatory and antioxidant effects (Fremont L, 1999; Lee SK, 1998; Athar M, 2007).

III.1.1. Chemical properties

Resveratrol is a molecule with low solubility in aqueous media, poor bioavailability, and it has propensity to oxidize (Walle T, 2004; Trela BC, 1996; Wenzel E, 2005). Regarding its solubility, *trans*-resveratrol is soluble in ethanol, DMSO, and other organic solvents, whereas different authors have put its solubility in water at 1 mg/mL, limiting its use in the food industry (Lopez-Nicolas JM, 2008; Caddeo C, 2008).
It exists as two geometric isomes: *cis*- (*Z*) and *trans*- (*E*). *Cis*- isomer is unactive, it has biological activity unuseful for our needs. The *trans*- form can undergo isomerisation to the *cis*- form when exposed to ultraviolet irradiation (Prokop J, 2006). Unfortunately, the use of trans-resveratrol in pharmaceutical and cosmetic field is problematic owing to its fast degradation mainly linked to the isomerization from the active *trans* form to the inactive *cis* one (Wang Y, 2002).
A knowledge of the protonation state of resveratrol is important to understand its biological activity. pk_{a1} = 8.8 (H-4', essential for cytogenetic, radical scavenging, antioxidant and antiproliferative activities), pk_{a2} = 9.8 (H-3 or H-5), pk_{a3} = 11.4 (H-5 or H-3) calculated on the basis of the variation on the fluorescence of emission signal (Lopez-Nicolas JM, 2008).

When the pH of the medium is higher than the first pk_a, the biological activity of resveratrol will be strongly reduced (Lopez-Nicolas JM, 2008).
The logarithm of octanol–water partition coefficient (log *P*) is used as a measure of the hydrophobicity of compounds and it is assumed to represent the general tendency of a chemical to partition between an aqueous and an organic phase. The value of log *P* for the resveratrol is 1.87 (Fabris S, 2008).

III.1.2. Pharmacological effects

The preventive anti-carcinogenic effects of resveratrol appear to be closely associated with its antioxidant activity. RSV, and it has been shown to inhibit hydroperoxidase, protein kinase C, Bcl-2 phosphorylation, Akt, focal adhesion kinase, NF-κB, matrix metalloprotease-9, and cell cycle regulators (Athar M, 2007).
Resveratrol has been shown to modulate lipoprotein metabolism (Frankel EN, 1993; Belguendouz L, 1998), eicosanoid synthesis (Kimura Y, 1985; Pace-Asciak CR, 1995; Rotondo S, 1998) and lipid oxidation (Belguendouz L, 1997). It inhibits the oxidation of low-density lipoproteins and platelet aggregation (Kimura Y, 1985; Frankel EN, 1993; Pace-Asciak CR, 1995; Bertelli AA, 1996; Belguendouz L, 1997; Rotondo S, 1998; Wang Z, 2002; Athar M, 2007).

III.1.2.1. In vitro anti-inflammatory activity

Resveratrol has a strong anti-inflammatory property acting through the inhibition of cyclo-oxygenases, thereby amongst others the arachidonic acid metabolism is disrupted (Pace-Asciak CR, 1995; Jang M, 1997). Resveratrol also suppresses the induction of nitric oxide synthase and disrupts arachidonic acid metabolism by inhibiting cyclooxygenase-2 (Chan MY, 2000; Moreno JJ, 2000; Athar M, 2007).
Kimura *et al.* reported that resveratrol strongly inhibited the formation of 5-lipoxygenase products, 5-hydroxy-6,8,11,14-eicosatetraenoic acid, leukotrienes B_4 and C_4, and the cyclooxygenase product thromboxane B_2 from arachidonic acid (Kimura Y, 1985*a*; 1985*b*; 1995).
Resveratrol significantly reduces both acute and chronic chemically induced oedema (Jang M, 1997; Bohm M, 2004; Chen G, 2005), lipopolysaccharide-induced airway inflammation (Birrell MA, 2005) and osteoarthritis (Elmali N, 2005) and helps to prevent allograft rejection (Wu SL, 2005).
Resveratrol exerts powerful antiinflammatory effects in the setting of ischemia/riperfusion, actions that may explain in part the cardioprotective effects associated with regular consumption of this type of alcoholic beverage. (Shigematsu S, 2003).
Resveratrol has been reported as a powerful antioxidant for the therapy of AD (Jang JH, 2003; Russo A, 2003; Sharma M, 2002).
In vitro studies on PC12 cells, human umbilical vein endothelial cells (HUVECs), SHSY5Y neuroblastoma cells and hippocampal neuronal cell cultures, had found that resveratrol protected cells from oxidative stress and apoptosis induced by Aβ (Jang JH, 2003; Russo A, 2003; Sharma M, 2002; Savaskan E, 2003; Han YS, 2004).
12-hr pre-incubation of resveratrol-loaded nanoparticles protected PC12 cells from Aβ-induced damage in a dose dependent manner (1-10μM) by attenuating intracellular oxidative stress and caspase-3 activity (Lu X, 2009).

III.1.2.2. In vivo anti-inflammatory activity

Although resveratrol behaves as a poor *in vitro* scavenger of ROS (Leonard S, 2003), it acts as a potent antioxidant *in vivo*. The *in vivo* antioxidant property of resveratrol probably arises from its ability to increase nitric oxide synthesis, which in turn functions as an *in vivo* antioxidant, scavenging superoxide radicals (Das DK, 2006).
It is becoming increasingly clear that resveratrol has two faces. On one hand, it protects cells by potentiating a survival signal. On the other hand, it selectively kills cancer cells. It behaves as an antioxidant, yet it can induce redox signalling or it behaves as a pro-oxidant, it is an antiproliferative agent for cancer (Das DK, 2006; Alarcón C, 2007). It induces apoptosis in tumor cells and sensitizes cancer cells by inhibiting cell survival signal transduction and antiapoptotic pathways (Das DK, 2006). Administration of high doses of resveratrol to rats promotes death signals (Jocelyn D, 2008). The potential beneficial effects of natural antioxidants cannot justify the risk of severe side effects (Mancuso C, 2007).
Resveratrol possesses anti-inflammatory properties: it exhibits toxicity towards RAW 264.7 mouse macrophages with a $IC_{50} \leq 25$ µM. This toxicity most probably arises from its 4'-hydroxyl group found on phenyl ring B (Billack B, 2008).
Resveratrol has been reported to protect several types of cells against β-Amyloid peptide (Aβ) toxicity by scavenging Reactive Oxygen Species (ROS) and inactivating caspase-3 at the concentrations of 5, 10 µM (Lu X, 2009).

III.1.2.3. In vitro chemopreventive activity

The cancer chemopreventive potential of resveratrol has been demonstrated in the models of carcinogenesis *in vivo* and in cells *in vitro* (Sale S, 2004).
Cancer chemopreventive activity of resveratrol was investigated in a mouse mammary gland culture model of carcinogenesis (Moon RC, 1990). Resveratrol inhibited, in a dose-dependent manner, the development of DMBA-induced preneoplastic lesions (ED_{50} = 3.1 µM). No signs of toxicity were observed, as judged by morphological examination of the glands (Jang M, 1997).

III.1.2.4. In vivo chemopreventive activity

Resveratrol inhibits tumor growth and causes apoptosis as a cancer chemopreventive mechanism (Jang M, 1997; Ciolino HP, 1998; Ragione FD, 1998; Fontecave M, 1998; Subbaranmaiah K, 1998; Sun NJ, 1998; Clèment MV, 1998; Carbò N, 1999).
Epidemiological evidence shows that long-term inhibition of cyclooxygenase significantly reduces the risk of developing many cancers and deletion of the gene that encodes cyclooxygenase 2 is protective in a mouse model of colorectal cancer (Oshima M, 1996).
In several studies, small doses (0.02-8 mg/kg) of resveratrol, given prophylactically, reduced or prevented the development of intestinal and colon tumors in rats given different carcinogens (Athar M, 2007).
Administration of 1–5 mg/kg daily of resveratrol failed to affect the growth or metastasis of breast cancer in mice, despite promising *in vitro* results (Bove K, 2002).
Resveratrol treatment appeared to prevent the development of mammary tumors in animal models; however, it had no effect on the growth of existing tumors. Paradoxically, treatment of pre-pubertal mice with high doses of resveratrol enhanced formation of tumors. Injected in high doses (40 mg/Kg) into mice, resveratrol slowed the growth of neuroblastomas (Chen G, 2004).
Topical application of resveratrol reduced the number of skin tumors per mouse by up to 98% (Jang M, 1997).

The *in vivo* studies appear to show that resveratrol is not an effective chemotherapeutic agent in inhibiting melanoma growth in animals, although more pre-clinical studies would be needed for confirmation (Athar M, 2007).
Topical application of resveratrol in mice, both before and after the UVB exposure, inhibited the skin damage and decreased skin cancer incidence (Athar M, 2007).

III.1.2.5. In vitro anticancer activity

Resveratrol's potential chemopreventive and chemotherapeutic activities have been demonstrated in all three stages of carcinogenesis (initiation, promotion, and progression) (Jang M, 1997; Athar M, 2007).
It was found to act as an antioxidant and antimutagen and to induce phase II drug-metabolizing enzymes (anti-initiation activity) (Jang M, 1997). Resveratrol was also found to inhibit events associated with tumor initiation: for example, it inhibited, in a dose-dependent manner, free-radical formation (ED_{50} = 27 µM) when human promyelocytic leukemia (HL-60) cells were treated with 12-O-tetradecanoylphorbol-13-acetate (Sharma S, 1994).
It mediated anti-inflammatory effects and inhibited cyclooxygenase COX-1 (median effective dose ED_{50} = 15 µM) and hydroperoxidase functions (anti-promotion activity) (Jang M, 1997).
In addition, it induced human promyelocytic leukemia cell differentiation (anti-progression activity) (Jang M, 1997). Suh *et al.* tested the ability of resveratrol to inhibit the progression stage of carcino-genesis by treating cultured HL-60 cells with resveratrol (Suh N, 1995).
Treatment of LLC cells *in vitro* with resveratrol significantly increased apoptotic cells. It induced cleavage of caspase-9 and caspase-3 (it was involved in *in vivo* apoptosis) (Lee EO, 2006).
Angiogenesis is required to support the growth of most solid tumors beyond a diameter of 2–3 mm. When delivered systemically at a dose of 2.5–100 mg/kg, resveratrol inhibits tumor-induced neovascularization (Kimura Y, 2001; Tseng SH, 2004) and wound healing (Brakenhielm E, 2001).
Murias *et al.* found that the catechol group formed by hydroxyl groups at the 3'- and 4'-positions of phenyl ring B increases the cytotoxic potential of stilbenes (Murias M, 2005).

III.1.2.6. In vivo anticancer activity

In contrast to a large number of studies demonstrating the antiproliferative effects of resveratrol on several tumor cell lines *in vitro*, very little is known about the antitumor activity of resveratrol *in vivo*. A few studies in which the antitumor effect of resveratrol on tumor growth *in vivo* was investigated, employed solid tumors only (Goldberg DM, 1995*a*; Langcake P, 1976). In our case that is good because only solid tumors display the EPR effect, i.e. passive targeting with nanoparticulate systems. For blood cancers, the evidence is equivocal, even if massive doses of resveratrol are used (Athar M, 2007).
Resveratrol suppressed solid hepatoma growth and metastasis in rats, which harboured s.c. implanted hepatoma cells (Miura D, 2003).
Gao *et al.* demonstrated that despite strong antiproliferative and apoptotic effects of resveratrol on 32Dp210 leukemia cells *in vitro*, resveratrol has only a weak if any antileukemic activity *in vivo when* administered orally at a dose of 8 mg/kg once a day, 5 d per week (Gao X, 2002).
Kimura *et al.* found that resveratrol, at doses of 2.5 and 10 mg/kg i.p., significantly reduced the tumor volume (42%), tumor weight (44%) and metastasis to the lung (56%) in mice

bearing highly metastatic Lewis lung carcinoma (LLC) tumors, but not at a dose of 0.6 mg/kg (Kimura Y, 2001).
In addition it reduced the number of tumor cell colonies that metastasized to the lung compared with the LLC-bearing mice and it inhibited tumor-induced neovascularization (Kimura Y, 2001).
Resveratrol partially inhibited the tumor growth and metastasis of Lewis lung carcinoma and T241 fibrosarcoma in mice (Kimura Y, 2001; Brakenhielm E, 2001).
Resveratrol prevented or delayed the development of esophageal (Li ZG, 2002) and mammary malignancies (Banerjee S, 2002; Bhat KPL, 2001) and intestinal adenomas in the Apc^{Min} mouse model (Schneider Y, 2001), although the latter effect was subsequently shown to be very weak (Sale S, 2005; Ziegler CC, 2004).
Resveratrol possesses antiangiogenic properties (Cao Y, 2005; Tseng SH, 2004); it inhibits vascularization in the corneal micropocket assay in mice at a dose of only 48 µg/kg when administered daily (Brakenhielm E, 2001).
Resveratrol (25 mg/kg, for 3 weeks) decreased angiogenesis and increased apoptotic index in Erα- Erβ+ MDA-MB-231 tumors in resveratrol-treated nude mice compared with controls (Garvin S, 2006).
So far, no results of human clinical trials for cancer have been reported (Athar M, 2007).

III.1.4. Toxicity

The maximum tolerated dose of resveratrol has not been thoroughly determined, but 300 mg/kg showed no detrimental effects in rats (Crowell JA, 2004) and doses up to 100 mg/kg p.o. have been used routinely in studies on rodents (Baur JA, 2006).
No patients experienced any toxicities while enrolled on the clinical trial, orally administred. Specifically, there were no reported changes in bowel habits (diarrhea or constipation), no abdominal bloating, no nausea or vomiting, and no gastrointestinal bleeding (Nguyen AV, 2009).

III.2. Materials and methods

III.2.1. Chemicals

Acetonitrile and methanol were HPLC grade and were purchased from Biosolve Ltd. (Valkenswaard, The Netherlands); ethanol absolute was provided by Merck (Darmstadt, Germany). Acetic acid was a product of Amersham (Roosendaal, The Netherlands). Phosphate buffered saline was purchased from B-Braun, Melsungen, Germany. All buffers and reversed osmosis water were filtered through 0.2 mm filters (Schleicher & Schuell MicroScience GmbH, Dassel, Germany) prior to use. NaCl was purchased from Sigma-Aldrich, Buchs SG, Switzerland. Resveratrol (purity by HPLC >98%) was provided by Chengdu Biopurify Phytochemicals Ltd. DPPC was purchased from Natterman Phospholipids, Gmb. Cholesterol was analytical grade and was purchased from Aldrich (Milan, Italy). Lipoid PE 18:0/18:0 PEG 2000 was purchased by Lipoid, art.no. 882. Triton X-100 was purchased from Sigma-Aldrich, Buchs SG, Switzerland. Bovine serum albumin and Albumin bovine cross-linked 4% beaded agarose (bead diameter: 45-165 microns) were purchased from Sigma-Aldrich, Buchs SG, Switzerland. FluoSpheres Size Kit #2, carboxylate-modified microspheres of 0.02–0.1–0.2–0.5–1.0–2.0 µm, yellow-green fluorescent (505/515), was purchased from Molecular Probes, Invitrogen, Breda, The Netherlands. LabelIT Fluorescein Nucleic Acid Labeling Kits were purchased from Mirus Bio, Madison, WI, USA.

III.2.2. Production of liposomes

Samples of liposomes were prepared with a phospholipid concentration of ca. 100 μmol PL/mL and with a varying amount of resveratrol.
Multilamellar vesicles were prepared according to the film hydratation method (Bangham AD, 1965). 5-10 ml of ethanol absolute were added in order to dissolve the lipids by heating at 50 ºC in a waterbath. The organic phase was evaporated using a rotavapor till a dry lipid film develops; the lipid film further was dried by flushing with nitrogen for 10 minutes. 5 ml of PBS were added to the lipid film and rotate the flask for 5-10 minutes at 50 ºC in the waterbath of the rotavapor without the vacuum. If the lipid film sticks to the glass wall, glass beads were used. Then the dimensions were reduced by extrusion technique. The liposomes were extruded twice through 2 polycarbonate filters with pore size 600 nm, putting the filters on top of each other, than twice through 2 polycarbonate filters with pore size 600 nm and 200 nm and, at last they were extruded 8 times through 2 filters with pore size 100 nm.

III.2.2.1. Production of fluorescent liposomes

Fluorescent liposomes were prepared with 3 different fluorescent labels:

- DiD
- NBD-PE
- calcein

III.2.2.1.a. Production of liposomes with the fluorescent label DiD

Fluorescent liposomes had a total lipid concentration of 16.436 mM.
The liposomes contained 0.1% mol of the fluorescence label DiD. DiD's bleuish stock solution has a concentration of 200 μg/mL in EtOH and it could be saved in freezer.

III.2.2.1.b. Production of liposomes with the fluorescent label NBD-PE

Fluorescent liposomes had a total lipid concentration of 16.436 mM.
The liposomes contained 1% mol of the fluorescence label NBD-PE (N-(7-nitrobenz-2-oxa-1,3-diazol-4-yl)-1,2-dihexadecanoyl-snglycero-3-phosphoethanolamine, triethylammonium salt). NBD-PE's yellowish stock solution has a concentration of 1 mg/mL in $CHCl_3$ and it could be saved in freezer.

III.2.2.1.c. Preparation of calcein solution

A solution of calcein at the concentration of 100 mg/mL in RO-water (161 mM) was prepared. One pellet of NaOH was added in order to dissolve the calcein and the pH of the solution of calcein was adjust with a 4 M NaOH solution to pH 7.5. The osmolality of the calcein solution was checked and it was diluted with RO-water until it was iso-osmotic (between 280-300 mOsmol/kg) using the Osmomat 030.

III.2.2.1.d. Production of liposomes with calcein

Liposomes with calcein had a total lipid concentration of 16.436 mM.
Multilamellar vesicles were prepared according to the film hydratation method (Bangham AD, 1965), as described above. 5 ml of calcein solution were added to the lipid film and

rotate the flask for 5-10 minutes at 50 ºC in the waterbath of the rotavapor without the vacuum. Then the dimensions were reduced by extrusion technique. The liposomes were extruded twice through 2 polycarbonate filters with pore size 600 nm, putting the filters on top of each other, than twice through 2 polycarbonate filters with pore size 600 nm and 200 nm and, at last they were extruded 8 times through 2 filters with pore size 100 nm.

III.2.3. Characterization of liposomes

III.2.3.1. Dynamic Light Scattering (DLS)

Dynamic Light Scattering is an ALV CGS-3 system (Malvern Instruments, Malvern, UK) equipped with a JDS Uniphase 22 mW He–Ne laser operating at 632.8 nm, an optical fiber-based detector, a digital LV/LSE-5003 correlator and a temperature controller (Julabowater bath) set at 25 °C. Time correlation functions were analyzed to obtain the hydrodynamic diameter of the particles (Z_h) and the particle size distribution (polydispersity index, PDI) using the ALV-60X0 software V.3.X provided by Malvern. Autocorrelation functions were analyzed by the cumulants method (fitting a single exponential to the correlation function to obtain the mean size (Z_{ave}) and polydispersity index (PDI)) and CONTIN (to fit a multiple exponential to the correlation function to obtain particle size distributions). The diffusion coefficients calculated from the measured autocorrelation functions were related to the hydrodynamic radius of the particles via the Stokes–Einstein equation

$$Z_h = (k_B T q^2)/(3\pi\eta\Gamma)$$

where Z_h is the hydrodynamic radius of the particles,
k_B is the Boltzmann constant,
T is the absolute temperature,
η is the solvent viscosity,
Γ is the decay rate,
q is the scattering vector

$$q = [4\pi n \sin(\Phi/2)]/\lambda$$

in which n is the refractive index of the solution,
Φ is the scattering angle,
λ is the wavelength of the incident laser light.
Scattering was measured in an optical quality 4 mL borosilicate cell at a 90° angle.

III.2.3.2. Disruption of liposomes by Triton X-100

After the purification of the surface of the liposomes, they were disrupted by 0.025% non ionic Triton X-100 in order to calculate the encapsulation efficacy. In order to prepare a 0.025% Triton X-100 solution, 25 mg of Triton X-100 were dissolved in 100 mL bidistilled water and heated until 70°C. 500µL of 0.025% Triton X-100 were added to liposomal dispersions and they were heated for 20 minutes at 70°C in a water bath. Allow the samples to cool at room temperature.
The same was done also with a know amount of resveratrol in order to calibrate the disruption method: resveratrol (100 µg/mL in EtOH) was added to a dispersion of empty liposomes. Empty liposomes have the same concentrations of the constituents of resveratrol-loaded liposomes. After 5 minutes of vortex, 0.025% Triton-100 was added to

this mixture. The concentration of resveratrol of the liposomes was determined by HPLC/PDA analysis.

III.2.3.3. Encapsulation efficacy (EE%)

Free resveratrol was removed by means of dialysis. The liposomes were transferred into a Slide-A-Lyzer cassette (cut off= 3000 kDa). This dialysis cassette was stirred in 1 liter PBS at 4-8 ºC for 24 hours; the PBS were refreshed four times within these 24 hours (equilibrium is obtained after ca. 4 hours) in order to remove all free resveratrol.
During dialysis, samples of the liposomes (50 µL each one) and samples of the medium (1 mL), were taken before refreshing the PBS in order to optimize the conditions of dialysis. These samples were collected and diluted with eluent. The concentration of resveratrol was determined by HPLC analysis, in order to check that all the free resveratrol is removed. The addition of the amount of resveratrol found in the liposomes with the amount found in the medium has to be ~100% for each sample.
In the case of the production of liposomes with calcein, the dialysis cassette was stirred in 1 liter PBS at 4-8 ºC for 48 hours; the PBS were refreshed eight times within these 48 hours in order to remove not only all free resveratrol but also free calcein.

III.2.3.4. HPLC/PDA analysis

An HPLC/PDA Waters System (Waters Associates Inc., Milford, MA) with a differential refractometer model 410 was used for analising the content of resevratrol inside the vesicles. Peak areas were determined with Empower Software Version 2 build 1154 (Waters Associates Inc). Resveratrol is determined by HPLC/PDA on column X-Terra RP-18 (5 µm, 4.6 x 25 mm, Waters), using an isocratic method and a gradient method already present in literature (Caddeo C, 2008; Juan ME, 2009) but modified. Resveratrol was detected at 306 and 288 nm (absorption of cis-resveratrol).

III.2.3.5. Recovery

A known amount of resveratrol (100 µg/mL in EtOH) was added to a dispersion of empty liposomes in order to check the percentage of recovery. This mixture was stirred for 5 minutes with vortex after both of the additions.

µL of empty liposomes	µL of RSV (100 µg/mL)	µL of eluent	dilution of conc. of RSV (times)	conc. of RSV (µg/mL)
100	-	9900	-	-
100	50	9850	200	0.5
100	100	9800	100	1
100	150	9750	66.7	1.5

III.2.4. Stability

III.2.4.1. Stability test of free resveratrol in solution

Two concentrations of resveratrol (1-10 mg/mL in eluent) were prepared in glass vials. These vials were kept under sunlight, in absence of light (covered with an alluminium sheet) and under UV lamp (60%, 5982 mW/cm^2, 717840 mJ/cm^2) in order to test the stability of resveratrol in solution in different conditions. These solutions were divided in six parts: 3 conditions, each one in duplo.

A sample of the solutions kept under sunlight and kept in absence of light was taken after 3, 7 hours and 1, 2, 3 and 4 days. These solutions were kept under UV lamp 1, 2, 4, 6, 8 and 16 minutes.
Every samples were collected and the samples with an initial concentration of resveratrol in solution of 1 mg/mL were diluted 100-times and the samples with an initial concentration of resveratrol in solution of 10 mg/mL were diluted 1000-times. They were transferred into some vials and were kept in freezer until HPLC/PDA analysis.

III.2.4.2. Stability test of resveratrol-loaded LC liposomes at different temperatures

Resveratrol-loaded long circulating liposomes with different initial concentrations of resveratrol were been prepared and they were kept at different temperatures in order to understand their stability in time and the future right way of stocking.
Resveratrol-loaded long circulating liposomes were been prepared as described before with different initial concentrations of resveratrol: 0.1, 0.2, 0.3, 0.5, 1 and 1.5 mg/mL.
Each liposomal dispersion was divided in 4 parts and was kept at diffent temperature values:

- room temperature (RT, about +20°C) covered by light with an alluminum sheet
- room temperature (RT, about +20°C) under the sunlight
- fridge (+4°C)
- oven at the body temperature (+37°C).

Samples were diluted 100-times with eluent in order to analyze them by HPLC/PDA and to quantified the chemical degradation of resveratrol in time.
Samples were diluted with PBS in order to analyze them by DLS for monitoring size and PD in time. The samples were taken after 0, 1, 3, 7, 24 hours and every week.

III.2.4.3. Photostability

A solution of resveratrol 1 mg/mL in eluent, a solution of resveratrol 10 mg/mL in eluent and resveratrol-loaded long circulating liposomes with the same initial concentration of resveratrol 1 mg/mL were irradiated in a dark cabinet (60%, 5982 mW/cm^2, 717840 mJ/cm^2). The distance from the light source to the test sample was 6.5 cm. At different times: after 10 sec., 30 sec, 1 minutes, 2, 4, 6, 8 and 16 minutes 3 samples (10 µL) of each solution were collected.
Samples were diluted 100-times with eluent in order to analyze them by HPLC/PDA and to quantified the chemical degradation of resveratrol in time.
Samples were diluted with PBS in order to analyze them by DLS for monitoring size and PDI in time.

III.2.5. Stability in presence of blood protein

The stability of the liposomal formulations in presence of blood protein (albumin at physiological concentration) was evaluated: size change in time by FACS analysis (Vorauer-Uhl K, 2000) and by fluorimeter analysis, leakage and extraction of drug from the formulation by incubation with albumine coated beads and than HPLC/PDA analysis.

III.2.5.1. Fluorescent Activated Cell Sorting (FACS)

Flow cytometry was performed using a FACSCalibur (Becton and Dickinson, Mountain View, CA, USA) benchtop flow cytometer equipped with an air-cooled Argon-ion laser at

488 nm and various flow speed controls or a FACSCanto II or FACSAria Cell Sorter (Becton and Dickinson, Mountain View, CA, USA) equipped with three air-cooled lasers at 488, 633 and 405 nm. Side scatter outcome was set to logarithmic and detected at a scattering angle of 90° with a threshold set on FL-1 (set to logarithmic amplification) to exclude side scatter values from non-fluorescent particulate matter. Flow rates and/or dilutions were chosen such that less than 2000 events/s were recorded to prevent coincidence. For each measurement a total number of 10000 events were recorded.
FACS parameters:

sample flow rate	0.5 µL/s
sample volume	5-20 µL
mixing volume	50 µL
mixing speed	100 µL/s
number of mixes	2
wash volume	400 µL

III.2.5.1.a. FACS data processing

FACSCalibur data were processed with Summit® software (Dako-Cytomation, Fort Collins, CO, USA) and FACSCanto II and FACSAria data with FACSDiva software (Becton and Dickinson, Mountain View, CA, USA) or FCS Express (http://www.denovosoftware.com). For calibration, histograms of SSC values were plotted and the geometric means of each peak corresponding to a bead size were derived. Bead sizes (y) and geometric means of SSC values (x) were then plotted in Graphpad Prism and fitted with non linear regression using $y=a+bx^c$
as described previously (Vorauer-Uhl K, 2000).
For size analysis of samples, raw data were converted to ASCI using the program MFI and FCSExtract for data obtained with the FACSCalibur data and FACSAria, respectively. Data were converted from 10-bit (1024 channels) to log4-scale using
$y=10^{(x/256)}$
Data from channel 0 were excluded from the analysis. The resulting log4-scale values were then converted to sizes by applying $y=a+bx^c$.

III.2.5.1.b. Incubation with albumin and FACS analysis

Empty liposomes and liposomes with initial concentrations of resveratrol of 1 mg/mL were incubated with a solution of albumin (40 mg/mL in PBS) at the body temperature in a shaking waterbath to mimic the *in vivo* condition.
They were labelled with NBD-PE 1% mol (N-(7-nitrobenz-2-oxa-1,3-diazol-4-yl)-1,2-dihexadecanoyl-snglycero-3-phosphoethanolamine, triethylammonium salt; λ_{ex}= 463 nm: λ_{em}= 536 nm), and analysed by FACS experiment.
200 µL of fluorescent liposomes were exposed to 2.2 mL of albumin solution (40 mg/mL). This volume of albumin was choosen because for *in vivo* mouse studies, the total blood volume of a mouse of approx. 25 grams is 2 mL, which equals approx 1.1 ml of serum (55% of 2 mL) and the maximum injection volume of 100 µL is used.
Fluorescent liposomes were sampled (150 µL) at 20, 40, 60, 90 and 120 minutes.
RSV-loaded liposomes and RSV-loaded liposomes after incubation with albumin were diluted 4 x 10^3-times in PBS and 4 x 10^2-times in PBS, respectively. They were subsequently analyzed by FACS for particle size. The experiment and the measurements were repeated in triplo.

III.2.5.1.c. Calibration curve by labeled beads

The size distribution of the liposomes was determined by correlating the side scattered signals of the vesicles and the side scattered signals of the calibration beads. Diameters of the fluorescent beads were confirmed by Dynamic Light Scattering (100, 210 and 500 nm bead). DLS was calibrated with 200 nm polystyrene latex standard beads (Duke Scientific, Leusden, The Netherlands).
The standard beads were analized by FACS and a calibration curve based on measurements of the labelled beads was calculated.

III.2.5.2. Fluorimeter analysis

The FLUOstar OPTIMA is a fully automated microplate based multi-detection reader for measuring the fluorescence Intensity. By integrating a high intensity xenon flash lamp and liquid light guide technology, the FLUOstar OPTIMA can cover the wavelength range from 240 to 740 nm. The FLUOstar OPTIMA can read all plate formats from 6- up to 384-well plates. The versatile optical system allows instant switching from top to bottom reading. Further, the instrument has a build-in incubator (from +8°C to +45°C) and is equipped with one reagent injector.

III.2.5.2.a. Incubation with albumin and fluorimeter analysis

Empty liposomes and liposomes with initial concentrations of resveratrol of 1 mg/mL were incubated with a solution of albumin (40 mg/mL in PBS, physiological concentration) at the body temperature in a shaking waterbath to mimic the *in vivo* condition.
Liposomes were labelled with calcein, a small hydrophilic fluorofore (λ_{ex}= 485 nm: λ_{em}= 512 nm), and analysed by the Fluorometer.
200 µL of fluorescent liposomes were exposed to 2.2 mL of albumin solution (40 mg/mL). This volume of albumin was choosen because for *in vivo* mouse studies, the total blood volume of a mouse of approx. 25 grams is 2 mL, which equals approx 1.1 ml of serum (55% of 2 mL) and the maximum injection volume of 100 µL is used.
Fluorescent liposomes were sampled (150 µL) at 20, 40, 60, 90 and 120 minutes. The samples were put directly in a well-plate and analyzed by fluorimeter. The experiment and the measurements were repeated in triplo.
The fluorescence of PBS, albumin, RSV-loaded liposomes and empty liposomes was measured as controls.

III.2.5.2.b. Calibration curve by disrupted liposomes

In order to quantified the amount of fluorescence, a calibration curve was prepared using increasing amount of disrupted liposomes. 2.2 mL of albumin (40 mg/mL) was added to 200 µL of liposomes: albumin was added in order to measure some potencial interferences in the fluorescence because of its presence. 200 µL of Triton X-100 (10% aqueous solution) was added to this mixture in order to disrup the vesicles. These solutions were heated at 70°C for 20 minutes and than they were allowed to cool at room temperature. Different volumes of disrupted liposomes were diluted with PBS in order to obtain a calibration curves.

III.2.5.3. Incubation with albumin coated beads

Liposomes with the initial concentrations of resveratrol of 1 mg/mL (%EE=42%, RSV final concentration 0.42 mg/mL) were incubated with a solution of albumin coated beads/PBS 50% v/v at the body temperature in a shaking waterbath to mimic the *in vivo* condition. The molar ratio between RSV and albumin were 1:1, 1:1.5 and 1:2. As controls, the same liposomes were incubated also with PBS only and resveratrol at the concentration of 0.42 mg/mL in EtOH was incubated with a solution of albumin coated beads/PBS 50% v/v.
Each experiment was repeated in duplo.

Molar ratio RSV:albumin	50% (v/v) Albumin gel in PBS (µmol)	µL of RSV-loaded liposomes	µL of a 50% (v/v) Albumin gel in PBS or PBS (reference)
1:1	0.184	100	2125
1:1.5	0.276	100	3188
1:2	0.368	100	4252

Some samples (250 µL per time point) were collected after 20, 40 minutes, after 1, 2, 4, 6, 24, 48 hours and 6 days. Each sample was centrifuge at 10.000 g for 6 minutes.
The supernatant was collected and diluted 100-times with eluent.
The concentration of resveratrol was determined by HPLC/PDA analysis.

III.2.6. *In vivo* activity: tumor growth

III.2.6.1. Cell lines

The Human Head and Neck Squamous Cell Carcinoma cell line, UM-SCC-14C, developed by Dr. T.E. Carey (Carey TE, 1990), Ann Arbor, MI, was kindly provided by Dr. G.A.M.S. van Dongen, Department of Otolaryngology/Head and Neck Surgery, VU University Medical Center, Amsterdam, The Netherlands.

III.2.6.2. Solutions for cell colture

Completed DMEM medium: Plain DMEM (Dulbecco's modification of Eagle's medium, with 3.7 g/l sodium bicarbonate, 4.5 g/l l-glucose, and L-glutamine (Cat. No: E15-810; PAA), completed with 5.7 ml antibiotics/antimycotics and 28 ml Foetal Bovine Serum (FBS) (final concentration 5%) stored as aliquots located in the freezer in the cell culture.
PBS: Phosphate buffered saline, containing 10 mM phosphate buffer (pH 7.2) and 145 mM NaCl. Trypsin/EDTA solution.

III.2.6.3. Materials for cell colture

Culture flasks with vented cap (depending on the number of cells: 182 or 75 cm^2, Greiner-Bio-one, cat. no. 661175/658175). 5, 10 and 25 ml pipettes (Greiner-Bio-one, cat. no. 606180, 607180, 760180). Biohazard safety cabinet (HB 2472, Holten B.V.) equipped with burner and aspiration device. CO_2-incubator 37°C (Heraeus). Ethanol 70% in sprayer.

III.2.6.4. Preparation of cell culture

The Biohazard was switched 30 minutes beforehand and the working surface was cleaned with 70% ethanol. PBS and completed DMEM medium were warmed in water bath to 37°C

for 15 minutes. The medium were aspirated from the cells by suction and they were washed with PBS (about 15 ml, 10 ml or 3 ml to 175 cm^2, 75 cm^2 or 25 cm^2 flasks, respectively) and than PBS was aspirated from the cells by suction.
Trypsin/EDTA solution was added (about 6 ml, 3 ml or 1 ml to 175 cm^2, 75 cm^2 or 25 cm^2 flasks, respectively). The cells were incubated with trypsin for no longer than 15 minutes.
Completed DMEM medium was added (about 3-4 times the trypsin/EDTA solution's volume added before). Trypsin is inactivated by serum present in the medium. Gently cells were suspended again in the medium to obtain a homogeneous cell suspension without the presence of air bubbles. Cells were bringed in one or more (175 cm^2, 75 or 25 cm^2) culture flasks. In general 1:3 to 1:5 part of the last passage is transferred to a new flask. Complete medium was bringed in culture flask and add a certain volume of cell suspension, to an end volume of 35 ml, 15 ml or 5 ml, according to the flask (175 cm^2, 75 or 25 cm^2, respectively). For maintaining this cell line 1:5 is satisfactory; if soon large numbers of cells are needed, less diluted passages (1:3) can be used. Place the culture flasks in the CO_2-incubator at 37°C and 5% CO_2. This procedure was repeated after a confluent monolayer has formed (twice a week).

III.2.6.5. Mice

Developed through crosses and back-crosses between BALB/cABom-nu and BALB/cAnNCrj-nu at Charles River Laboratories Japan (CRLJ). This mouse is inbred, and genetic monitoring results confirm it to be a BALB/c nude. The homozygous animals lack a thymus, so they are unable to produce T-cells and therefore they are immunodefficient. The coat colour is albino and they are hairless.

III.2.6.6. In vivo experiment: tumor growth

Balb/c nude female mice were housed in groups of 4–8 animals and had free access to water and food. All animal studies were performed in compliance with guidelines set by national regulations and were approved by the local animal experiments ethical committee. The head and neck squamous-cell carcinoma line 14C was introduced in the flank of the mice by inoculation (subcutaneous injection above the right hind leg) with 1 x 10^6 14C-tumor cells. Palpable subcutaneous tumors had developed over a period of 2-3 weeks. The tumor was measured with a digital caliper in order to calculate the tumor volume. When the tumor measured 4x4 mm, that means 30 mm^3, mice were treated with resveratrol-loaded long circulating liposomes intravenously (200 µL, via the tail vein of the mice) of the maximum concentration. During the whole experiment the tumor size was measured twice weekly. Tumor size was measured and volume calculated according to the formula $0,5 * a * b^2$ where a = the largest superficial diameter and b = the smallest.
When the tumors reached the humane endpoint (1000 mm^3) the mice were sacrificed one by one. After sacrificing, blood, tumor and organs were taken.

III.2.7. *In vivo* activity: biodistribution profile

III.2.7.1. Recovery of trans-resveratrol from plasma

Plasma was obtained by centrifugation at 1500 g for 15 minutes. 10 µL of a solution of resveratrol at the concentration of 40 µg/mL in eluent (0.4 µg of RSV) were added to 200 µL of blank plasma. In the literature two factors were described as useful to precipitate the

blood proteins: the cold temperature and the increasing of acidity (Derakhshanded K, 2005; Mathies JC, 1980). So, 500 µL of CH_3CN kept in freezer (-20°C) and 100 µL of $ChCl_3$, kept in freezer as well, were added to plasma. Also, 170 mg of finely powdered mixture of Na.bisulfate.monohydrate/NaCl in ratio 1/4 were added to plasma. As control, 500 µL of CH_3CN kept at room temperature and 100 µL of $ChCl_3$ at room temperature as well were added to plasma. Plasma samples were vortexed for 30 seconds and they were centrifuged until they were dried at 40°C for 1 hour under a nitrogen flow. After adding 125 µL of mobile phase, the samples were analysed by HPLC/PDA.

III.2.7.2. Recovery of trans-resveratrol from tissues

1 g of tissue was finely minced with scissors, and placed in a homogenizer vessel. Methanol 80% (4 mL) v/v acidified with acetic acid 2.5% v/v and 10 µL ascorbic acid (15%, w/v) as antioxidant were added. The samples were homogenized by Ultra-Turrax until they were homogeneous. The homogenizer was cleaned twice with 1 mL of acidified methanol, which were added to the 4 mL making a final volume of 8 mL. The recoveries of RSV from tissue were determined by spiking each tissues with the final concentration of 10 µmol/g tissues. 625 µL of RSV 1 mM were added to 500 µL of each homogenized samples.

III.2.7.2.a. Brain, testis, liver and lungs

The samples were vortexed for 5 minutes and were centrifuged at 3000 g for 30 min at 4°C. The residue was extracted two more times with 500 µL of acidified methanol by vigorous agitation in the vortex for 5 min, followed by centrifugation at 3000 g for 30 min at 4°C. The samples were diluted 50-times with eluent (isocratic method) or with EtOH 20% v/v (gradient method) and analysed by HPLC/PDA.

III.2.7.2.b. Kidney

500 µL of acidified methanol were added to 500 µL of homogenized tissue. Each sample was incubated at 60°C (oil bath with electrical thermometer connected to the hot plate) with constant stirring for 30 minutes. The samples were centrifuged at 3000 g for 30 min at 4°C. The residue was extracted one more time with 500 µL of acidified methanol by vigorous agitation in the vortex for 5 min, followed by centrifugation at 3000 g for 30 min at 4°C. The samples were diluted 50-times with eluent (isoratic method) or with EtOH 20% v/v (gradient method) and analysed by HPLC/PDA.

III.3. Results and discussion

Starting from literature data, we found an article where resveratrol-loaded liposomes were prepared and characterized; they had final resveratrol concentration of 1.3 mM, 70% of resveratrol incorporation efficacy and they were stable over 60-days period at 4°C (Caddeo C, 2008).
One of the aims of this project is to prepare resveratrol-loaded long-circulating liposomes with an improved final absolute concentration of resveratrol, with an optimized encapsulation efficacy and with the same stability in time at least.
Resveratrol-loaded long-circulating liposomes were prepared in order to find the best balance between final absolute concentration and encapsulation efficacy of resveratrol

inside the vesicles and also in order to understand the trend of the incapsulation efficacy towards initial concentrations of resveratrol.

III.3.1. Production and characterization of liposomes

In the table all the constituents of the bilayer of PEGylated liposomes were indicated with their molar ratio:

molecule	MW	molar ratio	mg/mL
DPPC	734	2	75.00
18:0/18:0 PEG 2000	2805.497	0.1	22.33
cholesterol	386.66	1	20.92

Twelve different initial resveratrol concentrations were used (0.1, 0.2, 0.3, 0.5, 1, 1.5, 2, 2.5, 2.75, 3, 3.5 and 4 mg/mL) to prepare liposomes in order to find the optimal balance between final absolute concentration and EE of resveratrol.

initial RSV conc. (mg/mL)	molar ratio (%)	mean diameter (nm)	polydispersity index (PDI)	final RSV conc. (mg/mL)	EE (%)
-	-	125.0±3.97	0.07±0.04	-	-
0.1	0.3	126.6	0.08	0.08±0.01	77.45±4.73
0.2	0.5	139.9	0.11	0.12±0.01	60.12±1.94
0.3	0.8	133.4	0.02	0.17±0.01	55.95±2.66
0.5	1.3	130.9±1.25	0.08±0.01	0.33±0.13	65.63±27.21
1	2.7	134.0±10.39	0.09±0.03	0.51±0.09	50.58±8.85
1.5	4.0	145.9±16.24	0.08±0.03	0.39±0.11	25.89±7.37
2	5.3	117.9	0.09	0.27	13.31
2.5	6.7	135.8	0.05	0.54±0.02	21.74±0.67
2.75	7.3	124.0	0.09	0.47±0.01	17.05±0.02
3	8.0	119.6	0.10	0.25±0.02	8.38±0.59
3.5	9.3	142.8	0.14	0.56±0.04	16.00±1.24
4	10.7	482.1	0.12	1.25	31.27

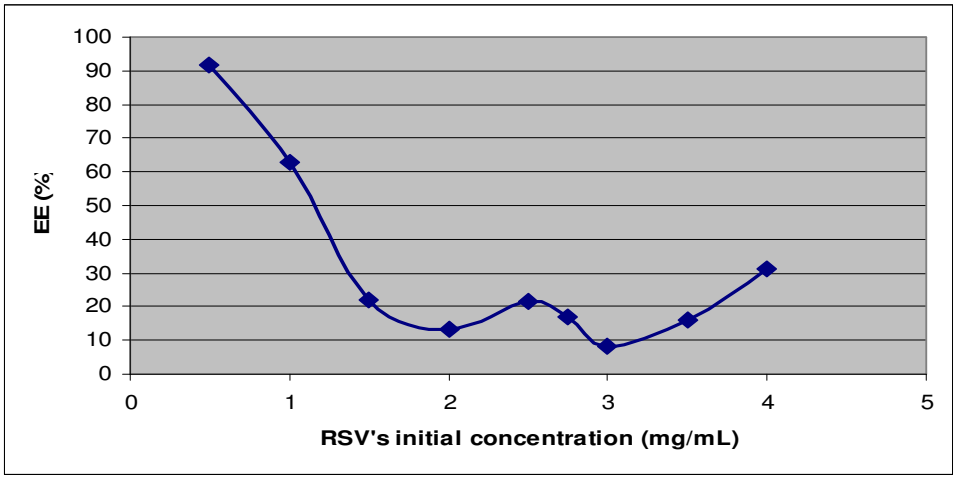

Fig 38. Resveratrol's initial concentration plotted versus encapsulation efficacy.

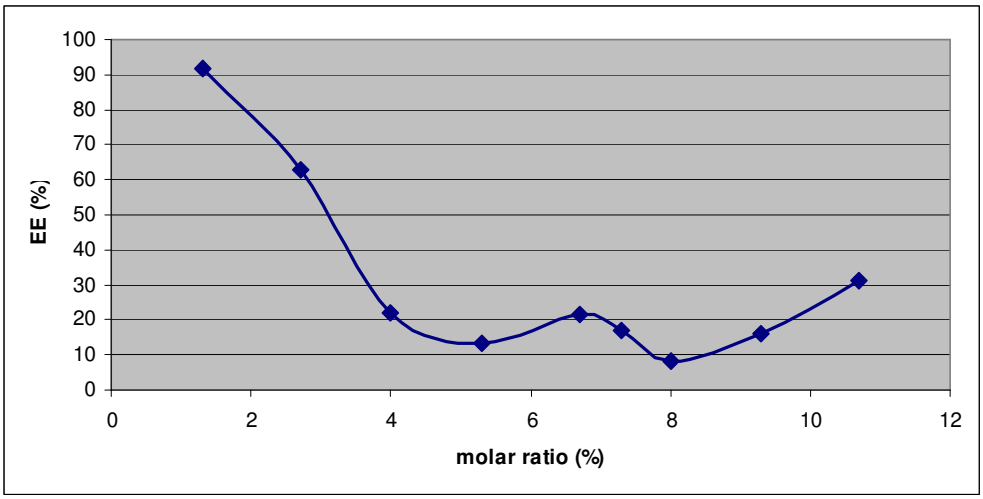

Fig 39. Molar ratio plotted versus encapsulation efficacy.

III.3.1.1. Optimization of method of disruption

The reproducibility of resveratrol quantification with or without the addition of Triton X-100 will be examined.
After the purification of the liposomes by dialisys, they were disrupted with Triton X-100 in different molar ratio or they were diluted 100-fold with eluent (MeOH/CH_3CN/water acidified with CH_3COOH 75:22.5:2.4:0.1 v/v).

initial RSV conc. (mg/mL)	molar ratio (%)	mean diameter (nm)	polydispersity index (PDI)	final RSV conc. (mg/mL)	EE (%)
2	5.3	117.9	0.09	0.27	13.31
2.5	6.7	135.8	0.05	0.54±0.02	21.74±0.67
3.5	9.3	142.8	0.14	0.56±0.04	16.00±1.24
4	10.7	482.1	0.12	1.25	31.27

samples	Triton X-100: RSV-LCL	initial RSV conc. (mg/mL)	final RSV conc. (mg/mL)	final RSV conc. (mM)	EE (%)
Caddeo, 2008*	not explained the ratio	~ 0.4	0.30	1.3	~70
RSV-LCL	-	2	0.27	1.17	13.31
RSV-LCL	1:1	2	0.26	1.12	12.83
RSV-LCL	-	2.5	0.54±0.02	2.38±0.0736	21.74±0.67
RSV-LCL	3:1	2.5	0.57±0.03	2.48±0.1554	22.68±1.42
RSV-LCL	2:1	2.5	0.64	2.81	25.62
RSV-LCL	1:1	2.5	0.56	2.44	22.26
RSV-LCL	-	3.5	0.56±0.04	2.45±0.1906	16.00±1.24
RSV-LCL	3:1	3.5	0.60±0.02	2.61±0.1119	17.05±0.73
RSV-LCL	2:1	3.5	0.57	2.49	16.24
RSV-LCL	1:1	3.5	0.56	2.48	16.15
RSV-LCL	-	4	1.25	5.48	31.27
RSV-LCL	1:1	4	0.40	1.74	9.95

[*]Caddeo C., Teskac K., Sinico C., Kristl J., **2008**. Effect of resveratrol incorporated in liposomes on proliferation and UV-B protection of cells. *International Journal of Pharmaceutics* 36, 183-19.

In every case the addition of Triton X-100 did not change the detected value. The eluent is probably already sufficient to disrupt the vesicles because of its high percentage of organic solvents. The only exeption is for the liposomes with a resveratrol's initial concentration of 4 mg/mL; in this case different results were obtained upon addition of Triton X-100. However, the dispersion was not homogeneous and so this discrepancy is presumably due to sample heterogeneity. This formulation probably had a too much high initial content of resveratrol, in fact it was not possible to extrude this dispersion through 2 filters with pore size of 600 and 200 nm. The size of liposomes was consequently not within the dimensional range wanted (70-130 nm).

III.3.1.2. HPLC/PDA analysis

III.3.1.2.a. Isocratic method

Resveratrol is determined by HPLC/PDA on column X-Terra RP-18 (5 µm, 4.6 x 25 mm, Waters), using a mixture of MeOH/CH_3CN/water and CH_3COOH (75:22.5:2.4:0.1 v/v) as mobile phase.

Flow rate: 0.8 mL/min.
Detection: λ=306 nm
λ=288 nm (absorption of *cis*-resveratrol)
Injection volume: 50 µL
Run time: 8 minutes
Temperature: 25°C

A calibration curve was prepared at concentration of 1 mg/mL in eluent as external standard (solution **a**) in order to quantify the amount of resveratrol present in the samples in a higher range of concentration. The range of this calibration curve is: 2 - 25 µg/mL. My dilution scheme was:

µg/mL	µM	µL of solution a	µL of eluent	dilution
2	8.762	2	998	**a**/500
4	17.525	4	996	**a**/250
6	26.287	6	994	**a**/166.6
8	35.049	8	992	**a**/125
10	43.812	10	990	**a**/100
14	61.336	14	986	**a**/71.4
16	70.098	16	984	**a**/62.5
20	87.623	20	980	**a**/50
25	109.529	25	975	**a**/40

Prepare a calibration curve using resveratrol at concentration of 1 µg/mL in eluent as external standard (solution **a**/1000) in order to quantify the amount of resveratrol present in the samples in a lower range of concentration.
The range of this calibration curve is: 1 µg/mL - 5 ng/mL. My dilution scheme was:

sol.	µg/mL	nM	µL of solution	µL of eluent	dilution
b	1	4381.161	**a** 10	9990	**a**/1000
c	0.5	2190.580	**b** 1000	1000	**b**/2
d	0.25	1095.290	**c** 1000	1000	**c**/2
e	0.125	547.645	**d** 1000	1000	**d**/2
f	0.025	109.529	**e** 1000	4000	**e**/5
g	0.0125	54.764	**f** 1000	1000	**f**/2
h	0.005	21.906	**f** 1000	4000	**f**/5

III.3.1.2.b. Gradient method

Resveratrol is determined by HPLC/PDA on column X-Terra RP-18 (5 µm, 4.6 x 25 mm, Waters), using a gradient eluent constituted by two mobile phases:
Phase A: CH_3CN/Phase B 80/20 v/v
Phase B: CH_3COOH 3% v/v.
The following multi-step linear gradient was applied:

time (minutes)	Phase B (%)	Phase A (%)
0	78	22
2	78	22
6	70	30
14	50	50
18	40	60
25	0	100
28	78	22

Flow rate: 1.5 mL/min.
Detection: λ=306 nm
λ=288 nm (absorption of *cis*-resveratrol)
Injection volume: 100 µL
Run time: 8 minutes
Temperature: 40°C
A calibration curve was prepared at concentration of 1 mg/mL in eluent as external standard (solution **a**) in order to quantify the amount of resveratrol present in the samples in a higher range of concentration. The range of this calibration curve is: 2 - 25 µg/mL. My dilution scheme was:

µg/mL	µL of RSV 1 mM	µL of EtOH 20% v/v	dilution (times)
22.825	100	900	10
18.26	80	920	12.5
14.836	65	935	15.38
11.4125	50	950	20
7.9887	35	965	28.57
4.565	20	980	50
2.2825	10	990	100
0.913	4	996	250
0.4565	4	1996	500
0.22825	1000 c	1000	c/2
0.114125	1000 d	1000	d/2
0.02282	1000 e	4000	e/5

0.0114125	1000 f	1000	f/2
0.004565	1000 f	4000	f/5

III.3.1.2.c. Recovery

Known amounts of resveratrol will be added to empty liposomes in order to check the percentage of recovery.

expected conc. of RSV (µg/mL)	found conc. of RSV (µg/mL)	Recovery (%)
-	-	-
0.5	0.40±0.01	79.20±1.70
1	0.92±0.01	92.45±1.34
1.5	1.27±0.03	84.90±2.30

The percentage of recovery with the isocratic method was satisfied, so it seems not necessary to perform the gradient elution. It could be used in perspective, during the in vivo experiments. In fact, resveratrol and its metabolites will be monitored in plasma and tissues samples where could be useful an gradient eluent whit a more efficient capacity of separation. For the in vitro characterization fo the optimized formulation, the isocratic method will be used because it is easier and faster than the other.

III.3.1.3. Optimization of method of dialysis

In order to be sure that all the free resveratrol was removed from the liposomal dispersion, the conditions of dialysis was optimized.
So, during the dialysis, samples of liposomes and of the medium will be collected before every refreshment. The concentration of resveratrol was determined by HPLC/PDA analysis. The addition of the amount of resveratrol found in the liposomes with the amount found in the medium has to be ~100% for each sample.

initial RSV conc. (mg/mL)	molar ratio (%)	mean diameter (nm)	polydispersity index (PDI)	final RSV conc. (mg/mL)	EE (%)
2.75	7.3	124.0	0.09	0.47±0.01	17.05±0.02
3	8.0	119.6	0.10	0.25±0.02	8.38±0.59

Liposomes with an initial conc. of RSV (mg/mL)	hours of dialysis	final absolute conc. of RSV in liposomes (mg/mL)	EE (%)	final absolute conc. of RSV in the medium (µg/mL)	Conc. of RSV liposome + medium (%)
2.75	0	0.41±0.01	15.07±0.06	0.000±0.00	14.9
2.75	3	0.53±0.01	19.19±0.08	0.018±0.01	19.3
2.75	6	0.47±0.02	17.04±0.93	0.010±0.01	17.1
2.75	9	0.47±0.01	17.05±0.02	0.007±0.01	17.1
2.75	24	0.34±0.03	12.23±1.17	0.007±0.01	12.4
2.75	27	0.36±0.01	13.22±0.01	0.011±0.01	13.1
2.75	30	0.35±0.01	12.93±0.02	0.009±0.01	12.7
2.75	33	0.34±0.01	12.36±0.01	0.010±0.01	12.4
3	0	0.16±0.01	5.32±0.36	0.000±0.00	5.3
3	3	0.29±0.02	9.62±0.60	0.009±0.00	9.7

3	6	0.29±0.01	9.58±0.07	0.007±0.01	9.7
3	9	0.25±0.02	8.38±0.59	0.008±0.01	8.3
3	24	0.15±0.01	5.16±0.10	0.006±0.01	5.0
3	27	0.18±0.01	5.98±0.37	0.010±0.01	6.0
3	30	0.19±0.02	6.32±0.57	0.012±0.01	6.3
3	33	0.16±0.01	5.35±0.01	0.011±0.01	5.3

The final absolute concentrations of resveratrol and EE are lower than expected values.
Each sample of liposomes was diluted with eluent 20-times instead of 100-times; probably this dilution is not sufficient to disrupt the vesicles completely. So the samples may be not homogeneous and it may explain also the increase of the concentration of resveratrol after 3 hours of dialysis in both of the samples.
The concentrations of resveratrol in the medium are quite constant in time; it means that presumably an equilibrium is reached after 3 hours, before every refreshment.
The final concentrations of resveratrol in the medium are lower than the value of its solubility in water that it is < 0.001 mol/mL = 228.25 µg/mL (Caddeo C, 2008); probably mostly of the uncapsulated resveratrol remain at the bottom of the beaker because of its poor solubility in the medium.
Dialysis could be stopped after 24 hours and every refreshment could be done every 3 hours.

III.3.2. Stability

III.3.2.1. Stability test of free resveratrol in solution

To our best knowledge no more studies have been reported on the stability of resveratrol in solution. Some authors had tested solid trans-resveratrol under accelerated stability conditions (75% humidity and 40°C) for up to 4 years and under ambient conditions (60% humidity and 25°C) in a mixture with other grape polyphenols for 2 years. No significant decay in the content of resveratrol was observed in the presence of atmospheric oxygen and humidity. In addition, no by-products attributable to the stilbenoid degradation, neither *trans–cis* isomerism or oxidation, were detected (Bertelli AA, 1998; Prokop J, 2006). Resveratrol content also stayed stable in the skins of grapes and pomace taken after fermentation and stored for a long period (Roy H, 2005).

100 µM aqueous solution of *trans*-resveratrol was stable for at least 8 h at room temperature when protected from light (resveratrol oxidation products were absent) (Camonta L, 2009). *Trans*-resveratrol in hydro-alcoholic solutions has been reported to be stable in the dark (Trela BC, 1996; Camonta L, 2009). The stability of *trans*-resveratrol is valuated in absence and in presence of sunlight.

The solubility of resveratrol is very low (< 0.001 mol/mL = 228.25 µg/mL by Caddeo C, 2008) so the stability in solution was evaluated for 2 concentrations (1 and 10 mg/mL) in the mobile phase of the HPLC/PDA isoctratic method.

Initial concentration of resveratrol in eluent was 1 mg/mL:

Condition	Time	Found concentration of resveratrol in eluent (mg/mL)	Amount of resveratrol (%)
darkness	**0**	**0.94±0.02**	**100**
darkness	3 hours	0.93±0.02	99.1
darkness	7 hours	0.92±0.01	97.4
darkness	1 day	0.90±0.03	95.4
darkness	2 days	0.90±0.02	96.2
darkness	3 days	0.91±0.03	97.1
darkness	4 days	0.90±0.01	95.5
darkness	9 days	0.89±0.18	94.2
darkness	10 days	0.83±0.01	88.3
darkness	14 days	0.85±0.10	90.9
darkness	16 days	0.87±0.01	92.7
darkness	18 days	0.74±0.09	78.6
darkness	21 days	0.73±0.00	77.8
sunlight	**0**	**0.83±0.01**	**100**
sunlight	3 hours	0.82±0.04	98.7
sunlight	7 hours	0.78±0.01	93.9
sunlight	1 day	0.77±0.01	91.9
sunlight	2 days	0.70±0.03	84.0
sunlight	3 days	0.60±0.05	72.5
sunlight	4 days	0.59±0.01	70.8
sunlight	9 days	0.60±0.07	72.5
sunlight	10 days	0.61±0.03	73.2
sunlight	14 days	0.55±0.03	66.0
sunlight	16 days	0.56±0.06	66.8
sunlight	18 days	0.50±0.02	59.8
sunlight	21 days	0.44±0.01	53.2

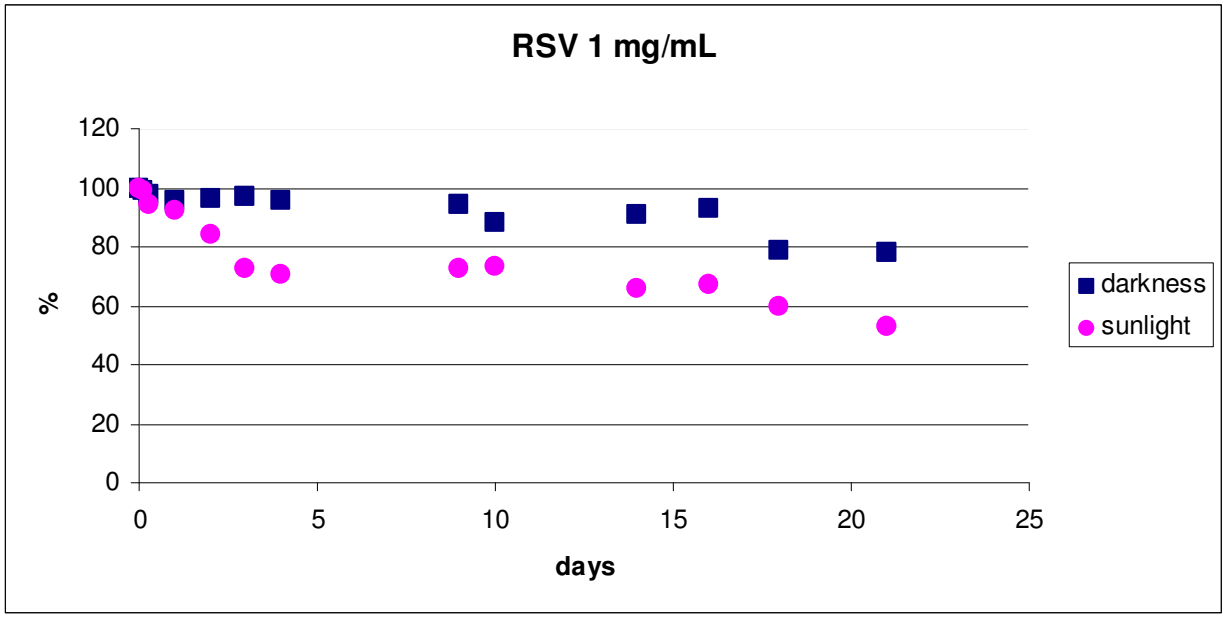

Fig 40. Stability in time of RSV 1 mg/mL in eluent.

Initial concentration of resveratrol in eluent was 10 mg/mL:

Condition	Time	Found concentration of resveratrol in eluent (mg/mL)	Amount of resveratrol (%)
darkness	**0**	**8.88±0.04**	**100.0**
darkness	3 hours	8.45±0.08	95.2
darkness	7 hours	8.53±0.01	96.0
darkness	1 day	8.62±0.09	97.8
darkness	2 days	8.33±0.01	93.8
darkness	3 days	8.04±0.02	90.5
darkness	4 days	7.88±0.01	88.7
darkness	9 days	7.98±1.74	89.9
darkness	10 days	7.72±0.14	87.0
darkness	14 days	8.04±0.55	90.5
darkness	16 days	7.58±0.73	85.4
darkness	18 days	7.24±1.07	81.6
darkness	21 days	6.37±0.01	71.7
sunlight	**0**	**9.76±0.04**	**100**
sunlight	3 hours	9.33±0.01	95.6
sunlight	7 hours	9.63±0.02	98.7
sunlight	1 day	8.36±0.03	85.6
sunlight	2 days	7.36±0.09	75.4
sunlight	3 days	7.90±0.13	80.9
sunlight	4 days	7.65±0.01	78.3
sunlight	9 days	6.99±0.30	71.6
sunlight	10 days	7.24±0.18	74.1
sunlight	14 days	5.98±0.43	61.2
sunlight	16 days	6.22±0.20	63.7
sunlight	18 days	5.66±0.49	58.0
sunlight	21 days	4.79±0.01	49.1

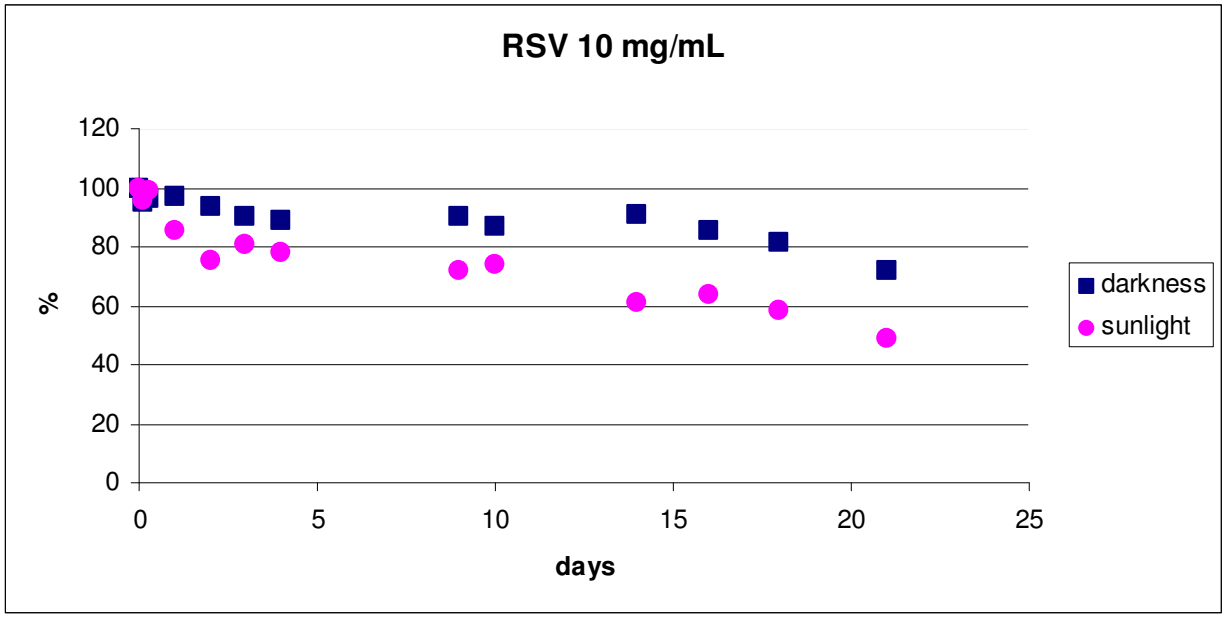

Fig 41. Stability in time of RSV 10 mg/mL in eluent.

The amount of resveratrol with the initial concentration of 1 mg/mL after 16 days is reduced to 92.7% keeping it covered by light and to 66.8% keeping it under the sunlight.
The amount of resveratrol with the initial concentration of 10 mg/mL after 14 days is reduced to 90.5% keeping it covered by light and to 61.2% keeping it under the sunlight.
So, resveratrol is stable in solution within 21 days if it is kept in the dark.

III.3.2.2. Stability test of resveratrol-loaded LC liposomes at different temperatures

The stability of long circulating liposomes formulation was evaluated keeping a batch of empty liposomes in fridge (+4℃) in order to evaluated their stability during time.

empty liposomes		**Time (days)**
diameter (nm)	**PDI**	
127.8	0.10	**0**
138.5	0.04	**1**
135.4	0.06	**9**
135.5	0.09	**13**
133.9	0.07	**15**
132.5	0.09	**17**
126.4	0.06	**20**

The formulation without the drug was stable after 20 days, kept at 4 ℃.
Resveratrol-loaded long circulating liposomes with different initial concentrations of resveratrol (0.1, 0.2 and 0.3 mg/mL) have been prepared. They were kept at different temperatures in order to understand their stability in time, resveratrol's chemical degradation profile and their future right way of stocking. At scheduled intervals, aliquots of liposomes were removed and the size in time and the content of resveratrol were determined.
Conditions:

- RTD room temperature (+20℃) and darkness
- RTS room temperature (+20℃) under the sunlight
- fridge (+4℃)
- oven (+37℃) at the body temperature.

Physical stability of vesicular dispersion was investigated by DLS measurements. Chemical stability that means resveratrol stability was checked by HPLC/PDA analysis.

Results derived from DLS analysis:

RSV 0.1 mg/mL loaded liposomes		**RSV 0.2 mg/mL loaded liposomes**		**RSV 0.3 mg/mL loaded liposomes**		**Time**	**condition**
diameter (nm)	**PDI**	**diameter (nm)**	**PDI**	**diameter (nm)**	**PDI**		
126.6	**0.08**	**139.9**	**0.11**	**133.4**	**0.02**	**0**	**RTD**
132.8	0.08	137.8	0.07	134.9	0.01	**1 hour**	**RTD**
131.6	0.02	136.1	0.10	132.6	0.06	**3 hours**	**RTD**
128.8	0.07	134.9	0.08	133.1	0.07	**7 hours**	**RTD**
131.2	0.05	138.1	0.07	133.1	0.08	**1 day**	**RTD**
129.9	0.04	135.1	0.09	133.5	0.07	**4 days**	**RTD**
126.6	**0.08**	**139.9**	**0.11**	**133.4**	**0.02**	**0**	**RTS**
132.5	0.08	138.6	0.07	136.8	0.04	**1 hour**	**RTS**
133.6	0.06	138.2	0.10	139.4	0.08	**3 hours**	**RTS**

134.0	0.07	136.5	0.05	133.3	0.08	**7 hours**	**RTS**
130.5	0.03	139.3	0.07	136.3	0.06	**1 day**	**RTS**
124.1	0.11	126.7	0.10	129.0	0.09	**4 days**	**RTS**
126.6	**0.08**	**139.9**	**0.11**	**133.4**	**0.02**	**0**	**+4℃**
133.0	0.08	134.0	0.08	135.9	0.04	**1 hour**	**+4℃**
131.3	0.03	137.8	0.06	135.8	0.09	**3 hours**	**+4℃**
130.0	0.07	136.1	0.09	132.1	0.04	**7 hours**	**+4℃**
134.1	0.02	138.1	0.07	132.7	0.09	**1 day**	**+4℃**
125.7	0.08	132.3	0.10	129.8	0.12	**4 days**	**+4℃**
126.6	**0.08**	**139.9**	**0.11**	**133.4**	**0.02**	**0**	**+37℃**
136.9	0.23	137.1	0.07	135.0	0.07	**1 hour**	**+37℃**
128.2	0.07	136.5	0.09	135.2	0.09	**3 hours**	**+37℃**
131.1	0.07	136.5	0.04	134.5	0.09	**7 hours**	**+37℃**
131.5	0.08	138.6	0.06	136.9	0.08	**1 day**	**+37℃**
128.9	0.08	137.9	0.31	133.8	0.10	**4 days**	**+37℃**

There were no differences between the formulations kept at different temperature regarding the physical stability in time.

Results derived from HPLC/PDA analysis:

initial conc. of RSV (mg/mL)	**final absolute conc. of RSV (mg/mL)**	**final absolute conc. of RSV (mM)**	**EE (%)**
0.1	0.077±0.01	0.339±0.02	77.45±4.73
0.2	0.120±0.01	0.527±0.02	60.12±1.94
0.3	0.168±0.01	0.735±0.03	55.95±2.66

RSV 0.1 mg/mL loaded liposomes		RSV 0.2 mg/mL loaded liposomes		RSV 0.3 mg/mL loaded liposomes		Time	Condition
EE (%)	RSV % of initial content	EE (%)	RSV % of initial content	EE (%)	RSV % of initial content		
77.45±4.73	**100**	**60.12±1.94**	**100**	**55.95±2.66**	**100**	**0**	**RTD**
77.45±4.73	100	60.12±1.94	100	45.00±1.51	80.43±2.70	**10 min.**	**RTD**
73.85±1.34	95.35±1.74	58.25±1.13	96.88±1.88	45.52±1.06	81.36±1.89	**30 min.**	**RTD**
75.75±1.63	97.80±2.10	59.45±1.41	98.87±2.35	47.20±0.47	84.36±1.83	**1 hour**	**RTD**
74.45±3.04	96.12±3.92	58.85±2.05	97.88±3.41	54.33±1.36	97.11±2.44	**3 hours**	**RTD**
77.95±5.87	100.64±7.57	57.37±4.56	95.42±7.59	54.11±0.26	96.72±0.47	**7 hours**	**RTD**
61.40	79.28	42.45	70.60	48.30	86.33	**1 day**	**RTD**
48.30	62.36	31.75	52.81	42.63	62.36	**4 days**	**RTD**
77.45±4.73	**100**	**60.12±1.94**	**100**	**55.95±2.66**	**100**	**0**	**RTS**
71.50±0.57	92.31±0.73	54.17±1.24	90.10±2.06	50.75±2.33	90.70±4.16	**10 min.**	**RTS**
68.30±0.61	88.18±0.91	51.15±1.62	85.08±2.69	47.53±2.88	84.96±5.15	**30 min.**	**RTS**
63.60±3.82	82.11±4.93	49.27±2.79	81.95±4.65	42.45±1.24	75.87±2.22	**1 hour**	**RTS**
48.10±0.42	62.10±0.54	36.70±1.98	61.04±3.29	32.11±0.26	57.40±0.47	**3 hours**	**RTS**
47.30±0.85	61.07±1.10	32.02±0.11	53.26±0.18	29.60±1.41	52.90±2.52	**7 hours**	**RTS**
41.00	52.94	27.50	45.74	27.70	49.51	**1 day**	**RTS**
35.30	45.58	23.85	39.67	21.23	37.94	**4 days**	**RTS**
77.45±4.73	**100**	**60.12±1.94**	**100**	**55.95±2.66**	**100**	**0**	**+4℃**
73.85±1.20	95.35±1.56	57.00±0.71	94.80±1.17	55.95±2.69	100	**10 min.**	**+4℃**
79.75±5.59	102.97±7.21	56.30±2.76	93.63±4.59	47.51±0.54	84.92±0.97	**30 min.**	**+4℃**
74.50±2.69	96.19±3.46	54.65±1.91	90.89±3.17	46.13±0.61	82.45±1.10	**1 hour**	**+4℃**
75.35±1.06	97.29±1.37	55.87±2.16	92.93±3.59	52.43±4.15	93.71±7.42	**3 hours**	**+4℃**
79.25±2.90	102.34±3.76	57.15±1.06	95.05±1.77	48.56±0.80	86.80±1.43	**7 hours**	**+4℃**
76.50	98.77	50.55	84.07	50.33	89.95	**1 day**	**+4℃**
69.80	90.12	50.05	83.24	48.10	85.97	**4 days**	**+4℃**
77.45±4.73	**100**	**60.12±1.94**	**100**	**55.95±2.66**	**100**	**0**	**+37℃**
78.15±2.62	100.90±3.39	54.35±4.10	90.39±6.82	51.93±6.55	92.82±11.72	**10 min.**	**+37℃**
76.35±2.05	98.58±2.64	53.32±3.08	88.69±5.12	49.68±2.67	88.95±4.55	**30 min.**	**+37℃**
77.90±1.41	100.58±1.82	54.75±4.18	91.06±6.94	50.93±4.19	92.58±5.31	**1 hour**	**+37℃**
77.20±2.69	99.67±3.47	54.10±2.47	89.98±4.11	51.43±2.45	91.93±4.38	**3 hours**	**+37℃**
75.00±1.27	96.83±1.65	53.85±1.98	89.56±3.29	47.83±2.47	85.48±5.31	**7 hours**	**+37℃**
75.5	96.19	51.75	86.07	49.43	88.35	**1 day**	**+37℃**
71.3	92.06	41.35	68.77	38.87	69.47	**4 days**	**+37℃**

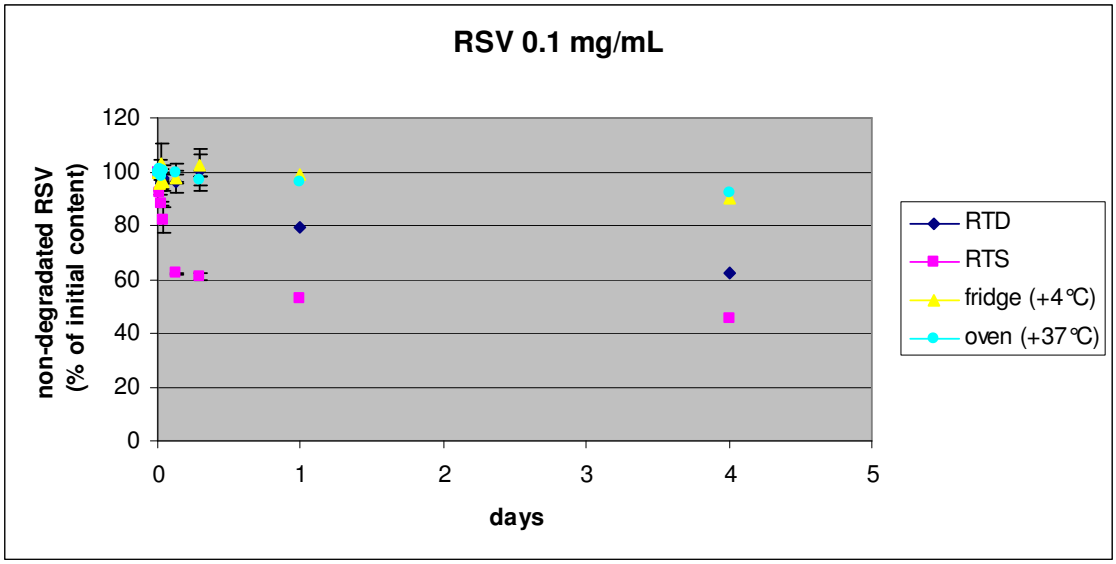

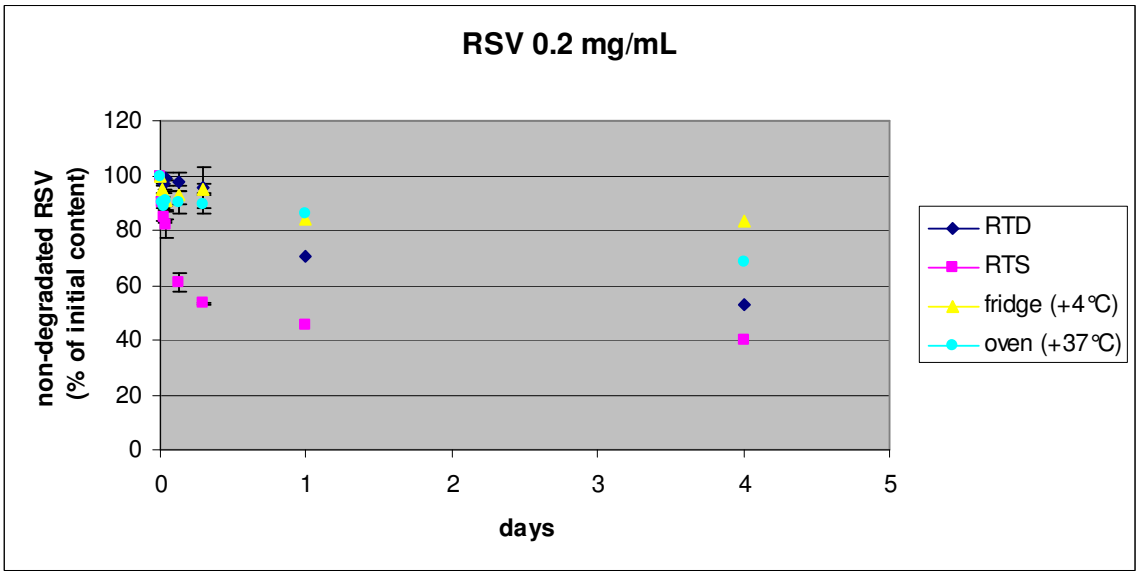

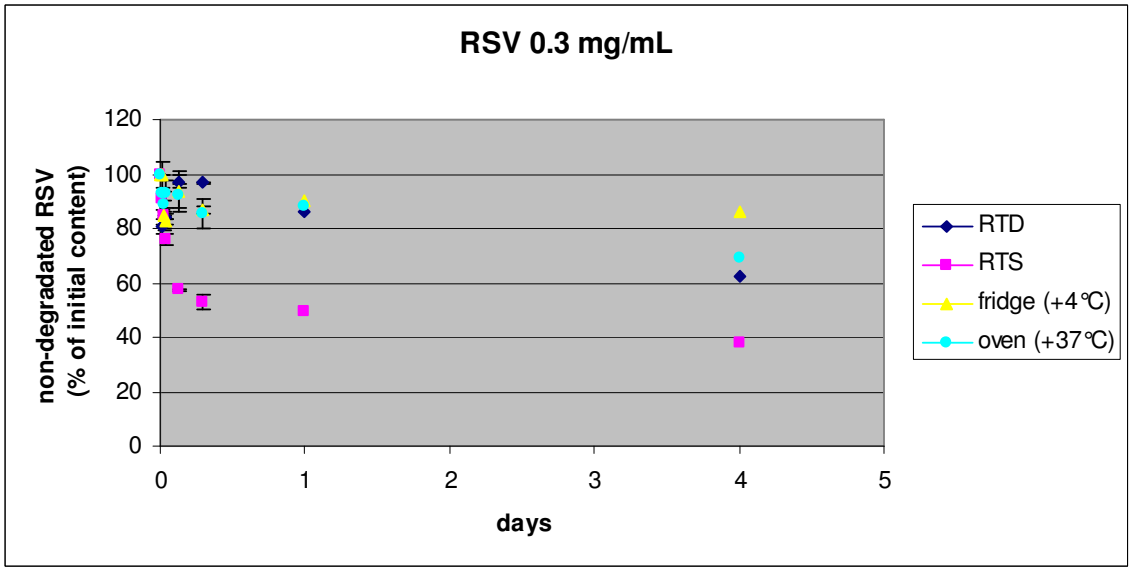

Fig 42. Stability in time of RSV-loaded LCL at different temperatures with initial concentrations of resveratrol of 0.1 mg/mL (up), 0.2 mg/mL (middle) and 0.3 mg/mL (down).

All the three tested formulations were stable at 4°C between the 83-90%. The best way of stocking is keeping them in the fridge before using.
The solar radiations were responsible of the chemical degradation of resveratrol, indeed in the formulation with initial concentration of the drug of 0.1, 0.2 and 0.3 mg/mL, the percentage of non-degradated resveratrol was 45.58, 39.67 and 37.94% respectively.
At the wavelength of 208 nm *cis*-resveratrol was not found, so other oxidated or degradated products were occurred during the storage of the formulations at room temperature under sunlight.
At the body temperature, in the formulation with initial concentration of the drug of 0.1, 0.2 and 0.3 mg/mL, the percentage of non-degradated resveratrol was 92.06, 68.77 and 69.47% respectively. The formulation with the lower initial concentration of resveratrol (0.1<0.2<0.3 mg/mL) but with the higher encapsulation efficacy than the others (77.45<60.12<55.95 %EE) was more stable. That means that the free resveratrol was more suscettible to degradation; if it was inside the vesicles it was more protected.

initial RSV conc. (mg/mL)	molar ratio (%)	mean diameter (nm)	polydispersity index (PDI)	final RSV conc. (mg/mL)	EE (%)
0.1	0.3	126.6	0.08	0.08±0.01	77.45±4.73
0.2	0.5	139.9	0.11	0.12±0.01	60.12±1.94
0.3	0.8	133.4	0.02	0.17±0.01	55.95±2.66

Initial concentration of resveratrol was increased in order to find the best balance between final absolute concentration and encapsulation efficacy of resveratrol inside the vesicles. So, resveratrol-loaded long circulating liposomes with different initial concentrations of resveratrol (0.5, 1 and 1.5 mg/mL) were been prepared and they were kept in the fridge (+4°C) and at scheduled intervals, aliquots of liposomes were removed and the size in time and the chemical degradation profile was determined.
Conditions:

- fridge (+4°C)
- oven (+37°C) at the body temperature.

Physical stability of vesicular dispersion was investigated by DLS measurements. Chemical stability that means resveratrol stability was checked by HPLC/PDA analysis.

Results derived from DLS analysis:

RSV 0.5 mg/mL loaded liposomes		**RSV 1 mg/mL loaded liposomes**		**RSV 1.5 mg/mL loaded liposomes**		**Time**	**condition**
diameter (nm)	**PDI**	**diameter (nm)**	**PDI**	**diameter (nm)**	**PDI**		
130.5	**0.08**	**132.0**	**0.11**	**150.0**	**0.09**	**0**	**+4°C**
134.0	0.04	132.1	0.07	150.6	0.07	**10 min.**	
131.9	0.09	132.2	0.06	150.7	0.06	**30 min.**	
132.3	0.11	133.2	0.07	152.1	0.08	**1 h**	
136.9	0.11	129.7	0.11	146.2	0.07	**3 h**	
135.8	0.07	132.8	0.08	152.7	0.05	**7 h**	
136.2	0.11	133.3	0.10	150.3	0.10	**1 day**	
134.0	0.10	135.3	0.09	151.7	0.06	**4 days**	
134.2	0.11	133.6	0.03	153.6	0.12	**6 days**	
142.3	0.11	140.6	0.12	160.4	0.11	**16 days**	
137.1	0.07	132.1	0.10	152.6	0.10	**21 days**	
153.9	0.03	164.9	0.11	159.5	0.07	**28 days**	

130.5	**0.08**	**132.0**	**0.11**	**150.0**	**0.09**	**0**	
133.0	0.07	130.8	0.09	152.5	0.04	**10 min.**	
130.7	0.10	131.4	0.09	150.9	0.11	**30 min.**	
133.0	0.07	132.8	0.10	148.2	0.09	**1 h**	
133.9	0.07	134.0	0.10	148.2	0.09	**3 h**	
133.6	0.09	131.1	0.07	152.1	0.06	**7 h**	**+37℃**
138.0	0.10	132.5	0.07	152.8	0.10	**1 day**	
137.5	0.07	136.1	0.05	151.2	0.07	**4 days**	
133.2	0.09	135.9	0.05	155.6	0.07	**6 days**	
142.9	0.08	144.6	0.09	173.2	0.07	**16 days**	
141.3	0.04	139.9	0.11	162.5	0.08	**21 days**	
165.2	0.06	161.4	0.08	179.8	0.05	**28 days**	

All the three tested formulations were stable within 21 days. After 28 days, the index of polidispersity were acceptable but the mean diameters were >140 nm.
The liposomes with the initial concentration of resveratrol of 1.5 mg/mL had a size >145 nm at time zero and a lower encapsulation efficacy (21.34%, table below), so the other two formulations seem more suitable.

Results derived from HPLC/PDA analysis:

Initial RSV concentration (mg/mL)	**Final RSV concentration (mg/mL)**	**Final RSV concentration (mM)**	**EE (%)**
0.5	0.34±0.04	1.48±0.19	67.79±8.50
1	0.49±0.07	2.15±0.30	49.02±6.60
1.5	0.32±0.01	1.40±0.05	21.34±0.72

RSV 0.5 mg/mL loaded liposomes		**RSV 1 mg/mL loaded liposomes**		**RSV 1.5 mg/mL loaded liposomes**		**Time**	**Condition**
EE (%)	**RSV % of initial content**	**EE (%)**	**RSV % of initial content**	**EE (%)**	**RSV % of initial content**		
67.79±8.50	**100**	**49.02±6.60**	**100**	**21.34±0.72**	**100**	**0**	
60.03±2.45	88.55±3.61	45.78±0.33	93.39±0.68	20.66±0.24	96.81±1.12	**10 min.**	
59.15±0.35	87.25±0.52	46.14±2.42	94.12±4.95	20.00±0.13	93.72±0.59	**30 min.**	
60.60±0.20	89.39±0.29	44.65±0.20	91.08±0.42	22.67±1.81	106.23±8.48	**1 h**	
68.99±6.89	101.74±10.12	45.36±0.60	92.53±1.22	21.23±1.07	99.48±5.04	**3 h**	
60.81±0.18	89.7±0.27	40.55±1.17	82.72±2.38	20.19±1.98	94.61±9.28	**7 h**	
66.70±0.45	98.39±0.66	39.25±0.57	80.06±1.16	20.72±0.49	97.09±2.32	**1 day**	**+4℃**
62.28±1.47	91.87±2.17	42.09±1.77	85.85±3.61	21.61±1.10	101.26±5.17	**4 days**	
69.48±8.23	102.49±12.14	42.43±1.00	86.54±2.04	21.77±1.10	102.04±5.13	**6 days**	
67.07±7.17	98.93±10.58	44.43±0.64	90.17±0.65	23.24±1.70	108.90±7.95	**16 days**	
63.02±0.40	92.96±0.59	34.08±3.94	69.52±8.04	20.69±1.81	96.95±8.48	**21 days**	
67.34±4.89	98.80±6.47	42.60±2.77	86.89±5.65	20.59±1.52	96.51±7.13	**28 days**	
67.79±8.50	**100**	**49.02±6.60**	**100**	**21.34±0.72**	**100**	**0**	**+37℃**
60.17±0.10	88.76±0.14	45.90±3.21	93.62±6.55	19.34±0.18	90.63±0.86	**10 min.**	
60.43±0.83	89.14±1.23	47.27±6.28	96.42±12.81	19.54±0.98	91.58±4.60	**30 min.**	
63.87±1.03	94.21±1.52	47.38±3.00	96.65±6.13	19.92±0.61	93.34±2.85	**1 h**	
66.39±3.27	97.93±4.81	48.60±2.86	99.13±5.82	20.62±0.95	96.63±4.44	**3 h**	
68.35±8.39	101.12±11.95	47.14±2.89	96.16±5.90	19.83±1.87	92.92±8.75	**7 h**	
62.46±1.92	92.13±2.83	45.52±1.77	92.85±3.61	20.61±0.03	96.57±0.13	**1 day**	
61.79±1.74	91.14±2.57	46.06±2.11	93.96±4.31	21.37±0.71	100.14±3.31	**4 days**	
60.23±1.09	88.84±1.60	46.63±2.04	95.11±4.15	21.92±0.71	102.74±3.35	**6 days**	
63.49±2.11	93.65±3.10	53.31±0.90	109.39±0.93	20.09±1.88	94.14±8.81	**16 days**	

57.83±0.49	85.30±1.02	44.75±0.21	91.28±0.44	16.75±0.99	78.49±4.64	**21 days**
64.65±8.36	95.37±12.33	46.66±1.27	95.18±2.58	20.06±3.05	94.02±14.28	**28 days**

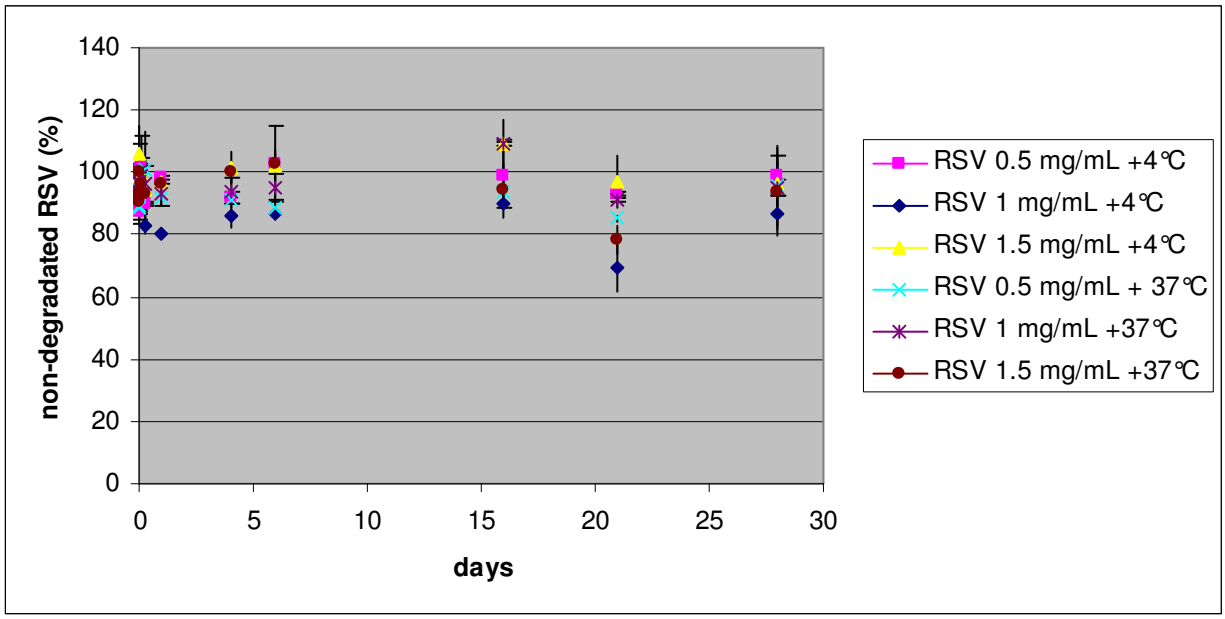

Fig 43. Stability in time of RSV-loaded LCL at different temperatures with initial concentrations of resveratrol of 0.5, 1 and 1.5 mg/mL.

At 4°C, in the formulation with initial concentration of the drug of 0.5, 1 and 1.5 mg/mL, the percentage of non-degradated resveratrol was 98.80, 86.89 and 96.51% respectively.
At the body temperature, in the formulation with initial concentration of the drug of 0.5, 1 and 1.5 mg/mL, the percentage of non-degradated resveratrol was 95.37, 95.18 and 94.02% respectively.
DLS measurements had pointed out that vesicles with the initial concentration of 1.5 mg/mL was not within the optimized dimensional range.
Within 21 days, both at 4°C and 37°C, neither resveratrol chemical degradation, nor vesicles size alteration occurred for the formulations with the initial resveratrol concentration of 0.5 and 1 mg/mL.
As you can see in the table below, the encapsulation efficacy of the formulation with an initial concentration of resveratrol of 0.5 mg/mL is higher than the formulation with an initial concentration of resveratrol of 1 mg/mL (65.63>50.58 %EE) but the final concentration of resveratrol encapsulated into the vesicles is higher in the formulation with an initial concentration of resveratrol of 1 mg/mL (0.51>0.33 mg/mL).

initial RSV conc. (mg/mL)	molar ratio (%)	mean diameter (nm)	polydispersity index (PDI)	final RSV conc. (mg/mL)	EE (%)
0.5	1.3	130.9±1.25	0.08±0.01	0.33±0.13	65.63±27.21
1	2.7	134.0±10.39	0.09±0.03	0.51±0.09	50.58±8.85
1.5	4.0	145.9±16.24	0.08±0.03	0.39±0.11	25.89±7.37

So, the formulation with an initial concentration of resveratrol of 1 mg/mL was investigated more with the perspective of *in vivo* experiments.

III.3.2.3. Photostability

Unfortunately, the use of trans-resveratrol in pharmaceutical and cosmetic field is problematic owing to its fast degradation mainly linked to the isomerization from the active

trans form to the inactive *cis* one (Wang Y, 2002). *Cis*- isomer is unactive, it has biological activity unuseful for our aims.

However, in the solid state, whether exposed to light or not, *cis*-resveratrol readily reverts to the *trans*- isomer, the thermodynamically more stable isomer (Trela BC, 1996). Thus, as a solid, resveratrol and its analogs exist predominantly as *trans*- isomers (Prokop J, 2006). *trans*-Resveratrolosides could convert to their *cis*- isomeric form and/or be oxidized in solution (Prokop J, 2006). *Trans*-resveratrol in hydro-alcoholic solutions has been reported to be stable in the dark, with a tendency to isomerise to *cis*-resveratrol when exposed to UV light or sunlight (Trela BC, 1996; Camonta L, 2009). 100 µM aqueous solution of *trans*-resveratrol was stable for at least 8 h at room temperature when protected from light (resveratrol oxidation products were absent) (Camonta L, 2009). Trela and Waterhouse (Trela BC, 1996) reported that the isomerisation yield was highly variable, and depended on the UV wavelength (10% vs 90% after 1 h irradiation at 254 and 366 nm, respectively). The use of natural UV from sunlight for isomerisation is probably less efficient than exposure to an UV lamp and the exact equilibrium mixture may depend on the specific spectrum of light reaching the sample (Camonta L, 2009).
So, the stability of resveratrol in solution will be tested under UV lamp at different concentrations: 1 and 10 mg/mL in eluent.
Initial concentration of resveratrol in eluent was 1 mg/mL:

time	found concentration of RSV in eluent (mg/mL)	amount of RSV (%)
0	**0.94±0.02**	**100**
10 seconds	0.69±0.02	73.4
30 seconds	0.55±0.01	58.4
1 minute	0.40±0.01	42.6
2 minutes	0.32±0.01	33.8
4 minutes	0.27±0.01	28.7
6 minutes	0.23±0.02	24.1
8 minutes	0.18±0.01	19.0
16 minutes	0.10±0.01	11.1

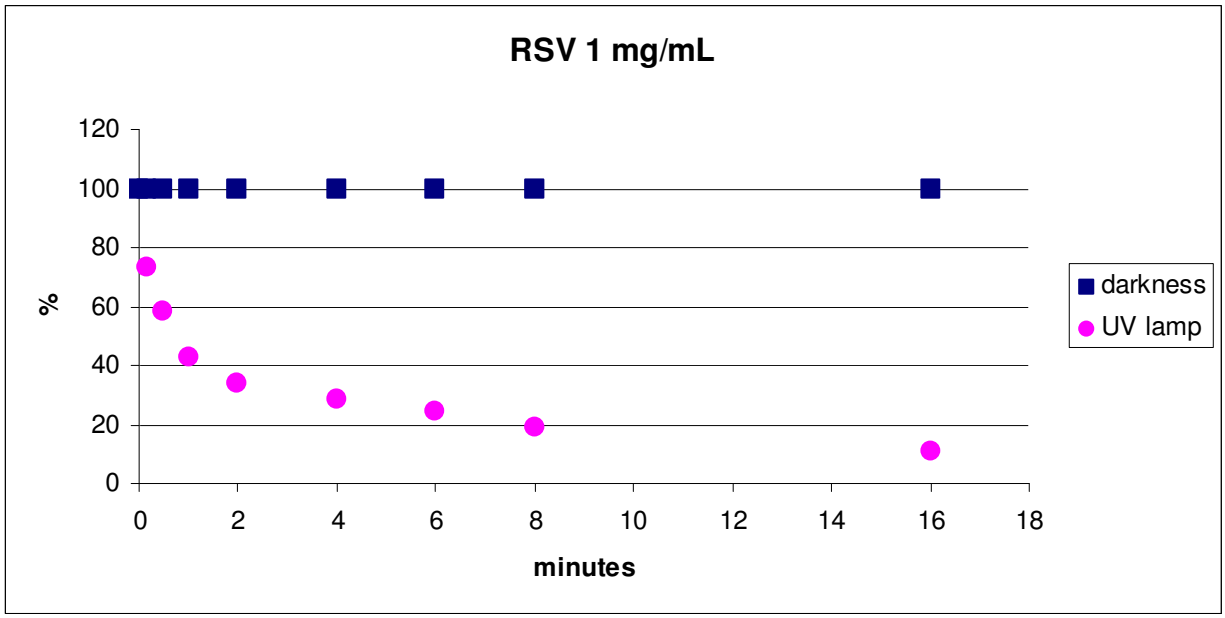

Fig 44. Photostability of RSV 1 mg/mL in eluent under UV lamp.

Initial concentration of resveratrol in eluent was 10 mg/mL:

time	found concentration of RSV in eluent (mg/mL)	amount of RSV (%)
0	9.76±0.04	**100**
10 seconds	8.32±0.00	85.3
30 seconds	6.57±0.48	67.3
1 minute	5.61±0.02	57.4
2 minutes	4.25±0.18	43.5
4 minutes	3.62±0.07	37.1
6 minutes	3.63±0.05	37.2
8 minutes	3.51±0.18	36.0
16 minutes	3.23±0.12	33.1

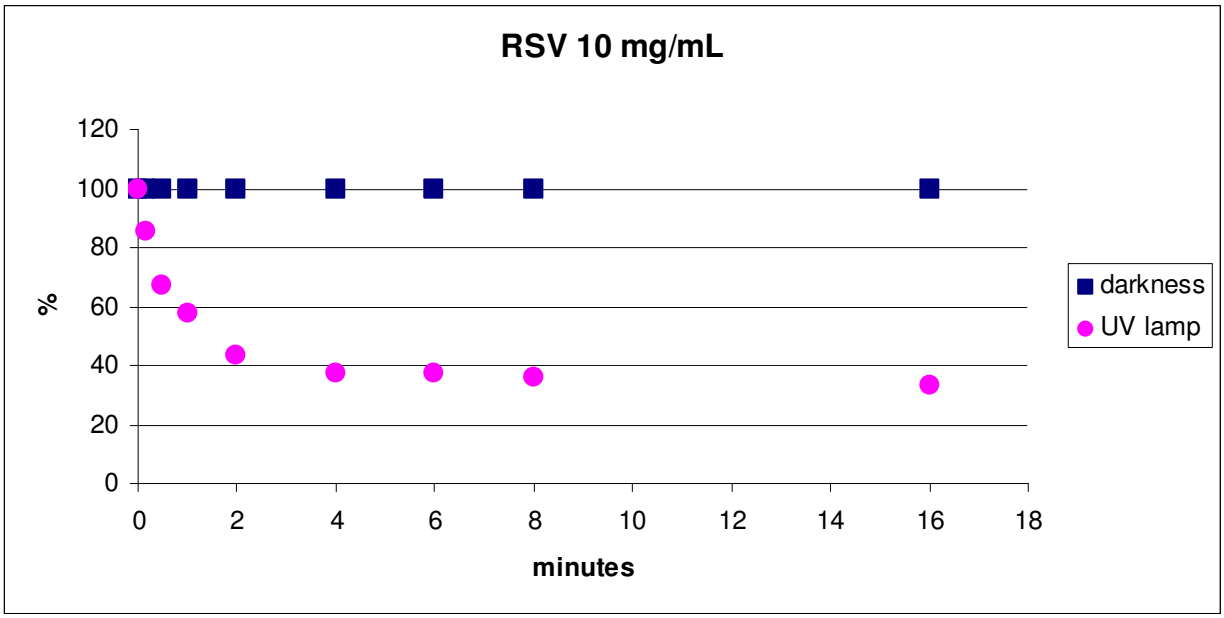

Fig 45. Photostability of RSV 10 mg/mL in eluent under UV lamp.

Under UV lamp (60%, 5982 mW/cm^2, 717840 mJ/cm^2), the amount of resveratrol with the initial concentration of 1 mg/mL after 1 minute is reduced to 42.6%. The amount of resveratrol with the initial concentration of 10 mg/mL after 1 minute is reduced to 57.4%.
A resveratrol-loaded long circulating liposomes with the same initial concentration of resveratrol 1 mg/mL of a solution of resveratrol in eluent was prepared to understand if vesicles can protect resveratrol from the photosensibilization that can provoke the *trans/cis*-isomeritation. Photostability of resveratrol-loaded long circulating liposomal formulations in comparison with resveratrol solution was measured.

Initial RSV concentration (mg/mL)	RSV concentration before dialysis (mg/mL)	RSV concentration after dialysis (mg/mL)	Final RSV concentration (mM)	EE (%)
1	0.64±0.06	0.49±0.05	2.13±0.20	48.6±4.66

Results derived from DLS analysis:

RSV 1 mg/mL loaded liposomes	Time

diameter (nm)	PDI	
177.7±0.01	0.11±0.01	**0**
174.6±0.02	0.07±0.01	**10 sec.**
176.1±0.03	0.05±0.01	**30 sec**
173.8±2.76	0.04±0.01	**1 min.**
168.1±0.28	0.07±0.01	**2 min.**
162.6±0.35	0.09±0.04	**4 min.**
162.7±3.96	0.08±0.01	**6 min.**
167.3±2.54	0.07±0.04	**8 min.**
164.3±1.77	0.06±0.01	**16 min.**

Results derived from HPLC/PDA analysis:

RSV 1 mg/mL	Found concentration of RSV (mg/mL)	Amount of RSV (%)	Time
in eluent	**0.94±0.02**	**100**	**0**
in eluent	0.69±0.02	72.6±2.55	**10 sec.**
in eluent	0.55±0.01	57.8±0.21	**30 sec**
in eluent	0.40±0.01	42.1±0.23	**1 min.**
in eluent	0.32±0.01	33.4±1.22	**2 min.**
in eluent	0.27±0.01	28.4±1.13	**4 min.**
in eluent	0.23±0.02	23.8±1.72	**6 min.**
in eluent	0.18±0.01	18.8±0.81	**8 min.**
in eluent	0.10±0.01	11.0±0.99	**16 min.**
loaded liposomes	**0.64±0.06**	**100**	**0**
loaded liposomes	0.60±0.01	94.3±0.01	**10 sec.**
loaded liposomes	0.60±0.01	93.8±0.20	**30 sec**
loaded liposomes	0.54±0.06	84.5±10.24	**1 min.**
loaded liposomes	0.47±0.02	73.8±2.76	**2 min.**
loaded liposomes	0.40±0.05	62.7±8.05	**4 min.**
loaded liposomes	0.49±0.23	69.3±5.40	**6 min.**
loaded liposomes	0.42±0.09	65.7±4.16	**8 min.**
loaded liposomes	0.43±0.15	67.4±4.40	**16 min.**

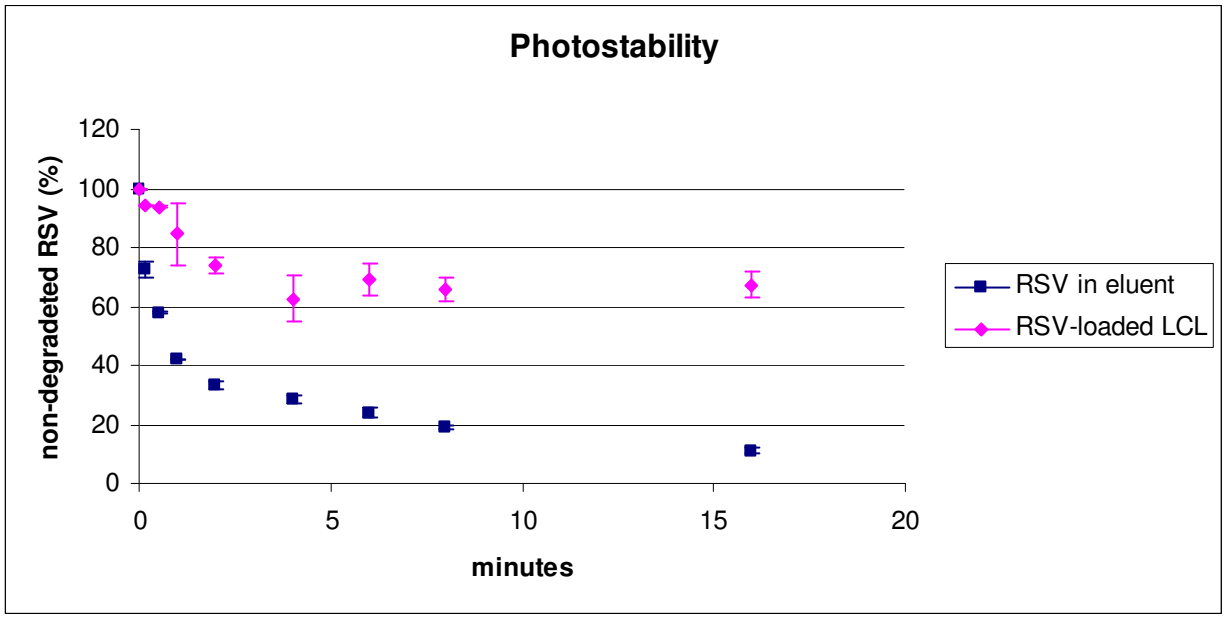

Fig 46. Photostability of RSV-loaded LCL with initial concentration of 1 mg/mL under UV lamp.

Under UV lamp the amount of resveratrol with the initial concentration of 1 mg/mL after 1 minute is reduced to 42.1%; if the same content of resveratrol was encapsulated in liposomes, it was reduced to 84.5%. It is clear that the vehicle is able to protect resveratrol from chemical degradation and photodegradation. Vesicles can protect resveratrol from the photosensibilization that can provoke the *trans/cis*-isomeritation.

III.3.3. Stability in presence of blood protein

To further advance biomedical application, it is important to characterize the interactions between liposomes and blood components, particularly with serum proteins that play an important role in the stability and properties of liposomes in blood e.g. in their circulation lifetimes (Panagi Z, 1999; Chonn A, 1992). The amount of serum proteins associated on the liposomes used was inversely related to their circulation half-lives (Chonn A, 1992).
The serum proteins associated onto the surface of liposomes systematically administered have been suggested to be one of the most important factors to determine their in vivo fate (Drummond DC, 1999; Luigi C, 2003). The amount of blood protein associated with liposomes in the circulation dramatically affects liposome clearance behaviour in vivo (Chonn A, 1992). Specific bounded proteins can have a direct effect on particle internalization and biodistribution. Certain proteins allow macrophages of the reticuloendothelial system (RES) to more easily recognize nanoparticles (Owens DE, 2006). On the other hand, dysopsonins such as albumin are said to promote prolonged circulation times in the blood (Goppert TM, 2005; Moghimi SM, 1993; Ogawara K, 2004).
It has been found that proteins partially penetrate (Sweet C, 1969; Law SL, 1986, 1988; Juliano, 1971; Sabin J, 2009) and modify the lipid bilayer (Lis LJ, 1967; Hoekstra H, 1979) when they are in contact with the membrane surface. This protein penetration into the liposomal membrane can change the properties of the bilayer with drastic consequences in their use as drug delivery systems (Sabin J, 2009).
Increase in the rate of efflux of different liposomal contents in contact with serum albumin has been reported (Sweet C, 1969 1970; Zborowski J, 1977), but the role of albumin in phospholipid transfer, leading to loss of bilayer integrity and release of liposomal contents, is controversial.

Near-physiological concentration (30 mg/mL) of albumin dissolved more then 50% of liposomes (Michnik A, 1997).
The addition of PEG can add protein/opsonization resistance properties by preventing interactions between the particle surface and the plasma proteins (Owens DE, 2006; Jeon SI, 1991). Often water-soluble polymers like polyethylene glycol (PEG) are attached to the surface of long-circulating liposomes to reduce adhesion of opsonic plasma proteins that would otherwise induce recognition and rapid removal from the circulation by macrophages in the liver and spleen (Woodle MC, 1992; 1994; Oku N, 1994; Aggarwal P, 2009, figure **47**). Using this approach, PEG-coated long-circulating liposomes can remain in the circulation with a half-life as long as 50 hours (Gabizon A, 1994; Hong RL, 2001).

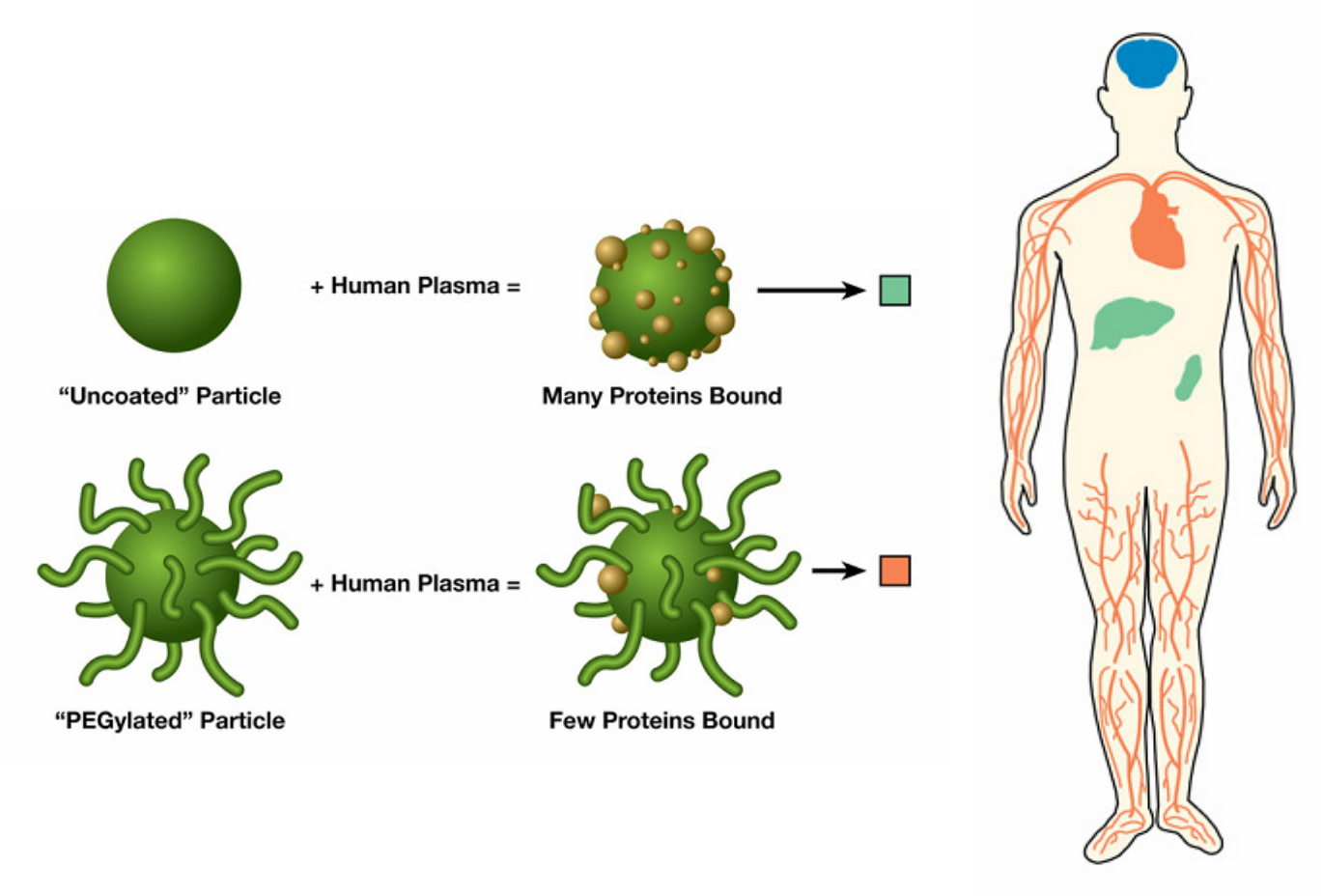

Fig 47. Biodistribution of nanoparticles with varying coatings and bound proteins.
Uncoated particles bind proteins and are taken up by the RES into the liver and spleen. PEGylated particles bind very fewproteins, avoid uptake by the RES, and are longer circulating in the blood (Aggarwal P, 2009).

Application of liposomes as drug carriers is associated with their stability in the bloodstream.
Stability test of resveratrol-loaded and empty long-circulating fluorescent liposomes in presence of blood protein like albumin was performed in order to assess the capacity of albumin to extract the constituents of the bilayer and modified or disrupt the vesicles (size changes) and to assess the capacity of albumin to extract resveratrol from the formulation (drug content changes).

III.3.3.1. Fluorescent Activated Cell Sorting (FACS)

Measure particle size do not allow reliable measurements in the presence of small particulate contaminations present in biological fluids as serum (Hsu CY, 2008). Serum is a complex fluid containing (amongst other) serum albumin, lipoproteins, immuno-, γ- and macrogobulins, and oleic acid (van Gaal E, 2009). This heterogeneous nature can give rise to significant background signals, whereas sizing techniques based on conventional light scattering require minimum levels of background noise for generation of accurate results. With imaging techniques such as electron microscopy individual particles can be studied, however, these techniques are laborious and have poor statistical power. Imaging is particularly valuable to obtain information regarding particle morphology, but when deriving sizes from images one should be aware of the risk for artefacts (Vorauer-Uhl K, 2000; van Gaal E, 2009).
Flow cytometry is a well established technique that integrates light scattering and fluorescence measurements to gather information regarding size, shape, morphology of cells and presence and intensity of diverse fluorescent signals. Flow cytometry was originally developed as a tool to study cells, which have typical sizes of 2–120 µm (with a majority being 10–20 µm), and attempts to apply this method to submicron particles are scarce. Recently this technique was exploited to study submicron matter, including unilamellar synthetic vesicles (Fuller LL, 1996), liposomes (Vorauer-Uhl K, 2000) and viral particles (Hercher M, 1979; Steen HB, 2004).
Each single particle is measured in a continuous flow system, which is in contrast to the well-established light scattering systems, where a suspension is measured in a closed containment. By FACS, the detection of particles may be performed at an angle of 10° forward scatter and at 90° side scatter (Vorauer-Uhl K, 2000). As with cells (Salgado FJ, 2003; 2005), the diffraction of the laser beam (forward scatter, FSC) is proportional to the liposome size while refraction plus reflection of the beam (side scatter, SSC) is proportional to the complexity of the liposome.
For a representative measurement, 10000 particles per sample were analyzed (Vorauer-Uhl K, 2000).

III.3.3.1.a. Incubation with albumin and FACS analysis

Empty liposomes and liposomes with initial concentrations of resveratrol of 1 mg/mL were incubated with a solution of albumin (40 mg/mL in PBS) at the body temperature in a shaking waterbath to mimic the *in vivo* condition.
They were labelled with NBD-PE 1% mol and analysed by FACS experiment.

constituent	mg/mL	MW	µmol
DPPC	7.5	734	51.090
18:0/18:0 PEG 2000	2.233	2750	4.060
cholesterol	2.092	387	27.030
DiD	0.0172	1052.1	0.082
NBD-PE	0.1572	956.24	0.822

initial RSV conc. (mg/mL)	diameter (nm)	polydispersity index (PDI)	final RSV conc. (mg/mL)	EE (%)
-	121.4	0.05	-	-
1	124.7	0.05	0.38±0.01	37.9±0.42

III.3.3.1.b. Calibration curve by *by labeled beads*

The size distribution of the liposomes was determined by correlating the side scattered signals of the vesicles and the side scattered signals of the calibration beads. The standard beads were analized by FACS and a calibration curve based on measurements of the labelled beads was calculated.

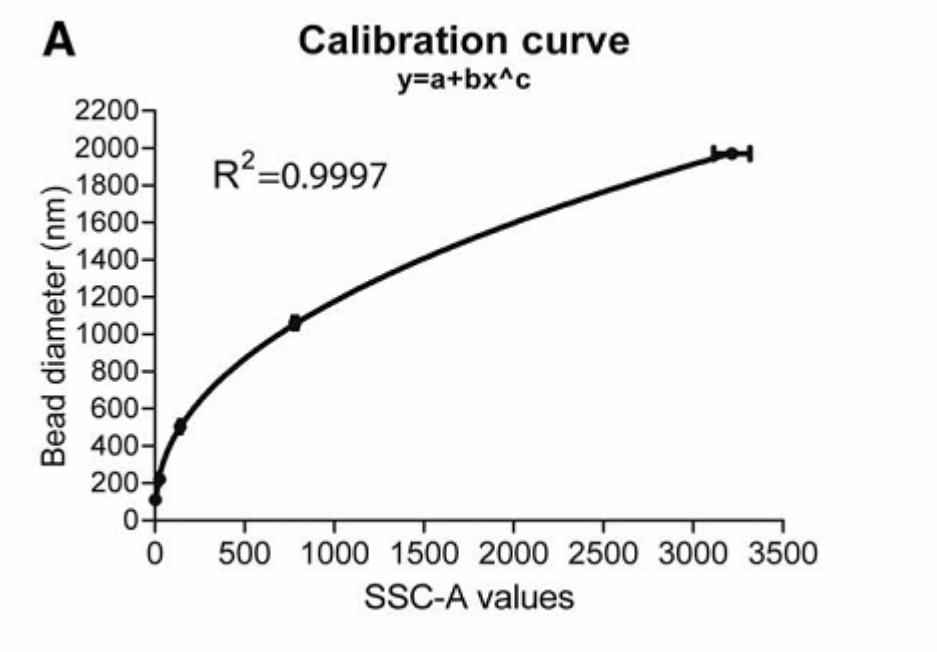

Fig 48. Calibration curve.

The correlation between the mean diameter of the latex beads and their side scatter signals was determined according to equation

$$y = a + bx^c$$

where a = 18.39, b = 52.36 and c = 0.4482 (figure **48**).
Based on this equation, the side scatter signals of different samples may be classified in several size ranges. The following table showa the classification ranges based on latex beads values.

size classes	size range (nm)
P1	4-178
P2	330-930
P3	3500-6500
P10	24000-36000
P11	90000-115000

RSV-loaded liposomes and RSV-loaded liposomes after incubation with albumin (40 mg/mL in PBS) were diluted 4 x 10^3-times in PBS and 4 x 10^2-times in PBS, respectively.

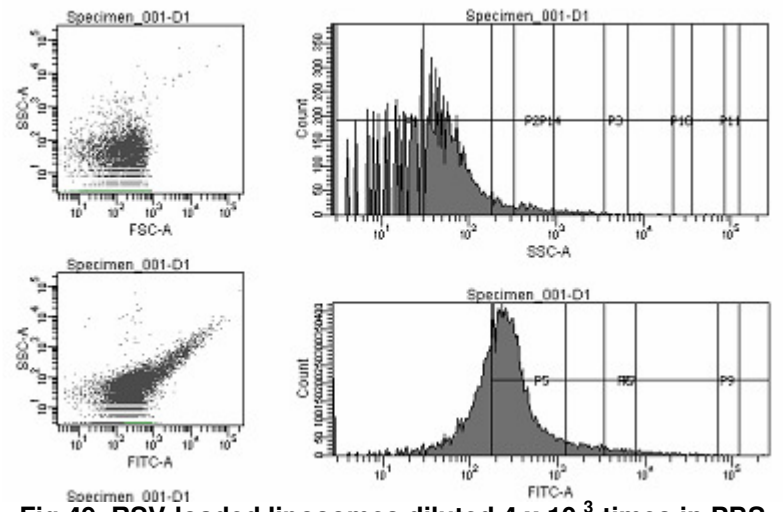

Fig 49. RSV-loaded liposomes diluted 4 x 10 ^{3}-times in PBS

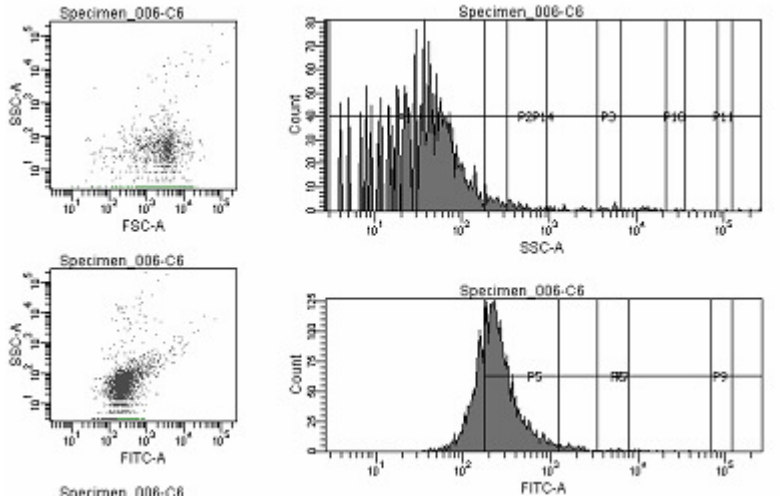

Fig 50. RSV-loaded liposomes after 2 hours of incubation with albumin (40 mg/mL in PBS) diluted 4 x 10^{2}-times in PBS

The dot plots represent the SCC-A (indicative of size) against FITC-A (fluorescence intensity of the particles).
The size of empty and RSV-loaded liposomes are around 100 nm, according with the DLS measurements.
Size is not affected by albumin. The vesicles that remain are stable and intact.

The incubation with albumin was monitored at different time points.
Liposomes were labelled with NBD-PE 1% mol, and this kind of fluorescent label is lipophilic and it forms the bilayer together with the other lipid. So, we expected a decreasing of fluorescent events in 10 second if the vesicles were disrupted because of the interaction with albumin.

The experiment was repeated in triplo and each plate was measured 3 times.
Count:

Sample	Events measured in 10 seconds
RSV-loaded LCL	**4919.4±1104.2**
RSV-loaded LCL + albumin after 20 minutes	1553.8±267.1
RSV-loaded LCL + albumin after 40 minutes	1583.6±500.2

RSV-loaded LCL + albumin after 1 hour	1856.1±296.7
RSV-loaded LCL + albumin after 1 hour and 30 min.	2196.7±298.6
RSV-loaded LCL + albumin after 2 hours	2592.1±218.4
empty LCL	**6924.2±1866.3**
empty LCL + albumin after 20 minutes	782.7±144.9
empty LCL + albumin after 40 minutes	859.2±186.8
empty LCL + albumin after 1 hour	598.7±187.2
empty LCL + albumin after 1 hour and 30 min.	952.4±242.8
empty LCL + albumin after 2 hours	752.3±106.6

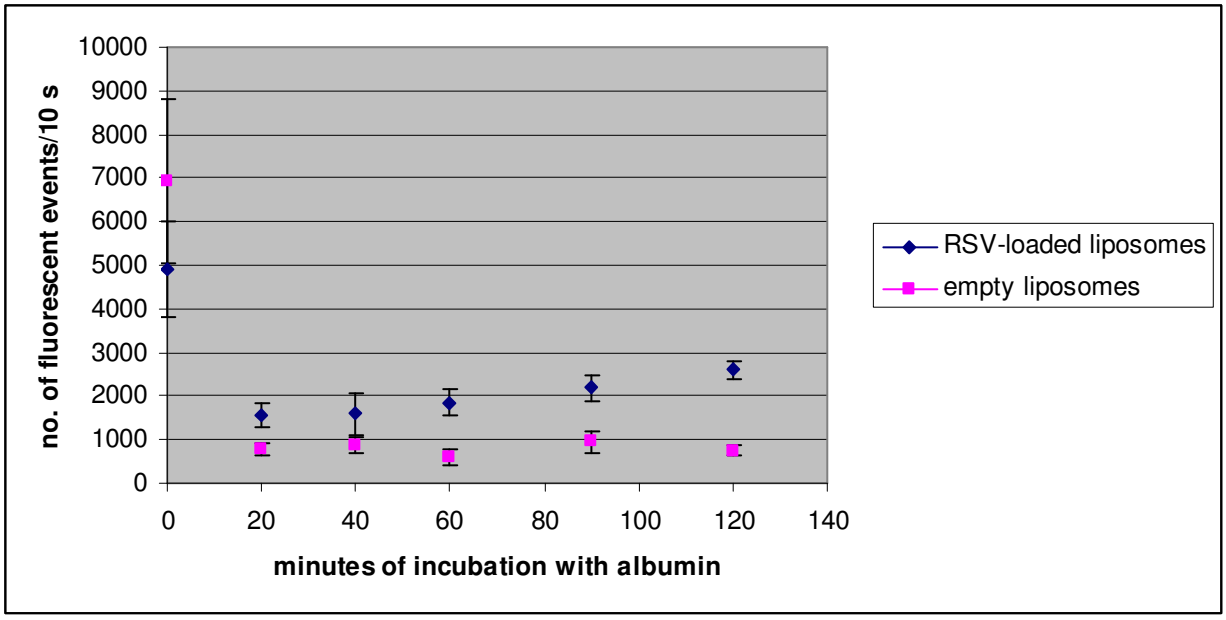

Fig 51. RSV-loaded liposomes after 2 hours of incubation with albumin.

The fluorescent signal decreases after only 20 minutes. It means that some vesicles are lost after incubation with albumin.
A decreasing of fluorescence should be measured also if NBD-PE might form a shell around the vesicles, but, in this case, the fluorescent signal should be shifted and it is not.
It seems that empty vesicles are less stable than RSV-loaded vesicles in presence of albumin. Probably the presence of encapsulated resveratrol may stabilize them.
Concluding, it is necessary an independent method to measure the interaction between vesicles and albumin in order to cross the informations.

III.3.3.2. Fluorimeter analysis

Leakage of water-soluble molecules from liposomes can be measured using fluorescent markers. For this purpose the fluorophore calcein can be used. Calcein is a small (620 g/mol), hydrophilic fluorophore, which shows self-quenching properties at high concentrations. When the concentration of calcein is higher than 40 mM, the self-quenching efficiency is about 90%. A concentration of 75-100 mM ensures an efficient self-quenching even when a considerable fraction of the encapsulated calcein has been release. Calcein can be encapsulated into the liposomes in a quenched concentration and when the liposomal membrane is destabilized, the encapsulated calcein will be released and diluted in the surrounding buffer. Upon dilution, the quenching effect is reduced and fluorescent signal increases.

III.3.3.2.a. Incubation with albumin and fluorimeter analysis

Empty liposomes and liposomes with initial concentrations of resveratrol of 1 mg/mL were incubated with a solution of albumin (40 mg/mL in PBS, physiological concentration) at the body temperature in a shaking waterbath to mimic the *in vivo* condition.

constituent	mg/mL	MW	µmol
DPPC	7.5	734	51.090
18:0/18:0 PEG 2000	2.233	2750	4.060
cholesterol	2.092	387	27.030

initial RSV conc. (mg/mL)	mean diameter by DLS (nm)	polydispersity index (PDI)
-	128.8	0.02
1	126.9	0.09

Liposomes were labelled with calcein, a small hydrophilic fluorofore (λ_{ex}= 485 nm: λ_{em}= 512 nm), and analysed by the Fluorometer.

III.3.3.2.b. Calibration curve by disrupted liposomes

In order to quantified the amount of fluorescence, a calibration curve was prepared using increasing amount of disrupted liposomes. Different volumes of disrupted liposomes were diluted with PBS in order to obtain the following calibration curves (figure **52**).

µL of liposomes disrupted by Triton X-100 (+ albumin)	µL of PBS	% of disrupted liposomes	fluorescence
0	150	0	2994.5
30	120	20	16922.5
45	105	30	22195.0
60	90	40	26675.0
75	75	50	31167.0
90	60	60	37734.0
105	45	70	41810.0
120	30	80	46814.0
135	15	90	51834.0
150	0	100	59562.5

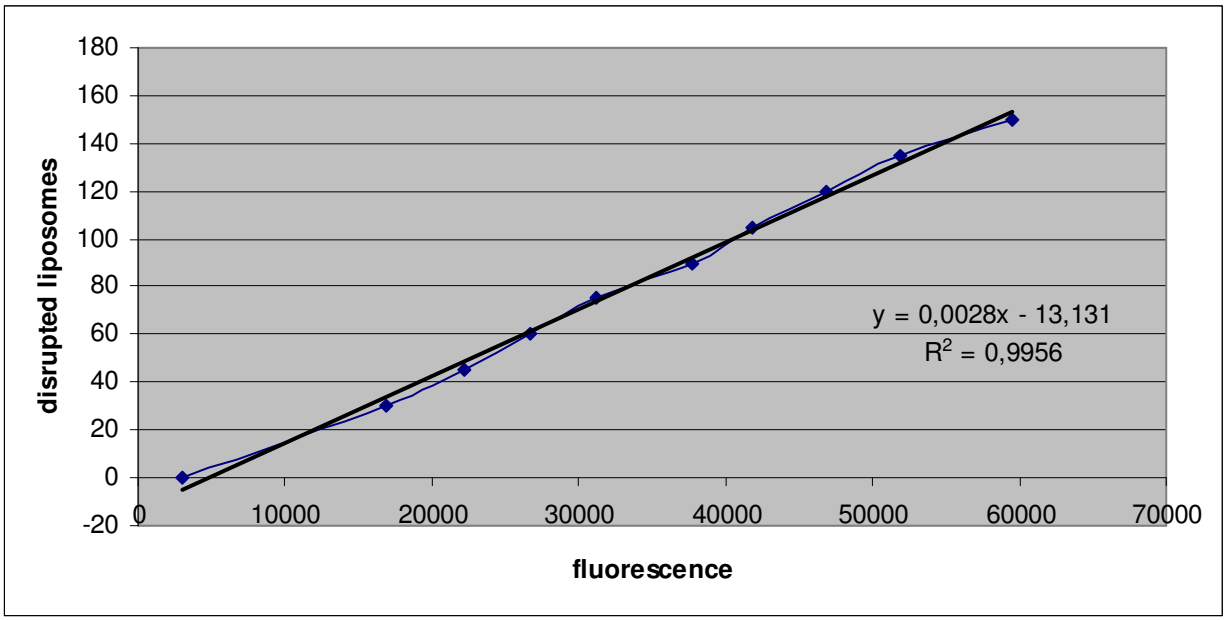

Fig 52. Calibration curve.

The incubation with albumin was monitored at different time points.
Each sample had the same dilution of the calibration curve.
Liposomes were labelled with calcein, and this kind of fluorescent label is hydrophilic and it naturally remains inside the vesicle, in the internal core. So, we expected an increasing of fluorescence if the vesicles were disrupted because of the interaction with albumin.
In the table below, the results obtained for empty liposomes were summarized:

time (min)	fluorescence	disrupted empty liposomes	% of disrupted empty liposomes
0	50780.7±461.5	129.05±1.29	86.0±0.82
20	41708.7±7258.9	103.65±20.32	65.0±6.73
40	48144.3±3595.6	121.67±10.07	81.1±6.06
60	49101.7±10193.0	124.35±28.54	89.9±18.7
90	44376.0±2543.7	111.12±7.12	74.1±4.25
120	51833.7±4631.7	132.00±12.97	88.0±7.86

In the table below, the results obtained for RSV-loaded liposomes were summarized:

time (min)	fluorescence	disrupted RSV-loaded liposomes	% disrupted RSV-loaded liposomes
0	50521.5±441.9	127.49±1.24	85.0±0.75
20	42155.3±7576.9	104.90±21.21	79.9±14.36
40	42755.0±2536.1	106.58±7.10	71.0±4.21
60	36591.3±5626.4	89.32±15.75	58.7±8.92
90	43260.3±3573.2	108.00±10.00	72.0±5.95
120	41618.0±5919.8	103.40±16.57	68.9±9.80

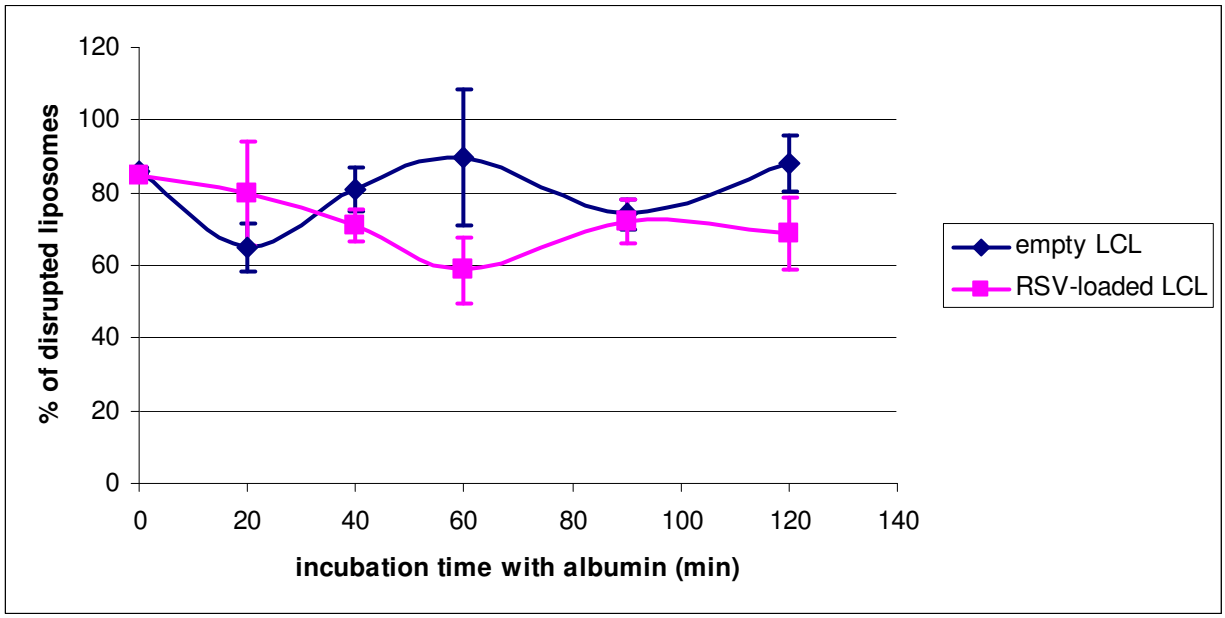

Fig 53. Disrupted RSV-loaded liposomes after 2 hours of incubation with albumin.

The amount of fluorescence in time is quite high, ranging from 65 to 88% for empty liposomes and from 58 to 85% for RSV-loaded liposomes, respectively.
It seem that the effect of albumin was instant. As soon as albumine was added to liposomal dispersion, calcein can escape.

III.3.3.3. Incubation with albumin coated beads

Resveratrol has poor water solubility (Belguendouz L, 1997; Caddeo C, 2009), so it must be bound to proteins to keep it at a high concentration in plasma. The efficiency of a therapeutic substance is related to its affinity to bind protein transporters (Khan MA, 2002). In the transport of resveratrol, it can bind to serum proteins (Jannin B, 2004) and can passively diffuse through the plasma membrane (Lancon A, 2004).
Resveratrol binds human serum albumin with association constant of $K = 2.56 \times 10^5 \ M^{-1}$. The resveratrol-protein binding is mainly through pigment H-bonding with polypeptide C=O, C-N, and NH groups. At low drug concentration, no major protein conformational changes occur, whereas at high pigment contents, an increase of protein α-helix and a decrease of β-sheet were observed. This is due to an additional stabilization of protein conformation induced at high resveratrol concentration (Soukpoé-Kossi CNN, 2006).

Stability test of resveratrol-loaded long-circulating liposomes in presence of blood protein like albumin was performed in order to assess the capacity of albumin to extract resveratrol from the vesicles. The molar ratio between RSV and albumin were 1:1, 1:1.5 and 1:2.
For the molar ratio RSV:albumin 1:1, results derived from HPLC/PDA analysis:

final RSV conc. (mg/mL)	%	Time of incubation with albumin	sample
0.42±0.04	**100**	**0**	**RSV-loaded liposomes in PBS**
0.44±0.01	104.8±1.68	**20 min.**	
0.41±0.10	97.0±23.74	**40 min.**	
0.42±0.07	99.9±17.68	**1 h**	

0.40±0.04	95.0±10.78	**2 h**	
0.40±0.04	95.9±10.78	**4 h**	
0.37±0.04	89.3±9.09	**6 h**	
0.37±0.05	89.3±12.79	**24 h**	
0.32±0.08	77.0±18.35	**48 h**	
0.34±0.01	80.4±3.53	**6 days**	
0.42±0.04	**100**	**0**	**RSV in albumin coated beads/PBS 50% v/v**
0.13±0.02	30.8±5.76	**20 min.**	
0.10±0.01	23.7±0.93	**40 min.**	
0.10±0.01	24.9±2.23	**1 h**	
0.09±0.01	21.7±0.37	**2 h**	
0.10±0.01	23.2±1.67	**4 h**	
0.09±0.01	22.1±1.29	**6 h**	
0.06±0.01	13.5±0.56	**24 h**	
0.04±0.00	9.4±0.00	**48 h**	
0.02±0.01	5.8±0.37	**6 days**	
0.42±0.04	**100**	**0**	**RSV-loaded liposomes in albumin coated beads/PBS 50% v/v**
0.19±0.03	44.6±7.24	**20 min.**	
0.16±0.01	37.5±3.20	**40 min.**	
0.17±0.03	42.9±3.95	**1 h**	
0.16±0.01	39.3±3.37	**2 h**	
0.13±0.02	32.3±2.77	**4 h**	
0.13±0.01	30.9±2.69	**6 h**	
0.09±0.01	22.4±0.68	**24 h**	
0.08±0.01	17.5±1.39	**48 h**	
0.04±0.01	9.57±1.68	**6 days**	

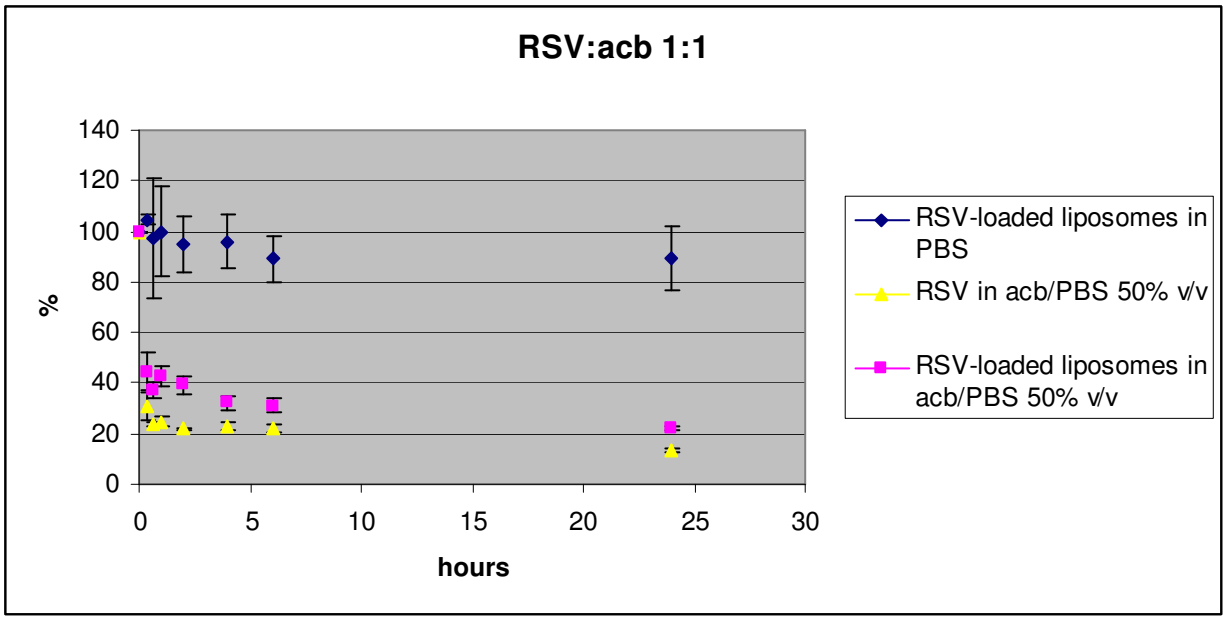

Fig 54. Stability test of RSV-loaded LCL in presence of albumin. Molar ratio between RSV and albumin was 1:1.

For the molar ratio RSV:albumin 1:1.5, results derived from HPLC/PDA analysis:

final RSV conc. (mg/mL)	%	Time of incubation with	sample

		albumin	
0.42±0.04	**100**	**0**	**RSV-loaded liposomes in PBS**
0.43±0.03	102.5±7.91	**20 min.**	
0.41±0.03	97.3±6.23	**40 min.**	
0.41±0.02	96.9±5.72	**1 h**	
0.40±0.01	94.4±0.16	**2 h**	
0.43±0.04	101.9±10.44	**4 h**	
0.40±0.01	96.5±0.50	**6 h**	
0.39±0.02	93.9±4.21	**24 h**	
0.41±0.06	98.8±14.8	**48 h**	
0.29±0.08	70.3±19.9	**6 days**	
0.42±0.04	**100**	**0**	**RSV in albumin coated beads/PBS 50% v/v**
0.11±0.01	27.4±3.37	**20 min.**	
0.07±0.01	17.7±1.97	**40 min.**	
0.08±0.00	20.3±0.00	**1 h**	
0.08±0.01	18.3±1.12	**2 h**	
0.09±0.01	21.5±1.68	**4 h**	
0.08±0.01	18.5±3.08	**6 h**	
0.06±0.00	14.3±0.00	**24 h**	
0.05±0.00	11.1±0.00	**48 h**	
0.03±0.01	8.3±0.00	**6 days**	
0.42±0.04	**100**	**0**	**RSV-loaded liposomes in albumin coated beads/PBS 50% v/v**
0.12±0.03	28.2±6.23	**20 min.**	
0.10±0.01	24.3±1.70	**40 min.**	
0.10±0.01	23.0±2.15	**1 h**	
0.09±0.01	21.1±0.56	**2 h**	
0.11±0.01	25.6±2.52	**4 h**	
0.12±0.01	28.1±2.01	**6 h**	
0.10±0.01	23.8±0.68	**24 h**	
0.07±0.01	17.7±0.27	**48 h**	
0.05±0.01	11.9±3.37	**6 days**	

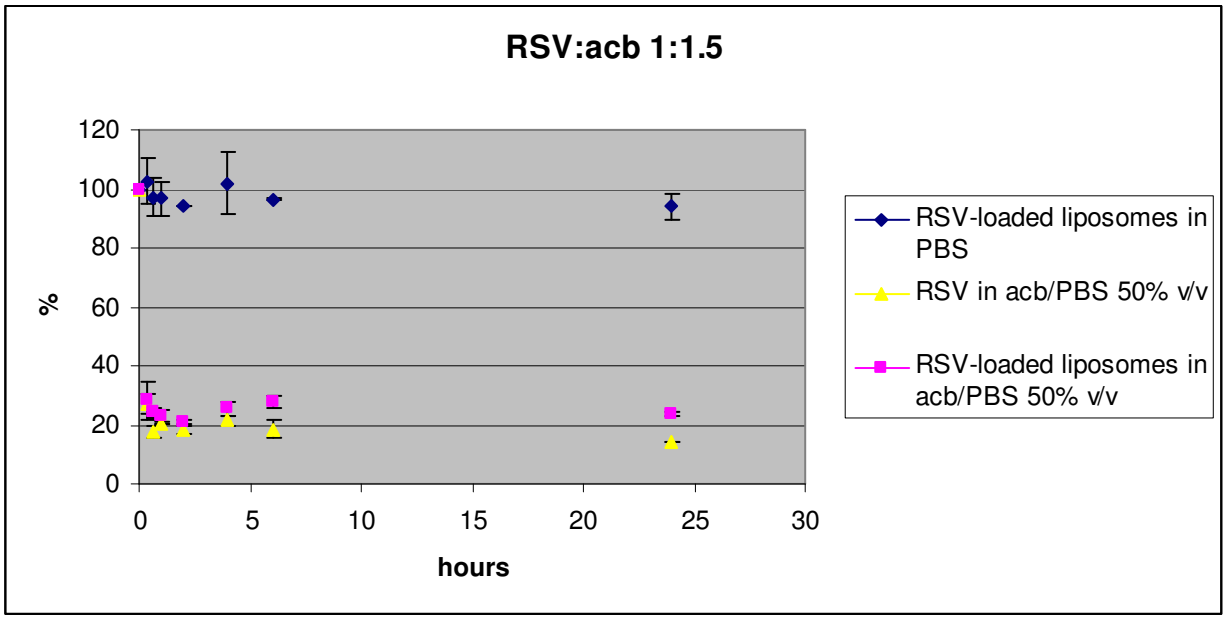

Fig 55. Stability test of RSV-loaded LCL in presence of albumin. Molar ratio between RSV and albumin was 1:1.5.

For the molar ratio RSV:albumin 1:2, results derived from HPLC/PDA analysis:

final RSV conc. (mg/mL)	%	Time of incubation with albumin	sample
0.42±0.04	**100**	**0**	**RSV-loaded liposomes in PBS**
0.50±0.02	119.4±5.22	**20 min.**	
0.48±0.11	115.6±26.4	**40 min.**	
0.50±0.05	118.7±12.29	**1 h**	
0.45±0.06	107.4±14.14	**2 h**	
0.38±0.03	90.5±8.08	**4 h**	
0.46±0.05	110.2±13.13	**6 h**	
0.37±0.09	88.3±21.55	**24 h**	
0.36±0.06	85.5±13.81	**48 h**	
0.21±0.06	50.5±13.47	**6 days**	
0.42±0.04	**100**	**0**	**RSV in albumin coated beads/PBS 50% v/v**
0.08±0.01	20.0±0.75	**20 min.**	
0.06±0.01	15.5±3.33	**40 min.**	
0.06±0.02	13.4±4.09	**1 h**	
0.06±0.01	13.9±0.37	**2 h**	
0.07±0.01	17.9±2.24	**4 h**	
0.06±0.01	14.7±0.74	**6 h**	
0.05±0.01	12.9±1.87	**24 h**	
0.04±0.01	10.8±3.35	**48 h**	
0.04±0.01	8.9±1.48	**6 days**	
0.42±0.04	**100**	**0**	**RSV-loaded liposomes in albumin coated beads/PBS 50% v/v**
0.11±0.01	26.5±1.84	**20 min.**	
0.09±0.02	21.4±4.14	**40 min.**	
0.08±0.00	19.5±0.00	**1 h**	
0.09±0.01	21.8±0.37	**2 h**	
0.08±0.01	18.7±0.37	**4 h**	
0.09±0.01	22.4±1.12	**6 h**	
0.09±0.00	21.6±0.00	**24 h**	
0.09±0.01	20.5±2.23	**48 h**	
0.06±0.01	14.2±1.49	**6 days**	

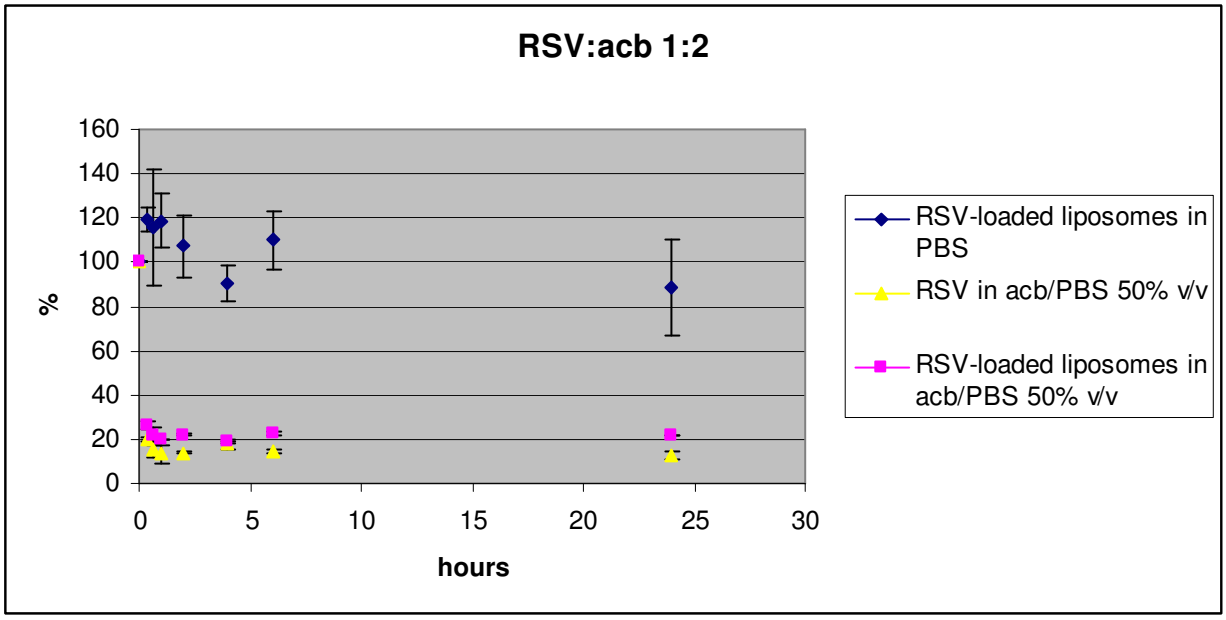

Fig 56. Stability test of RSV-loaded LCL in presence of albumin. Molar ratio between RSV and albumin was 1:2.

In the experiment with the molar ratio RSV:albumin 1:1, resveratrol in contact with albumin coated beads/PBS 50% v/v had a residual percentage of 30.8% after only 20 minutes. Its level was manteined around 20% within 6 hours.
If encapsulated in liposomes, it was reduced to 44.6% after 20 minutes. Its content was manteined around 40% within 2 hours and around 30% within 6 hours.
In the experiment with the molar ratio RSV:albumin 1:1.5, resveratrol in contact with albumin coated beads/PBS 50% v/v was reduced to 27.4% after only 20 minutes. Its level was manteined around 20% within 6 hours.
If encapsulated in liposomes, it was reduced to 28.2% after 20 minutes. Its content was manteined around 20-25% within 24 hours.
In the experiment with the molar ratio RSV:albumin 1:2, resveratrol in contact with albumin coated beads/PBS 50% v/v had a residual percentage of 20.0% after only 20 minutes. Its level was manteined around 10-15% within 48 hours.
If encapsulated in liposomes, it was reduced to 26.5% after 20 minutes. Its content was manteined around 20% within 24 hours.
The results indicated appreciable destructive effects of serum albumin on the liposomal content after only 20 minutes.

III.3.4. *In vivo* activity: tumor growth

Liposomes containing polyethylene glycol (PEG) derivatives (Blume G, 1990; Klibanov AL, 1990; Allen TM, 1991; Maruyama K, 1992; Woodle MC, 1992; Yuda T, 1996) are not readily taken up by the macrophages in reticuloendothelial system (RES), and hence remain in the blood circulation for a relatively long period of time.
The addition of polyethylene glycol (PEG) is the most common and preferred method of “masking” nanoparticles from immune recognition (Gref R, 2000; Peracchia MT, 1999; Owens DE, 2006). It has been shown to decrease interactions of various nanoparticles with blood proteins and help avoiding recognition by the RES, in essence prolonging blood circulation (Gref R, 1994; 2000; Peracchia MT, 1999; Paciotti GF, 2004; Lemerchand C, 2006; Kim HR, 2007).

Particularly, PEG-modified liposomes have been utilized as a particulate carrier for anti-tumor therapy due to their long circulation time (Jun-ichi Y, 2008). The capillary permeability of the endothelium in newly vascularized tumors is significantly greater than that of normal organs and the integrity of the endothelial barrier is perturbed, via EPR effect: enhanced permeability and retention effect (Gabizon A, 1992; Jang SH, 2003).
Studies with radiolabels entrapped in PEG liposomes have indicated that PEG liposomes can selectively extravasate in inflammatory tissues, by virtue of the increased permeability of the local vascular endothelium (Laverman P, 1999; Dams ET, 2000).
So, long-circulating PEG liposomes are preferentially delivered and accumulated into the tumors which provides a great opportunity for passive targeting into tumor tissues (Maeda H, 2000; Luigi C, 2003).

III.3.4.1. In vivo experiment: tumor growth

Balb/c nude female mice were inoculated with 1 x 10^6 14C-tumor cells (the head and neck squamous-cell carcinoma line 14C). Palpable subcutaneous tumors was developed over a period of 2-3 weeks. The tumor was measured with a digital caliper in order to calculate the tumor volume. When the tumor measured 30 mm^3, mice were treated with resveratrol-loaded long circulating liposomes with an initial concentration of resveratrol of 1 mg/mL intravenously (0.102 µg of resveratrol in 200 µL of injected liposomal dispersion). During the whole experiment the tumor size was measured twice weekly. When the tumors reached the humane endpoint (1000 mm^3) the mice were sacrificed one by one.

initial RSV conc. (mg/mL)	molar ratio (%)	mean diameter (nm)	polydispersity index (PDI)	final RSV conc. (mg/mL)	EE (%)
1	2.7	134.0±10.39	0.09±0.03	0.51±0.09	50.58±8.85

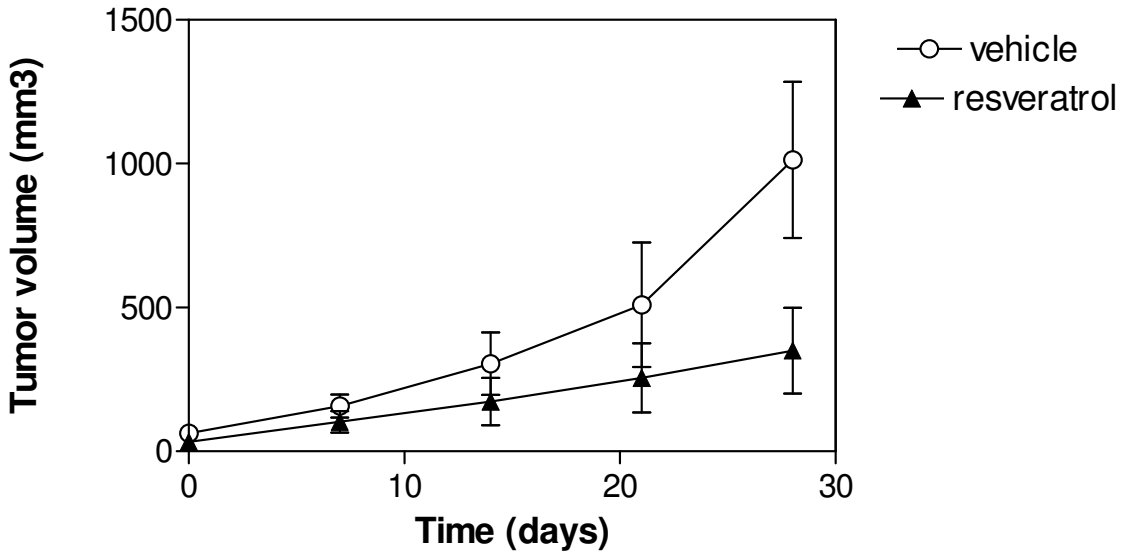

Fig 57. Tumor growth after administration of RSV-loaded LCL.
The tumor volume was reduced in an impressive way in comparison with the vehicle (empty liposomes without resveratrol).

III.3.4.2. Tumor: microscopy

Laser Scanning Confocal Microscopy or fluorescence microscopy can be used to determine binding of fluorescence labeled liposomes in histological samples (Cavalletti G, 2009). Tumors were saved with the perspective to do that. No results yet.

III.3.5. *In vivo* activity: biodistribution profile

Our understanding of the bioavailability, metabolism and tissue distribution of this compound is limited. Orally ingested *trans*-resveratrol is extensively metabolized in the enterocyte (Gonzalez-Pons E, 2004) before its entry into blood and target organs (Baur JA, 2006). To improve our understanding of the mechanism of action of *trans*-resveratrol, it is necessary to know if this compound or its metabolites are present in the body and in which organs they are found. A methodology of extraction and quantification of *trans*-resveratrol and its metabolites was performed after the intravenous administration of 15 mg/kg to healthy rats (Juan ME, 2009). Because of the limited information on the distribution available at present, we modified the existent method for simultaneous determination of *trans*-resveratrol and its metabolites in homogenized mice blood and tissues. The tissues that we analised were brain, liver, lungs, testis and kidney.

III.3.5.1. Recovery of trans-resveratrol from plasma

Blank plasma samples were spiked with the amount of RSV of 0.4 µg.
Results derived from HPLC analysis for the isocratic method:

Sample	recovery (µg/mL)
Organic solvent RT	2.16
Organic solvent -20°C	7.55
Organic solvent -20°C and salts	9.68

III.3.5.2. Recovery of trans-resveratrol from tissues

Blank brain, testis, liver, lungs and kidneys were spiked with the final concentration of 10 µmol/g tissue. The samples were than analysed by two different HPLC methods.
Results derived from HPLC analysis for the isocratic method:

Sample	recovery (%)
liver 1	93.1±9.79
liver 2	103.0±2.27
kidney 1	82.1±7.11
kidney 2	98.6±6.85
lung 1	85.1±8.22
lung 2	95.4±2.47
testis	96.3±6.26
brain	89.3±5.84

Results derived from HPLC analysis for the gradient method:

Sample	recovery (%)
liver 1	60.6

liver 2	77.8±3.79
kidney 1	61.1±0.00
kidney 2	67.0±3.05
lung 1	60.6±2.21
lung 2	76.9
testis	79.9±21.33
brain	71.1

III.3.5.3. In vivo experiment: biodistribution profile

Blood and tissues were saved for defining a biodistribution profile. No results yet.

III.4. Future perspectives

Tumors will be observed by Laser Scanning Confocal Microscopy or fluorescence microscopy to determine binding of fluorescence labeled liposomes in histological samples (Cavalletti, 2009).
Blood and tissues from treated mice were saved in order to assess a biodistribution profile after parenteraly administration of resveratrol-loaded PEGylated liposomes.

III.5. References

- Aggarwal P, Hall JB, McLeland CB, Dobrovolskaia MA, McNeil SE. **2009**. Nanoparticle interaction with plasma proteins as it relates to particle biodistribution, biocompatibility and therapeutic efficacy. *Advanced Drug Delivery Reviews*, *in press.*
- Alarcón de la Lastra C, Villegas I. **2007**. Resveratrol as an antioxidant and prooxidant agent: mechanisms and clinical implications. *Biochem. Soc. T.* 35, 1156-1160.
- Allen TM, Hansen C, Martin F, Redemann C, Yau-Young A. **1991**. Liposomes containing synthetic lipid derivatives of poly(ethylene glycol) show prolonged circulation half-lives *in vivo. Biochim. Biophys. Acta* 1066, 29–36.
- Athar M, Back JH, Tang X, Kim KH, Kopelovich L, Bickers DR, Kim AL. **2007**. Resveratrol: A review of preclinical studies for human cancer prevention. *Toxicology and Applied Pharmacology.* 224(3), 274–283.
- Banerjee S, Bueso-Ramos C, Aggarwal BB. **2002**. Suppression of 7,12-dimethylbenz(a)anthracene-induced mammary carcinogenesis in rats by resveratrol: role of nuclear factor-nB, cyclooxygenase 2, and matrix metalloprotease 9. *Cancer Res*. 62, 4945 – 54.
- Baur JA, Sinclair DA. **2006**. Therapeutic potential of resveratrol: the *in vivo* evidence. *Nature reviews* 5, 493 – 506.
- Bavaresco L. **2003**. Role of viticultural factors on stilbene concentrations of grapes and wine. *Drugs Exp. Clin. Res.* 29, 181–187.
- Belguendouz L, Fremont L, Gozzelino MT. **1998**. Interaction of transresveratrol with plasma lipoproteins. *Biochem. Pharmacol*. 55, 811–816.
- Belguendouz L, Fremont L, Linard A. **1997**. Resveratrol inhibits metal ion dependent and independent peroxidation of porcine low density lipoproteins. *Biochem. Pharmacol*. 53, 1347–1355.
- Bertelli AA, Giovannini L, Bernini W, Migliori M, Fregoni M, Bavaresco L, Bertelli A. **1996**. Antiplatelet activity of cis resveratrol. *Drugs Exp. Clin. Res*. 22, 61–63.
- Bertelli AA, Gozzini A, Stradi R, Stella S, Bertelli A. **1998**. Stability of resveratrol over time and in the various stages of grape transformation. *Drugs Exp Clin Res* 24 (4), 207–11.
- Billack B, Radkar V, Adiabouah C. **2008**. *In Vitro* Evaluation Of The Cytotoxic And Antiproliferative Properties Of Resveratrol And Several Of Its Analogs. *Cellular & Molecular Biology Letters*, 13, 553 - 569.
- Birrell MA, *et al*. **2005**. Resveratrol, an extract of red wine, inhibits lipopolysaccharide induced airway neutrophilia and inflammatory mediators through an NF-κB-independent mechanism. *FASEB J.* 19, 840–841.
- Blume G, Cevc G. **1990**. Liposomes for the sustained drug release *in vivo. Biochim. Biophys. Acta* 1029, 91–97.
- Bohm M, Rosenkranz S, Laufs U. **2004**. Alcohol and red wine: impact on cardiovascular risk. *Nephrol. Dial. Transplant.* 19, 11–16.
- Boocock DJ, Faust GES, Patel KR, Schinas AM, Brown VA, Ducharme MP, Booth TD, Crowell JA, Perloff M, Gescher AJ, Steward WP, Brenner DE. **2007**. Phase I Dose Escalation Pharmacokinetics Study in Healthy Volunteers of Resveratrol, a Potential Cancer Chemopreventive Agent. *Cancer Epidemiol Biomarkers Prev*, 16 (6), 1264-52.
- Bove K, Lincoln DW, Tsan MF. **2002**. Effect of resveratrol on growth of 4T1 breast cancer cells *in vitro* and *in vivo. Biochem. Biophys. Res. Commun*. 291, 1001–1005
- Brakenhielm E, Cao R, Cao Y. **2001**. Suppression of angiogenesis, tumor growth, and wound healing by resveratrol, a natural compound in red wine and grapes. *FASEB J.* 15, 1798–1800.
- Caddeo C, Teskac K, Sinico C, Kristl J. **2008**. Effect of resveratrol incorporated in liposomes on proliferation and UV-B protection of cells. *International Journal of Pharmaceutics* 36, 183-19.

- Camonta L, Cottarta CH, Rhayema Y, Nivet-Antoinea V, Collinc RDF, Beaudeuxa JL, Bonnefont-Rousselota D. **2009**. Simple spectrophotometric assessment of the trans-/cis-resveratrol ratio in aqueous solutions. *Analytica Chimica Acta* 634, 121–128.
- Cao Y, Fu ZD, Wang F, *et al.* **2005**. Anti-angiogenic activity of resveratrol, a natural compound from medicinal plants. *J Asian Nat Prod Res*. 7, 205 – 13.
- Carbò N, Costelli P, Baccino FM, Lòpez-Soriano FJ, Argile JM. **1999**. Resveratrol, a natural product present in wine, decreases tumor growth in rat tumor model. *Biochem. Biophys. Res. Commun.* 254, 739–743.
- Carey TE, Wolf GT, Baker SR, Krause CJ. **1990**. Cell surface antigen expression and prognosis In: Fee WE , Goephert H , Johns ME , Strong EW , Ward PH. Head and neck cancer. Philadelphia: BC Decker. p 77-82.
- Cavaletti G, Cassetti A, Canta A, Galbiati S, Gilardini A, Oggioni N, Rodriguez-Menendez V, Fasano A, Liuzzi GM, Fattler U, Ries S, Nieland J, Riccio P, Haas H. **2009.** Cationic Liposomes Target Sites of Acute Neuroinflammation in Experimental Autoimmune Encephalomyelitis. *Molecular Pharmaceutics*, *in press.*
- Chan MY, Mattiacci JA, Hwang HS, Shah A, Fong D. **2000**. Synergy between ethanol and grape polyphenols, quercetin, and resveratrol, in the inhibition of the inducible nitric oxide synthase pathway. *Biochem. Pharmacol*. 60, 1539–1548.
- Chen G, *et al.* **2005**. Synthesis and anti-inflammatory activity of resveratrol analogs. *Chem. Pharm. Bull.* (Tokyo) 53, 1587–1590.
- Chonn A, Semple SC, Cullis PR. **1992**. Association of blood proteins with large unilamellar liposomes in vivo: relation to circulation lifetimes. *J. Biol. Chem*. 267, 18759–18765.
- Ciolino HP, Daschner PJ, Yeh GC. **1998**. Resveratrol inhibits transcription of CYP1A1 in vitro by preventing activation of the aryl hydrocarbon receptor. *Cancer Res*. 58, 5707–5712.
- Clèment M-V, Hirpara JL, Chawdhury S-H, Pervaiz S. **1998**. Chemopreventive agent resveratrol, a natural product derived from grapes, triggers CD95 signaling-dependent apoptosis in human tumor cells. *Blood* 92, 996–1002.
- Creasy LL, Coffee M. **1988**. Phytoalexin production potential of grape berries. *J. Am. Soc. Hortic. Sci.* 113, 230-234.
- Crowell JA, Korytko PJ, Morrissey RL, Booth TD, Levine BS. **2004**. Resveratrol-associated renal toxicity. *Toxicol. Sci.* 82, 614–619.
- Dams ET, Oyen WJ, Boerman OC, Storm G, Laverman P, Kok PJ, *et al.* **2000**. 99mTc-PEG liposomes for the scintigraphic detection of infection and inflammation: clinical evaluation. *J Nucl Med* 41, 622–30.
- Das DK and Maulik N. **2006**. Resveratrol in cardioprotection: a therapeutic promise of alternative medicine. *Molecular Interventions* 6(1), 36 - 46.
- Delmas D, Lancon A, Colin D, Jannin B, Latruffe N. **2006**. Resveratrol as a chemopreventive agent: a promising molecule for fighting cancer. *Curr. Drug Targets* 7, 423–442.
- Derakhshanded K, Dadashzadeh S. **2005**. Liquid chromatographic quantitation of the lactone and the total of lactone and carboxylate forms of 9-nitrocamptothecin in human plasma. *Journal of Chromatography B* 818, 199-204.
- Drummond DC, Meyer O, Hong K, Kirpotin DB, Papahadjopoulos D. **1999**.Optimizing liposomes for delivery of chemotherapeutic agents to solid tumors. *Pharmacol. Rev.* 51, 691–743.
- Elmali N, *et al.* **2005**. Effect of resveratrol in experimental osteoarthritis in rabbits. *Inflamm. Res.* 54, 158–162.
- Fabris S, Momo F, Ravagnan G, Stevanato R. **2008**. Antioxidant properties of resveratrol and piceid on lipid peroxidation in micelles and monolamellar liposomes. *Biophysical Chemistry* 135, 76–83.
- Fontecave M, Lepoivre M, Elleingand E, Gerez C, Guittelet O. **1998**. Resveratrol, a remarkable inhibitor of ribonucleotide reductase. *FEBS Lett*. 421, 277–279.
- Frankel EN, Waterhouse AL, Kinsella JE. **1993**. Inhibition of human LDL oxidation by resveratrol. *Lancet* 341, 1103–1104.

- Fremont L, Belguendouz L, Delpal S. **1999**. Antioxidant activity of resveratrol and alcohol-free wine polyphenols related to LDL oxidation and polyunsaturated fatty acids. *Life Sci* 64, 2511 – 21.
- Fuller RR, Sweedler JV. Characterizing submicron vesicles with wavelength-resolved fluorescence in flow cytometry, Cytometry 25 (1996) 144–155.
- Gabizon A, Catane R, Uziely B, Kaufman B, Safra T, Cohen R, *et al.* **1994.** Prolonged circulation time and enhanced accumulation in malignant exudates of doxorubicin encapsulated in polyethyleneglycol coated liposomes. *Cancer Res* 54, 987–92.
- Gabizon A, Papahadjopoulos D. **1992**. The role of surface charge and hydrophilic groups on liposome clearance *in vivo. Biochim. Biophys. Acta* 1103, 94–100.
- Gao X, Xu YX, Divine G, Janakiraman N, Chapman RA, Gautam SC. **2002**. Disparate *in vitro* and *in vivo* antileukemic effects of resveratrol, a natural polyphenolic compound found in grapes. *J. Nutr*. 132(7), 2076-81.
- Garvin S, Ollinger K, Dabrosin C. **2006**. Resveratrol induces apoptosis and inhibits angiogenesis in human breast cancer xenografts *in vivo. Cancer Letters* 231, 13–122.
- Goldberg DM, Hahn SE, Parkes JG. **1995*a***. Beyond alcohol: beverage consumption and cardiovascular mortality. *Clin. Chim. Acta* 237, 155–187.
- Goldberg DM, Yan J, Ng E, Diamandis EP, Karuman-chiri A, Soleas G, Waterhouse AL. **1994**. Direct injection gaschromatography mass spectrometric assay for trans-resveratrol. *Anal. Chem*.66, 3959-3963.
- Goldberg DM, Yan J, Ng E, Diamandis EP, Karumanchiri A, Soleas G, Waterhouse AL. **1995b**. A global survey of trans-resveratrol concentrations in commercial wines. *Am.J. Enol. Vitic*. 46, 159-165.
- Gonzalez-Pons E, Juan ME, Bolufer J, Planas JM. **2004**. *J.Physiol. Biochem*. 60, 126.
- Goppert TM, Muller RH. **2005**. Adsorption kinetics of plasma proteins on solid lipid nanoparticles for drug targeting. *Int. J. Pharm*. 302, 172–186.
- Gorham J. **1980**. The stilbenoids. In Progress in Phytochemistry; Reinhold L, Harborne J B, Swain T, Eds.; Pergamon Press: Oxford, U. K.,; 203-252.
- Gref R, Luck M, Quellec P, Marchand M, Dellacherie E, Harnisch S, Blunk T, Muller RH. **2000**. 'Stealth' corona–core nanoparticles surface modified by polyethylene glycol (PEG): influences of the corona (PEG chain length and surface density) and of the core composition on phagocytic uptake and plasma protein adsorption. *Colloids Surf., B Biointerfaces* 18, 301–313.
- Gref R, Minamitake Y, Peracchia MT, Trubetskoy V, Torchilin V, Langer R. 1994. Biodegradable long-circulating polymeric nanospheres. *Science* 263, 1600–1603.
- Han YS, Zheng WH, Bastianetto S, Chabot JG, Quirion R. **2004**.Neuroprotective effects of resveratrol against beta-amyloid-induced neurotoxicity in rat hippo- campal neurons: involvement of protein kinase C. *Br. J. Pharmacol*. 141, 997–1005.
- Hercher M, Mueller W, Shapiro HM. Detection and discrimination of individual viruses by flow cytometry, J. Histochem. Cytochem. 27 (1979) 350–352.
- Hoekstra D, Scherphoft G. **1979**. *Biochim. Biophys. Acta* 551, 109–121.
- Hong RL, Tseng YL. **2001**. Phase I and pharmacokinetic study of a stable, polyethylene-glycolated liposomal doxorubicin in patients with solid tumors: the relation between pharmacokinetic property and toxicity. *Cancer* 91, 1826–33.
- Hsu CY, Uludag H. Effects of size and topology of DNA molecules on intracellular other submicroscopic particles, Cytometry A 57 (2004) 94–99.
- Ingham JL. **1976**. 3,5,4′-Trihydroxystilbene as a phytoalexin from groundnuts (*Arachis hypognea). Phytochemistry* 15, 1791-1793.
- Jang JH, Surh YJ. **2003**. Protective effect of resveratrol on beta-amyloid- induced oxidative PC12 cell death. *Free Radical Biol. Med*. 34, 1100–1110.
- Jang M, Cai L, Udeani GO, Slowing KV, Thomas CF, Beecher CWW, Fong HHS, Farnsworth NR, Kinghorn AD, Mehta RG, Moon RC, Pezzuto JM. **1997**. Cancer chemopreventive activity of resveratrol, a natural product derived from grapes. *Science* 275, 218–220.

- Jang SH, Wientjes MG, Lu D, Au JLS. **2003**. Drug delivery and transport to solid tumors. *Pharm. Res*. 20, 1337–1350.
- Jannin B, Menzel M, Berlot JP, Delmas D, Lancon A, Latruffe N. **2004**. Transport of resveratrol, a cancer chemopreventive agent, to cellular targets: plasmatic protein binding and cell uptake. *Biochem Pharmacol* 68, 1113–1118.
- Jeandet P, Bessis R, Gautheron B. **1991**. The production of resveratrol (3,5,4′-trihydroxystilbene) by grape berries in different developmental stages. *Am. J. Enol. Vitic.* 42, 41-46.
- Jeandet P, Bessis R, Sbaghi M, Meunier P. **1995**. Production of the phytoalexin resveratrol by grapes as a response to Botrytis attacks under natural conditions. *J. Phytopathol.* 143, 135-139.
- Jeon SI, Lee JH, Andrade JD, Degennes PG. **1991**. Protein surface interactions in the presence of polyethylene oxide. 1. Simplified theory. *J. Colloid Interface Sci*. 142, 149–158.
- Jocelyn D, Samarjit D, Subhendu M, Dipak KD. **2008**. Resveratrol, a unique phytoalexin present in red wine, delivers either survival signal or death signal to the ischemic myocardium depending on dose. *Journal of Nutritional Biochemistry*.
- Juan ME, Maijo M, Planas MJ. **2009.** Quantification of trans-resveratrol and its metabolites in rat plasma and tissues by HPLC. *Journal of Pharmaceutical and Biomedical Analysis*, *accepted*.
- Juliano RL, Kimelberg HK, Papahadjopoulos D. **1971**. *Biochim. Biophys. Acta* 241, 894–905.
- Khan MA, Muzammil S, Musarrat J. **2002**. Differential binding of tetracyclines with serum albumin and induced structural alterations in drug-bound protein. *Int J Bio Macromol* 30, 243–249.
- Kim HR, Andrieux K, Delomenie C, Chacun H, Appel M, Desmaele D, Taran F, Georgin D, Couvreur P, Taverna M. **2007**. Analysis of plasma protein adsorption onto PEGylated nanoparticles by complementary methods: 2-DE, CE and Protein Labon-chip system. *Electrophoresis* 28, 2252–2261.
- Kimura Y, Okuda H, Arichi S. **1985*a***. Effects of stilbene derivatives on arachidonate metabolism in leukocytes. *Biochim. Biophys. Acta* 837, 209–212.
- Kimura Y, Okuda H, Arichi S. **1985*b***. Effects of stilbenes on arachidonate metabolism in leukocytes. *Biochim. Biophys. Acta* 834, 275–278.
- Kimura Y, Okuda H. **2001**. Resveratrol Isolated from *Polygonum cuspidatum* Root Prevents Tumor Growth and Metastasis to Lung and Tumor-Induced Neovascularization in Lewis Lung Carcinoma-Bearing Mice. *J. Nutr.* 131(6), 1844-9.
- Klibanov AL, Maruyama K, Torchilin VP, Huang L. **1990**. Amphipathic polyethyleneglycols effectively prolong the circulation time of liposomes. *FEBS Lett.* 268, 235–237.
- Krishna P, Bhat L, Lantvit D, Christov K, Mehta RG, Moon RC, Pezzuto JM. **2001**. Estrogenic and Antiestrogenic Properties of Resveratrol in Mammary Tumor Models. *CANCER RESEARCH* 61, 7456–7463.
- Lancon A, Delmas D, Osman H, Thénot JP, Jannin B, Latruffe N. **2004**. Human hepatic cell uptake of resveratrol: involvement of both passive diffusion and carrier-mediated process. *Biochem Biophys Res Commun* 316, 1132–1137.
- Langcake P, Pryce RJ. **1976**. The production of resveratrol by Vitis vinifera and other members of the Vitaceae as a response to infection and injury. *Physiol. Plant Pathol*. 9, 77–86.
- Langcake P, Pryce RJ. **1976**. The production of resveratrol by *Vitis vinifera* and other members of the Vitaceae as a response to infection or injury. *Physiol. Plant Pathol*. 9, 77-86.
- Laverman P, Boerman OC, Oyen WJ, Dams ET, Storm G, Corstens FH. **1999**. Liposomes for scintigraphic detection of infection and inflammation. *Adv Drug Deliv Rev* 37, 225–35.
- Law SL, Lo WY, Pai SH, Tech GW, Kou FY. **1986**. *Int. J. Pharm*. 32, 237–241.
- Law SL, Lo WY, Pai SH, Tech GW. **1988**. *Int. J. Pharm*. 43, 257–260.

- Lee EO, Lee HJ, Hwang HS, Ahn KS, Chae C, Kang KS, Lu J, Kim SH. **2006**. Potent inhibition of Lewis lung cancer growth by heyneanol A from the roots of *Vitis amurensis* through apoptotic and anti-angiogenic activities. *Carcinogenesis*. 27(10), 2059–2069.
- Lee SK, Mbwambo ZH, Chung H, *et al.* **1998**. Evaluation of the antioxidant potential of natural products. *Comb Chem High Throughput Screen* 1, 35 – 46.
- Lemarchand C, Gref R, Passirani C, Garcion E, Petri B, Muller R, Costantini D, Couvreur P. **2006**. Influence of polysaccharide coating on the interactions of nanoparticles with biological systems. *Biomaterials* 27, 108–118.
- Leonard S, Xia C, Jiang BH, Stinefelt B, Klandorf H, Harris GK, Shi X. **2003**. Resveratrol scavenges reactive oxygen species and effects radical-induced cellular responses. *Biochem. Biophys. Res. Commun.* 309, 1017–1026.
- Li ZG, Hong T, Shimada Y, *et al.* **2002**. Suppression of N-nitrosomethylbenzylamine (NMBA)-induced esophageal tumorigenesis in F344 rats by resveratrol. *Carcinogenesis* 23,1531 – 6.
- Lis LJ, Kauffman JW, Shriver DF. **1976**. *Biochim. Biophys. Acta* 436, 513–522.
- Lopez-Nicolas JM, Garcia-Carmona F. **2008**. Aggregation state and pk_a values of (*E*)-resveratrol as determined by fluorescence spectroscopy and UV-Visible Absorption. *Journal of Agricultural and Food Chemistry* 56, 7600-5.
- Lu X, Ji C, Xu H, Li L, Ding H, Ye M, Zhu Z, Ding D, Jiang X, Ding X, Guo X. **2008**. Resveratrol-loaded polymeric micelles protect cells from Aβ-Induced oxidative stress. *International Journal of Pharmaceutics*.
- Luigi C, Maurizio C, Franco D. **2003**. From conventional to stealth liposomes. A new frontier in cancer chemotherapy. *Tumori* 89, 237–249.
- Maeda H, Wu J, Sawa T, Matsumura Y, Hori K. **2000**. Tumor vascular permeability and the EPR effect in macromolecular therapeutics. *J. Control.Release* 65, 271–284.
- Mancuso C, Bates TE, Butterfield DA, Calafato S, Cornelius C, Lorenzo AD, Kostova ATD, Calabrese V. **2007**. Natural antioxidants in Alzheimer's disease. *Expert Opin. Investig. Drugs,* 16, 1921-1931.
- Maruyama K, Yuda T, Okamoto A, Kojima S, Suginaka A, Iwatsuru M. **1992**. Prolonged circulation time *in vivo* of large unilamellar liposomes composed of distearoyl phosphatidylcholine and cholesterol containing amphipathic poly(ethylene glycol). *Biochim. Biophys. Acta* 1128, 44–49.
- Mathies JC, Austin MA. **1980**. Modified acetonitrile protein precipitation method of sample preparation for drug assay by liquid chromatography. *Clinical Chemistry* 26, 12, 1760.
- Michnik A, Sulkowska A. **1997.** Destabilisation of liposomes by bovine serum albumin; Sepharose 2B-Cl experiment. *Chromatographia* 45, 155 – 157.
- Miura D, Miura Y, Yagasaki K. **2003**. Hypolipidemic action of dietary resveratrol, a phytoalexin in grapes and red wine, in hepatoma-bearing rats. *Life Sci* 73, 1393 – 400.
- Moghimi SM, Muir IS, Illum L, Davis SS, Kolb-Bachofen V. **1993**. Coating particles with a block co-polymer (poloxamine-908) suppresses opsonization but permits the activity of dysopsonins in the serum. *Biochim. Biophys. Acta* 1179, 157–165.
- Moon RC, Mehta RG. **1990**. In: Chemistry and Biology of Retinoids. Dawson MI, Okamura WH, Eds. (CRC Press, Boca Raton, FL, 1990), 501–518.
- Moreno JJ. **2000**. Resveratrol modulates arachidonic acid release, prostaglandin sysnthesis, and 3T6 fibroblast growth factor. *J. Pharm. Exp. Ther.* 294, 333–338.
- Murias M, Jager W, Handler N, Erker T, Horvath Z, Szekeres T, Nohl H, Gille L. **2005**. Antioxidant, prooxidant and cytotoxic activity of hydroxylated resveratrol analogues: structure-activity relationship. *Biochem. Pharmacol*. 69, 903-912.
- N' soukpoé-Kossi CN, St-Louis C, Beauregard M, Subirade M, Carpentier R, Hotchandani S, Tajmir-Riahi HA. **2006**. Resveratrol Binding to Human Serum Albumin. *Journal of Biomolecular Structure &Dynamics* 24, 3.
- Nguyen AV, Martinez M, Stamos MJ, Moyer MP, Planutis K, Hope C, Holcombe RF. **2009**. Results of a phase I pilot clinical trial examining the effect of plant-derived resveratrol and

grape powder on Wnt pathway target gene expression in colonic mucosa and colon cancer. *Cancer Management and Research* 1, 25–37.

- Ogawara K, Furumoto K, Nagayama S, Minato K, Higaki K, Kai T, Kimura T. **2004**. Pre-coating with serum albumin reduces receptor-mediated hepatic disposition of polystyrene nanosphere: implications for rational design of nanoparticles. *J. Control Release* 100, 451–455.
- Oku N, Namba Y. **1994**. Long-circulating liposomes. *Crit Rev Ther Drug Carrier Syst* 11, 231–70.
- Oshima M, *et al.* **1996**. Suppression of intestinal polyposis in Apcδ716 knockout mice by inhibition of cyclooxygenase 2 (COX-2). *Cell* 87, 803–809.
- Owens DE, Peppas NA. **2006**. Opsonization, biodistribution, and pharmacokinetics of polymeric nanoparticles. *Int. J. Pharm*. 307, 93–102.
- Pace-Asciak CR, Hahn S, Diamandis EP, Soleas G, Goldberg DM. **1995**. The red wine phenolics trans-resveratrol and quercetin block human platelet aggregation and eicosanoid synthesis:implications forprotection against coronary heart disease. *Clin. Chim. Acta* 235, 207–219.
- Paciotti GF, Myer L, Weinreich D, Goia D, Pavel N, McLaughlin RE, Tamarkin L. **2004**. Colloidal gold: a novel nanoparticle vector for tumor directed drug delivery. *Drug Deliv*. 11, 169–183.
- Panagi Z, Avgoustakis K, Evangelatos G, Ithakissios DS. **1999**. *Int. J. Pharm*. 176, 203–207.
- Peracchia MT, Fattal E, Desmaele D, Besnard M, Noel JP, Gomis JM, Appel M, d'Angelo J, Couvreur P. **1999**. Stealth PEGylated polycyanoacrylate nanoparticles for intravenous administration and splenic targeting. *J. Control. Release* 60, 121–128.
- Peracchia MT, Harnisch S, Pinto-Alphandary H, Gulik A, Dedieu JC, Desmaele D, d'Angelo J, Muller RH, Couvreur P. **1999**. Visualization of *in vitro* protein-rejecting properties of PEGylated stealth polycyanoacrylate nanoparticles. *Biomaterials* 20, 1269–1275.
- Prokop J, Abrman P, Seligson AL, Sovak M. **2006**. Resveratrol and its glycon piceid are stable polyphenols. *J Med Food* 9 (1), 11–4.
- Ragione FD, Cucciolla V, Borriello A, Pietra VD, Racioppi L, Soldati G, Hanna C, Galletti P, Zappia V. **1998**. Resveratrol arrests the cell division cycle at S/G2 phase transition. *Biochem. Biophys. Res. Commun*. 250, 53–58.
- Roggero JP. **2000**. Study of the ultraviolet irradiation of resveratrol and wine. *J. Food Compost. Anal.* 13, 93–97.
- Rotondo S, Rajtar G, Manarini S, Celardo A, Rotilio D, de Gaetano G, Evangelista V, Cerletti C. **1998**. Effects of trans-resveratrol, a natural polyphenolic compound, on human polymorphonuclear leukocyte function. *Br. J. Pharmacol*. 123, 1691–1699.
- Roy H, Lundy S. **2005**. Resveratrol. Pennington Nutrition Series, No. 7 .
- Russo A, Palumbo M, Aliano C, Lempereur L, Scoto G, Renis M. **2003**. Red wine micronutrients as protective agents in Alzheimer like induced insult. *Life Sci*.72, 2369–2379.
- Sabín J, Prieto G, Ruso JM, Messina PV, Salgado FJ, Nogueira M, Costas M, Sarmiento F. **2009**. Interactions between DMPC Liposomes and the Serum Blood Proteins HSA and IgG. *J. Phys. Chem. B* 113, 1655–1661.
- Sale S, Tunstall RG, Ruparelia KC, *et al.* **2005**. Comparison of the effects of the chemopreventive agent resveratrol and its synthetic analogue trans-3,4,5,4-tetramethoxystilbene (DMU-212) on adenoma development in the Apc(Min+) mouse and cyclooxygenase-2 in human-derived colon cancer cells. *Int J Cancer* 115,194 – 201.
- Salgado FJ, Lojo J, Alonso-Lebrero JL, Lluis C, Franco R, Cordero OJ, Nogueira M. **2003**. *J. Biol. Chem*. 278, 24849–24857.
- Salgado FJ, Pineiro A, Canda-Sanchez A, Lojo J, Nogueira M. **2005**. *Mol. Membr. Biol*. 22, 163–76.
- Savaskan E, Olivieri G, Meier F, Seifritz E, Wirz-Justice A, Muller-Spahn F. **2003**. Red wine ingredient resveratrol protects from beta-amyloid neurotoxicity. *Gerontology* 49, 380–383.

- Schneider Y, Duranton B, Gosse F, Schleiffer R, Seiler N, Raul F. **2001**. Resveratrol inhibits intestinal tumorigenesis and modulates host-defense-related gene expression in an animal model of human familial adenomatous polyposis. *Nutr Cancer* 39, 102 – 7.
- Sharma M, Gupta YK. **2002**. Chronic treatment with trans resveratrol prevents intra-cerebroventricular streptozotocin induced cognitive impairment and oxidative stress in rats. *Life Sci*. 71, 2489–2498.
- Sharma S, Stutzman JD, Kelloff JG, Steele VE. **1994**. Screening of potential chemopreventive agents using biochemical markers of carcinogenesis. *Cancer Res*. 54, 5848.
- Shigematsu S, Ishida S, Hara M, Takahashi N, Yoshimatsu H, Sakata T and Korthuis RJ. **2003**. Resveratrol, a red wine constituent polyphenol, prevents superoxide-dependent inflammatory responses induced by ischemia/reperfusion, platelet-activating factor, or oxidants. *Free Radical Biology & Medicine* 34, No. 7, 810–817.
- Steen HB. **2008**. Flow cytometer for measurement of the light scattering of viral and delivery with non-viral gene carriers. *BMC Biotechnol*. 8, 23.
- Subbaranmaiah K, Chung WJ, Michaluart P, Telang N, Tanabe T, Inoue H, Jang M, Pezzuto JM, Dannenberg AJ. **1998**. Resveratrol inhibits cyclooxygenase-2 transcription and activity in phorbol ester-treated human mammary epithelial cell. *J. Biol. Chem*. 273, 21875–21882.
- Suh N, Luyengi L, Fong HHS, Kinghorn AD, Pezzuto JM. **1995**. *Anticancer Res.* 15, 233.
- Sun NJ, Woo SH, Cassady JM, Snapka RM. **1998**. DNA polymerase and topoisomerase II inhibitors from Psoralea corylifolia. *J. Nat. Prod*. 61, 362–366.
- Sweet C, Zull JE. **1969**. *Biochim. Biophys. Acta* 173, 94–103.
- Sweet C, Zull JE. **1970**. *Biochim. Biophys. Acta* 219, 253.
- Trela BC, Waterhouse AL. **1996**. Resveratrol: isomeric molar absorptivities and stability. *J Agric Food Chem* 44:1253–1257.
- Tseng SH, Lin SM, Chen JC, *et al.* **2004**. Resveratrol suppresses the angiogenesis and tumor growth of gliomas in rats. *Clin Cancer Res* 10, 2190 – 202.
- van Gaal EVB, Spierenburg G, Hennik WE, Crommelin DJA, Mastrobattista E. **2009**. Flow cytometry for rapid size determination and sorting of nucleic acid containing nanoparticles in biological fluids. *Journal of controlled release, in press.*
- Vorauer-Uhl K, Wagner A, Borth N, Katinger H. **2000.** Determination of Liposome Size Distribution by Flow Cytometry. *Cytometry* 39,166–171.
- Vrhovsek U, Eder R, Wendelin S. **1995**. The occurrence of trans-resveratrol in Slovenian red and white wines. *Acta Aliment*. 24, 203-212.
- Walle T, Hsieh F, Delegge MH Jr, Walle UK. **2004**. High absorption but very low bioavailability of oral resveratrol in humans. *Drug Metab. Dispos*. 32, 1377–1382.
- Wang Y, Catana F, Yang Y, Roderick R, van Breemen RB. **2002**. An LC-MS method for analyzing total resveratrol in grape juice, cranberry juice and in wine. *J. Agric. Food Chem.* 50, 431–435.
- Wang Z, Huang Y, Zou J, Cao K, Xu Y, Wu JM. **2002**. Effects of red wine and wine polyphenol resveratrol on platelet aggregation *in vivo* and *in vitro*. *Int. J. Mol. Med*. 9, 77–79.
- Wenzel E, Somoza V. **2005**. Metabolism and bioavailability of trans-resveratrol. *Mol. Nutr. Food Res*. 49, 472–481.
- Woodle MC, Lasic DD. **1992**. Sterically stabilized liposomes. *Biochim. Biophys. Acta* 1113, 171–199.
- Woodle MC, Newman MS, Cohen JA. **1994**. Sterically stabilized liposomes: physical and biological properties. *J Drug Target* 2, 397–403.
- Wu SL, Pan CE, Yu L, Meng KW. **2005**. Immunosuppression by combined use of cyclosporine and resveratrol in a rat liver transplantation model. *Transplant. Proc*. 37, 2354–2359.

- Yokoe J, Sakuragi S, Yamamoto K, Teragaki T, Ogawara K, Higaki K, Katayama N, Kai T, Sato M, Kimura T. **2008**. Albumin-conjugated PEG liposome enhances tumor distribution of liposomal doxorubicin in rats. *International Journal of Pharmaceutics* 353, 28–34.
- Yuda T, Maruyama K, Iwatsuru M. **1996**. Prolongation of liposome circulation time by various derivatives of polyethyleneglycols. *Biol. Pharm. Bull.*19, 1347–1351.
- Zborowski J, Roerdink E, Scherphof G. **1977**. *Biochim. Biophys. Acta* 497, 183.
- Ziegler CC, Rainwater L, Whelan J, McEntee MF. **2004**. Dietary resveratrol does not affect intestinal tumorigenesis in Apc(Min/+) mice. *J Nutr* 134, 5 – 10.

Concluding remarks

During my PhD, innovative formulations were developed in order to try giving answers to different therapeutic emergencies.

First of all, **malaria**, a neglected illness, which continues to be one of the major public problems to solve in Africa, Asia and Latin America. The World Health Organisation (WHO) has recommended that all the antimalarial drugs must be combined. In particular, artemisinin and its derivatives are suggested as first line treatment against malaria but only in combination therapy (ACT) (Ioset JR, 2009; Eastman RT, 2009). Recently, it has been reported that curcumin, a very safe natural polyphenol, is active against malaria and it has synergistic effects if administered with artemisinin. In view of their abundance and safety, further investigations related to their combination to develop low-cost antimalarial therapies are mandatory (Reddy RC, 2005; Nandakumar DN, 2006). Several innovative formulations containing artemisinin were developed and were testing for their stability.
In vivo studies showed improved pharmacokinetic parameters of artemisinin-loaded liposomes and PEGylated liposomes. These results are encouraging and, in a preliminary investigation, liposomes have been also positively tested in *Plasmodium berghei* infected mice for their antiplasmodial activity. In the future also the PEGylated liposomes, having the best pharmacokinetic performance, will be compared with conventional liposomes for the antimalarial activity. Subsequently, artemisinin-curcumin loaded liposomes have been developed with the aim of producing an appropriate formulation to be suggested as an artemisinin-based combination therapy.

Secondly, **neuropathic pain**, is a widespread disorder induced by autoimmune diseases, drug or toxin exposure, infections, metabolic insults or trauma and it is defined by OMS as an untreatable disease. The underlying molecular mechanisms of neuropathic pain are still not completely understood, and as a consequence, treatments are unsatisfactory in mostly of the cases (Syndrup SH, 1999). There is an urgent need to develop novel therapeutics for an effective treatment of this disease. From our study it was found that a β-cyclodextrin formulation containing verbascoside 300 mg/kg showed the same antihyperalgesic profile of 300 mg/kg verbascoside saline solution when orally administered in a chronic constriction injury of the sciatic nerve and in an intra-articular injection of sodium monoiodoacetate in the rat paw-pressure test. Conversely, a liposome formulation containing verbascoside 100 mg/kg administered i.p. showed a longer lasting antihyperalgesic effect in comparison with a 100 mg/kg verbascoside saline solution. To the best of our knowledge no study has been reported on the activity of verbascoside on neuropathic pain, neither free nor formulated.
In addition, stability studies revealed that vesicles were physically stable for 90 days and neither verbascoside leakage or degradation nor vesicle size alteration occurred during this period.

Finally, a model of **tumor** (Human Head and Neck Squamous Cell Carcinoma in BALB/c nude mice) was treated with resveratrol-loaded PEGylated liposomes. Although the stability of PEGylated liposomes containing resveratrol in presence of blood protein, like albumin, seemed scarce, in our *in vivo* experiments, the tumor growth was strikingly reduced by resveratrol-loaded PEGylated liposomes in comparison with the vehicle.

Acknowledgments

University of Florence - Italy

Department of Pharmaceutical Sciences
Prof. Franco F Vincieri, for his experience, his openness and his personal style.
Prof. Anna Rita Bilia, for her care, her passion and her will power.
Dr. Maria Camilla Bergonzi
Dr. Anastasia Karioti
Dr. Marzia Innocenti

Department of Preclinical and Clinical Pharmacology
Prof. Carla Ghelardini
Prof. Nicoletta Galeotti
Elisa Vivoli

Department of Preclinical and Clinical Pharmacology
Prof. Andrea Novelli
Dr. Silvia Arrigucci

Department of Anatomy, Histology and Forensic Medicine, Section of Histology
Prof. M Giuliana Vannucchi
Mr. Patrizio e Daniele Guasti

Department of Chemistry
Dr. Debora Berti

Mass Spectrometry Laboratory, A. Meyer Children's Hospital
Dr. Giancarlo la Marca

Magnetic Resonance Center CERM
Mr. Fabio Calogiuri

University of Cagliari - Italy

Dipartimento Farmaco Chimico Tecnologico
Prof. Anna Maria Fadda's research group

University of Utrecht – The Netherlands

Department of Pharmaceutics, Utrecht Institute of Pharmaceutical Sciences UIPS
Prof. Gert Storm
Prof. Raymond Schiffelers
Dr. Cristianne JF Rijcken
Joris P Schillemans
Ethlinn VB van Gaal

Enceladus Pharmaceuticals Company, Amsterdam
Dr. Josbert M. Metselaar

Index